ISSN 0021-9673

VOL. 694 NO. 2 10 MARCH 1995

THIS ISSUE COMPLETES VOL. 694

JOURNAL OF CHROMATOGRAPHY A

INCLUDING ELECTROPHORESIS AND OTHER SEPARATION METHODS

ELSEVIER

JOURNAL OF CHROMATOGRAPHY A

INCLUDING ELECTROPHORESIS AND OTHER SEPARATION METHODS

Scope. The *Journal of Chromatography A* publishes papers on all aspects of **chromatography, electrophoresis** and related methods. Contributions consist mainly of research papers dealing with chromatographic theory, instrumental developments and their applications. In the *Symposium volumes*, which are under separate editorship, proceedings of symposia on chromatography, electrophoresis and related methods are published. *Journal of Chromatography B: Biomedical Applications* —This journal, which is under separate editorship, deals with the following aspects: developments in and applications of chromatographic and electrophoretic techniques related to clinical diagnosis or alterations during medical treatment; screening and profiling of body fluids or tissues related to the analysis of active substances and to metabolic disorders; drug level monitoring and pharmacokinetic studies; clinical toxicology; forensic medicine; veterinary medicine; occupational medicine; results from basic medical research with direct consequences in clinical practice.

Submission of Papers. The preferred medium of submission is on disk with accompanying manuscript (see *Electronic manuscripts* in the Instructions to Authors, which can be obtained from the publisher, Elsevier Science B.V., P.O. Box 330, 1000 AH Amsterdam, Netherlands). Manuscripts (in English; *four* copies are required) should be submitted to: Editorial Office of *Journal of Chromatography A*, P.O. Box 681, 1000 AR Amsterdam, Netherlands, Telefax (+31-20) 485 2304, or to: The Editor of *Journal of Chromatography B: Biomedical Applications*, P.O. Box 681, 1000 AR Amsterdam, Netherlands. Review articles are invited or proposed in writing to the Editors who welcome suggestions for subjects. An outline of the proposed review should first be forwarded to the Editors for preliminary discussion prior to preparation. Submission of an article is understood to imply that the article is original and unpublished and is not being considered for publication elsewhere. For copyright regulations, see below.

Publication information. *Journal of Chromatography A* (ISSN 0021-9673): for 1995 Vols. 683–714 are scheduled for publication. *Journal of Chromatography B: Biomedical Applications* (ISSN 0378-4347): for 1995 Vols. 663–674 are scheduled for publication. Subscription prices for *Journal of Chromatography A*, *Journal of Chromatography B: Biomedical Applications* or a combined subscription are available upon request from the publisher. Subscriptions are accepted on a prepaid basis only and are entered on a calendar year basis. Issues are sent by surface mail except to the following countries where air delivery via SAL is ensured: Argentina, Australia, Brazil, Canada, China, Hong Kong, India, Israel, Japan, Malaysia, Mexico, New Zealand, Pakistan, Singapore, South Africa, South Korea, Taiwan, Thailand, USA. For all other countries airmail rates are available upon request. Claims for missing issues must be made within six months of our publication (mailing) date. Please address all your requests regarding orders and subscription queries to: Elsevier Science B.V., Journal Department, P.O. Box 211, 1000 AE Amsterdam, Netherlands. Tel.: (+31-20) 485 3642; Fax: (+31-20) 485 3598. Customers in the USA and Canada wishing information on this and other Elsevier journals, please contact Journal Information Center, Elsevier Science Inc., 655 Avenue of the Americas, New York, NY 10010, USA, Tel. (+1-212) 633 3750, Telefax (+1-212) 633 3764.

Abstracts/Contents Lists published in Analytical Abstracts, Biochemical Abstracts, Biological Abstracts, Chemical Abstracts, Chemical Titles, Chromatography Abstracts, Current Awareness in Biological Sciences (CABS), Current Contents/Life Sciences, Current Contents/Physical, Chemical & Earth Sciences, Deep-Sea Research/Part B: Oceanographic Literature Review, Excerpta Medica, Index Medicus, Mass Spectrometry Bulletin, PASCAL-CNRS, Referativnyi Zhurnal, Research Alert and Science Citation Index.

US Mailing Notice. *Journal of Chromatography A* (ISSN 0021-9673) is published weekly (total 52 issues) by Elsevier Science B.V., (Sara Burgerhartstraat 25, P.O. Box 211, 1000 AE Amsterdam, Netherlands). Annual subscription price in the USA US$ 5389.00 (US$ price valid in North, Central and South America only) including air speed delivery. Second class postage paid at Jamaica, NY 11431. **USA POSTMASTERS**: Send address changes to *Journal of Chromatography A*, Publications Expediting, Inc., 200 Meacham Avenue, Elmont, NY 11003. Airfreight and mailing in the USA by Publications Expediting.

See inside back cover for Publication Schedule, Information for Authors and information on Advertisements.

0021-9673/95/$09.50

Printed in the Netherlands

CONTENTS

(Abstracts/Contents Lists published in Analytical Abstracts, Biochemical Abstracts, Biological Abstracts, Chemical Abstracts, Chemical Titles, Chromatography Abstracts, Current Awareness in Biological Sciences (CABS), Current Contents/Life Sciences, Current Contents/Physical, Chemical & Earth Sciences, Deep-Sea Research/Part B: Oceanographic Literature Review, Excerpta Medica, Index Medicus, Mass Spectrometry Bulletin, PASCAL-CNRS, Referativnyi Zhurnal, Research Alert and Science Citation Index)

REGULAR PAPERS

Column Liquid Chromatography

Gas Chromatography

(Continued overleaf)

ELSEVIER

Journal of Chromatography A, 694 (1995) 321–331

JOURNAL OF CHROMATOGRAPHY A

Determination of the apparent transverse and axial dispersion coefficients in a chromatographic column by pulsed field gradient nuclear magnetic resonance

Edgar Baumeister[a], Uwe Klose[b], Klaus Albert[a], Ernst Bayer[a], Georges Guiochon[a,1,*]

[a] *Institut für Organische Chemie, University of Tübingen, D-72076 Tübingen, Germany*
[b] *Abteilung für Neuroradiologie, University of Tübingen, D-72076 Tübingen, Germany*

First received 1 August 1994; revised manuscript received 28 October 1994

Abstract

Pulsed field gradient nuclear magnetic resonance permits the direct determination of the coefficient of apparent dispersion of a solute in a chromatographic column. Axial and transverse dispersion coefficients can be measured independently as a function of the flow velocity of the mobile phase. Experiments have been carried out using water as the mobile phase, porous C18 silica as the stationary phase, and water as the probe (self-dispersion). The results are reported and compared to similar ones obtained previously by various authors, using conventional chromatographic techniques. The NMR method shows potential for the investigation of the structure and homogeneity of the packing of large diameter columns for preparative chromatography. It permits direct access to local values of these coefficients instead of measuring averages as classical methods do.

1. Introduction

Despite numerous investigations of column performance and of its relationship with the characteristics of the stationary phase, column packing has remained an art to this day. New materials require the development of new packing methods or at least the proper adjustment of conventional methods. The situation is potentially worse in preparative chromatography. First, conventional packing methods for analytical columns, which use high flow velocities, are unacceptable because the walls of preparative columns cannot be made thick enough to withstand the required high inlet pressures. Second, the column performance and essentially its separation power are critically influenced by large scale fluctuations of the local mobile phase velocity, themselves caused by an inhomogeneous packing density [1]. Deleterious fluctuations of the packing density are more prone to take place in wide columns.

Finally, it is difficult to control the homogeneity of the packed bed when the factors which influence its density and structure are not fully understood, nor even all clearly identified.

* Corresponding author.
[1] Present address: Department of Chemistry, University of Tennessee, Knoxville, TN, 37996-1600 and Division of Chemical and Analytical Sciences, Oak Ridge National Laboratory, Oak Ridge, TN, 37831-6120, USA.

0021-9673/95/$09.50
SSDI 0021-9673(94)01062-5

The local value of the permeability is related to the local density of the stationary phase through the external porosity, or fraction of the volume which is not occupied by the particles. Kozeny–Karman equation shows that the permeability increases slightly faster than the fourth power of this porosity [2]. As a result, the local average mobile phase flow velocity may fluctuate significantly across the column cross-sectional area and the surfaces of constant solute concentration are no longer planar and perpendicular to the column axis, as they should be for maximum performance. They become warped. Since the exit section of the column is flat and the whole mobile phase stream exiting from the column is admitted in the same time into the detector cell (in analytical applications) or the fraction collector (in preparative applications), the bands have an apparent width which is enlarged by the contribution of these warps [3].

The structure of a chromatographic bed is complex. The particle size distribution has a finite width and, as a consequence, the formation of a homogeneous, regularly structured bed, which might have been questionable in a cylindrical tube anyway, is impossible to achieve. The distance between particles varies widely across the bed and so does the average diameter of the channels which form between and around the particles. The range of channel diameters extends from 0.1 to 0.5 particle diameter (d_p), with significantly lower or larger values being possible occasionally. These channels are tortuous and constricted [4]. Furthermore, over an average distance of the order of one particle diameter, channels fork and/or merge. Because of the lack of homogeneity of the channels of a packed column at the particle level and of the anastomosis of the various channels available to the mobile phase percolating through the bed, the distribution of linear velocities of the mobile phase across a column section is chaotic, both in space and time. Like in a mountain brook flowing through a layer of boulders, eddies form in the large pools which lie between particles, where the cross-sectional area of a channel increases abruptly. However, by contrast with the quasi-planar surface of the water flow in a river, these eddies are in a 3-D fluid. Therefore, the eddies do not necessarily have a fixed vertical axis around which to revolve. This axis tumbles and its direction fluctuates randomly. This explains why the flow velocity in any given point of the column may fluctuate chaotically in time.

Accordingly, we are not interested in knowing the exact distribution of the flow velocities in a packed column. The only parameter of importance is the distribution of velocities averaged over scales of space and time which are large compared to a particle but small compared to the distance over which the packing density, permeability, transverse[a] and axial dispersion coefficients and other characteristics of the band broadening and mass transfer kinetics vary significantly. It is obvious that averaging the flow velocity over distances of the order of a few particle diameters will give values which are practically constant in time at a given location and which vary smoothly in all spatial directions. These average values are different from the average flow velocity classically used in chromatography, u, a velocity which is averaged over the entire cross-sectional area of the column and over a period of time which is usually large compared to the band width.

All measurements of the local average velocity across the diameter of a column, be it in chromatography [5–10] or in chemical engineering [11,12], have concluded that significant varia-

[a] Previous authors [5–8] have considered only the radial dispersion, i.e., the dispersion in the radial direction. This assumes implicitly that the column is cylindrical, which is not strictly correct [8], and that the injection is simultaneous and homogeneous over the entire cross-sectional area of the column inlet. If both assumptions are valid, the radial dispersion coefficient is a function of the distance to the column axis and, possibly, of the column length, but is independent of the direction. If one of these two assumptions is not valid, we must consider the transverse dispersion coefficients, which, at any point of the packing, may vary to a larger or smaller extent, depending upon the direction. Thus, we have to consider the distribution of these coefficients across the whole column. In chromatography, we may assume the column to be nearly cylindrical and consider a radial apparent dispersion coefficient. In NMR, we measure a transverse apparent dispersion coefficient.

tions are observed, with a central core region where the velocity is constant, a peak velocity at a distance from the wall depending on the average size of the packing particles, and a significant drop close to the wall. Such large scale variations of the velocity have a considerable influence on the column efficiency. Knox [13] has suggested that this might be the single most important cause of band broadening in analytical chromatography. This point was never seriously challenged. Admittedly, however, this result was obtained using long, narrow columns, packed with relatively coarse particles ($\rho = d_c/d_p = 10–40$). As a consequence, the wall region where the packing density fluctuates considerably occupies a relatively more important volume fraction of the column than in current short columns, packed with small particles ($\rho = 100–1000$) which have become the standard in HPLC.

Because only transverse dispersion can relax the transverse concentration gradients caused by large-scale drifts of the average velocity in the direction perpendicular to the column axis, it is important to investigate the transverse rate of mass transfer. If the column is homogeneous and if we consider a location which is not very close to the wall, the apparent dispersion coefficient is the same in all transverse directions. For the moderate degrees of angular fluctuations of the packing density which have been observed [8], the variations of the apparent transverse dispersion coefficient with the direction should be small and we can assume the apparent transverse and radial dispersion coefficients to be the same. Because, as a first approximation, non-homogeneous columns can be assumed to have a cylindrical symmetry, it is convenient to characterize the transverse rate of mass transfer by an apparent radial dispersion coefficient or as the radial HETP [5–8] and to compare the rates of axial and radial dispersion. Note also that if the column has a cylindrical symmetry, i.e., if the mobile phase velocity is only a function of r, the distance to the column axis, and not of the angular position, and provided that during the entire injection of the feed the local concentration is independent of the radial position, there is no radial concentration gradient and only the apparent radial dispersion coefficient matters.

To the extent of our knowledge, the measurement of the radial coefficient of apparent dispersion in liquid chromatography columns has been made so far only by Knox et al. [6] and by Eon [8]. Both groups used rather wide columns (12 and 18 mm I.D., respectively), packed with glass beads, water as the eluent, and *p*-nitrophenol as the analyte. They measured the axial and radial dispersion of very small samples injected with a syringe whose needle enters into the top layer of the column bed, by recording as a function of time the signal of a polarographic detector. The distance between the microelectrodes of this detector can be adjusted as desired. This work, although quite promising, has not been continued by the systematic investigation of the dependence of the radial dispersion coefficient on the parameters of the column. As a result, a number of issues have been left unresolved. Although not critical for analytical applications of chromatography, these issues have to be revisited in connection with the recent development of preparative liquid chromatography. It has been shown that the column efficiency may have a serious influence on the production rate and the recovery yield achieved with this method [14,15].

Nuclear magnetic resonance (NMR) offers an attractive possibility of monitoring diffusion processes [16] and measuring the dispersion coefficients in the direction of a stream and in the perpendicular direction. The frequency at which a certain nucleus (e.g., a proton) resonates is proportional to the local magnetic field. By superimposing a small magnetic field gradient to the field used to perform NMR measurements (such as is done in a scanner or more elaborately in the 2-D or 3-D Fourier techniques) it is possible to determine the position of a nucleus [16]. This process, called NMR imaging, is frequently used in medicine as a powerful diagnosis tool (NMR tomography). A proper combination of field gradient pulses permits the determination of the change of the position of tagged nuclei after a known period of time. As this signal is a function of the local velocity of

the solvent and because the gradients are applicable in different directions, it is possible to measure separately the axial and transverse components of dispersion. This technique developed after the work of Stejskal and Tanner [17] is called pulsed field gradient spin echo (PGSE) [18] or pulsed field gradient NMR (PFG) [19]. Today, it is frequently used in the determination of diffusion and dispersion coefficients [18,19]. The combination of PGSE and NMR imaging allows space resolved determination of flow, diffusion and dispersion [20,21]. However, depending on the nature of the magnetic field gradient used, different average values of the dispersion coefficient are measured. The smaller the volume over which the averaging takes place, the lower the signal/noise ratio and the more difficult the determination.

The goal of this first publication is a comparison of the results obtained with the conventional methods of measurements of the dispersion in chromatographic columns and by NMR. As we show, this provides a validation of the new approach, and a discussion of the limitations of the results which can be obtained by this method.

2. Theory

In this section, we discuss first the relationships between the axial and radial apparent dispersion coefficients in chromatographic columns and the experimental conditions. In the last part, we review briefly the procedure used for the derivation of these dispersion coefficients from the results of NMR measurements.

2.1. Definitions

The height equivalent to a theoretical plate was defined by Giddings [4] as the slope of the dependence of the band variance on its migration distance. This definition is more general than the classical one, using the square of the ratio of the retention time to the band standard deviation (or using the relationships $N = (L/\sigma_t)^2$, and $H = \sigma_t^2/L$). For example, it allows the consideration of a plate height function of the distance along the column, which is most useful in GC and TLC. With this definition, the axial and radial reduced HETP's are respectively given by

$$h_a = H_a/d_p = (1/d_p)(\partial\sigma_a^2/\partial z) \quad (1)$$

$$h_r = H_r/d_p = (1/d_p)(\partial\sigma_r^2/\partial z) \quad (2)$$

where H_a and H_r are the axial and radial plate height, respectively, h_a and h_r are the reduced plate heights, σ_a^2 and σ_r^2 are the variance of the band in the axial and radial direction, respectively, and z is the column length. For the purpose of this definition, the band is assumed to have the same variance in all radial directions (cylindrical symmetry). Although this may not be true in actual practice [8,10], deviations from cylindrical symmetry remain small compared to the variation of the dispersion coefficients across the column.

2.2. Plate height equations

As suggested by Knox [22] and confirmed by the results of many experimental investigations [15], the relationship between the axial reduced plate height and the mobile phase velocity is given by

$$h_a = B/\nu + A\nu^n + C\nu \quad (3)$$

where A, B, and C are numerical coefficients, function of the nature of the packing material used, of the analyte studied, and of the homogeneity of the packed bed. n is a numerical coefficient, typically between 0.25 and 0.35 and usually taken equal to 1/3. In their work, however, both Knox et al. [6] and Eon [8] took $n = 0.20$. ν is the reduced velocity or particle Peclet number

$$Pe_p = \nu = \bar{u}d_p/D_m \quad (4)$$

where $\bar{u}$ is the cross-sectional average velocity, d_p the average particle diameter, and D_m the diffusion coefficient in the bulk mobile phase or diffusivity.

In Eq. 3, the structure of the packed bed and eddy diffusion, axial diffusion, and the mass

transfer resistance are characterized by A, B, and C, respectively. A depends on the homogeneity of the packing and is a complex function of the fluctuations of the packing density on short, medium, and long distance. It includes the contribution of eddy diffusion to axial dispersion, and possible contributions of the width of the particle size distribution. Since diffusion is hindered by the presence of the particles, B is smaller than 2 (as would be implied by Eq. 2) and seems, most often, to be close to 1.5. It is a function of the tortuosity of the packing [4]. Because determinations of B require measurements of band profiles at low values of the mobile phase velocity, this coefficient is not known accurately and its possible dependence on the column packing technology has not been studied carefully. C includes the contributions of the kinetics of mass transfer between the stream of mobile phase percolating through the bed and the particles, of the kinetics of mass transfer through the particle pore network, and of the kinetics of adsorption/desorption or more generally of the kinetics of the retention mechanism. The contribution of the kinetics of mass transfer through the mobile phase stream (outside the particles) is included in the coefficient A. In this work, we are mainly interested in the coefficients A and B.

The reduced radial plate height is related to the mobile phase velocity by the Eq. 7

$$h_r = B/\nu + D \tag{5}$$

where B and ν have the same meaning as in Eqs. 3 and D is a coefficient accounting for the contribution of eddy diffusion to radial dispersion. This contribution has been explained in the literature by the phenomenon of "stream splitting", the mechanism of which has been discussed by Horne et al. [7], Saffman [23,24], and Littlewood [25]. When a mobile phase streamlet hits a particle, it separates into several unequal, smaller streamlets which pass between the hit particle and its neighbours, and merge with other streamlets of similar origin. Because the minimum width of these streamlets is very narrow, typically less than 0.1 d_p, they homogenize quickly. This process accelerates radial dispersion, in much the same way as the entrapment of molecules in the eddies taking place in the large pools between particles enhance axial dispersion.

The plate heights defined in chromatography are related to the corresponding apparent dispersion coefficients, $D_{ap,a}$ and $D_{ap,r}$ by the classical relationships [7]

$$D_{ap,a} = H_a \bar{u}/2 = h_a \nu D_m/2 \tag{6a}$$

$$D_{ap,r} = H_r \bar{u}/2 = h_r \nu D_m/2 \tag{6b}$$

These equations permit the conversion of the apparent dispersion coefficients measured by NMR into reduced plate heights or conversely.

2.3. Radial dispersion and stream splitting

This relationship has been discussed in detail by Horne et al. [7], Saffman [23,24], and Littlewood [25]. These authors have demonstrated that a band migrating along a porous bed is dispersed both in the axial and the radial directions by a combination of molecular and convective dispersions. The former results essentially from the axial molecular diffusion, slowed by the fact that migration along a straight line is impossible in a porous bed, as a new packing particle would be hit after a distance which, on the average, is equal to d_p [4,7]. As shown by Saffman [23,24], the results depends on the range of values of the Reynolds and the Peclet numbers encountered in the experiment. The Reynolds number can be written

$$Re = \bar{u} d_p \rho/\eta = \nu D_m \rho/\eta \tag{7}$$

where ρ is the density of the fluid and η its viscosity. Liquid chromatography is typically carried out in a range of reduced velocities from 2 to 100. ρ is of the order of 1 g cm^{-3} and η of the order of $1 \cdot 10^{-2}$ Poise. D_m is between $2 \cdot 10^{-5}$ and $5 \cdot 10^{-7}$ cm^2 s^{-1}. Thus, the Reynolds number is always smaller than 0.2 and is often more than ten times smaller than that. This is the range of *creeping flow*, in which Darcy law is certainly valid [8].

The assumptions made by Saffman are that there is no adsorption of the compound, that the

medium is isotropic and its local average velocity or mean pressure gradient is constant. He considered a model of the column packing consisting of randomly oriented capillary tubes and made a rigorous random-walk treatment. A further approximation is that molecular diffusion is negligible compared to convective dispersion [23]. A more complex derivation, using a more sophisticated model, provided a solution in the case in which molecular diffusion is significant [24]. Since in chromatography the reduced velocity is always larger than 2 and often of the order of 10 or more, we can consider only the results of the first theoretical development

$$D_{ap,r} = \gamma D_m + 3 \bar{u} / (16 d_p) \quad (8)$$

Hence

$$h_r = 2 \gamma/\nu + 0.375 \quad (9)$$

Using a much simpler model, treating the dispersion in an anastomosed network of pores in the same way as molecular diffusion is handled in molecular kinetics, Littlewood [25] derived an equation similar to Eq. 8 for the apparent dispersion and obtained a value of less than 0.40 for the constant term in Eq. 9. His experimental data suggested a value close to 0.20 in gas chromatography.

Horne et al. [7] used the classical random-walk model of band broadening in chromatography developed by Giddings [4], and showed that the constant term in Eq. 9 should rather be between 0.10 and 0.15. Their model assumes the particles to be spherical. When a streamlet impinges on a particle, it divides equally around the sphere, causing the average molecule to undergo a transverse step with an average length of d_p/π [7]. If one lateral step is taken for every ω_3 d_p moved axially (where ω_3 is a number between 0 and 1), the radial variance, σ_r^2, according to the random-walk model is the product of the number of steps ($n = L / (\omega_3 d_p)$) and the square of the step length (d_p/π)

$$\sigma_r^2 = L(d_p/\pi)^2 / (\omega_3 d_p) = L d_p/(\omega_3 \pi^2) \quad (10)$$

Hence, the contribution, h_c

$$h_c = \sigma_r^2 / (L d_p) = 1 / (\pi^2 \omega_3) \quad (11)$$

It is reasonable to assume that, in a dense packing, one lateral move is made for every progression by one half to one particle diameter, corresponding to ω_3 is between 0.5 and 1. Hence a value of D intermediate between 0.1 and 0.2 [7]. It is obvious, however, that D will vary within this range depending on the packing density. This is probably sufficient to explain the scattering of experimental results found in the literature.

Determination of the apparent dispersion coefficients by NMR

In an homogeneous magnetic field, the spin of a nucleus precesses around the direction of the magnetic field, at the Larmor frequency, ν, given by

$$\nu = \underline{\gamma} B_0 \quad (12)$$

where $\underline{\gamma}$ is the gyromagnetic ratio of the nucleus and B_0 is the intensity of the magnetic field. At equilibrium, the total magnetization of the sample is a vector aligned parallel to the direction of the constant magnetic field. In this case, however, the precession of the individual spins remains invisible on a macroscopic scale. All the difficulty in NMR is to produce a non-equilibrium state in which the spin precession is detectable. The application of a 90° RF pulse turns the total magnetization vector into the plane perpendicular to the direction of the main magnetic field. Only this radial component of the magnetization is detectable in NMR. The flexibility of the NMR methods result from the wide variety of the possible approaches to detect this component. The pulsed field gradient spin echo (PGSE) technique [17,18] is a combination of a spin echo sequence (90°–τ–180°–τ–echo), which minimizes the effects of the inhomogeneities of the magnetic field, and of two short field gradient pulses with a time interval Δ for the determination of the dispersion coefficients (Fig. 1). The 180° refocussing RF pulse is applied between the two field gradient pulses.

Since the Larmor frequency is proportional to the intensity of the magnetic field, the superimposition of a magnetic field gradient on a

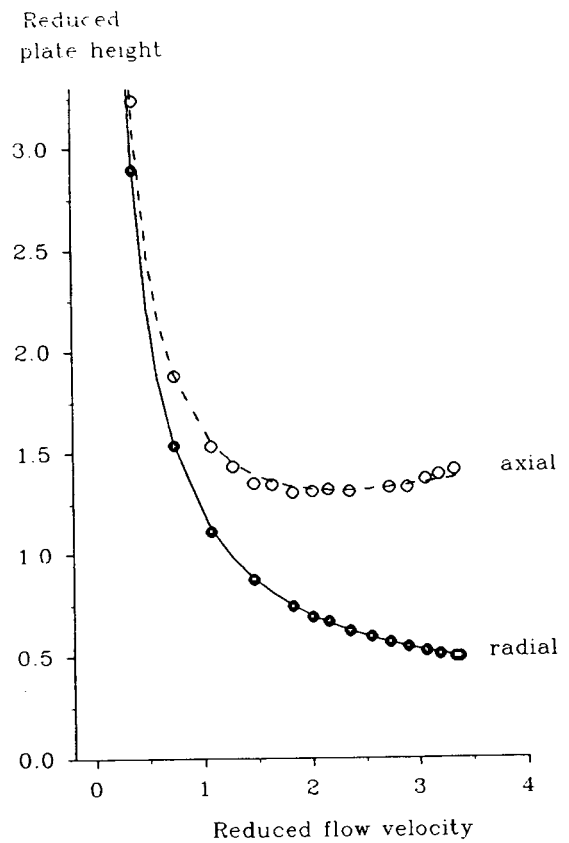

Fig. 1. Reduced axial (○) and radial (●) plate heights as a function of the mobile phase velocity. Column: 15 × 2.6 cm, packed with 15-μm LiChrospher C18 silica. Mobile phase: water. Self-diffusion coefficient of water in the bulk, $2.2 \cdot 10^{-9}$ m^2 s^{-1}.

constant magnetic field causes protons at different locations to precess at different frequencies. Hence, a short gradient pulse (with a duration, δ, of the order of 10 ms) causes a phase shift which depends on the position of the nucleus. A distribution of the phase shifts within the sample causes a decrease in the signal intensity. The 180° pulse inverts the phase shifts. If the nuclei do not change their positions in the time interval Δ (150 ms), an identical gradient pulse eliminates the phase shift caused by the first gradient pulse. Then, the magnetization would reach the same value as it does when there are no magnetic field gradient pulses. Any movement of the nuclei between the beginning of the first and the end of the second gradient pulse causes the refocussing to be incorrect. In this case, there is a loss of the amount of magnetization measured. This loss depends on the amplitude of the field gradient, g, and on the dispersion coefficient. It is given by the Stejskal–Tanner equation [17]

$$\ln A/A_0 = -\underline{\gamma}^2 D_{ap} g^2 \delta^2 (\Delta - \delta/3) \quad (13)$$

where A is the signal intensity measured, A_0 is the unattenuated signal intensity (in the absence of field gradient pulses), g is the intensity of the field gradient, and D_{ap} is the apparent dispersion coefficient.

The use of strong field gradient pulses renders negligible the influence of the inherent magnetic gradients. The influence of the relaxation effects is made negligible by keeping constant the pulse duration (δ) and pulse intervals (Δ), while changing the field gradient strength (g). Because the field gradient pulses can be sent in any direction inside the magnet of the NMR instrument, it is possible to measure the apparent dispersion coefficient in any direction, for example in the direction of the mobile phase stream (i.e., axial) or in the perpendicular direction (i.e., radial). Because of limitations due to the signal/noise ratio and the time available for the experiment, the cross-sectional average transverse dispersion coefficient in the only one transverse direction was measured. The column efficiency was high ($h_a \approx 2$) in these experiments, so the apparent transverse and radial dispersion coefficients are equal or at least very close.

3. Experimental

3.1. NMR measurements

The experiments were carried out in the head coil of a 1.5 Tesla whole-body tomograph (Magnetom, Siemens, Erlangen, Germany). We used a spin echo sequence with slice selective excitation RF pulses and a read out gradient at data acquisition. This combination allows the selection of a small slice of the column, perpendicular to its main axis and the acquisition, with the read

out gradient, of the profile of the signal originating from this slice, with spatial resolution in one direction. Thus, the results of the measurements can be related to a well-defined region of the column. Because the gradient pulses induce (magnetic) eddy currents, there was a small space shift in the detected signal. To eliminate this effect, we used only the integrated signal of the profile. Measurements were made at 128 different amplitudes of the field gradient pulses, between 0.2 and 9.7 mT/m. The results were plotted as $\ln (A/A_0)$ against g^2. A straight line was obtained, showing that the influence of the background gradients in our experiments is negligible. The apparent dispersion coefficient is calculated from the slope of this line.

Measurements of the self-dispersion coefficients of water in the chromatographic column measured in the absence of flow gave values of 1.23 and $1.15 \cdot 10^{-9}$ m^2/s for the axial and radial coefficients, respectively. For pure water in an otherwise empty column, the values observed were 2.33 and $2.16 \cdot 10^{-9}$ m^2/s, respectively, while the value generally accepted is $2.4 \cdot 10^{-9}$ m^2/s at room temperature. In still water, the apparent dispersion coefficients should obviously be the same in all directions. Thus, there is an inaccuracy of 5 to 7% in the measurements. It is important to note that, for $\nu = 0$, the ratio D_{ap}/D_m should be equal to $B/2$ (combination of Eqs. 3 and 6a or 5 and 6b). The value obtained is 0.53, in excellent agreement with the value 0.50 derived from the whole set of experimental data (see later).

3.2. Chromatographic system

NMR cannot be carried out on systems incorporating any magnetic metal. Accordingly, the columns used must be made of plastic, glass or silica. We used a silica tube (Merck, Darmstadt, Germany). Accordingly, the inlet pressure is limited to low values, and in spite of the rather large particle size, only values of the reduced velocity below 4 were attainable. The column was packed with 15-μm particles of C18 bonded silica. The column was packed by letting a 30% slurry sediment for three days. This is a marked deviation from conventional packing procedures. The column exhibited an excellent efficiency. The minimum value of h for toluene and ethylbenzene in acetonitrile–water (80:20) was close to 2). Its packing density was probably lower than usual, which may have affected its long-term stability, but this was never studied. The mobile phase is pure water. A non-magnetic high pressure pump was used. The flow rate was measured manually. The signal recorded corresponds to protons of water, thus giving the self-dispersion coefficient of water. The experiments were conducted at room temperature.

The reduced velocity, ν, is derived from the measured flow rate using the classical relationship $\nu = u\, d_p/D_m = (4\, F\, d_p) / (\epsilon_T\, \pi\, d_c^2\, D_m)$, with $d_p = 15$ μm, $D_m = 2.4 \cdot 10^{-9}$ m^2/s, F_v, the measured flow rate, ϵ_T, the total porosity of the stationary phase (0.75), and d_c, the column diameter (26 mm). The reduced plate height is derived from the apparent dispersion coefficient using Eq. 6.

4. Results and discussion

Knox et al. [6] derived the values of the apparent axial and radial dispersion coefficients of *p*-nitrophenol in 0.1 *M* aqueous KCl solution, using a 77.5×1.15 cm column packed with 64-μm glass beads. Eon [8] determined the apparent axial and radial dispersion coefficients of the same compound in the same eluent, using 60×1.58 cm columns packed with 76-μm glass beads. In both cases, the axial and radial dispersion coefficients are measured by recording the passage of the zone using a dual polarographic detector 6 with two 0.2 mm diameter microelectrodes. The electrodes can be moved to measure the concentration at any radial position. Injections of very small volumes of sample solution are made with a syringe needle, allowing the introduction into the column of small initial bands and permitting the easy determination of both radial and axial dispersion. Alternately reversing the direction of the flow several times permits a study of the progressive broadening of

the bands in the radial direction [8]. This procedure permitted the determination of the dependence of the axial and radial dispersion on the reduced mobile phase velocity for values of ν between 16 and 250 [6] or 0.6 and 1000 [8]. The axial and radial reduced plate heights were found to be given by the following equations for the data by Knox et al. (KLR) [6] and by Eon [8]

$$h_a(\text{KLR}) = 1.4/\nu + 0.73\ \nu^{0.20} \quad (14a)$$

$$h_r(\text{KLR}) = 1.4/\nu + 0.060 \quad (14b)$$

$$h_a(\text{EON}) = 1.5/\nu + 0.64\ \nu^{0.21} \quad (14c)$$

$$h_r(\text{EON}) = 1.5/\nu + 0.075 \quad (14d)$$

There is an excellent agreement between these two sets of data. As concluded by Knox et al. [6], the axial dispersion coefficient is nearly ten times larger than the radial dispersion coefficient for values of the reduced velocity around 12, a value typical of the conditions used in liquid chromatography, while these coefficients are close for values of the reduced velocities around 1, which are prevalent in thin-layer chromatography. This explains why spots obtained in TLC tend to be circular, while LC bands are more elongated.

Measurements of the apparent self-dispersion coefficients of water were carried out by NMR, on porous silica, using the experimental set-up described earlier in this paper and the procedure whose theory has been explained. The range of reduced velocities explored is much narrower, between 0.4 and 3.5, hardly one order of magnitude. This is due to the pressure limitations introduced by the use of a silica column. The results are reported in Fig. 2. The apparent axial and transverse (i.e., radial, see previous discussion) dispersion coefficients were found to follow the equations

$$h_a = 0.994/\nu + 0.406\ \nu^{0.2} + 0.204\ \nu \quad (15a)$$

$$h_r = 0.994/\nu + 0.201 \quad (15b)$$

where h_t is the reduced transverse dispersion coefficient. We have adopted the same value of n as found by Knox et al. [6] and Eon [8]. The range of values of reduced velocities explored in our work is too narrow to attempt an accurate determination of the exponent, n, of the eddy diffusion term by introducing an additional degree of freedom when fitting the experimental data to Eq. 3. This limitation results also in part from the need to introduce a mass transfer resistance term, $C\,\nu$ in Eq. 3 (see below). Accordingly, there are two degrees of freedom in Eq. 3, A and C, the same number as in the problem solved by Knox et al. (A and n). It is legitimate to assume that the first term or axial diffusion term of this equation is the same in Eq. 15b as in Eq. 15a, given the data obtained at low values of the reduced velocity. However, the introduction of another degree of freedom in Eq. 3 would not permit an accurate determination of n. For this purpose, the acquisition of data in a

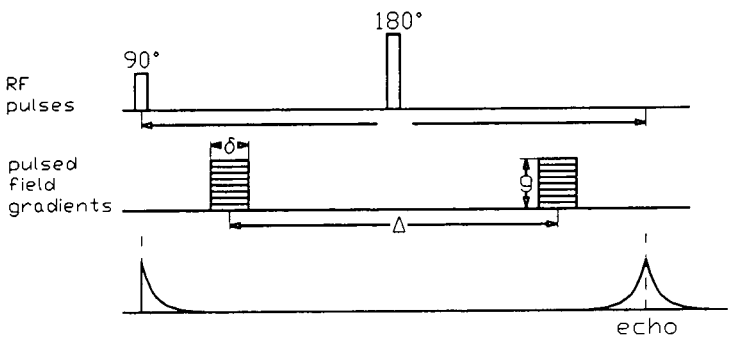

Fig. 2. Events in the PGSE technique. Top, timing of the RF pulses. Middle, timing of the field gradient pulses. Bottom, signal measured.

much wider range of values of ν would be necessary.

The three sets of experimental results, those by Knox et al. [6], by Eon [8], and ours, are qualitatively extremely similar. Quantitatively, the values of h_f observed are very close to those reported by these authors [6,8], although the numerical values of the constants B and D are different. The major differences between our results and those previously published are (i) our much smaller value of the tortuosity factor, 0.50 versus a more typical 0.75; (ii) our larger value of the coefficient D, arising from stream splitting; and (iii) the presence of a third term in the equation we used for the axial plate height (Eq. 15a). These three points are discussed in the next paragraphs. We note here, however, that these differences might be explained in a large part (j) by the narrow range of values of the mobile phase velocity explored (with a wider range of ν, there might have been better agreement); and (jj) by the difference in the quantity actually measured, the average radial apparent dispersion coefficient, by Knox et al. and Eon, or the average transverse apparent dispersion coefficient, by us. Although the column is highly efficient, some small differences between these two dispersion coefficients are possible.

There is no good explanation for the difference between the values of the B coefficient obtained by Knox et al. [6] and by Eon [8], and the one found in this work. There are few papers in the literature reporting systematic measurements of the coefficient B, as explained above. The general agreement that the tortuosity coefficient, γ, should be close to 0.75 is based on the opinion of Knox [6,7,13,22], itself based mostly on the experimental data reported in his earlier experimental work in gas chromatography [26]. Although there are no reasons to doubt that, in most cases of practical importance in chromatography, B should be of the order of 1.4 to 1.8, it is still unclear whether lower values, of the order of 1, are possible under some particular conditions. Nevertheless, this value is consistent with the ratio of the self-dispersion and self-diffusion coefficients of water measured in still water (flow rate = 0).

The theoretical work of Littlewood [25] concluded that the value of D should be less than 0.40. His experimental results, obtained in gas chromatography, concluded that D was of the order of 0.20. Depending on the columns used, however, values between 0.13 and 0.24 were obtained, the larger values corresponding to the smaller particles. Similarly, Horne et al. [7] concluded that values between 0.10 and 0.20 are more probable than the high theoretical values of 0.375 [23] and 0.40 [25]. These conclusions are in excellent agreement with our experimental results. The fact that our value of D (0.201) is in the high range is probably related to the packing procedure used. Since the chromatographic column used for the NMR determinations was packed by mere sedimentation, its packing density is in the low range of experimentally possible values, suggesting that the largest reasonable value of ω_3 should apply.

Finally, we need to account for the resistance to mass transfer in the particles of packing. Knox et al. [6] and Eon [8] used solid core glass beads with which such a term would be 0 or negligible. In the case of porous silica particles, this is no longer true, even for a small molecule such as water.

5. Conclusion

The great advantage of NMR measurements in this type of studies is that it is possible to determine simultaneously the axial and transverse dispersion coefficients in several locations inside the column. It would be easy also to measure the degree of isotropy of the cross-sectional averaged apparent transverse dispersion coefficient. As a consequence, it is possible to carry out systematic determinations of these local values and to study the dependence of these dispersion coefficients or local plate heights on the position in the column. Systematic determination of local values of h_a and h_r could shed much needed light on the "wall effect" issue. It should also be possible to study the influence of the packing density on the values of

the different parameters of the plate height equation.

Measurements of dispersion coefficients by NMR are done on time and space scales that are orders of magnitude smaller than those on which conventional measurements are made. In chromatography, the space scale is the column length, the time scale is the band width. In NMR, the time scale is Δ. During that time, dispersion causes the molecules to move from their initial position by an average distance l, such that $l^2 = 2 D_{ap} \Delta$. Since $\Delta = 147$ ms and the values of D_{ap} are all larger than $1 \cdot 10^{-9}$ m^2 s^{-1}, and, only in a few cases, at high velocities, are less than four times as large, the average molecule disperses by more than 17 μm and, except in a few experiments, by less than 35 μm. During that time, convection causes the molecules to migrate downstream by between 11 μm ($\nu = 0.5$) and 75 μm ($\nu = 3.5$). Most of these dimensions are only slightly larger than the average size of the pores between the packing particles, which are estimated to be between 0.1 and 0.5 d_p [4–8]. Thus, our results describe the behaviour of the water molecules in a volume equivalent to that of several particles, hence account for the same phenomena as those obtained by conventional techniques. Therefore the two series of data are fully comparable. The use of shorter periods for the field gradient pulses would easily permit a reduction of the volume available to the molecules during the measurement to a small fraction of the average particle volume. If the packing is made of solid core beads, the values obtained for the dispersion coefficients should tend toward those in the bulk liquid when the pulse period decreases. If, however, the particles are porous, a weighted average between the effects of dispersion in the pores of the particles and dispersion in the bulk would be measured. Clearly, the study of the influence of the pulse period could supply new and useful data.

Acknowledgement

This work has been supported in part by Grant CHE-9201663 of the National Science Foundation and by the cooperative agreement between the University of Tennessee and the Oak Ridge National Laboratory. We thank the Alexander von Humboldt Stiftung (Bonn, Germany) for the Research Award received by G.G. E.B. thanks F. Eisenbeiss (Merck, Darmstadt, Germany) and S. Marmée (University of Mainz) for the gift of the column and the packing material.

References

[1] J.C. Giddings, *J. Gas Chromatogr.*, 1 (1) (1963) 12.
[2] R.B. Bird, W.E. Stewart and E.N. Lightfoot, *Transport Phenomena*, Wiley, New York, NY, 1960.
[3] T. Yun and G. Guiochon, *J. Chromatogr.*, 672 (1994).
[4] J.C. Giddings, *Dynamics of Chromatography*, M. Dekker, New York, NY, 1960.
[5] J.H. Knox and J. Parcher, *Anal. Chem.*, 41 (1969) 1599.
[6] J.H. Knox, G.R. Laird and P.A. Raven, *J. Chromatogr.*, 122 (1976) 129.
[7] D.S. Horne, J.H. Knox and L. McLaren, *Separat. Sci.*, 1 (1966) 531.
[8] C. Eon, *J. Chromatogr.*, 149 (1978) 29.
[9] J.E. Baur, E.W. Kristensen and R.M. Wightman, *Anal. Chem.*, 60 (1988) 2338.
[10] T. Farkas and G. Guiochon, *J. Chromatogr.*, (1994) in Press.
[11] R.A. Bernard and R.H. Wilhelm, *Chem. Eng. Progr.*, 46 (1950) 233.
[12] C.E. Schwartz and J.M. Smith, *Ind. Eng. Chem.*, 45 (1953) 1209.
[13] J. Knox, *Anal. Chem.*, 38 (1966) 253.
[14] A. Felinger and G. Guiochon, *AIChE J.*, 40 (1994).
[15] G. Guiochon, S. Golshan-Shirazi and A.M. Katti, *Fundamentals of Preparative and Nonlinear Chromatography*, Academic Press, Boston, MA, 1994.
[16] M. Ilg, B. Pfleiderer, K. Albert, W. Rapp and E. Bayer, *Macromolecules*, 27 (1994) 2778.
[17] E. O. Stejskal and J.E. Tanner, *J. Phys. Chem.*, 42 (1965) 288.
[18] P. Stilbs, *Prog. NMR Spectrosc.*, 19 (1987) 1.
[19] S. Gibbs, E.N. Lightfoot and T.W. Root, *J. Phys. Chem.*, 96 (1992) 7458.
[20] Y. Xia and P.T. Callaghan, *Macromolecules*, 24 (1991) 4777.
[21] P.T. Callaghan, *Principles of Nuclear Magnetic Resonance Microscopy*, Oxford University Press, Oxford, 1991.
[22] J.H. Knox, *J. Chromatogr. Sci.*, 15 (1977) 352.
[23] P.G. Saffman, *J. Fluid Mech.*, 6 (1959) 321.
[24] P.G. Saffman, *J. Fluid Mech.*, 7 (1960) 194.
[25] A.B. Littlewood, *Anal. Chem.*, 38 (1966) 2.
[26] J.H. Knox and L. McLaren, *Anal. Chem.*, 36 (1964).

ELSEVIER

Journal of Chromatography A, 694 (1995) 333–345

JOURNAL OF CHROMATOGRAPHY A

Synthesis and characterization of unsaturated bonded phases for high-performance liquid chromatography

Jutta Schmid, Klaus Albert, Ernst Bayer*

Institut für Organische Chemie der Universität Tübingen, Auf der Morgenstelle 18, D-72076 Tübingen, Germany

First received 7 September 1994; revised manuscript received 4 November 1994; accepted 8 November 1994

Abstract

New reversed-phase materials containing unsaturated fatty acids on a silica support were prepared by a two-stage modification of LiChrospher silica and characterized by chromatographic and NMR spectroscopic techniques.

Chromatographic properties of the chemically modified silica were evaluated by separation of two test mixtures, one containing three basic drugs, the other being a homologous series of four *p*-hydroxybenzoic acid esters. The dynamic behaviour of the bonded alkenyl chains was studied by means of NMR relaxation time measurements in the solid and suspended state and correlated with chromatographic properties.

Spectroscopic and chromatographic results were compared to data of the corresponding saturated phases: the unsaturated packings showed higher overall mobility together with better separation characteristics. This is ascribed to different degrees of order in unsaturated and saturated phases and to specific interactions of the double bonds.

1. Introduction

Conventional reversed phases for HPLC are bonded saturated alkyl chains of various length. The interaction between phase and analyte is in general predominantly of hydrophobic nature. Analogue bonding forces in principle occur in biological membranes where molecular self organization of the phospholipid bilayer and of enzymes and receptors in the membrane is also due to Van der Waals interactions [1]. In natural membranes, phospholipids containing unsaturated fatty acid moieties also do occur in addition to those composed exclusively of saturated fatty acyl chains. Although little is known about the influence of such unsaturated lipids upon the mechanisms of self organization of membranes, one can assume certain specific interactions. It was our goal to study the properties and chromatographic behaviour of bonded phases containing alkenyl chains, in expectation that they might show a novel type of selectivity for analytes and that these results could shed insight into the question of why nature has created lipid molecules with unsaturated as well as saturated fatty acids.

A correlation of chromatographic properties and mobility as determined by solid- and suspended-state NMR spectroscopic relaxation time measurements should also reveal relations between structure and chromatographic efficacy of the synthesized packings. For the synthesis of such new reversed-phase materials, in a first reaction step (I) the silica was modified with a functionalized γ-aminopropylsilane (mono- or trifunctional) [2], the reaction creating siloxane

* Corresponding author.

0021-9673/95/$09.50
SSDI 0021-9673(94)01097-8

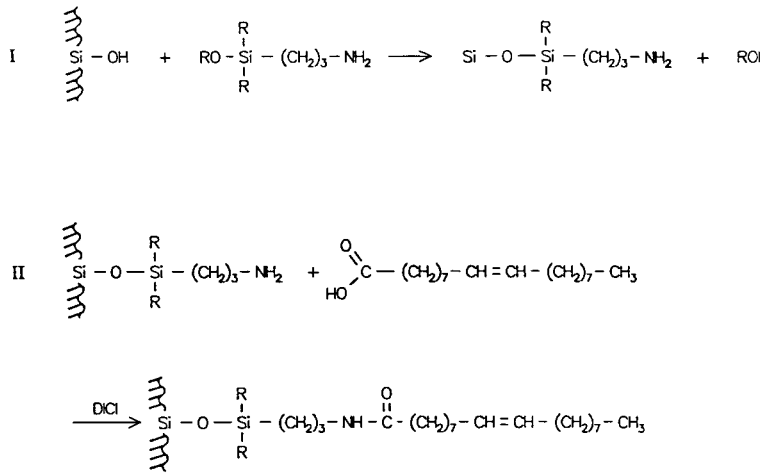

Fig. 1. Synthesis of the unsaturated packings. (I) Silanization of the silica. (II) Carbodiiminide (DICI) coupling with an unsaturated fatty acid.

bonds between the silane and the silica support (Fig. 1, I).

Whereas the reaction of silica with a monofunctional silane results in a well defined monolayer on the silica surface, reaction with a trifunctional silane leads to a more complex surface chemistry [3]. The various possibilities of crosslinking and polymerization as well as the effects of various silane functionalities on the chromatographic properties of the resulting packings have been discussed by Dorsey and Dill [4] and Pfleiderer et al. [5]. In this connection, Dorsey and Dill conclude that partitioning, rather than adsorption, is a dominant mechanism of chromatographic retention. Partitioning, again, depends on chain ordering and, thus, partly on the functionality of the bonded silane, as polymeric phases are more ordered than the corresponding monomeric ones [6,7]. Thus, a distinction between monofunctional and trifunctional packings is also important when discussing mobility and ordering effects.

In a second step (II), the γ-aminopropylsilane-modified silica was treated with an unsaturated fatty acid (oleic acid or elaidic acid) by carbodiimide coupling [8,9] with addition of N-hydroxybenzotriazole, resulting in an amide bond (Fig. 1, II). The saturated analogues were obtained by reaction of the aminopropylsilane-modified silica with stearoyl chloride.

According to elemental analysis, this second reaction step proceeds only to the extent of about 50%. Thus, the resulting packings are "mixed phases" containing both fatty acid amide and free amino groups which might have special characteristics for HPLC separations.

In order to investigate analogies between the synthesized packings and biomembranes the interaction with cholesterol was chosen. Cholesterol decreases the fluidity of biomembranes [10]. Therefore we added cholesterol to the synthesized packings and checked by NMR spectroscopic relaxation time measurements whether it incorporates between the alkyl chains and decreases the mobility of the bonded fatty acyl chains as it does in biomembranes.

2. Experimental

2.1. Materials

LiChrospher silica (batch 5025, particle diameter 5 μm, average pore diameter 60 Å, specific surface area 570 m^2/g) was kindly donated by Merck (Darmstadt, Germany). Dimethyl-

methoxy-γ-aminopropylsilane and triethoxy-γ-aminopropylsilane were obtained from Bayer (Leverkusen, Germany) and Fluka (Neu-Ulm, Germany), respectively, and used without further purification. Diisopropylcarbodiimide (DICI), oleic acid and elaidic acid were obtained from Aldrich (Steinheim, Germany). Morpholine was obtained from Riedel de Haën (Seelze, Germany). N-Hydroxybenzotriazole (HOBT) was prepared by reaction of *o*-chloronitrobenzene and hydrazine hydrate [11]. Stearoyl chloride was prepared by reaction of stearic acid with $SOCl_2$.

Acetonitrile for HPLC was of LiChrosolv grade (Merck), deuterated solvents for NMR spectroscopy were of Uvasol grade (Merck). Test solutes for HPLC were obtained from Merck, Aldrich and Hoffmann-La Roche.

2.2. Solid-state and suspended-state NMR measurements

NMR spectra in solution and in the suspended state were measured in 5-mm sample tubes on a Bruker AC 250 NMR spectrometer. Modified silica samples were suspended in perdeuterated acetonitrile. Solid-state ^{29}Si and ^{13}C magic-angle spinning (MAS) spectra were obtained on a Bruker MSL 200 NMR spectrometer at 4.7 T. Quantities of 200-300 mg of modified silica gel were packed into double bearing rotors of ZrO_2 which were spun at 3.6 kHz by dry air gas drive.

Solid-state NMR experiments were performed by combination of MAS [12], cross polarization (CP) [13] and high-power decoupling [14] in order to obtain high-resolution spectra.

The Hartmann–Hahn condition for CP was calibrated with glycine or Q_8M_8, the trimethylsilyl ester of the octameric form of silicic acid, for ^{13}C and ^{29}Si NMR, respectively. Typically, ^{13}C CP-MAS spectra were recorded with a pulse length of 5 μs, contact times of 1 and 3 ms for monofunctionally and trifunctionally modified packings, respectively, and a repetition time of 2 s. Chemical shifts were externally referenced to liquid tetramethylsilane.

The error limits of relaxation time values are in the order of approximately 5% as was revealed by repeated measurement of the same parameters.

2.3. Chromatography

HPLC separations were performed with an S 1110 HPLC pump (Sykam, Germany), a UV 655 A variable-wavelength detector (Hitachi) and a C-R6A Chromatopac integrator (Sykam).

The modified silica were packed into 60 × 4.6 mm tubes (Bischoff, Leonberg, Germany) by a high-pressure slurry-packing procedure on a Shandon packing pump (Shandon, Frankfurt, Germany).

Chromatographic conditions

Mobile phases: 156 ml acetonitrile + 340 ml phosphate buffer, pH 2.3 (6.66 g of KH_2PO_4 + 4.8 g of 85% H_3PO_4 in 1 l of water for HPLC) for separation of the basic drugs and acetonitrile–water (45:55) for separation of *p*-hydroxybenzoic acid esters; UV detection wavelength: 220 nm for separation of the basic drugs and 254 nm for separation of *p*-hydroxybenzoic acid esters; flow: 0.5 and 0.9 ml/min for basic drugs and esters, respectively; temperature 25°C.

2.4. Procedures

Silanization of the silica

A small quantity of the silica (5 g) was dried under vacuum (10^{-2} Torr; 1 Torr = 133.322 Pa) at 180°C for 12 h. After cooling to 120°C, the flask was aerated, and 1 ml of the γ-aminopropylsilane per g silica was added without any addition of solvent. The flask was covered with a frit (G3) and the mixture held at 120°C for another 12 h. The product was filtered off, washed three times with 25 ml of toluene, methanol and *n*-hexane, respectively and finally air dried (for coverage densities obtained in this first reaction step see Table 1).

Reaction of the γ-aminopropylsilane-modified silica with unsaturated fatty acids

A 5-mmol amount of the unsaturated fatty acid and 6 mmol of HOBT were dissolved in 30 ml of dimethylformamide. After cooling the

Table 1
Characteristics of the synthesized packings

No. of packing	Type of silane	Fatty acid	Coverage				
			P_C(C-3)	P_N(C-3)	α_{C-3}	P_C(C-21)	α_{C-21}
1	M	Stearic acid	7.18	1.59	2.46	15.58	1.15
2	M	Oleic acid	7.18	1.59	2.46	18.66	1.51
3	M	Elaidic acid	7.18	1.59	2.46	19.30	1.60
4	T	Stearic acid	5.33	1.84	3.06	14.33	1.30
5	T	Oleic acid	5.33	1.84	3.06	19.10	1.98
6	T	Elaidic acid	5.33	1.84	3.06	20.51	2.19

Silanes: M = dimethylmethoxy-γ-aminopropylsilane (monofunctional); T = triethoxy-γ-aminopropylsilane (trifunctional). Carbon and nitrogen contents P_C(C-3) and P_N(C-3)/P_C(C-21) (%) and coverage densities $\alpha_{C-3}/\alpha_{C-21}$ (μmol/m^2) of the aminopropylsilane-modified silica and the C_{21} phases, respectively, are given.

solution to 0°C in an ice-bath 5.5 mmol DICI in 3 ml dichloromethane were slowly added. The ice-bath was then removed, the solution stirred for 15 min and a quantity of silica containing 5 mmol of NH_2 groups (2.9 g of the trifunctional or 3.6 g of the monofunctional γ-aminopropylsilane-silica) added. The reaction mixture was then stirred at room temperature for 12 h. The product was filtered off, washed three times with 30 ml of dimethylformamide, methanol and *n*-hexane, respectively and air dried.

Reaction of the γ-aminopropylsilane-modified silica with stearic acid

A 2-g amount of the γ-aminopropylsilane-modified silica was vacuum-dried (10^{-2} Torr) at 100°C for 8 h. After cooling down to 50–60°C, the flask was aerated and 2.6 ml stearoyl chloride and 2.6 ml morpholine were quickly added without any solvent.

The flask was covered with a frit (G3) and the reaction mixture stirred slowly at 100°C overnight. Finally the product was filtered off, washed three times with 30 ml of toluene, methanol and *n*-hexane, respectively and dried under air.

Coverage densities α_{C-3} of the γ-aminopropylsilane-modified silica were calculated according to [15] from carbon and nitrogen contents, as determined with a Model 1104 CHN analyzer (Carlo Erba, Milan, Italy). The degree of reaction of amino to amide groups in the second reaction step and thus the coverage density with the fatty acid moiety α_{C-21} was determined from the carbon content of the C_{21}-amide phase, relative to the theoretical calculated carbon content derived from the known α_{C-3} coverage density.

The specific surface area S_{BET} of LiChrospher was determined by nitrogen sorption using a Model 1800 Sorptomatic instrument (Carlo Erba).

Incorporation of cholesterol into C_{21}-amide phases

A 1-g amount of the C_{21}-amide phase was suspended in a mixture of 20 ml of methanol and 20 ml of water. A 0.5-g amount of cholesterol was added and the mixture stirred slowly overnight. The silica was then filtered off, washed three times with 5 ml of methanol and then air dried.

3. Results

Table 1 contains characteristic data of the synthesized packings. The use of trifunctional γ-aminopropylsilane results in slightly higher coverage densities α_{C-3} than the use of monofunctional silane, the partially cross-linked trifunctional species allowing a closer packing than the monofunctional silanes which contain relatively voluminous methyl groups.

Further on, comparing the coverage densities of oleic acid and elaidic acid packings, it seems that the *trans* double bond allows closer packing of the alkenyl chains than the *cis* double bond. This effect will be correlated with molecular modelling and NMR spectroscopic and chromatographic results.

Coverage densities of the saturated C_{21} phases are clearly lower than those of the unsaturated packings. At present it is unclear whether this is an effect of chain packing or of the different reaction modes (step II) for saturated and unsaturated packings.

3.1. NMR studies

The packings were characterized by ^{29}Si and ^{13}C solid-state CP-MAS-NMR spectra in order to verify that silanes and fatty acids were chemically bonded (Fig. 2).

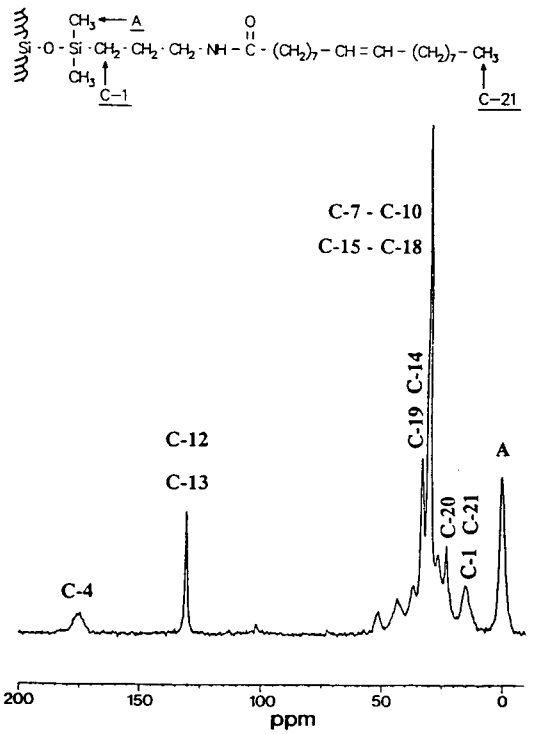

Fig. 2. ^{13}C CP-MAS-NMR spectrum of monofunctionally modified LiChrospher containing elaidic acid.

$T_{1\rho H}$-measurements

NMR relaxation time measurements permit the description of the dynamic behaviour of certain atoms in chemical systems.

$T_{1\rho H}$, the spin lattice relaxation time in the rotating frame, describes motions in the kHz range [16,17]. A systematic determination of $T_{1\rho H}$ values of the various packings according to a pulse sequence developed by Schaefer et al. [18] showed that there is an increase in $T_{1\rho H}$ values from the carbon anchored to the silica to the carbon of the terminal methyl group (Fig. 3a), as has been shown previously for conventional reversed phases [19,20]. Temperature-dependent measurements on comparable systems have shown that increased $T_{1\rho H}$ values indicate higher mobility of the respective carbon atoms [21]. While the increase in mobility towards the terminal methyl group occurs in both conventional and the new C_{21} packings, the absolute $T_{1\rho H}$ values are much lower in the case of our C_{21} packings (up to a factor of about 5), i.e. the aminopropyl spacer together with the planar amide group renders the whole system quite rigid.

The $T_{1\rho H}$ values and thus the mobility of the respective carbon atoms are higher for monofunctionally modified packings than for trifunctionally modified ones. This can be explained by the cross-linking of the trifunctional aminopropylsilane-modified species which renders the system more rigid.

In each of the two groups the packing containing oleic acid (unsaturated *cis*) shows the highest $T_{1\rho H}$ values, followed by the elaidic acid packing (unsaturated *trans*), whereas the corresponding saturated phase (monofunctionally modified) shows relatively low $T_{1\rho H}$ values. This indicates an increase in mobility of the fatty acid chains caused by the C = C double bond, the effect of a *cis* double bond being significantly stronger than that of a *trans* double bond.

The molecular organization of saturated stationary phase chains has been described by Dorsey and Dill [4]: chains which are aligned parallel one to another should be orientated normal to the silica surface resulting in a relatively ordered structure. Pfleiderer et al. [21]

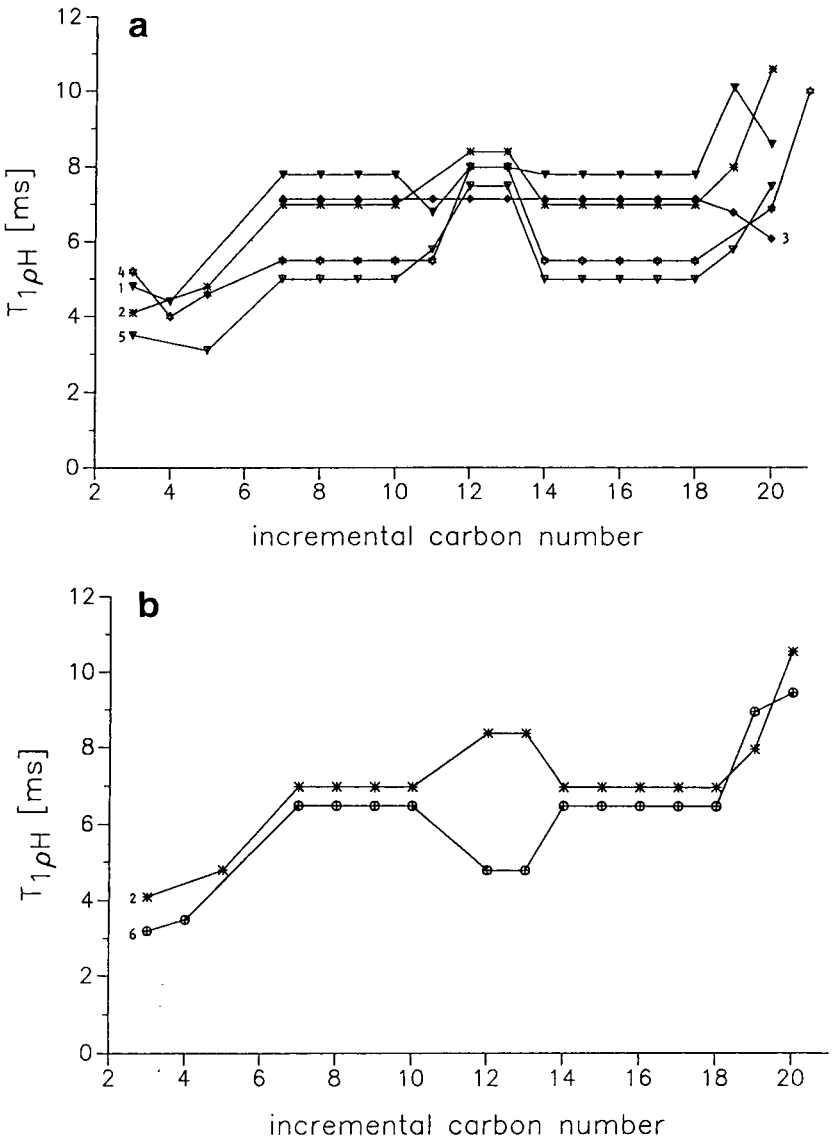

Fig. 3. (a) Dependence of the $T_{1\rho H}$-values on the carbon position within the alkenyl chain. 1 = Monofunctional oleic acid packing; 2 = monofunctional elaidic acid packing; 3 = monofunctional stearic acid packing; 4 = trifunctional oelic acid packing; 5 = trifunctional elaidic acid packing. $T_{1\rho H}$ values of the carbon atoms C_7–C_{10} and C_{14}–C_{18} are not resolved because in the NMR chemical shift range these carbon atoms all result in an overlaped peak at 29.7 ppm. (b) $T_{1\rho H}$ values of the monofunctionally modfied elaidic acid packing before and after addition of the cholesterol. 2 = Monofunctional elaidic acid packing; 6 = monofunctional elaidic acid packing + cholesterol

showed that the alkyl chains of common (saturated) C_{18} phases are indeed almost parallel one to another and much less mobile than the shorter chains e.g. of C_6 or C_8 phases.

An ideally parallel orientation of such alkyl chains is possible in the case of all-*trans* conformation of the carbon atoms only. A double bond always causes a kink in the chain preventing parallel orientation of the chains. The packing thus becomes less ordered and motional freedom increases. This effect is much stronger for *cis* double bonds than for *trans* double bonds.

This result corresponds to the slightly higher coverage densities of the oleic acid packings compared to the elaidic acid packings and has been supported by molecular mechanics calculations of these systems [22].

$T_{1\rho H}$ values decrease significantly after incorporation of cholesterol (Fig. 3b). This influence of cholesterol on relaxation times shows that the cholesterol is really incorporated between the fatty acyl chains of the RP packing and decreases mobility. The lower $T_{1\rho H}$ values are ascribed to lower mobility and thus correspond to the influence of cholesterol on the fluidity of biological membranes which are stabilized by cholesterol [10]. In this respect, the synthesized packings mimic biomembranes.

Contact time experiments

The results evaluated by $T_{1\rho H}$ measurements were verified by contact time experiments.

In these experiments the signal intensity is a function of the contact time. Depending on the carbon atom mobility various contact times are necessary to obtain maximum signal intensity in CP experiments: The higher the mobility, the longer is the contact time to obtain a maximum signal-to-noise ratio ($C_{p\,max}$) of comparable carbon atoms.

The results of the contact time experiments as presented in Fig. 4 clearly confirm the higher mobility of the unsaturated phases compared to the corresponding saturated ones.

^{13}C NMR T_1 measurements in the suspended state

In order to investigate the dynamic behaviour of the packings under actual HPLC conditions, mobility studies in the suspended state were performed. ^{13}C T_1 values can be obtained by inversion recovery experiments [180°–τ–90°–free induction decay (FID)]. Again, higher T_{1C} values can be correlated with higher mobility in the MHz range [23]. Fig. 5 shows a typical set of inversion recovery spectra obtained after various τ values. The dynamic behaviour of the packings in the suspended state is in accordance with solid-state mobilities (Fig. 6). This finding indicates that there is no principal difference between the solid and suspended state.

3.2. Chromatography

DMD test [24]

This test has been developed to determine chromatographic properties of RPLC bonded phases particularly for separation of basic substances. The three compounds of the test mixture are diphenhydramine hydrochloride, diazepam and 5-(*p*-methylphenyl)-5-phenylhydantoin (MPPH).

Daldrup and Kardel [24] described some criteria which a good RPLC column should fulfil with respect to the separation of these three substances:

(1) The elution order should always be diphenhydramine · HCl–MPPH–diazepam. This indeed was found for all our C_{21}-amide-bonded phases (Fig. 7a).

(2) Diphenhydramine is a basic drug which is extremely sensitive to the residual polarity especially that arising from free silanol groups. Ideally it should be eluted in a symmetrical peak without any tailing. Deviations from this situation however can be expressed by an asymmetry factor (which is calculated by a BASIC program on the C-R6A Chromatopac integrator) defined in the usual manner as $f_{as} = (B_{0.1}/A_{0.1})$ [25].

(3) Selectivity: the RRT value (relative retention time) of diazepam which is determined with MPPH as reference substance indicates the resolution; it depends on the degree of effective surface concentration of bonded alkyl phase.

(4) High numbers of theoretical plates/m: theoretical plate numbers (N/m) are calculated based on the retention and elution of MPPH which can be used as a referent substance, because different properties of the bonded phase (according to the variable manufacturing process) have a negligible effect on this component, using Gaussian peak form calculation.

The results obtained are given in Table 2.

The monofunctional as well as the trifunctional unsaturated phases allow very good separation of the basic drugs. Especially, the monofunction-

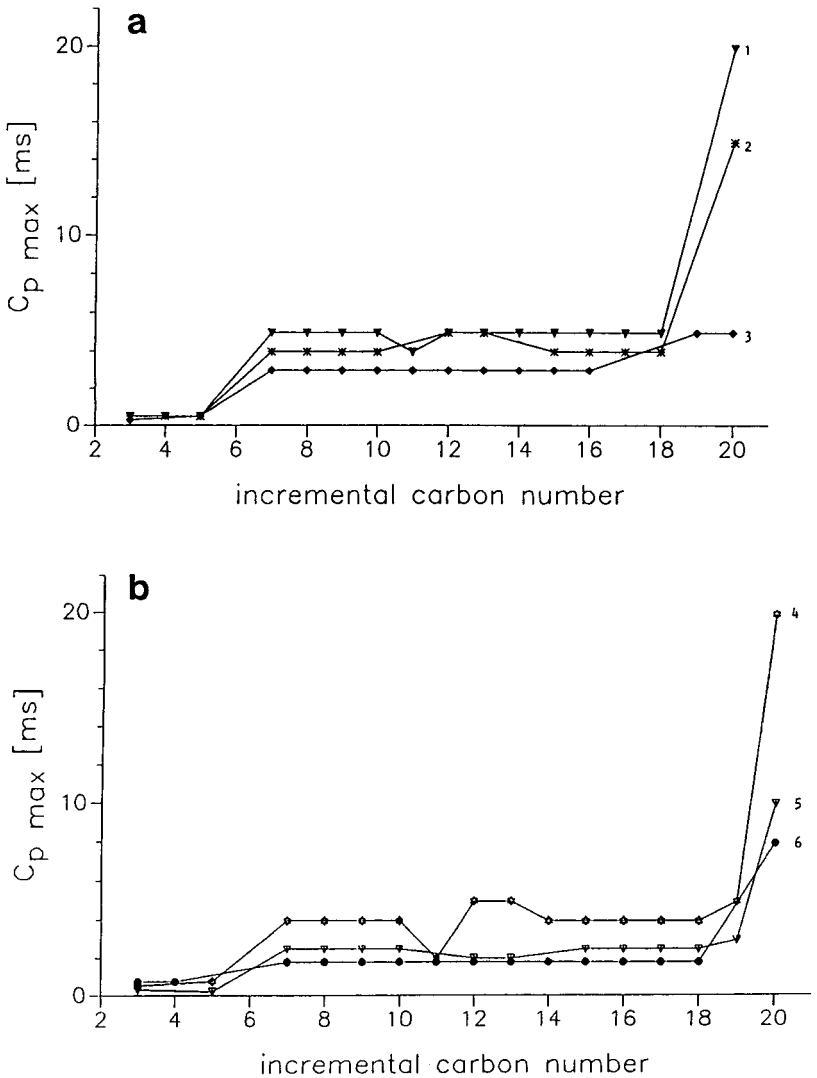

Fig. 4. (a) Contact times for maximum signal-to-noise ratio in dependence on the carbon position within the alkenyl chain of monofunctionally modified packings. 1 = Monofunctional oleic acid packing; 2 = monofunctional elaidic acid packing; 3 = monofunctional stearic acid packing. (b) Contact times for maximum signal-to-noise ratio in dependence on the carbon position witin the alkenyl chain of trifunctionally modified packings. 4 = Trifunctional oleic acid packing; 5 = trifunctional elaidic acid packing; 6 = trifunctional stearic acid packing.

al phases show very high numbers of theoretical plates (for MPPH) even on 60 × 4.6 mm columns, indicating a high quality of the packings. RRT values of all packings and thus the resolution obtained are comparable to commercially available packings [26].

The asymmetry factors for diphenhydramine varying from 1.3 to 2.0 (calculated as aforementioned) indicate a good screening of free silanol groups which results in a small residual polarity of the RP packings. The monofunctionally modified phases show slightly better

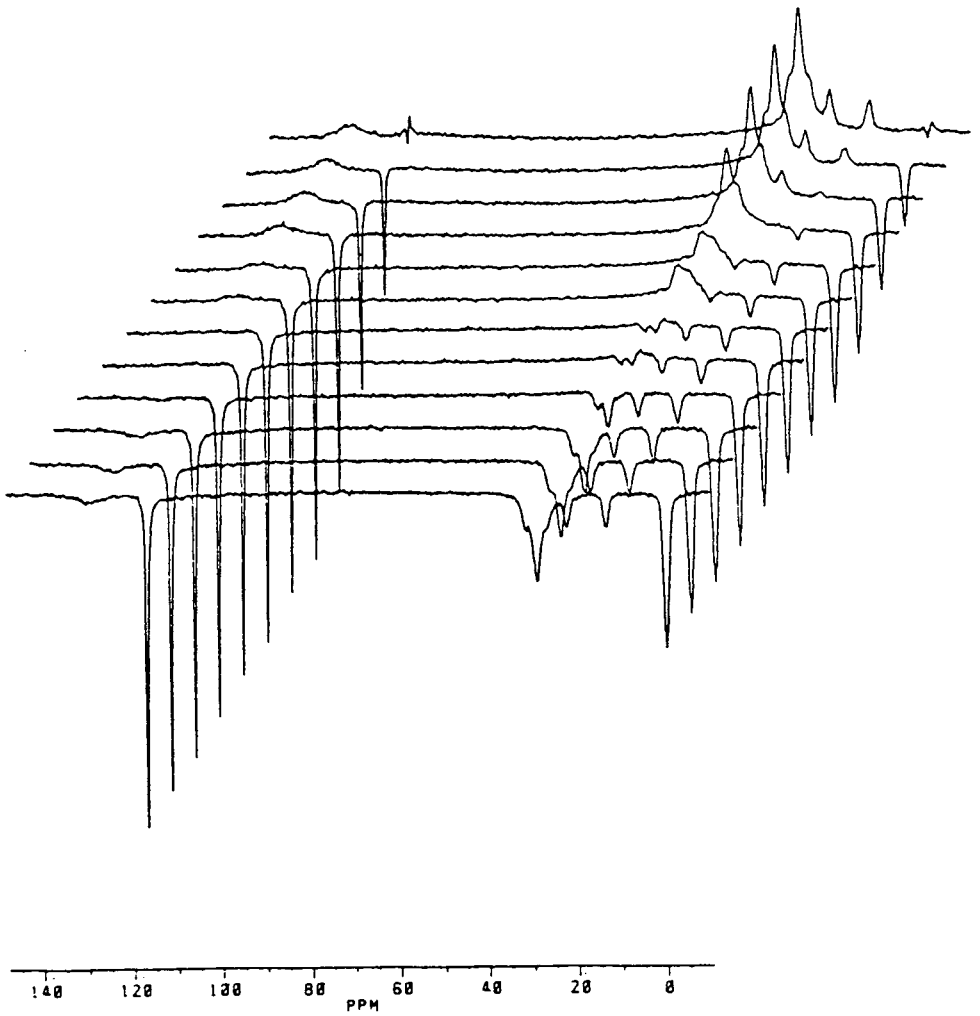

Fig. 5. Inversion recovery spectra of the monofunctional oleic acid packing obtained after different τ values varying from $\tau_{min} = 50$ ms (1st spectrum) to $\tau_{max} = 5$ s (12th spectrum).

asymmetry factors than the corresponding trifunctional phases.

Separation of alkylbenzenes

The homologous series of *p*-hydroxybenzoic acid esters (methyl, ethyl, propyl and butyl ester) was used as a second test mixture: Fig. 7b depicts the chromatogram of *p*-hydroxybenzoic acid esters eluted on the monofunctional modified C_{21}-oleic acid phase. Log k' values obtained on the monofunctional packings are shown in Fig. 8.

All packings showed excellent separation of the esters in very short time on 60×4.6 mm columns. Especially, the selectivity obtained on the unsaturated packings (*cis* and *trans*) is better than that obtained on the corresponding saturated packings.

The stability of the described phases was checked in a three years time period. No remarkable differences could be found in the

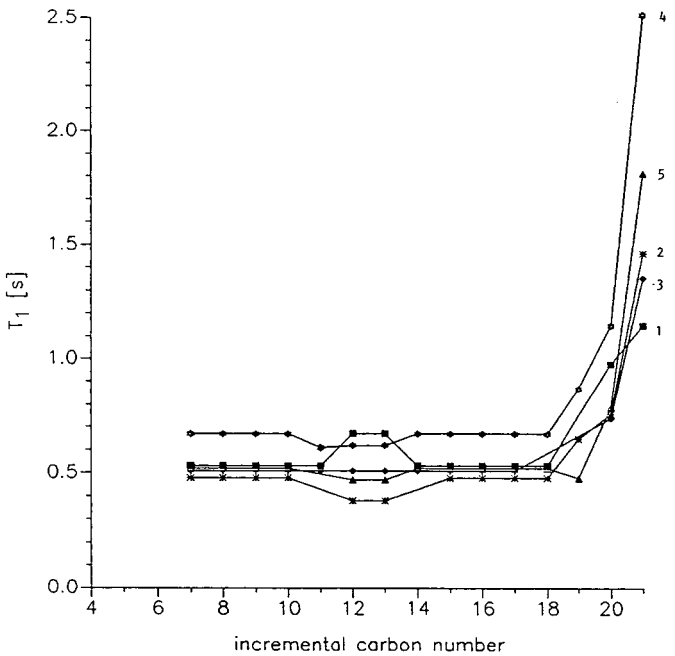

Fig. 6. Dependence of the T_{1C} values in the suspended state on the carbon position within the alkenyl chain. 1 = Monofunctional oleic acid packing; 2 = monofunctional elaidic acid packing; 3 = monofunctional stearic acid packing; 4 = trifunctional oleic acid packing; 5 = trifunctional elaidic acid packing.

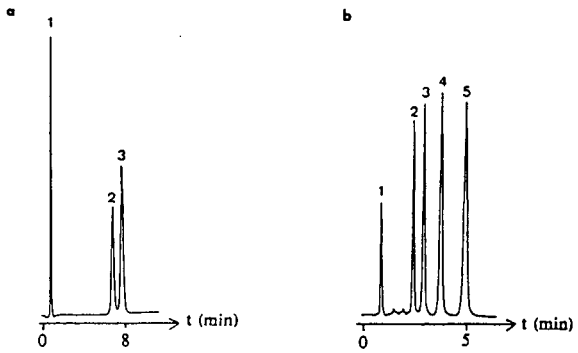

Fig. 7. Separation of two test mixtures on the monofunctional oleic acid packing. (a) 1 = Diphenhydramin hydrochloride, 2 = diazepam, 3 = 5-(*p*-methylphenyl)-5-phenylhydantoin (MPPH); mobile phase: 156 ml acetonitrile + 340 ml phosphate buffer, pH 2.3 (6.66 g of KH_2PO_4 + 4.8 g of 85% H_3PO_4 in 1 l of water for HPLC), flow-rate 0.5 ml/min; UV detection wavelength 254 nm; temperature 25°C. (b) *p*-Hydroxybenzoic acid esters: 1 = KNO_3, 2 = methyl ester, 3 = ethyl ester, 4 = propyl ester, 5 = butyl ester; mobile phase: acetonitrile–water (45:55), flow-rate 0.9 ml/min; UV detection wavelength 254 nm; temperature 25°C.

Table 2
Asymmetry factors f_{as} (diphenhydramine · HCl), RRT values (diazepam/MPPH) and theoretical plate numbers N/m (MPPH) obtained for separation of three basic drugs (diphenhydramine · HCl, diazepam, MPPH) on various packings

Packing	f_{as}	RRT value	N/m
Mono-*cis*	1.7	1.15	74 000
Mono-*trans*	1.8	1.15	69 000
Mono-saturated	1.3	1.06	44 000
Tri-*cis*	2.0	1.24	33 000
Tri-*trans*	1.9	1.19	30 000
Tri-saturated	1.6	1.24	24 000

chromatographic properties and in the solid-state NMR spectra between a newly prepared stationary phase and a stationary phase after three years of use [27].

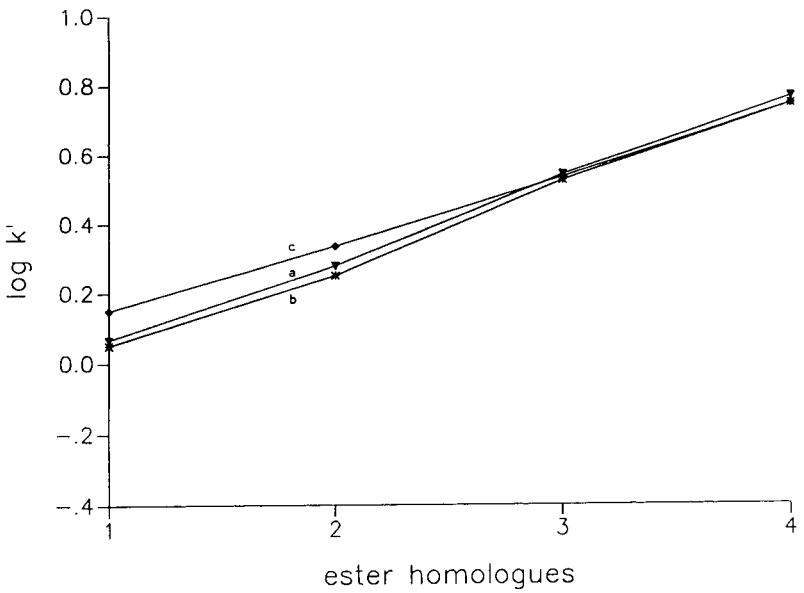

Fig. 8. Log k' values of *p*-hydroxybenzoic acid esters, obtained with acetonitrile–water mixture (45:55). 1 = Methyl ester; 2 = ethyl ester; 3 = propyl ester; 4 = butyl ester. a = Monofunctional oleic acid packing; b = monofunctional elaidic acid packing; c = monofunctional stearic acid packing. Flow-rate 0.9 ml/min, UV detection wavelength 254 nm, temperature 25°C.

4. Discussion

The newly designed packings containing unsaturated fatty acid amides show excellent chromatographic properties as demonstrated on the examples of basic drugs and of *p*-hydroxybenzoic acid esters. Especially, they show better selectivities both for separation of *p*-hydroxybenzoic acid esters and of the basic drugs as well as much higher numbers of theoretical plates than the corresponding saturated phases for both test mixtures.

NMR relaxation time measurements showed increased mobility of the unsaturated packings compared to the saturated ones. This effect proved to be stronger in the case of the naturally occurring *cis* double bonds than in the case of *trans* double bonds. Comparing HPLC and NMR results of oleic and elaidic acid packings with the results obtained on the corresponding saturated ones, it appear that higher mobility of the alkenyl chains grafted to the silica support results in improved HPLC properties of the RP phase for the separation of both basic drugs and *p*-hydroxybenzoic acid esters. This could be explained by a better adjustment of the equilibrium between stationary and mobile phase. The mobility of these phases is, however, lower than that of customary RP phases without aminopropylsilane spacer: $T_{1\rho H}$ values for C-4–C-15 of monofunctional RP-18 materials are in the order of 30 ms (e.g. 28.9 ms for monofunctional LiChrospher Si 100, 10 μm RP-18 material) [19]. This shows that increased mobility cannot be the only reason for the good chromatographic properties of these phases.

Another explanation for the excellent separations on unsaturated packings could be the ability of the double bond to undergo specific Van der Waals interactions with the solutes resulting in an improvement in separation.

We showed earlier [2] that also the saturated C_{21} packings containing amide bonds can be superior (in the sense of better resolution and/or

selectivity) to conventional C_{18} phases e.g. for the separation of basic substances. Therefore we assume a favourable influence of the amide bond and of the unreacted free amino groups on chromatographic properties. Specific interactions of these structural units are more probable the better accessible they are. As shown by the NMR studies, the unsaturated packings show higher mobility than the saturated analogues, which is considered to be an effect of the less ordered structure of the unsaturated materials [22,28]. Here, again, we can assume that a less ordered structure where the fatty acyl chains are not aligned parallel one to another, but having kinks and being somewhat bent around, significantly increases the accessibility of the amide group at least for smaller solute molecules like the described *p*-hydroxybenzoic acid esters and basic drugs.

In addition, such a less ordered structure does not only increase the accessibility of the amide group itself, but also of the whole hydrophobic surface of the fatty acyl chains and thus increases the mass transfer rate.

Comparing the separation characteristics for basic drugs on monofunctionally and trifunctionally modified packings we can assume that theoretical plate heights are much smaller in the case of monomeric packings although coverages are slightly higher for the trifunctional packings. As monomeric phases are less ordered than polymeric ones we suppose that this effect is also due to a higher mass transfer caused by the less ordered structure. This point, again, supports the idea that partitioning (which strongly depends on ordering) is a dominant mechanism of reversed-phase chromatography as proposed by Dorsey and Dill [4].

We can now summarize that incorporation of unsaturated fatty acids into RP packing materials results in higher mobility as compared to the saturated analogues, an effect we ascribe to a less ordered structure. The good chromatographic properties of these unsaturated packings are supposed to be partly due to this less ordered structure which leads to a better accessibility of the hydrophobic region and of the amide bonds. Specific hydrophobic interactions between the double bonds and solute molecules are supposed to improve chromatographic characteristics, too.

Looking at biological systems now, unsaturated fatty acids are known to increase fluidity of biomembranes. This effect as well as the decreased mobility after incorporation of cholesterol absolutely corresponds to our results obtained on the synthesized RP packings. Therefore, we can be sure that the synthesized packings can indeed be used as simple model systems for biological membranes.

We propose now that, together with the increase of mobility itself, ordering and conformation effects as found for the chromatographic packings could play a certain role in biomembranes, too, for example for the build-up of a suitable surrounding for ion channels or peptide binding sites. Additionally, specific hydrophobic interactions of the double bonds probably also have an influence upon self organization of biological membranes.

It is remarkable that *trans* double bonds induce much less differences in mobility as compared to the saturated analogues than *cis* double bonds. This could be a reason why nature has selected the more effective stereochemistry of *cis* double bonds for influencing membrane fluidity.

The transfer of structural characteristics from biomembranes to chromatographic systems has thus resulted in a new class of unsaturated bonded phases with very good separation characteristics which, by correlation of chromatographic and NMR spectroscopic results, could be ascribed to certain structural and ordering features. Analogue influences of unsaturated fatty acids are proposed to be present in biological membranes, too.

References

[1] C. Pidgeon, *Chem. Eng.*, 66 (1988) 23.
[2] B. Buszewski, J. Schmid, K. Albert and E. Bayer, *J. Chromatogr.*, 552 (1991) 415.
[3] D.W. Sindorf and G.E. Maciel, *J. Am. Chem. Soc.*, 105 (1983) 3767.
[4] J.G. Dorsey and K.A. Dill, *Chem. Rev.*, 89 (1989) 331.
[5] B. Pfleiderer, K. Albert and E. Bayer, *J. Chromatogr.*, 506 (1990) 343.

[6] P. Shah, L.B. Rogers and J.C. Fetzer, *J. Chromatogr.*, 388 (1987) 411.
[7] S.A. Wise and L.C. Sander, *J. High Resolut. Chromatogr. Chromatogr. Commun.*, 8 (1985) 248.
[8] W. König and R. Geiger, *Chem. Ber.*, 103 (1970) 788.
[9] F. Weygand, W. Steglich, J. Bjarnson, R. Akhtar and N. Chytil, *Chem. Ber.*, 101 (1968) 3633.
[10] G. Karp, *Cell Biology*, McGraw-Hill, New York, 1979.
[11] E. Müller and G. Zimmermann, *J. Prakt. Chem.*, 11 (1925) 284.
[12] E.R. Andrew, *Prog. Nucl. Magn. Reson. Spectrosc.*, 8 (1971) 1.
[13] A. Pines, M.G. Gibby and J.S. Waugh, *J. Chem. Phys.*, 59 (1973) 569.
[14] J. Schaefer and E.O. Stejskal, *J. Am. Chem. Soc.*, 98 (1976) 1030.
[15] P. Staszczuk and B. Buszewski, *Chromatographia*, 25 (1988) 881.
[16] G.E. Maciel and D.W. Sindorf, *J. Am. Chem. Soc.*, 102 (1982) 7606.
[17] K. Albert and E. Bayer, *J. Chromatogr.*, 544 (1991) 345.
[18] J. Schaefer, E.O. Stejskal and R. Buchdahl, *Macromolecules*, 10 (1977) 384.
[19] K. Albert, B. Pfleiderer and E. Bayer, in D.E. Leyden and W.T. Collins (Editors), *Chemically Modified Surfaces*, Vol. 3, Gordon & Breach, New York, 1990, p. 233.
[20] D.W. Sindorf and G.E. Maciel, *J. Am. Chem. Soc.*, 105 (1983) 1848.
[21] B. Pfleiderer, K. Albert, K.D. Lork, K.K. Unger, H. Brückner and E. Bayer, *Angew. Chem., Int. Ed. Engl.*, 28 (1989) 327.
[22] J. Schmid, *Diploma Thesis*, University of Tübingen, Tübingen, 1989.
[23] K. Albert, B. Evers and E. Bayer, *J. Magn. Reson.*, 62 (1985) 428.
[24] T. Daldrup and B. Kardel, *Chromatographia*, 18 (1984) 81.
[25] J.P. Foley and J.G. Dorsey, *Anal. Chem.*, 55 (1983) 730.
[26] W. Jost, R. Gasteier, G. Schwinn and M. Tüylü, *GIT Fachz. Lab.*, 32 (1988) 357.
[27] J. Schmid, *Thesis*, University of Tübingen, Tübingen, 1993.
[28] K. Albert, J. Schmid, B. Pfleiderer and E. Bayer, in H.A. Mottola and J.R. Steinmetz (Editors), *Chemically Modified Surfaces*, Vol. 4, Elsevier, Amsterdam, 1992, p. 105.

ELSEVIER

Journal of Chromatography A, 694 (1995) 347–354

JOURNAL OF CHROMATOGRAPHY A

Computational studies on chiral discrimination mechanism of cellulose trisphenylcarbamate

Eiji Yashima, Makiko Yamada, Yuriko Kaida, Yoshio Okamoto*

Department of Applied Chemistry, School of Engineering, Nagoya University, Chikusa-ku, Nagoya 464-01, Japan

First received 19 July 1994; revised manuscript received 17 October 1994; accepted 24 October 1994

Abstract

The calculation of interaction energies between cellulose trisphenylcarbamate (CTPC) and enantiomers of (±)-*trans*-stilbene oxide (**1**) and (±)-*trans*-1,2-diphenylcyclopropane (**2**) was performed using QUANTA/CHARMm and MOLECULAR INTERACTION programs to gain an insight into the chiral recognition mechanism of phenylcarbamate derivatives of cellulose. The structure of CTPC was optimized with the CHARMm force field based on the proposed structure of CTPC by X-ray analysis. In chromatographic enantioseparation on CTPC, **1** was completely resolved ($\alpha = 1.46$) and the (*R*,*R*)-(+)-isomer eluted first followed by the (*S*,*S*)-(−)-isomer, but **2** was not resolved ($\alpha \approx 1$). The results of calculation of interaction energies between CTPC and the enantiomers **1** suggested that the most important adsorbing site of CTPC for **1** may be the NH protons of the carbamate moieties at the 3-position of glucose units, and the (*S*,*S*)-(−)-isomer of **1** may interact more closely than the (*R*,*R*)-(+)-isomer with CTPC. In contrast, there was little difference in the minimum interaction energies between the enantiomers **2**. These calculations agreed with the observed results for the chromatographic resolution on CTPC.

1. Introduction

Understanding chiral recognition at a molecular level is of great interest and importance in many fields of chemistry and biology. Chiral recognition plays an essential role in the field of enantioseparation. Chromatographic enantioseparation has become the most practical way of separating enantiomers, and many chiral stationary phases (CSPs) have been developed [1–4]. Recently, some approaches to the clarification of the chiral recognition mechanism on CSPs for gas and liquid chromatography have been attempted by means of NMR [5–10] and computational methods [8,11–17]. The CSPs that have been most intensively studied in this respect were cyclodextrin-based CSPs [8,9] and Pirkle's type CSPs [11–14]. Based on nuclear Overhauser effect studies, rational models of interactions between the CSPs and enantiomers have been proposed [6,7,10]. The interaction energies between the CSPs and enantiomers were calculated by quantum mechanical calculations [8,11–15,17], and chiral recognition mechanisms have been proposed on the basis of the above calculations and molecular dynamics simulations. Macromolecules such as proteins, polysaccharide derivatives and synthetic chiral polymers have also been used as polymeric CSPs to separate a wide range of racemates and many polymeric

* Corresponding author.

0021-9673/95/$09.50
SSDI 0021-9673(94)01039-0

CSPs are now commercially available [1–4]. However, the chiral recognition mechanism on the polymeric CSPs is still obscure, probably because the polymers usually have a number of different types of chiral binding sites and the determination of their exact structures may be laborious.

Phenylcarbamate derivatives of polysaccharides such as cellulose and amylose appear to be among the most useful polymeric CSPs. They can separate a broad range of enantiomers and give practically useful HPLC columns when they are coated on macroporous silica gel [3]. The chiral recognition mechanism at a molecular level on the polysaccharide-based CSPs is not obvious, although the most important adsorbing site for chiral recognition has been considered to be carbamate residues on the basis of the results of chromatographic enantioseparation. NMR spectroscopy is a useful tool for revealing the chiral recognition at a molecular level, as reported for small-molecule CSPs [5–10], but most of the phenylcarbamate derivatives of polysaccharides with a high chiral resolving power as CSPs are soluble only in polar solvents such as tetrahydrofuran, acetone and pyridine. In such polar solvents, the phenylcarbamate derivatives cannot show high chiral recognition for enantiomers because the solvents must interact strongly with the polar carbamate residues, which are the most important binding site for chiral recognition [18]. Recently, we found that cellulose tris(4-trimethylsilylphenylcarbamate) (CTSP), having a high chiral recognition ability as a CSP for HPLC, is soluble in chloroform, which, for the first time, allowed the chiral recognition mechanism of the phenylcarbamate derivatives to be studied by NMR [19]. In the ^{1}H NMR of (±)-*trans*-stilbene oxide (**1**), methine protons of the oxirane ring were enantiomerically discriminated to show a set of two peaks in the presence of CTSP in $CDCl_3$ [19]. The NMR study of competition experiments with acetone suggests that *trans*-stilbene oxide may be adsorbed on the NH proton of the carbamate residues of CTSP. These NMR studies also indicate that the most important adsorbing sites for effective chiral separation are the carbamate residues, which can interact with enantiomers mainly through hydrogen bonding.

In this paper, we report computational studies on the chiral discrimination mechanism of cellulose trisphenylcarbamate (CTPC). CTPC is the most suitable phenylcarbamate derivatives because its structure has been determined on the basis of X-ray analysis. CTPC shows a high chiral resolving ability as a CSP for HPLC [18]. As a racemate, *trans*-stilbene oxide (**1**) and *trans*-1,2-diphenylcyclopropane (**2**) were selected because **1** has an ether oxygen capable of hydrogen bonding and can be sufficiently separated by HPLC on CTPC, but **2** cannot be resolved on the same column (Fig. 1).

2. Experimental

2.1. Computational methods

Molecular modelling, molecular mechanics (MM) calculations and molecular dynamics (MD) simulations were performed with the

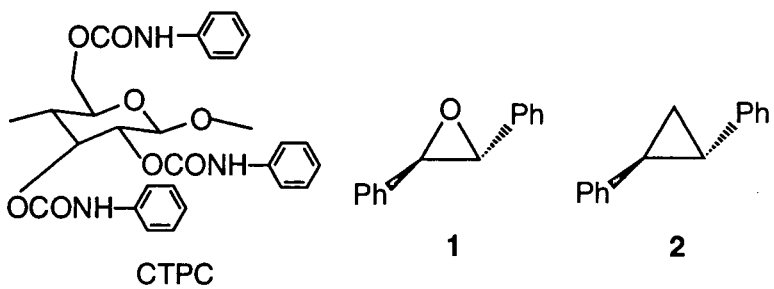

Fig. 1. Structures of CTPC, **1** and **2**.

CHARMm forcefield [20–22] (version 3.2) as implemented in a Polygen's QUANTA/CHARMm program [8,23–28] (Polygen, Waltham, MA, USA) running on a Stellar and a Personal Iris computer (Silicon Graphics). Bond lengths, bond angles, force constants and force field parameters employed in the present calculations were supplied by Polygen. The calculated total energy (E) is expressed in the form

$$E = E_{\text{bond length}} + E_{\text{bond angle}} + E_{\text{dihedral angle}} + E_{\text{improper torsion}} + E_{\text{electrostatic}} + E_{\text{Van der Waals}}$$

The polymer models and the enantiomers **1** and **2** were created by ChemNote in QUANTA. Energy minimizations were performed by steepest descents, followed by conjugate gradient and adopted-basis Newton Raphson minimization. Each step was continued until the value of the "energy value tolerance" became less than 0.001 kcal/mol and all minimizations were carried out using a non-bonded cut-off of 12.0 Å, with a switching window of 7.5–11.5 Å. All energies were given as a root mean square (rms) for a dielectric constant of 1.5. The MD simulation was implemented using Polygen's protocol; heating for 10 ps at 1000 K followed by equilibration for 10 ps with a step size of 0.001 ps.

2.2. Calculation of interaction energy between CTPC and enantiomers

The interaction energies (E') derived from Van der Waals force and electrostatics force between an atom i and an atom j can be calculated with the following equation:

$$E' = E_{\text{electrostatic}} + E_{\text{Van der Waals}}$$

where

$$E_{\text{electrostatic}} = \sum_{i,j>i} (q_i q_j)/(4\pi\varepsilon_0 r_{ij})$$

$$E_{\text{Van der Waals}} = \sum_{i,j>i} (A_{ij}/{r_{ij}}^{12} - B_{ij}/{r_{ij}}^{6})$$

q_i and q_j represent electric charge of atoms i and j, respectively, ε_0 is the effective dielectric constant and r_{ij} is the interatomic distance computed from the Cartesian coordinates. The two non-bonded parameters A_{ij} and B_{ij} are derived from the atom polarizabilities and the effective number of outer shell electrons. This calculation is performed for all combinations between the atoms of CTPC and enantiomers.

This energy was obtained by the MOLECULAR INTERACTION program supplied by Polygen. The calculation method using this program is described below. First, a centre of a cubic sampling box is placed on an atom i of CTPC. Here, the size of the cubic sampling box is specified as r. Then, the mesh size is specified as r', and an enantiomer is placed at the grid points and allowed to rotate from 0° to 360° along the x, y and z axes individually at angle (ω_x, ω_y, ω_z) intervals. The interaction energies are calculated for a given set of grid points and (ω_x, ω_y, ω_z).

3. Results and discussion

3.1. Coordinates of racemates and CTPC

The energy minimizations were carried out using the CHARMm force field developed by Brooks et al. [20], which has been widely utilized to construct molecular models of not only biopolymers such as nucleic acids [23,24], polypeptides [25] and synthetic polymers [26], but also small molecules such as cyclodextrin [8] and porphyrin derivatives [28]. The optimized structure of (*S*,*S*)-(−)-*trans*-stilbene oxide [(*S*,*S*)-(−)-**1**] obtained by the MM calculations is shown in Fig. 2. The final energies of both the enantiomers of **1** were 27.54 kcal/mol.

The optimization of CTPC was performed as follows. First, a full energy minimization of one unit of CTPC, containing CH_3O groups at the 1- and 4-positions of a glucose unit, was accomplished in the same way as that for (*S*,*S*)-(−)-**1**. Next, the optimized units were allowed to construct an octamer (8-mer) with a left-handed threefold (3/2) helix according to the structure of CTPC reported by Vogt and Zugenmaier [29] on the basis of X-ray analysis of a CTPC fibre. The dihedral angles defined by H1–C1–O–C4′

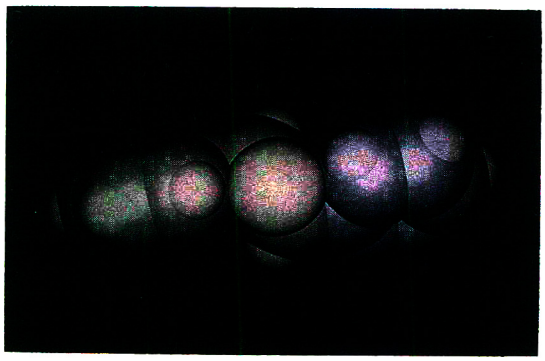

Fig. 2. Optimized structure of (*S*,*S*)-(−)-**1**.

(ϕ) and H4′–C4′–O–C1 (φ) were fixed to be 60° and 0°, respectively, as shown in Fig. 3.

Then, the eight units of CTPC as a starting structure was optimized by the steepest descents method. In the end of the minimization a metastable structure was obtained. The 8-mer has hydrogen bonds between the NH protons of the carbamate moieties at the 6-positions and the carbonyl oxygens at the 2-positions. The distance between the NH proton of the 6-position and the carbonyl oxygen at the 2-position is 2.634 Å. Then the minimization was further performed by using the conjugate gradient followed by the adopted-basis Newton Raphson methods.

The MD simulation was applied to the optimized 8-mer of CTPC. The structures with lower energies were extracted from the trajectory files obtained from the MD simulation and the MM calculations as described above were performed

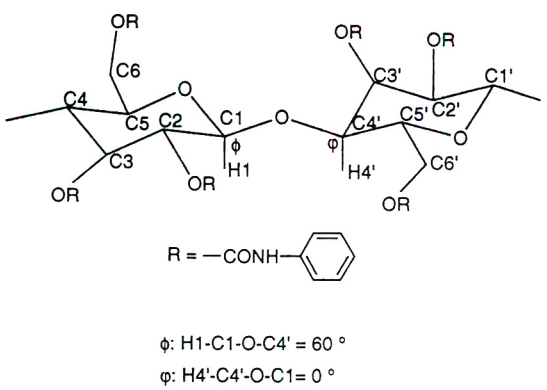

Fig. 3. The linkage of eight units of CTPC.

for these extracted structures again. However, significant changes were not observed before and after MD simulation. The resultant final, most stable, structure is shown in Fig. 4a and b together with the structure of CTPC reported by Vogt and Zugenmaier [29] on the basis of X-ray analysis (Fig. 4c). This structure is more stable than the metastable structure by 1.24 kcal/mol, and the distance between the NH proton and the carbonyl oxygen is 2.724 Å, which is longer than that of the metastable CTPC.

The structure of CTPC in Fig. 4b thus obtained in this study is similar to the structure in Fig. 4c; for example, the side-groups at the 2- and 3-positions and that at the 6-position of the neighbouring glucose unit are close to each other. However, some differences were observed between the calculated and the reported structures. The former is not exactly a 3/2 helix; the rotation angles around at each C1–C4 axis is in the range 110–113° depending on the number of the glucose unit (Table 1), and the conformation between the carbonyl carbon and the ether oxygen of the side-chain at the 2-position is *s-cis*. Further, those at the 3- and 6-positions are *s-trans*, whereas all the conformations of the reported ones are *s-trans*. The conformation of the starting 8-mer before minimization was *s-trans*. Therefore, the conformation at the 2-position was changed to *s-cis* from *s-trans* in the course of the minimization.

3.2. Calculation of interaction energy between CTPC and enantiomers

As mentioned earlier, the most important adsorbing site of CTPC for *trans*-stilbene oxide (**1**) may be the NH protons of the carbamate moieties (Fig. 5).

Therefore, the sampling boxes ($r = 6$, 5, 4 and 3 Å) were placed as centred by the NH proton, then the mesh size (r') was specified as 1 Å, and at each grid point (*R*,*R*)-(+)-**1** or (*S*,*S*)-(−)-**1** was rotated at 60° intervals for the x, y and z axes, individually. This means that $5^3 \times 6^3$ (= 27 000) times calculations are implemented if $r = 4$ Å. First, the calculations were carried out

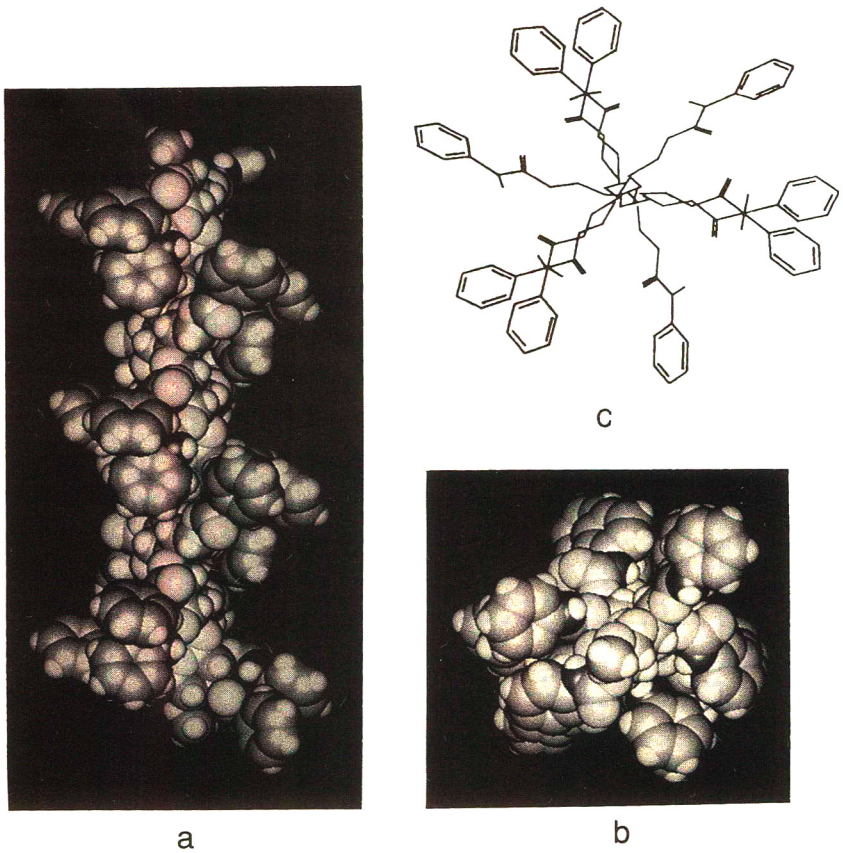

Fig. 4. (a and b) Optimized and (c) reported structures of CTPC. (a) Perpendicular to the chain axis; (b) and (c) along to the chain axis.

at $r = 3$–6 Å and $r' = 1$ Å, and it became clear that when r was 3 Å, the lowest interaction energy was over 100 kcal/mol. When r was 5 or 6 Å, the sampling boxes seemed large enough, and $r = 4$ Å was found to be suitable for the calculation of the interaction energies between CTPC and (±)-**1**. Such a box ($r = 4$ Å) centred by the NH proton covers the area as shown in Fig. 5.

Table 1
Dihedral angles of O–Cl–Cl′–O

Glucose No.	Dihedral angle (°)
1–2	112
2–3	110
3–4	112
4–5	111
5–6	111
6–7	113
7–8	111

The calculation was carried out at each NH proton at the 2-, 3- and 6-positions of glucose units 3, 4, 5 and 6 (Fig. 6) in order to avoid the influence of the end-groups, since CTPC is a polymer (degree of polymerization ≈ 100).

The results of the calculations are shown in Table 2. The minimum interaction energies were very different depending on the number of the glucose unit and the position of the NH. The interaction energies between CTPC and (*S*,*S*)-(−)-**1** were lower than those between CTPC and (*R*,*R*)-(+)-**1** except on 6–2 (2-position at glucose unit No. 6). This suggests that (*S*,*S*)-(−)-**1** may be more tightly adsorbed than (*R*,*R*)-(+)-**1** on

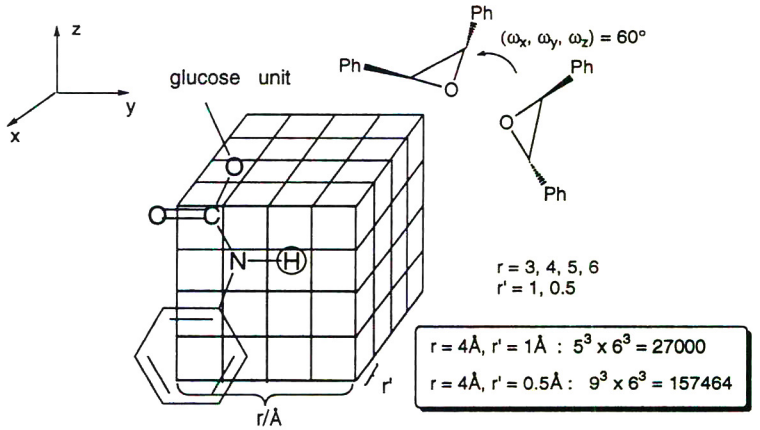

Fig. 5. Method of calculation of interaction energy between CTPC and an enantiomer of **1**.

the CTPC, and that **1** may preferentially interact with the NH protons at the 3-positions of the CTPC because most of interaction energies at the 3-positions were lower than those at the 2- and 6-positions except for glucose unit No. 6. In the chromatographic resolution of (±)-**1** using CTPC as chiral stationary phase, the (*R*,*R*)-isomer elutes first, followed by the (*S*,*S*)-isomer, and the separation factor (α) has been determined to be 1.46 [18]. Therefore, the results obtained by the above calculations are consistent with the results of the chromatographic enantioseparation on CTPC.

Next, a finer sampling box ($r = 4$ Å, $r' = 0.5$ Å) was placed at the NH-proton [4–3 (3-position at glucose unit No. 4)] where the lowest interaction energies appeared for both enantiomers. The results of the distribution of interaction energies are shown in Table 3. The total number of interaction energies under 0 kcal/mol was seven for (*R*,*R*)-(+)-**1** and ten for (*S*,*S*)-(−)-**1**. The lowest interaction energies for (*S*,*S*)-(−)-**1** and (*R*,*R*)-(+)-**1** were −21.42 and −19.10 kcal/mol, respectively. This also indicates that (*S*,*S*)-(−)-**1** may interact more tightly with the CTPC than (*R*,*R*)-(+)-**1**. The calculation described above may still be rough, so to obtain more precise interaction energies at the position 4–3,

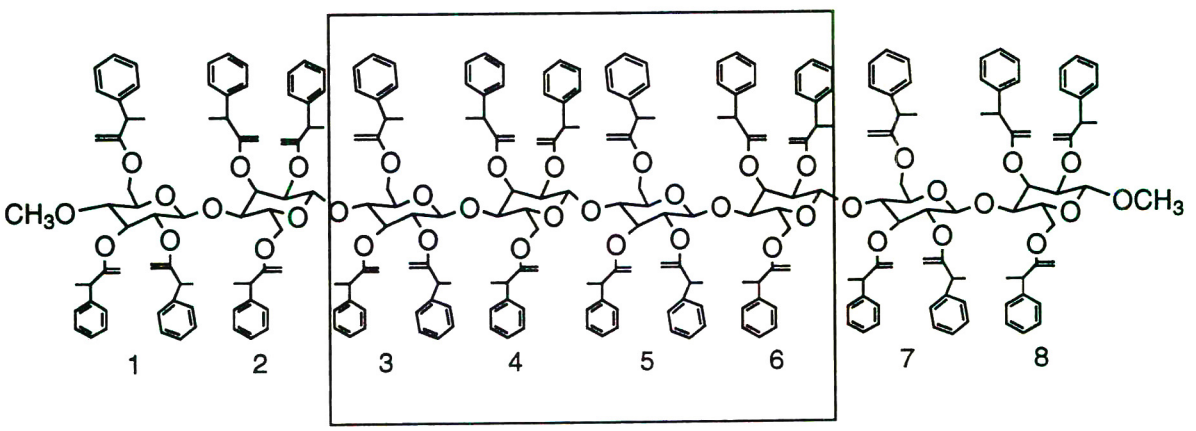

Fig. 6. Octamer of CTPC.

Table 2
Minimum interaction energy between CTPC and **1**

Glucose No. and position	(*R*,*R*)-(+)-**1** (kcal/mol)	(*S*,*S*)-(−)-**1** (kcal/mol)
3–2	–[a]	74.10
3–3	5.62	5.13
3–6	–	–
4–2	32.24	15.53
4–3	−17.62	−19.87
4–6	–	–
5–2	23.01	18.14
5–3	−5.87	−7.45
5–6	–	–
6–2	42.72	56.02
6–3	87.42	44.71
6–6	–	46.87

$r = 4$ Å, $r' = 1$ Å, 60°; total numbers, 27 000.
[a] Dashes indicate over 100 kcal/mol (1 cal = 4.184 J).

each enantiomer was rotated manually at that point along the x, y and z axes to find the orientations of **1** with lower interaction energies.

The lowest interaction energies between CTPC and (*S*,*S*)-(−)-**1** is −22.16 kcal/mol, whereas that of (*R*,*R*)-(+)-**1** is −19.73 kcal/mol. The decrease in the interaction energies in this operation for (*S*,*S*)-(−)-**1** is 0.74 kcal/mol and that for (*R*,*R*)-(+)-**1** is 0.63 kcal/mol. The difference in the interaction energy between the two enantiomers was 2.4 kcal/mol. This value seems to be large compared with that estimated by the chromatographic separation of (±)-**1** on CTPC. The energy difference ($\Delta\Delta G$) of the interaction between a CSP and a pair of enantiomers is correlated with the α value by $\Delta\Delta G = -RT \ln \alpha$.

Table 3
Distribution of interaction energy between CTPC and (*R*,*R*)- and (*S*,*S*)-**1**

Energy (kcal/mol)	Numbers	
	(*R*,*R*)-(+)-**1**	(*S*,*S*)-(−)-**1**
<−20	0	1
−20 to −10	2	4
−10 to 0	5	5

$r = 4$ Å, $r' = 0.5$ Å, 60°; total numbers, 157 464.

Therefore, $\Delta\Delta G$ for $\alpha = 1.46$ is estimated to be 0.23 kcal/mol. The α value must reflect the sum of the differences in interaction energies between CTPC and a pair of enantiomers. The computer graphics of the interaction between CTPC and (*S*,*S*)-(−)-**1** with the lowest energy is shown in Fig. 7. (*S*,*S*)-(−)-**1** is bound in a chiral groove existing along the main chain of CTPC, and each phenyl group of (*S*,*S*)-(−)-**1** may interact with the phenyl groups of CTPC via π–π interactions and the ether oxygen of the (*S*,*S*)-isomer seems to interact with the NH proton of CTPC via hydrogen bonding. The distance between the ether oxygen of (*S*,*S*)-(−)-**1** and the NH proton of CTPC is 2.502 Å, which is short enough to form hydrogen bonding, while the distance for (*R*,*R*)-(+)-**1** is 3.187 Å. This suggests that (*S*,*S*)-(−)-**1** may interact with the NH proton through the hydrogen bonding, but (*R*,*R*)-(+)-**1** may not interact effectively in such a way.

The same calculation was performed for 1,2-diphenylcyclopropane (**2**). The results of the calculation using the sampling box ($r = 4$ Å, $r' = 1$ Å) at glucose units Nos. 4 and 5 suggest that there was little difference in the minimum interaction energies between the enantiomers. The lowest interaction energies for (*S*,*S*)-(−)-**2** and (*R*,*R*)-(+)-**2** were −12.68 and −12.22 kcal/mol, respectively, which appeared at the 3-position of glucose unit No. 4. Moreover, the number of the

Fig. 7. Computational graphics of the interaction between CTPC and (*S*,*S*)-(−)-**1** (arrowed) exhibiting the lowest energy.

interaction energies under 0 kcal/mol was two for both enantiomers. It is considered that **2** cannot interact with CTPC through hydrogen bonding because of the absence of an ether oxygen as in **1**. The chromatographic resolution of (±)-**2** on CTPC as chiral stationary phase was unsuccessful. This agreed with the results of the chromatographic enantioseparation on CTPC.

4. Conclusions

The interaction energies between CTPC and (*R*,*R*)- and (*S*,*S*)-*trans*-stilbene oxide and between CTPC and (*R*,*R*)- and (*S*,*S*)-1,2-diphenylcyclopropane were calculated by using QUANTA/CHARMm. The results indicate that the most important adsorbing site of CTPC for *trans*-stilbene oxide may be the NH proton at the 3-position and the (*S*,*S*)-isomer may interact more closely with CTPC than the (*R*,*R*)-isomer. The interaction energies between the CTPC and enantiomers of 1,2-diphenylcyclopropane, which has a similar structure to *trans*-stilbene oxide but with no ether oxygen, showed almost no difference.

These calculations agreed with the observed results for the chromatographic resolution on CTPC, although the difference in the calculated interaction energy between the two enantiomers of *trans*-stilbene oxide is large compared with that estimated by the chromatographic enantioseparation. This may be due to the uncertainty in the calculated interaction energy values, which may be dependent on the structure of CTPC. However, we believe that the method reported here may be useful for a qualitative understanding of the chiral recognition mechanism of CTPC. The adaptability of this method to various kinds of enantiomers must be investigated. This approach is not restricted to the study of chiral recognition and should be applicable to a variety of polymer–analyte interactions.

References

[1] S. Ahuja, in S. Ahuja (Editor), *Chiral Separations by Liquid Chromatography* (*ACS Symposium Sereis*, No. 471), American Chemical Society, Washington, DC, 1991, p. 1.
[2] D.R. Taylor and K. Maher, *J. Chromatogr. Sci.*, 30 (1992) 67.
[3] Y. Okamoto and Y. Kaida, *J. Chromatogr. A*, 666 (1994) 403.
[4] W.H. Pirkle and T.C. Pochapsky, *Chem. Rev.*, 89 (1989) 347.
[5] B. Feibush, A. Figueroa, R. Charles, K.D. Onan, P. Feibush and B.L. Karger, *J. Am. Chem. Soc.*, 108 (1986) 3310.
[6] W.H. Pirkle and T.C. Pochapsky, *J. Am. Chem. Soc.*, 109 (1987) 5975.
[7] G.U.-Barretta, C. Rosini, D. Pini and P. Salvadori, *J. Am. Chem. Soc.*, 112 (1990) 2707.
[8] K.B. Lipkowitz, S. Raghothama and J. Yang, *J. Am. Chem. Soc.*, 114 (1992) 1554.
[9] J.E.H. Köhler, M. Hohla, M. Richters and W.A. König, *Angew. Chem., Int. Ed. Engl.*, 31 (1992) 319.
[10] K. Lohmiller, E. Bayer and B. Koppenhoefer, *J. Chromatogr.*, 634 (1993) 65.
[11] K.B. Lipkowitz, D.A. Demeter and C.A. Parish, *Anal. Chem.*, 59 (1987) 1731.
[12] K.B. Lipkowitz, D.A. Demeter, R. Zegarra, R. Larter and T. Darden, *J. Am. Chem. Soc.*, 110 (1988) 3446.
[13] K.B. Lipkowtiz and B. Baker, *Anal. Chem.*, 62 (1990) 770.
[14] S. Topiol, M. Sabio, J. Moroz and W.B. Caldwell, *J. Am. Chem. Soc.*, 110 (1988) 8367.
[15] M.G. Still and L.B. Rogers, *J. Comput. Chem.* 11 (1990) 242.
[16] E. Francotte and R.M. Wolf, *Chirality*, 2 (1991) 43.
[17] T. Hanai, H. Hatano, N. Nimura and T. Kinoshita, *J. Liq. Chromatogr.*, 16 (1993) 801.
[18] Y. Okamoto, M. Kawashima and K. Hatada, *J. Chromatogr.*, 363 (1986) 173.
[19] E. Yashima, M. Yamada and Y. Okamoto, *Chem. Lett.*, 1994, 579.
[20] B.R. Brooks, R.E. Bruccoleri, B.D. Olafson, D.J. States, S. Swaminathan and M. Karplus, *J. Comput. Chem.*, 4 (1983) 187.
[21] F.A. Momany and R. Rone, *J. Comput. Chem.*, 13 (1992) 888.
[22] I.K. Roterman, M.H. Lambert, K.D. Gibson and H.A. Scheraga, *J. Biomol. Struct. Dyn.*, 7 (1989) 421.
[23] D.R. Langley, J. Golik, B. Krishnan, T.W. Doyle and D.L. Beveridge, *J. Am. Chem. Soc.*, 116 (1994) 15.
[24] H.-J. Schneider, T. Blatter, B. Palm, U. Pfingstag, V. Rüdiger and I. Theis, *J. Am. Chem. Soc.*, 114 (1992) 7704.
[25] J.D. Madura, A. Wierzbicki, J.P. Harrington, R.H. Maughon, J.A. Raymond and C.S. Sikes, *J. Am. Chem. Soc.*, 116 (1994) 417.
[26] S.B. Clough, X.-F. Sun, S. Subramanyam, N. Beladakere, A. Blumstein and S.K. Tripathy, *Macromolecules*, 26 (1993) 597.
[27] H.-Y. Zhang, A. Blaskó, J.-Q. Yu and T.C. Bruice, *J. Am. Chem. Soc.*, 114 (1992) 6621.
[28] Ö. Almarsson, A. Sinha, E. Gopinath and T.C. Bruice, *J. Am. Chem. Soc.*, 115 (1993) 7093.
[29] U. Vogt and P. Zugenmaier, *Ber. Bunzenges. Phys. Chem.*, 89 (1985) 1217.

ELSEVIER

Journal of Chromatography A, 694 (1995) 355–363

JOURNAL OF CHROMATOGRAPHY A

Liquid chromatographic separation of the enantiomers of antihistaminic 3,3′-di(1,3-thiazolidin-4-one) derivatives with two and four stereogenic centres

Salvatore Caccamese[a,*], Grazia Principato[a], Rosaria Ottanà[b], Tindara Previtera[b], Carmela Zappalà[b]

[a]*Dipartimento di Scienze Chimiche, Università di Catania, Viale A. Doria 6, 95125 Catania, Italy*
[b]*Dipartimento Farmaco-Chimico, Università di Messina, Villaggio SS Annunziata, 98168 Messina, Italy*

First received 26 July 1994; revised manuscript received 25 October 1994; accepted 26 October 1994

Abstract

The enantiomers of anti-inflammatory and antihistaminic 3,3′-(1,2-ethanediyl)bis(2-aryl-1,3-thiazolidin-4-one) derivatives possessing two stereogenic centres were separated on Chiralcel OD stationary phase without derivatization. The *meso* form was also well separated from the enantiomers. The good resolution afforded a milligram-scale separation and subsequent measurement of the circular dichroism spectra of an enantiomeric pair. Addition of racemic α-mercaptopropionic acid to the N,N′-dibenzylideneethylenediamine yielded ten possible stereoisomers with four stereogenic centres. Two centres (2 and 2′) bear the same groups; the other two (5 and 5′) also bear the same groups, but these are different from the groups at 2 and 2′. In this situation four enantiomeric pairs and two *meso* forms exist; all of them were separated and identified using a Chiralpak AD column.

1. Introduction

3,3′-Di(1,3-thiazolidin-4-one) derivatives bearing an aryl group in positions 2 and 2′ (Fig. 1, R = H) were previously synthesized and investigated for their anti-inflammatory and antihistaminic properties [1,2]. Some of them, particularly those bearing an ethylenic chain between the 3- and 3′-nitrogen atoms and a 3-F or 3-Cl-phenyl group in position 2 and 2′, showed good anti-inflammatory and/or antihistaminic activity and also analgesic and antipyretic properties, their acute toxicity levels being lower than those of indomethacin and phenylbutazone used as reference compounds. Potency differences between racemic and *meso* isomers were often observed [2,3], the former usually being more active than the latter.

Since major differences in stereoselective ac-

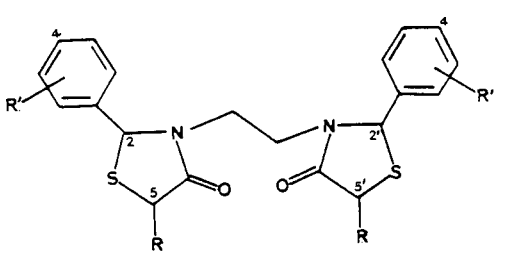

Fig. 1. Structures of compounds **1–16**: R = H, CH_3; R′ = 3 – Cl, 3-Br, 3-F, 3-CF_3, 3,4-Cl_2, 3,4-$(OCH_3)_2$.

* Corresponding author.

0021-9673/95/$09.50
SSDI 0021-9673(94)01055-2

tivities between the enantiomers of chiral antihistamines are well documented [4,5] and as a guide towards the pharmacokinetic and toxicological profiles of enantiomeric drugs has recently been issued [6], we decided to separate the enantiomers of the racemic compounds in order to submit single enantiomers to pharmacological evaluations.

This paper reports the enantiomeric resolution of several compounds with two stereogenic centres and one compound with four stereogenic centres due to an additional methyl in positions 5 and 5′ (Fig. 1, $R = CH_3$). The resolution was obtained without any derivatization using Chiralcel OD or, in one instance, Chiralpak AD as the stationary phase. The optimum mobile phase composition depended on the 2,2′ substituent group in the structure of the compound. The resolution of compound **5** ($R' = 3-F$, $R = H$) afforded a milligram-scale separation and measurement of the circular dichroism (CD) spectra of the individual enantiomers.

2. Experimental

Compounds **1–12** were available from previous studies [2,7]. The synthesis of the **13–16** is reported elsewhere [8]. The general procedure involves the addition of an aqueous solution of 1,2-diaminoethane to the appropriate aldehyde (0.5 molar ratio in ethanol) to obtain an N,N′-dibenzylideneethylendiamine that precipitates and is subsequently purified. To this compound, dissolved in toluene, an excess of mercaptoacetic acid (or racemic α-mercaptopropionic acid for the synthesis of **13–16**) is added and refluxed. After work-up, the title compounds are isolated.

The purity of **1–12** was checked by TLC (one distinct spot). Compounds **13–16**, all stereoisomers coming from a unique reaction, gave four distinct spots (see later). TLC was carried out on silica gel plates (Merck) using $CHCl_3$–Et_2O (9:1) as the eluent. Radial TLC was carried out by a Chromatotron apparatus (Harrison Research, Model 7924T) with silica gel 60P F_{254} gypsum-containing plates, by using light petroleum–Et_2O 9:1) as the eluent.

The HPLC system consisted of a Varian Model 5060 liquid chromatograph with Valco 10- or 50-μl sample loops, a Jasco Uvidec III UV spectrophotometric detector operating at 240 nm and a Varian CDS 401 data system or a Houston Omniscribe recorder for fraction collection. CD spectra were recorded on a Jasco Model 600 spectropolarimeter. The mobile phases were HPLC-grade *n*-hexane–2-propanol or *n*-hexane–dichloromethane mixtures as specified in the tables. As chiral phases a Chiralcel OD column (cellulose tris-3,5-dimethylphenylcarbamate) and a Chiralpak AD column (amylose tris-3,5-dimethylphenylcarbamate) coated on silica gel (each 25 cm × 0.46 cm I.D., particle size 10 μm), both from Daicel (Tokyo, Japan) were used. For normal-phase separations an Ultrasphere silica gel column from Beckman (15 cm × 2 mm I.D.) was used. Retention factors (k'), separation factors (α) and resolution (R_S) were calculated as usual. The column void time (t_0) was measured by injection of tri-*tert*-butylbenzene as a non-retained sample. Retention times were mean values of two replicate determinations. All separations were carried out at ambient temperature.

3. Results and discussion

3.1. 3,3′-Di(1,3-thiazolidin-4-one) derivatives with two stereogenic centres

The chromatographic results on silica gel for compounds **1–12** are presented in Table 1. Racemate and *meso* compounds were very well separated, exhibiting differences in the k' values of more than 1 and the *meso* form was more retained than the racemic mixture (2*R*,2′*R* and 2*S*,2′*S*) for all the compounds. The retention times were reasonably short and only **11** and **12** required a high content of 2-propanol in hexane for better elution.

The results on Chiralcel OD stationary phase (CSP) are summarized in Table 2. Good separation factors between the enantiomers (α = 1.20–1.66) were obtained, and were slightly improved by a decrease in the percentage of

Table 1
Normal-phase HPLC of compounds **1–16**

Compound	R	R′	Configuration	A (%)[a]	t_1 (min)	k'
1	H	3-Cl	*dl*	5	4.26	0.91
2	H	3-Cl	*meso*	5	7.17	2.22
3	H	3-Br	*dl*	5	4.31	0.94
4	H	3-Br	*meso*	5	7.23	2.24
5	H	3-F	*dl*	10	3.05	0.37
6	H	3-F	*meso*	10	5.19	1.33
7	H	3,4-Cl_2	*dl*	5	5.33	1.39
8	H	3,4-Cl_2	*meso*	5	11.36	4.10
9	H	3-CF_3	*dl*	5	5.91	1.66
10	H	3-CF_3	*meso*	5	8.80	2.95
11	H	3,4-$(OCH_3)_2$	*dl*	5	–[b]	
				30	6.31	1.83
12	H	3,4-$(OCH_3)_2$	*meso*	30	8.59	2.81
13	CH_3	3-F	$(dl)_1(A_1)$[c]	70[d]	6.56[e]	6.29
			$(dl)_2(A_1)$[c]	70[d]	5.90[f]	5.55
14	CH_3	3-F	$dl(A_2)$[c]	70[d]	9.09	9.10
15	CH_3	3-F	dl + $meso(B_1)$[c]	70[d]	15.50[g]	16.22
16	CH_3	3-F	$meso(B_2)$[c]	70[d]	16.43	17.25

[a] Percentage of 2-propanol in *n*-hexane at a flow-rate of 0.3 ml/min, $t_0 = 2.23$ min.
[b] Retained in the column.
[c] See text.
[d] Percentage of dichloromethane in *n*-hexane at a flow-rate of 1.0 ml/min, $t_0 = 0.9$ min.
[e] Elution time of the more abundant diastereomer $(dl)_1$.
[f] Elution time of the less abundant diastereomer $(dl)_2$.
[g] Broad peak with large tail.

2-propanol in the mobile phase. The resolution (R_S) was strongly improved by a decrease in the polarity of the mobile phase and in some instances (**1** and **3**) baseline separation was obtained only by decreasing the polarity of the eluent.

The *meso* forms did not follow a predictable elution order when compared with their *dl* forms, some of them possessing a higher retention factor than those of the enantiomers (**1** and **2**, **3** and **4**, and **5** and **6**), some having intermediate elution times with respect to the enantiomers (**7** and **8**, and **11** and **12**). The R′ substituent in the 2,2′-aryl groups strongly influences the interaction with the CSP and a different polarity of the mobile phase was necessary for reasonable elution of various compounds, as shown by the comparison of the behaviours of **1** and **11**.

Typical chromatograms are shown in Figs. 2 and 3, which show how the enantiomeric resolution was affected by the polarity and the flow-rate of the mobile phase. Elution of the *meso* form as a mixture with the *dl* form is also shown in Fig. 3.

The resolution (R_S) of compound **5** afforded a milligram-scale separation and measurement of the CD spectra of the enantiomeric pair, by repeated 50-μl injections of the racemic compound and collection of the eluate from the two chromatographic peaks. The CD spectra were mirror images of each other, as shown in Fig. 4. Analytical HPLC re-runs of the eluates indicated 100% enantiomeric purity of the first peak and 97% enantiomeric purity of the second peak. Their UV spectra were also identical.

We should mention also that the X-ray structures of the *meso* compound **6** and of the racemic

Table 2
Resolution of compounds **1–12** by HPLC on Chiralcel OD

Compound	R	R′	Configuration	A (%)[a]	k'_1		k'_2	α	R_S
1	H	3-Cl	*dl*	10	3.09		4.04	1.31	3.0
				30	1.36		1.67	1.23	1.0
2	H	3-Cl	*meso*	30		2.13			
3	H	3-Br	*dl*	30	1.88		2.26	1.20	1.4
				70	1.21		1.46	1.20	0.8
4	H	3-Br	*meso*	70		1.77			
5	H	3-F	*dl*	30	1.72		2.22	1.29	1.6
				70	0.79		0.98	1.24	1.1
6	H	3-F	*meso*	70		1.21			
7	H	3,4-Cl_2	*dl*	30	1.74		2.90	1.66	3.6
				70	1.20		1.86	1.55	2.5
8	H	3,4-Cl_2	*meso*	70		1.47			
9	H	3-CF_3	*dl*	30[b]	1.02		1.44	1.41	2.4
				30	1.12		1.56	1.39	1.9
				50[b]	0.68		0.95	1.39	1.7
				50	0.54		0.75	1.38	1.2
10	H	3-CF_3	*meso*	50		0.90			
11	H	3,4-$(OCH_3)_2$	*dl*	70	2.32		3.44	1.48	2.3
				70[b]	3.03		4.57	1.51	2.9
				90	2.83		4.21	1.48	1.9
				90[b]	3.23		4.72	1.46	2.7
12	H	3,4-$(OCH_3)_2$	*meso*	70		2.67			

[a] Percentage of 2-propanol in *n*-hexane at flow-rate of 1.0 ml/min, unless specified otherwise, $t_0 = 3.80$ min.
[b] Flow-rate 0.5 ml/min, $t_0 = 6.45$ min.

5 established their absolute stereochemistry [9], leading to a correction of a previously reported NMR assignment [2].

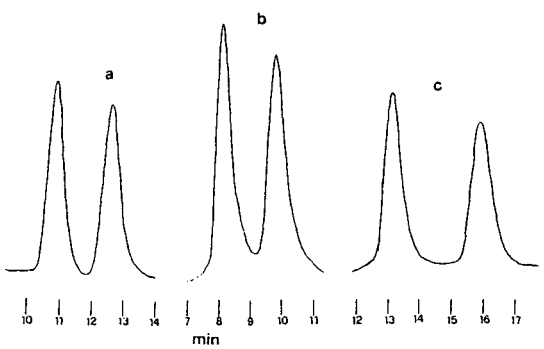

Fig. 2. HPLC separation of the enantiomeric pair of compound **9**. Mobile phase: *n*-hexane–2-propanol. (a) 5:5 at 0.5 ml/min, (b) 7:3 at 1 ml/min, (c) 7:3 at 0.5 ml/min.

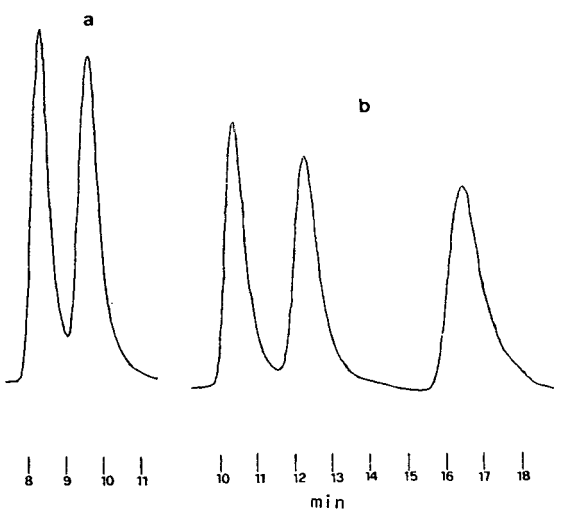

Fig. 3. HPLC separation (mobile phase: *n*-hexane–2-propanol) at 1 ml/min. Mobile phase composition: (a) compound **5**, 5:5; (b) compounds **5** and **6**, 7:3: first and second peaks, *dl* pair; third peak, *meso*.

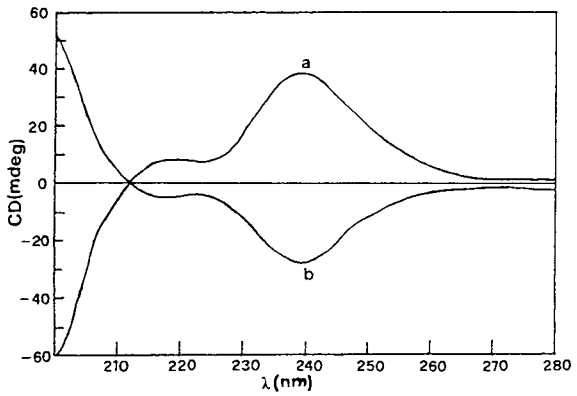

Fig. 4. CD spectra of the enantiomeric pair of compound **5** obtained from the first-eluted peak (positive) and from the second-eluted peak (negative) in ethanol at 25°C.

3.2. 3,3′-Di(1,3-thiazolidin-4-one) derivatives with four stereogenic centres

The chromatographic behaviour of **13–16** was more complicated. In fact, the nucleophilic addition of racemic α-mercaptopropionic acid to the N,N′-dibenzylideneethylenediamine resulted in ten possible stereoisomers with four stereogenic centres, as reported in Fig. 5. A degeneracy due to the presence of *meso* isomers reduced the maximum number of stereoisomers from the expected sixteen to ten. Two of these centres (2 and 2′) bear the same groups, and the remaining two (5 and 5′) also bear the same groups, but these are different from the groups at 2 and 2′. In this situation, four enantiomeric pairs and two *meso* forms exist; all of them were separated and

	C-2	C-2'	C-5	C-5'	2-5/2'-5'	Type	Compd.
Enantiomers	R	R	R	R	trans/trans	A	13
	S	S	S	S		A	
Enantiomers	R	R	R	S	trans/cis	A	13
	S	S	S	R		A	
Enantiomers	R	R	S	S	cis/cis	A	14
	S	S	R	R		A	
Enantiomers	R	S	R	R	trans/cis	B	15
	S	R	S	S		B	
Meso	R	S	R	S	trans/trans	B	15
	R	S	S	R	cis/cis	B	16

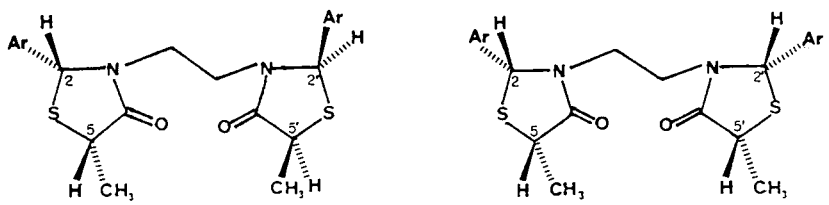

2R5S,2'R5'S 2R5S,2'S5'R

Fig. 5. Possible diastereomers of a 3,3′-di(1,3-thiazolidin-4-one) bearing a 3-fluorophenyl group in positions 2 and 2′. Stereochemistries of the enantiomer *2R5S,2′R5′S* of the racemic compound **14** and of the *2R5S,2′S5′R meso* compound **16** are shown. H-2 and H-5 exhibit an NOE effect in ^{1}H NMR spectra in a *cis* relative configuration. Ethylene protons appear as an AA′XX′ system in type A compounds and as an AA′BB′ system in type B compounds.

identified using polysaccharide-derived CSPs, as shown in Fig. 5.

From repeated crystallizations in methanol and radial TLC of the reaction mixture, partial purification resulted in four products. These appeared on silica gel TLC plates [$CHCl_3$–Et_2O (9:1) as the eluent] as two pairs of close spots, A_1 and A_2 at R_F 0.93 and 0.90, respectively, and B_1 and B_2 at R_F 0.74 and 0.67, respectively. In a detailed ^1H NMR study, we found that, in analogues with two stereogenic centres, an *RR* (or *SS*) relative configuration of the 2,2′-carbons causes the appearance of the ethylene protons as an AA′XX′ system (type A ^1H NMR spectra), whereas an *RS* (or *SR*) relative configuration gives an AA′BB′ system (type B ^1H NMR spectra) [2,3]. This observation applies also to type A and type B products, respectively, carrying four stereogenic centres [8], and it is summarized in Fig. 5. In addition, in the ^1H NMR spectra of **14** (A_2) and **16** (B_2), protons 2 and 5 (or 2′ and 5′) reciprocally exhibited a good nuclear Overhauser enhancement (NOE) effect which established a *cis* configuration between them. Also, the 5-methyl irradiation did not give an NOE effect on the proton 2. These results established a racemic 2*R*5*S*,2′*R*5′*S*/2*S*5*R*,2′*S*5′*R* structure for **14** and a *meso* 2*R*5*S*,2′*S*5′*R* structure for **16**, as shown in Fig. 5. Moreover, these results ruled out a "mixed" *trans*/*cis* relationship, i.e., a 2*S*5*S*, 2′*S*5′*R* stereochemistry.

The results of normal-phase and chiral liquid chromatography are summarized in Tables 1 and 3, respectively. On silica gel HPLC, the products B_2 and A_2 were slightly impure (6%) with the diastereomers B_1 and A_1, respectively. Instead, the product B_1 appeared as a broad peak and the width increased with decreasing eluent polarity, suggesting that it is an unseparable mixture of two diastereomers. Co-injection with B_2 gave, however, two distinct peaks, thus ruling out the possibility of B_2 being one of the diastereomers

Table 3
HPLC resolution of the stereoisomers **13**–**16** (R = CH_3, R′ = 3 − F in Fig. 1)

Compound	Configuration	A (%)[a]	k'_1	k'_{meso}	k'_2	α	R_S
13	$(dl)_1$	5	1.47		3.67	2.49	6.3
		10	1.07		2.27	2.13	5.4
	$(dl)_1$	7[b]	3.18		6.77	2.13	9.8
	$(dl)_2$	7[b]	4.89		11.49	2.35	12.5
14	*dl*	5	1.25		1.45	1.15	0.9
		10	0.89		1.02	1.14	0.6
		30	0.46			NS[c]	
15	*dl* + *meso*	7[d]	3.48	3.66	5.81	1.67	3.4
		10[d]	2.75	2.91	4.04	1.47	2.5
		10	2.48	2.85	4.07	1.64	3.5
		15	1.86	2.08	2.40	1.29	1.6
		15[e]	1.45	2.79[f]	2.79		
		25[e]	1.22	1.39[f]	1.39		
		30	0.75	1.02	0.88	1.18	0.5
		30[e]	0.76	1.05	0.91	1.20	0.7
16	*meso*	10		2.94			
		15		2.08			
		30		1.06			

[a] Percentage of 2-propanol in *n*-hexane at a flow-rate of 1 ml/min, unless specified otherwise, $t_0 = 3.65$ min.
[b] Stationary phase Chiralpak AD, $t_0 = 3.91$ min.
[c] Not separated.
[d] Flow-rate 1.2 ml/min, $t_0 = 2.90$ min.
[e] Flow-rate 0.7 ml/min, $t_0 = 4.90$ min.
[f] *Meso* compound overlapped with the last-eluting enantiomer.

in B_1. In addition, from Table 1, it can be observed that the pair A_1–A_2 had an elution time range much lower than the pair B_1–B_2, in agreement with the TLC results.

Confirmation of the *meso* nature of the stereoisomer **16** came from the chromatographic behaviour on Chiralcel OD. Compound **16** appeared as a unique, sharp peak, as shown in Table 3, with various percentages of 2-propanol in hexane.

In Chiralcel OD chromatography **14** appeared as two distinct peaks of the same area, as shown in Table 3 and Fig. 6. Therefore, it is a racemic compound that, according to the ^{1}H NMR features illustrated above, is identified as the enantiomeric pair *2R5S,2'R5'S/2S5R,2'S5'R* (Fig. 5). It is interesting to note the crucial effect of the polarity of the mobile phase on the enantiomeric resolution of **14**. A concentration of 30% of 2-propanol in hexane did not afford resolution and resulted in a single peak on Chiralcel OD, as shown in Fig. 6c.

In Chiralced OD chromatography **13** (A_1) appeared as two distinct major peaks of the same area at $k' = 1.47$ and 3.67 on eluting with *n*-hexane–2-propanol (95:5), as shown in Table 3, accompanied by a minor distinct peak ($k' = 2.58$, same eluent). This behaviour was maintained at various percentages of 2-propanol in *n*-hexane and various detection wavelengths.

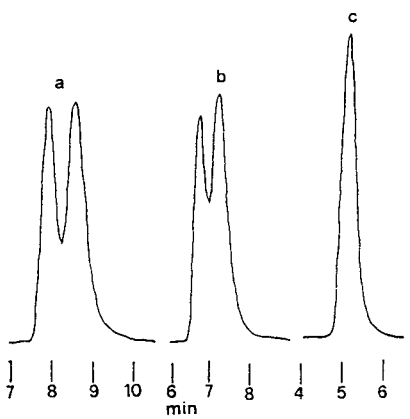

Fig. 6. HPLC separation of the enantiomeric pair of compound **14**. Mobile phase: *n*-hexane–2-propanol at 1 ml/min: (a) 95:5; (b) 9:1; (c) 7:3.

However, as one *meso* form was identified as **16**, as shown above, and the only other *meso* form possible according to Fig. 5 was identified as **15** (as shown below), the appearance of a single minor peak was suspicious. Therefore, we chromatographed **13** on a chiral stationary phase, Chiralpak AD, structurally similar to Chiralcel OD (the same carbamate moieties) but with a wider helicity deriving from the amylose matrix. In this experiment, as shown in Table 3 and Fig. 7, **13** was resolved into two enantiomeric pairs, $(dl)_1$ more abundant and $(dl)_2$ much less abundant. The relative areas of the peaks were confirmed in several experiments. Moreover, the area ratios of the diastereomers in Fig. 7a and b are approximately the same, as expected. Thus, according to the A nature of the ^{1}H NMR spectrum of **13**, as shown in Fig. 5, the two racemates resolved were *2R5R,2'R5'S/2S5S,2'S5'R* and *2R5R,2'R5'R/2S5S,2'S5'S*. The resolution for both enantiomeric pairs was excel-

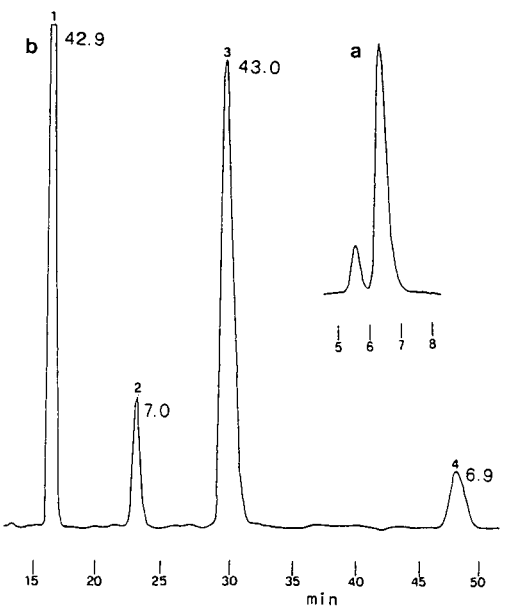

Fig. 7. HPLC separation of the enantiomeric pairs in product **13** (a) on silica gel, mobile phase *n*-hexane–dichloromethane (3:7) at 1 ml/min; (b) on Chiralpak AD, mobile phase *n*-hexane–2-propanol (93:7) at 1 ml/min. Numbers near the peaks represent the relative areas. Peaks 1 and 3 represent the separation of $(dl)_1$; peaks 2 and 4 represent the separation of $(dl)_2$.

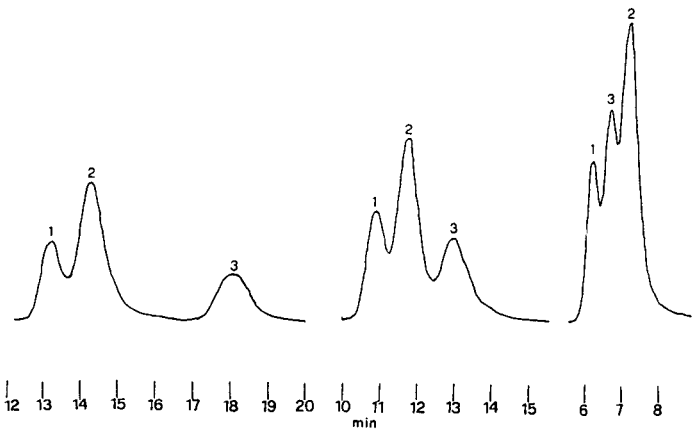

Fig. 8. HPLC separation of the enantiomeric pair and *meso* form in product **15**. Mobile phase: *n*-hexane–2-propanol at 1 ml/min: (a) 9:1; (b) 85:15; (c) 7:3. Peaks 1 and 3 represent the separation of dl; peak 2 is due to the *meso* form.

lent ($R_S = 9.8$ and 12.5), and this can afford a milligram-scale separation of the enantiomers for pharmacological assays. However, k'_2 of $(dl)_2$ was extremely high (11.49, corresponding to an elution time of 48.8 min).

The chromatographic behaviour on Chiralcel OD of **15** (B_1) was also complex. In fact, as shown in Table 3 and Fig. 8, this compound exhibited three peaks under several experimental conditions (various polarities and flow-rates of the mobile phase). Peaks 1 and 3 can be attributed to an enantiomeric pair as their area ratio is about 1 and it remains constant at various polarities and flow-rates of the mobile phase. Their separation and resolution are good and also in this instance a semi-preparative isolation of pure enantiomers appears feasible. The peak 2 can instead be attributed to the remaining *meso* structure (Fig. 5). In fact, this peak did not split under the various experimental conditions reported in Table 3 and also under other conditions not reported. Moreover, the ^{1}H NMR spectrum of **15** suggests clearly an *RS* configuration at the 2,2′ centres (AA′BB′ ethylenic system). This steric requirement is present only in the remaining *meso* form 2*R*5*R*,2′*S*5′*S* and in the racemic 2*R*5*R*,2′*S*5′*R*/2*S*5*S*,2′*R*5′*S* structure, thus identifying also peaks 1 and 3.

In conclusion, by chiral HPLC we separated all ten stereoisomers from the reaction of *dl*-thiolactic acid with N,N′-dibenzylideneethylenediamine. For **13** the excellent resolution opens the way to the isolation of its enantiomers in sizeable amounts. Analogously, by choosing the optimum eluent composition, the last-eluting enantiomer present in **15** can be isolated in pure form and the first-eluting enantiomer can also be isolated, although probably impure with the *meso* diastereomer (peak 2). The stereochemistry and the pharmacological activities of these individual stereoisomers will be investigated.

References

[1] M.G. Vigorita, T. Previtera, M. Basile, G. Fenech, R. Costa De Pasquale, F. Occhiuto and C. Circosta, *Farmaco, Ed. Sci.*, 39 (1984) 1008.

[2] T. Previtera, M. Basile, M.G. Vigorita, G. Fenech, F. Occhiuto, C. Circosta and R. Costa De Pasquale, *Eur. J. Med. Chem.*, 22 (1987) 67.

[3] T. Previtera, M.G. Vigorita, M. Basile, F. Orsini, F. Benetollo, G. Bombieri, *Eur. J. Med. Chem.*, 29 (1994) 317.

[4] A.F. Casy, in D.F. Smith (Editor), *Handbook of Stereoisomers; Therapeutic Drugs*, CRC Press, Boca Raton, FL, 1989, p. 149.

[5] D.G. Cooper, R.C. Young, G.J. Durant and C.R. Ganellin, in C. Hansch (Editor), *Comprehensive Medicinal Chemistry*, Vol. 3, Pergamon Press, Oxford, 1990, p. 371.

[6] *FDA's Policy Statement for the Development of New Stereoisomeric Drugs*, Food and Drug Administration, Washington, DC, 1992.
[7] I. Grillone, *Doctoral Thesis*, University of Messina, Messina, 1992.
[8] M.G. Vigorita, T. Previtera and R. Ottanà, in preparation.
[9] F. Benetollo, G. Bombieri, A. Del Pra, M. Basile, T. Previtera and M.G. Vigorita, *J. Crystallogr. Spectrosc. Res.*, 21 (1991) 113.

ELSEVIER

Journal of Chromatography A, 694 (1995) 365–373

JOURNAL OF CHROMATOGRAPHY A

Separations of molecular species of phosphatidic acid by high-performance liquid chromatography

S.L. Abidi*, T.L. Mounts

Food Quality and Safety Research, National Center for Agricultural Utilization Research, Agricultural Research Service, US Department of Agriculture, 1815 North University Street, Peoria, IL 61604, USA

Received 19 October 1994; accepted 11 November 1994

Abstract

Molecular species of phosphatidic acid (PA) were separated by reversed-phase high-performance liquid chromatography with mobile phases of acetonitrile–methanol–water containing quaternary ammonium phosphates (QAPs). Effective resolution of PA complexes was achieved by using low-mass QAPs at concentrations ≥ 50 mM or high-mass QAPs at concentrations ≥ 10 mM. Capacity factor (k') values were found to be dramatically influenced by the type and concentration of QAP, stationary phase specifications, and mobile phase solvent compositions. An increase in the acetonitrile–methanol ratio of the mobile phase tended to enhance the retention and separation of the polar lipid components. Correlation of logarithmic k' values with the total number of carbon atoms in QAP appeared to yield non-linear relationships. Compositions of major molecular species in various PA samples were determined by calibration with synthetic PA standards. Distribution patterns of PA molecular species in samples derived from animal and plant sources were compared.

1. Introduction

Clusters of phosphatidic acid (PA) (Fig. 1) are negatively charged polar lipids occurring in small amounts in cell membranes of animals and plants. They are important metabolic intermediates of phospholipid (PL) biosyntheses. Because of high activity of plant phospholipases, PA is known to be the major breakdown product of various PL classes in plants through specific enzymatic hydrolysis by phospholipase D. Several studies [1–4] show that high levels of PA has been found in PL fractions of soybeans stored for extended periods of time, elevated temperatures, and high moisture contents. Degummed soybean oils contain predominantly PA in the polar lipid isolates [4–7]. Our current research on the assessment of the impact of genetic modifications on oil quality required development of reliable, sensitive chromatographic techniques for analyses of PL classes and their molecular species. Normally, the polar lipid fractions of soybeans comprise primarily phosphatidylcholine (PC), phosphatidylethanolamine (PE), phosphatidylinositol (PI) and PA. Of these, PA amounts to ca. 5% of the total PL in the standard crude oils. Consequently, the low abundance of PA in oilseeds necessitates investigations of chromatographic methodology that would provide assay procedures for sensitive measurements of PA species.

The literature information on the separation

* Corresponding author.

SSDI 0021-9673(94)01239-3

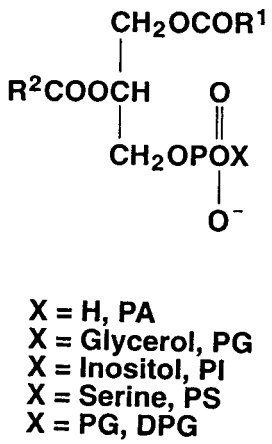

Fig. 1. General structure of negatively charged phospholipids. R^1 and R^2 represent alkyl or alkenyl groups of fatty acid chains.

and quantification of PA molecular species is sparse in contrast to the vast volume of available HPLC methods for the analysis of the major soybean PL (PE, PI and PC). Recently, certain derivatives of PA subcomponents have been separated by reversed-phase high-performance liquid chromatography (HPLC) [8–14]. In all of the published methods, the PA analytes are first converted to their dimethyl esters [8–13], dibenzyl esters [10] or monomethyl esters [14] prior to HPLC analyses. Due to the highly polar nature of PA molecules, HPLC speciation of molecular species of intact underivatized PA complexes has met with difficulties. Earlier attempts to resolve PA complexes failed, even though HPLC conditions employed were identical to those under which the corresponding species of monomethyl esters of PA were well separated [14]. Since direct HPLC separations of intact PA subcomponents are not known, this paper reports the results of a reversed-phase HPLC study on the baseline separation of the molecular species of intact PA molecules.

2. Experimental

2.1. Chemicals and reagents

Egg- and soybean PA were obtained from Avanti Polar Lipids (Alabaster, AL, USA). Wheat germ- and bovine brain PA were obtained from Matreya (Pleasant Gap, PA, USA). Degummed and modified soybean PA were prepared from respective oils following procedures as described previously [4,15]. Synthetic PA standards were obtained either from Avanti Polar Lipids or Sigma (St. Louis, MO, USA). All commercial natural PA samples were prepared from corresponding natural PC by transphosphatidylation with phospholipase D. Alkyltriethylammonium phosphates (ATEAP) and tetrabutylammonium phosphate (TBAP) were obtained from Regis (Morton Grove, IL, USA). Most of the symmetrically substituted tetraalkylammonium phosphates (TAAP) (carbon chains C_1 to C_3) were prepared from the corresponding hydroxides (Aldrich, Milwaukee, WI, USA) by titration with 85% phosphoric acid (Fisher Chemicals, Fair Lawn, NJ, USA) until desired pH values were obtained. HPLC-grade acetonitrile and methanol were products of EM Separations (Gibbstown, NJ, USA). Ultra-pure HPLC water was obtained by filtering through a Waters–Millipore (Milford, MA, USA) Milli-Q water purifier.

2.2. High-performance liquid chromatography

All HPLC experiments were performed on a Spectra-Physics (Thermo Separations, San Jose, CA, USA) liquid chromatograph Model SP 8700 solvent-delivery system. The LC unit was interfaced with an LDC Analytical (Riviera Beach, FL, USA) SpectroMonitor D multiple-wavelength UV detector. The polar lipid analytes were detected at a wavelength of 208 nm. Detector signals were recorded with an OminiScribe recorder (Houston Instruments, Houston, TX, USA). Mobile phases consisted of acetonitrile, methanol, water and quaternary ammonium phosphates (QAPs). In optimization experiments, QAP concentrations in the range 5–50 m*M* were employed. The HPLC eluents, prepared freshly before assays, were filtered, degassed, and pumped isocratically through a reversed-phase column at a flow-rate of 1 ml/min unless specified otherwise.

Analytical samples in aliquots of 0.5–5 μl 1% solutions were injected onto a column via a

Rheodyne (Cotati, CA, USA) Model 7125 injector equipped with a 10-μl loop. Three replicate injections were made for all sample analyses. Samples were stored in amber vials in a freezer at −30°C whenever not in use. Stationary phases were obtained from different commercial suppliers: (1) Ultrasphere C_{18}, 5 μm, 250 (or 150) × 4.6 mm I.D. (Beckman Instruments, San Ramon, CA, USA), (2) NovaPak C_{18}, 4 μm, 300 × 3.9 mm I.D. (Waters Chromatography, Milford, MA, USA), (3) Adsorbsphere HS C_{18}, 5 μm, 250 × 4.6 mm I.D. (Alltech, Deerfield, IL, USA), (4) YMC-Pak ODS-A, 5 μm, 250 × 4.6 mm I.D. (YMC, Wilmington, NC, USA), and (5) LiChrospher RP-18, 3 μm, 250 × 4 mm I.D. (EM Separations).

For confirmation purposes, individual HPLC peaks attributable to PA molecular species were collected and subjected to fatty acid analyses by a published HCl–methanol/gas chromatographic procedure [16]. Fatty acids were characterized as methyl esters using a Varian Model 3400 gas chromatograph equipped with a flame ionization detector. Samples were injected onto a 30 m × 0.25 mm fused-silica capillary column coated with 0.2 μm SP 2330 (Supelco, Bellefonte, PA, USA). Helium was used as the carrier gas. The column temperature was programmed from 200 to 220°C at 10°C/min after an initial hold of 15 min.

3. Results and discussion

In addition to the four major PL classes, there are phosphatidylserine (PS), phosphatidylglycerol (PG) and diphosphatidylglycerol (DPG) present in soybeans as minor PL constituents. The majority of these soybean PLs are negatively-charged compounds (PA, PG, PI, PS and DPG) as depicted in Fig. 1. Neutralization of the negative charges by cationic QAP counter ions in mobile phases should facilitate differential partition between the PL solutes and the hydrocarbonaceous phase in reversed-phase HPLC systems. With the exception of PA, molecular species of the negatively charged soybean lipids including N-derivatives of PE have recently been separated by reversed-phase ion-pair HPLC [17–21].

Examination of the PA structure (Fig. 1) indicates that the doubly anionic PA molecules devoid of hydrocarbonaceous functionality in the head group are relatively less hydrophobic than other negatively charged PL compounds found in soybeans. The mobile phase conditions used in HPLC of the more hydrophobic negatively-charged PLs [17–21] are apparently inadequate to confer a certain degree of hydrophobicity required for solvophobic interactions in the reversed-phase separation processes. Therefore, the strategy of increasing the concentration of QAP or using high-molecular-mass QAPs proved fruitful and led to the first separation of the intact PA molecular species. This direct approach to the analysis of intact PA species is advantageous over the existing chemical derivatization methods. Since the latter methods entail structural modifications, the molecular integrity of the analytes may not be preserved under drastic derivatization conditions.

Fig. 2 shows typical separations of PA molecular species under various HPLC conditions. As observed in HPLC of other negatively charged polar lipids [17–21], no appreciable retention and resolution of PA molecular species were observed in initial exploratory experiments where no QAP electrolytes were used in mobile phases. HPLC of a mixture of PA components on an octadecylsilica (ODS) column with a mobile phase of acetonitrile–methanol–water containing a QAP at a low concentration (0.5–5 m*M*) produced a broad band with some peak tailing [14] or, at best, ill-defined multiple bands (Fig. 2A). Adding more QAP to the mobile phases resulted in near-baseline separations of the PA molecular species as illustrated in Fig. 2B–D.

Retention data in Table 1 clearly demonstrate that the six major egg PA components were more strongly retained (higher k' values) by octadecylsilica (ODS) in mobile phases containing higher concentrations of QAP counter-ions. In the presence of increased concentrations of the cationic buffers, the anionic characteristics of the analytes appeared to be neutralized to further extent by the counter-ions, enhancing hy-

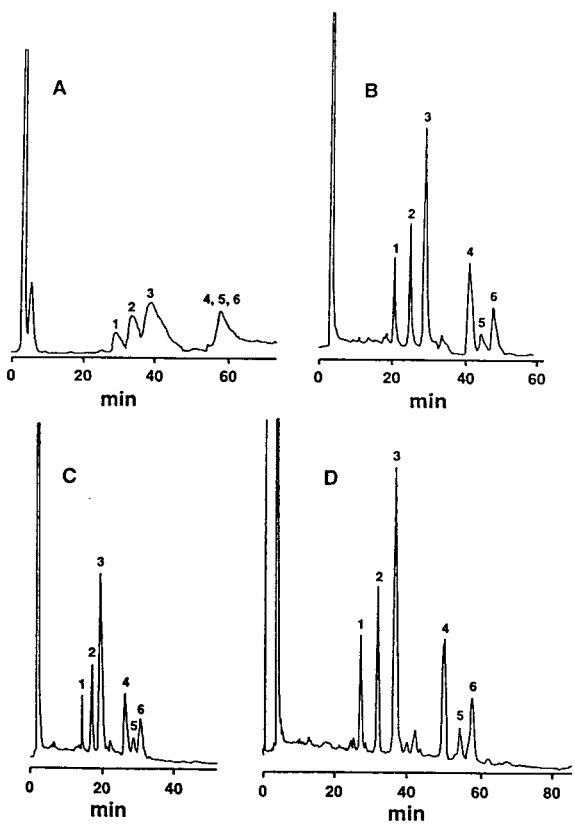

Fig. 2. HPLC separations of egg PA components. Columns: Beckman Ultrasphere C_{18}, 250 × 4.6 mm I.D. (A, B), or 150 × 4.6 mm I.D. (C); YMC-ODS (D). Mobile phases: acetonitrile–methanol–water (70:22:8) containing 5 m*M* PTAP at pH 6.5 (A); acetonitrile–methanol–water (70:26:4) containing 20 m*M* TBAP at pH 6.5 (B); acetonitrile–methanol–water (49:49:2) containing 50 m*M* TMAP at pH 6.5 (C, D). Peaks: 1 = 16:0–22:6; 2 = 16:0–20:4; 3 = 16:0–18:2; 4 = 16:0–18:1, 5 = 18:0–20:4 + 18:1–18:1; 6 = 18:0–18:2.

drophobic interactions in the reversed-phase chromatographic processes. The counter-ion concentration effects were more pronounced in HPLC experiments with higher water contents and heavier QAP in mobile phases [Table 1, conditions A1 (HTAP) *vs.* conditions A2 (OTAP)], which partly reflected the effect of the change in QAP types. On the other hand, the differences in k' values between the corresponding PA components were relatively small, when the retention data obtained with 25 m*M* TMAP were compared with those obtained with 50 m*M* TMAP (Table 1, conditions B). The positive concentration effects (k' values increase with increasing QAP concentrations) were found independent of the type of stationary phases evaluated (Table 1, conditions A *vs.* B), as observed in the HPLC studies on other soybean PL classes [17–21].

Two structural series of QAPs were chosen for study to determine if the retention behavior of the resolved PA components would be affected by incorporation of different types of QAP counter-ions in mobile phases. The tetraalkylammonium phosphate (TAAP) series includes four symmetrically substituted alkyl-ammonium phosphates: tetramethylammonium phosphate (TMAP), tetraethylammonium phosphate (TEAP), tetrapropylammonium phosphate (TPAP) and tetrabutylammonium phosphate (TBAP). The alkyltriethylammonium phosphate (ATEAP) series includes four unsymmetrically substituted ammonium phosphates: pentyltriethylammonium phosphate (PTAP), heptyltriethylammonium phosphate (HTAP), octyltriethylammonium phosphate (OTAP) and dodecyltriethylammonium phosphate (DTAP). Table 2 shows examples of structural effects of QAPs on the retention characteristics (k' values) of PA molecular species. As expected, greater k' values of the analyte components were observed in HPLC with QAP of higher molecular mass. In other words, PA analytes had longer retention times in mobile phases containing a higher-molecular-mass member of QAP in both structural series (Table 2 and Fig. 3).

Attempts to correlate the total number (n) of carbon atoms in QAP with logarithmic k' values failed to produce straight lines. The correlation results seems to be in variance with the linear relationships observed previously in HPLC of all other anionic polar lipids [17–21]. The $\ln k'$–n plots in Fig. 3 exhibit two sets of curves with marked differences in curvature. Evidently, changes in the magnitude of hydrophobicity (a function of n) of the QAP electrolyte caused greater responses in k' values for the ATEAP series than for the TAAP series.

Inspection of the HPLC data in Table 3 indicates that k' values and separation factors

Table 1
Concentration effects of quaternary ammonium phosphates on capacity factors, k', of molecular species of egg PA derived from egg PC

HPLC conditions[a]	QAP	QAP concentration (mM), pH 6.5	Capacity factor, k'					
			Component 1	Component 2	Component 3	Component 4	Component 5	Component 6
A1	TMAP	10.00	2.50	2.91	3.30	4.67	5.00	5.41
		50.00	6.48	7.75	8.90	12.2	13.0	13.8
	HTAP	5.00	2.19	2.58	3.22	4.50	4.85	5.14
		10.00	2.52	3.06	3.67	4.95	5.42	5.81
A2	OTAP	5.00	9.67	11.3	12.7	19.5	24.6	40.8
		10.00	16.8	20.3	22.9	36.3	43.2	69.3
B	TMAP	25.0	4.34	5.51	6.92	9.00	9.99	11.2
		47.7	4.67	5.75	7.15	9.33	10.2	11.5

TMAP = Tetramethylammonium phosphate; HTAP = heptyltriethylammonium phosphate; OTAP = octyltriethylammonium phosphate.
[a] HPLC conditions: A1 = mobile phase acetonitrile–methanol–water (49:49:2), pH 6.50; Beckman Ultrasphere C_{18} column, 250 × 4.6 mm I.D.; A2 = mobile phase acetonitrile–methanol–water (70:22:8), pH 7.50; column as A1; B = mobile phase acetonitrile–methanol–water (70:28:2), pH 7.50; column NovaPak 18, 300 × 3.9 mm I.D.

(α) for adjacent components were dramatically influenced by the variation in solvent compositions of mobile phases. As described in the Experimental section, the mobile phase solvents employed acetonitrile, methanol and water throughout the study. Few separations ($\alpha = 1.00$) of the lipid species were achieved when acetonitrile was not used in mobile phases (Table 3,

Table 2
Effects of the type of quaternary ammonium phosphates on the capacity factors, k', of molecular species of egg PA derived from egg PC

QAP (n)[a]	Capacity factor, k'					
	Component 1	Component 2	Component 3	Component 4	Component 5	Component 6
TAAP series						
TMAP (4)	2.48	2.89	3.29	4.64	4.95	5.37
TEAP (8)	2.53	3.00	3.44	4.77	5.10	5.53
TPAP (12)	2.69	3.24	3.74	5.10	5.47	5.93
TBAP (16)	3.00	3.66	4.17	5.65	6.02	6.50
ATEAP series						
PTAP (11)	2.17	2.58	3.09	4.16	4.50	4.91
HTAP (13)	2.49	3.06	3.67	4.95	5.42	5.81
OTAP (14)	2.83	3.49	4.18	5.69	6.11	6.55
DTAP (18)	7.84	10.3	11.7	15.9	16.8	18.5

HPLC conditions: mobile phase, acetonitrile–methanol–water (49:49:2) containing 10 mM QAP at pH 6.5; stationary phase, Beckman Ultrasphere C_{18}. TAAP = Tetraalkylammonium phosphate; TMAP = tetramethylammonium phosphate; TEAP = tetraethylammonium phosphate; TPAP = tetrapropylammonium phosphate; TBAP = tetrabutylammonium phosphate; ATEAP = alkyltriethylammonium phosphate; PTAP = pentyltriethylammonium phosphate; HTAP = heptyltriethylammonium phosphate; OTAP = octyltriethylammonium phosphate; DTAP = dodecyltriethylammonium phosphate.
[a] n = Total number of carbon atoms in QAP.

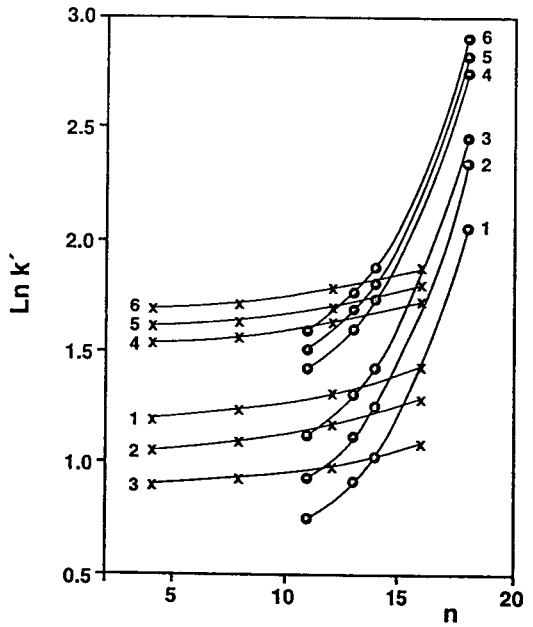

Fig. 3. Non-linear relation between $\ln k'$ of PA components and the total number (n) of carbon atoms in QAP. Curves with dots and crosses represent experiments with ATEAP and TAAP, respectively. HPLC conditions, column: Beckman Ultrasphere C_{18}, 250 × 4.6 mm I.D.; mobile phase: acetonitrile–methanol–water (49:49:2) containing 10 m*M* QAP at pH 6.5. For component identification, see Fig. 2.

conditions A). The k' and α values had the tendency to increase with increasing proportions of acetonitrile in acetonitrile–methanol–water mobile phases. Conversely, the presence of high methanol content in mobile phases had an adverse effect on component separations, as evidenced by low α values (Table 3, conditions A and B).

In consideration of the acidic properties of PA molecules, it was worthwhile to conduct a pH study to probe the effect of mobile phase pH on their retention characteristics as measured by the k' values. Generally, at a higher mobile phase pH value, the PA analytes were less retained (lower k' values) on the ODS phase (Table 4). In addition, notable enhancement in the pH effect was manifested in experiments with high water contents of mobile phases (Table 4, B). The inverse relationship between pH values and k' values of PA analytes may be explained in terms of an ion suppression rationale. The results of this pH study are parallel to those described in an earlier work [14] in which phosphoric acid and ammonia solutions were added to mobile phases and a polystyrene–divinylbenzene resin column was used.

A number of commercial ODS stationary

Table 3
Effects of the mobile phase solvent composition on the capacity factors, k', of molecular species of egg PA derived from egg PC

Conditions	Mobile phase solvent ratio ACN–MeOH–water	Component 1		Component 2		Component 3		Component 4		Component 5		Component 6
		k'	α	k'	α	k'	α	k'	α	k'	α	k'
A	49:49:2	3.38	(1.18)	4.00	(1.19)	4.75	(1.27)	6.05	(1.16)	6.99	(1.00)	6.99
	0:98:2	3.95	(1.00)	3.95	(1.00)	3.95	(1.33)	5.25	(1.00)	5.25	(1.00)	5.25
B	64:34:2	7.67	(1.22)	9.33	(1.20)	11.2	(1.38)	15.4	(1.14)	17.5	(1.33)	18.4
	49:49:2	6.48	(1.20)	7.75	(1.15)	8.90	(1.37)	12.2	(1.07)	13.0	(1.06)	13.8
C	70:22:8	15.5	(1.21)	18.7	(1.14)	21.3	(1.58)	33.6	(1.18)	39.5	(1.18)	46.5
	49:49:2	3.00	(1.22)	3.66	(1.14)	4.17	(1.35)	5.65	(1.07)	6.02	(1.08)	6.50
D	70:26:4	7.41	(1.23)	9.10	(1.19)	10.8	(1.45)	15.7	(1.10)	17.2	(1.09)	18.8
	49:49:2	5.58	(1.16)	6.50	(1.16)	7.51	(1.33)	10.0	(1.07)	10.7	(1.08)	11.6

HPLC conditions: mobile phases contained (A, B, D) 50 m*M* tetramethylammonium phosphate and (C) 10 m*M* tetrabutylammonium phosphate at pH values of (A, D) 7.50 and (B, C) 6.50; stationary phases, (A) Beckman Ultrasphere C_{18} (150 × 4.6 mm I.D.) and (B, C, D) Beckman Ultrasphere C_{18} (250 × 4.6 mm I.D.). ACN = Acetonitrile.

Table 4
Effects of the mobile phase pH on the capacity factors, k', of molecular species of egg PA derived from egg PC

Mobile phase pH	Capacity factor, k'					
	Component 1	Component 2	Component 3	Component 4	Component 5	Component 6
(A) Acetonitrile–methanol–water (49:49:2), 50 mM TMAP						
7.50	5.58	6.50	7.51	10.0	10.7	11.6
6.50	6.48	7.75	8.90	12.2	13.0	13.8
(B) Acetonitrile–methanol–water (70:22:8), 10 mM TBAP						
7.50	8.00	9.58	10.8	16.7	19.5	20.5
6.50	15.5	18.7	21.3	33.6	39.5	46.5

HPLC conditions: stationary phase, Beckman Ultrasphere C_{18} column (250 × 4.6 mm I.D.)

phases were studied under identical HPLC conditions to evaluate their separation potential for the PA species interest. The data in Table 5 indicate that, with the exceptions of experiments C and E, variations in α and k' values among the ODS columns studied are fairly small. In view of the higher degree of hydrocarbonaceous surface coverage (20% carbon loading and 3.27 μmol/m^2 bonded phase) in Adsorbsphere ODS with 60 Å pore size, reversed-phase HPLC of PA on this stationary phase would be expected to lead to separations of components with highest k' values. However, the experimental results showed otherwise (Table 5, D). In fact, the use of a YMC ODS phase gave longest retention times (higher k' values) of the PA components as noted in experiment C of Table 5, presumably due to the relatively large pore size (120 Å) of the column packings. A divinylbenzene polymer-based ODS column (Table 5, E) showed lower selectivity (α values = 1.00 for the adjacent peaks 4, 5 and 6) for most of the PA species than a silica-based ODS phase (Table 5, F).

Table 6 shows the calibration data for six commercially available synthetic PA standards. Plotting the injected amounts of individual PA compounds against peak areas yielded linear correlation lines with slope values (m) ranging 0.088–8.005 $cm^2/\mu g$. Coefficients of variation in peak measurements and correlation coefficients averaged 2.82% and 0.9987, respectively. The amounts of PA components in unknown samples can be determined by the equation $Y = mX$, where Y and X represent the respective peak

Table 5
Stationary phase effects on the capacity factors, k', of molecular species of egg PA derived from egg PC

Stationary phase	Component 1		Component 2		Component 3		Component 4		Component 5		Component 6
	k'	α	k'	α	k'	α	k'	α	k'	α	k'
A	6.48	(1.20)	7.75	(1.15)	8.90	(1.37)	12.2	(1.07)	13.0	(1.06)	13.8
B	5.83	(1.20)	7.00	(1.19)	8.33	(1.33)	11.1	(1.15)	12.8	(1.04)	13.3
C	10.3	(1.19)	12.3	(1.17)	14.4	(1.35)	19.5	(1.10)	21.5	(1.07)	23.0
D	5.27	(1.20)	6.33	(1.20)	7.60	(1.34)	10.2	(1.13)	11.5	(1.06)	12.2
E	2.50	(1.10)	2.75	(1.05)	2.88	(1.98)	5.69	(1.00)	5.69	(1.00)	5.69
F	7.46	(1.20)	8.97	(1.16)	10.4	(1.41)	14.7	(1.08)	15.9	(1.08)	17.1

HPLC conditions: mobile phase, acetonitrile–methanol–water (49:49:2) containing 50 mM TMAP at pH 6.5; stationary phases: (A) Beckman Ultrasphere C_{18} (250 × 4.6 mm I.D.), (B) EM Separations LiChrospher RP-18 (250 × 4 mm I.D.), (C) YMC-ODS-A (250 × 4.6 mm I.D.), (D) Alltech Adsorbsphere HS C_{18} (250 × 4.6 mm I.D.), (E) AsahiPak ODP-50 (150 × 4.6 mm I.D.), (F) Beckman Ultrasphere C_{18} (150 × 4.6 mm I.D.). Flow-rates: (A–D) 1 ml/min, (E, F) 0.5 ml/min.

Table 6
Linear correlation between peak areas and injected amounts of selected synthetic PA species on a Beckman Ultrasphere C_{18} column (250 × 4.6 mm I.D.) in HPLC with a mobile phase of acetonitrile–methanol–water (49:49:2) containing 50 m*M* TMAP at pH 6.5

PA species	Slope (*m*) $cm^2/\mu g$	R.S.D. (%)	Correlation coefficient (*r*)
18:0–20:4-PA	8.005	2.83	0.9998
16:0–20:4-PA	4.804	2.76	0.9999
18:2–18:2-PA	2.399	2.40	0.9998
16:0–18:2-PA	1.682	2.71	0.9979
18:1–18:1-PA	0.392	3.02	0.9966
16:0–18:1-PA	0.088	3.20	0.9980

Calibration lines expressed by $Y = mX$, where X, Y and m represent the amount injected, the peak area and the slope, respectively. Relative standard deviations (R.S.D.s) are based on mean values of three determinations of peak areas.

area and amount of a PA species present in a sample. The calibration equation implies that all the curves crossed the origin at zero. In light of the different degree of UV absorptivity among the PA molecular species analyzed, construction of calibration plots is an indispensable procedure for the quantitative analysis of the polar lipids by HPLC–UV detection [15].

With the aid of the calibration data in Table 6, compositions of the major PA components in some PA samples derived from various commercial sources were determined. The results are summarized in Table 7. The PA components were identified by peak matching with synthetic PA standards and by fatty acid analyses. Similar to the findings in a previous HPLC study on the separation of diverse groups of PL subcomponents [22], the distribution patterns of PA molecular species in samples of animal origins are generally more complex than those derived from plants (Fig. 4A–C *vs.* Fig. 4D and E). The chromatographic profile of a crude sample of degummed soybean oil revealed extra peaks due to contamination by impurities presumably derived from other PL species (Fig. 4C).

In conclusion, the results of this study represent the first report on the reversed-phase HPLC separation of molecular species of intact PA without derivatization. Using the HPLC–UV detection technique developed, quantitative analyses of the PA samples can be achieved by calibration with individual synthetic standards. The essence of attaining satisfactory component resolution lies in the modification of the polar anionic PA solutes with QAP cationic electrolytes in the mobile phase systems for strengthening hydrophobic interactions during

Table 7
Determination of the composition of major PA molecular species in animal and plant samples

Molecular species	Composition (%)				
	Egg	Brain	Soybeans	Soybeans (degummed)	Wheat
18:3–18:3	ND	ND	4.52	4.07	6.33
18:2–18:3	ND	ND	12.7	10.4	17.9
18:1–18:2	ND	ND	6.79	6.37	5.09
18:0–20:4	3.94	11.3	ND	ND	ND
16:0–20:4	3.35	3.18	ND	ND	ND
18:2–18:2	ND	ND	43.4	31.7	36.6
16:0–18:2	19.1	7.31	18.1	21.3	9.94
18:1–18:1	3.00	ND	ND	ND	ND
16:0–18:1	43.6	37.6	TR	TR	TR
18:0–18:2	9.37	4.52	3.60	3.09	2.70
18:0–18:1	16.8	13.8	ND	ND	ND
Others	0.84	22.3	10.9	23.1	21.4

HPLC conditions were same as in Table 6. ND = None detected; TR = trace.

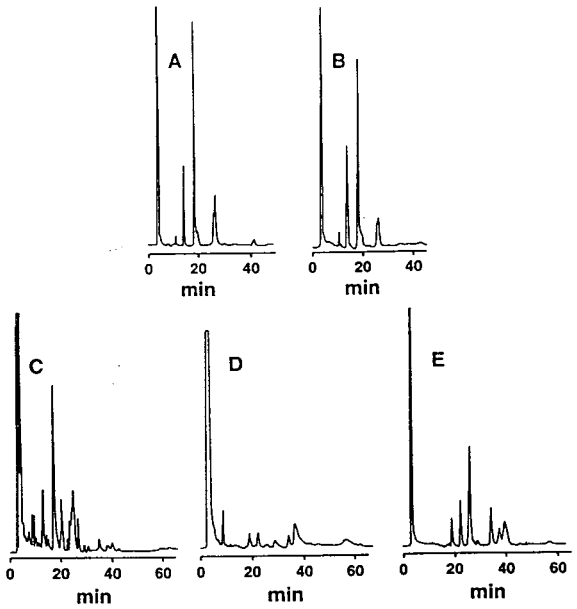

Fig. 4. HPLC separations of PA components in samples derived from animals and plants. (A) Soybeans, (B) wheat germ, (C) degummed soybean oil, crude sample, (D) bovine brain, (E) egg. HPLC conditions, column: Beckman Ultrasphere C_{18}; mobile phase as in Fig. 2C and D.

the separation processes. Thus, mobile phases in reversed-phase HPLC of the doubly charged PA require more hydrocarbonaceous electrolyte additives than those of singly charged PL. Optimization of HPLC conditions in the context of mobile phase variables and column specifications facilitates baseline resolution of the PA components with reasonable retention times. The method may be applicable to the characterization of PA molecular species in a wide range of biological and physiological sample matrices derived from cell membranes of animals and plants.

References

[1] Y. Nakayama, K. Saio and M. Kito, *Cereal Chem.*, 58 (1981) 260.
[2] G.W. Chapman, Jr. and J.A. Robertson, *J. Am. Oil. Chem. Soc.*, 54 (1977) 195.
[3] T.L. Mounts and A.M. Nash, *J. Am. Oil Chem. Soc.*, 67 (1990) 757.
[4] T.L. Mounts, S.L. Abidi and K.A. Rennick, *J. Am. Oil Chem. Soc.*, 69 (1992) 438.
[5] R. Kanamoto, Y. Wada, G. Miyajima and M. Kito, *J. Am. Oil Chem. Soc.*, 58 (1981) 1050.
[6] A. Hvolby, *J. Am. Oil Chem. Soc.*, 48 (1971) 503.
[7] T.L. Mounts, G.R. List and A.J. Heakin, *J. Am. Oil Chem. Soc.*, 56 (1979) 883.
[8] J.Y. Hsieh, *Ph.D. Dissertation*, University of Rhode Island, Kingston, RI, 1979, pp. 60–105.
[9] J.G. Turcotte, S.P. Srivastava, W.A. Meresak, B.A. Rizkalla, F. Louzon and T.P. Wunz, *Biochim. Biophys. Acta*, 619 (1980) 604.
[10] J.Y. Hsieh and J.G. Turcotte, *J. High Resolut. Chromatogr. Chromatogr. Commun.*, (1980) 481.
[11] J.G. Turcotte, J.Y. Hsieh and D.K. Welch, *Lipids*, 16 (1981) 761.
[12] J.Y. Hsieh, D.K. Welch and J.G. Turcotte, *J. Chromatogr.*, 208 (1981) 398.
[13] Y. Nakagawa and K. Waku, *J. Chromatogr.*, 381 (1986) 225.
[14] S.L. Abidi, *J. Chromatogr.*, 587 (1991) 193.
[15] S.L. Abidi, T.L. Mounts and K.A. Rennick, *J. Liq. Chromatogr.*, (1994) in press.
[16] W.W. Christie, *Lipid Analysis*, Pergamon Press, New York, 1973, p. 85.
[17] S.L. Abidi, T.L. Mounts and K.A. Rennick, *J. Liq. Chromatogr.*, 14 (1991) 573.
[18] S.L. Abidi and T.L. Mounts, *J. Liq. Chromatogr.*, 15 (1992) 2487.
[19] S.L. Abidi and T.L. Mounts, *J. Chromatogr. Sci.*, 31 (1993) 231.
[20] S.L. Abidi, T.L. Mounts and K.A. Rennick, *J. Chromatogr.*, 639 (1993) 175.
[21] S.L. Abidi and T.L. Mounts, *J. Liq. Chromatogr.*, 17 (1994) 105.
[22] S.L. Abidi and T.L. Mounts, *J. Chromatogr.*, 598 (1992) 209.

ELSEVIER

Journal of Chromatography A, 694 (1995) 375–380

JOURNAL OF CHROMATOGRAPHY A

Retention properties of triacylglycerols on silver ion high-performance liquid chromatography

Boryana Nikolova-Damyanova[a], William W. Christie[a,*], Bengt G. Herslöf[b]

[a]*Scottish Crop Research Institute, Invergowrie, Dundee DD2 5DA, Scotland, UK*

[b]*LipidTeknik AB, P.O. Box 6686, S-11384 Stockholm, Sweden*

First received 15 August 1994; revised manuscript received 29 November 1994

Abstract

The retention properties of series of synthetic disaturated–monounsaturated (1 to 6 double bonds) triacylglycerols and the common seed oil triacylglycerols on a silver ion high-performance liquid chromatography column have been studied in quantitative terms. Retention factors were found to increase stepwise, with a saturated dimonoenoic species being held ten times and trilinolenin ten thousand times more strongly than a disaturated monoenoic species, for example. Formation of chelate-type of pi-complexes between silver ions and double bonds, with participation of the carbonyl oxygen in the complexation, have been assumed in order to explain the high separation power and specificity of the silver ion column.

1. Introduction

In recent years, high-performance liquid chromatography (HPLC) has become one of the most widely applied separation techniques in lipid analysis [1]. Until recently, separation of triacylglycerols by reversed-phase HPLC (RP-HPLC) had no rival, but with the introduction of a stable silver-loaded column [2] silver ion HPLC (Ag-HPLC) has become an established technique, which has been reviewed recently [3]. The advantage of Ag-HPLC is that unlike RP-HPLC it separates species according to a single property: the number (with the configuration) of their double bonds. This simplifies the analysis of natural triacylglycerol mixtures to a great extent as they are resolved into groups with equal unsaturation [4]. It is evident that Ag-HPLC and RP-HPLC applied in a complementary way are to date the most powerful tools in the isolation and analysis of triacylglycerols [5–11].

The general elution order of triacylglycerols obtained with the silver-loaded column described by Christie [5] is:

SSS > SSM > SSD > MMM > SMD > MMD > SDD = SST > SMT = MDD > MMT > SDT = DDD > MDT ≥ STT > DDT > MTT > DTT > TTT

where S = saturated, M = monoenoic, D = dienoic and T = trienoic residues. One dienoyl residue is retained more strongly then two monoenoyls in one triacylglycerol molecule and one trienoyl (e.g. α-linolenoyl) residue is the equivalent of two dienoyls [5], but there are no quan-

* Corresponding author.

0021-9673/95/$09.50
SSDI 0021-9673(94)01180-X

titative data on the retention characteristics. The aim of the present work was to acquire such data for the most common constituents of natural seed oils as an aid to the understanding of the underlying separation mechanism. Also, for the latter purpose, a series of disaturated monounsaturated (1 to 6 double bonds) triacylglycerols was synthesised and the chromatographic behaviour was examined.

2. Experimental

2.1. Materials

All solvents were HPLC grade and were used without further purification. Oleic, linoleic, α-linolenic, arachidonic, eicosapentaenoic, docosahexaenoic acids, tripalmitin and 1,2-dipalmitin were purchased from Sigma (Poole, UK). Olive oil and sunflower were supplied by LipidTeknik AB (Sweden); linseed oil was from a local shop. The pure triacylglycerols fractions were isolated from each oil by eluting the crude sample through an Isolute silica cartridge (Crawford Scientific, Strathaven, UK) with hexane–acetone (99:1, v/v; 10 ml).

2.2. Triacylglycerol synthesis

Dipalmitoyl monounsaturated triacylglycerols were synthesised via 1,2-dipalmitin and the appropriate acid chlorides [12]. The latter were produced by reacting the free fatty acid (20 mg) with oxalyl chloride (0.5 ml) (Aldrich, Gillingham, UK) at room temperature for 36 h in a test tube [12]. The excess reagents were then removed in a stream of nitrogen and finally by a vacuum pump. The acid chloride was redissolved in 0.5 ml of toluene and was immediately added to dipalmitin (10 mg) in toluene (1 ml)/pyridine (0.2 ml). The mixture was left overnight at 50°C. The excess reagents were removed in a stream of nitrogen and the residue was dried under vacuum. It was then redissolved in hexane (5 ml), washed twice with water (5 ml) and cleaned by elution through a Florisil mini-column (Pasteur pipette) with hexane–acetone (99:1, v/v; 10 ml). The purity was checked by TLC on silica gel with a mobile phase of hexane–acetone (100:8, v/v), and eventually by silver ion HPLC.

2.3. Silver ion high-performance liquid chromatography

A Hitachi L-6200A HPLC pump was used with a Varex Model IIA evaporative light-scattering detector (P.S. Instruments, Sevenoaks, UK). A Nucleosil 5SA column (25 cm × 4.6 mm I.D.) (Hichrom Ltd, Reading, UK) was converted to the silver form as described earlier [2]. The integrator response was regulated by using tripalmitin as test substance. The temperature of the drift tube in the detector was 90°C.

The temperature of the column was maintained at 20.0 ± 1.0°C by fitting it into a water jacket through which water was pumped from a temperature control unit. Dichloroethane–dichloromethane (1:1, v/v) and either acetone or acetonitrile were used in the mobile phases, the compositions of which are listed in Tables 1 and 2.

Table 1
Mobile phase composition (Volume %) for elution of the synthetic disaturated triacylglycerols

Mobile phase composition[a]	Triacylglycerols resolved	
DCE–DCM–AcN, 1:1:0.01	16:0 16:0 18:1	16:0 16:0 18:2
DCE–DCM–AcN, 1:1:0.02	16:0 16:0 18:2	16:0 16:0 18:3
DCE–DCM–AcN, 1:1:0.03	16:0 16:0 18:3	16:0 16:0 20:4
DCE–DCM–AcN, 1:1:0.04	16:0 16:0 20:4	16:0 16:0 20:5
DCE–DCM–AcN, 1:1:0.05	16:0 16:0 20:5	16:0 16:0 22:6

[a] Abbreviations: DCE, dichloroethane; DCM, dichloromethane; AcN, acetonitrile.

Table 2
Experimental conditions for resolution of natural triacylglycerols mixtures on a silver ion loaded ion-exchange column

Oil	Mobile phase composition	Triacylglycerols resolved[a]
Olive oil	DCE–DCM–Acetone (1:1:0.1)	SSM, SMM
	DCE–DCM–Acetone (1:1:1)	SSM, SMM, MMM, SMD
	Acetone (100)	SMM, MMM, SMD, MMD
Sunflower	Acetone (100)	SMM, MMM, SMD, MMD
	Acetone–AcN (100:1)	SMD, MDD, SDD, MDD
	Acetone–AcN (100:2)	SDD, MDD, DDD
Linseed	Acetone–AcN (100:2)	MMM, SMD, MMD, SDD + SST, MDD, SMT
	Acetone–AcN (100:3)	SMT + MDD, MMT, DDD + SMT
	Acetone–AcN (100:4)	MMT, DDD + SDT, MDT
	Acetone–AcN (100:6)	MDT, STT, DDT, MTT
	Acetone–AcN (100:7)	MDT, STT, DDT, MTT, DTT
	Acetone–AcN (100:8)	MDT, STT, DDT, MTT, DTT, TTT

[a] Abbreviations: S, saturated; M, monoenoic; D, dienoic; T, trienoic fatty acid moieties; see also footnote to Table 1.

3. Results and discussion

Triacylglycerols are resolved by silver ion chromatography according to the total number of double bonds in the fatty acid moieties. The position of double bonds in a fatty acyl chain, the chain length of the fatty acids and the position of an unsaturated acyl group on the glycerol moiety have relatively small or negligible effects and are not considered. The principle question addressed here is whether a triacylglycerol molecule participates in complexation as a single entity or whether the general effect is a sum of the separate retention properties of the different fatty acid moieties. It has been established from crystallographic studies that a single silver ion can form a complex with two double bonds in the same or different molecules [13], and the specificity of this type of Ag-HPLC column has been interpreted as due to a dual interaction between a silver ion and either two double bonds or one double bond and an electron-rich centre [5].

Saturated acyl moieties have no significant participation in the retention. PPP (P = palmitic acid) had a k' value of 0.193 with a mobile phase of dichloroethane–dichloromethane (1:1, v/v), compared to PPO (O = oleic acid) with one double bond which eluted with a retention factor of 10.1.

When the polarity of the mobile phase was increased, the k' value of PPP equalled that of a non-retained substance, docosane. If palmitoyl moieties are neglected, triacylglycerols of the SSU type (U = unsaturated acyl moiety) can be treated as derivatives of fatty acids with 1 to 6 double bonds and their chromatographic behaviour can be compared with that of the methyl esters of the same fatty acids. There was no simple relationship between the fatty acid component of a triacylglycerol and its retention on the column, and the results for the k' values of the synthetic PPU triacylglycerols in Table 3 clearly reveal this. The ratio k'_{PPU}/k'_{PPO} is also listed since it expresses the increase in retention with an increasing number of double bonds in the molecule. If a fatty acid moiety were the only factor to affect the retention of a fatty acid derivative in the column, through the interaction of its double bond(s) with silver ion(s), the retention of the different types of derivative would be similar. The general patterns were comparable. As has been found with the methyl esters [5], the greatest relative increase in retention of the PPU triacylglycerols was observed when the number of double bonds in the mole-

Table 3
Calculated k' values of the synthetic dipalmitoyl monounsaturated triacylglycerols for a mobile phase of dichloroethane–dichloromethane–acetonitrile (1:1:0.1 by volume)

Triacylglycerols	k'	k'_{PPU}/k'_{PPO}	$k'_{UFA}/k'^{a}_{18:1}$
16:0–16:0–18:1	0.95	1.0	1.0
16:0–16:0–18:2	20.1	21.2	2.9
16:0–16:0–18:3	35.9	37.8	7.1
16:0–16:0–20:4	53.2	56.4	10.3
16:0–16:0–20:5	134.4	141.8	16.7
16:0–16:0–22:6	196.9	207.7	21.5

[a] For the corresponding fatty acid methyl ester [5].

cule increased from one to two. This could be ascribed to the appearance of a second complexing site in the molecule which enables the formation of a chelate type of complex, i.e. there is a simultaneous interaction of two double bonds and one silver ion. While methyl esters and triacylglycerols are similar in qualitative terms, there are quantitative differences. Methyl linoleate, for example, is held three times as strongly as methyl oleate, but dipalmitoyllinolein is held twenty times more strongly than dipalmitoylolein. Generally, the retention factor of a triacylglycerol was about 5 to 10 times greater than that of a comparable methyl ester.

The higher retention factors of triacylglycerols can be explained through two possible interactions: formation of a stronger silver ion complex because the triacylglycerol molecule is more rigid so that the double bond is approached more easily, and simultaneous interaction of a silver ion with the free electron pair of any of the three carbonyl oxygens. Both effects may play a part. Adsorption effects with the silica gel would not be expected to differ appreciable between methyl esters and triacylglycerols, and with the mobile phases used, hydrophobic interactions with the propylphenyl spacer should be minimal.

Table 4 presents the k' values of the most abundant natural triacylglycerols from olive, sunflower and linseed oil, i.e. the full series of triacylglycerols with zero to 9 double bonds. It is clear from the results that the retention of a monoacid or mixed acid triacylglycerol is not a simple sum of the k' values of the respective monounsaturated triacylglycerols. The data reveal that much more complex interactions occur when the number of double bonds increases. From an SSM triacylglycerol (1 double bond) to TTT (9 double bonds), the relative k' values increased from 1.0 to 10 000. As has been already observed, between triacylglycerols with an equal number of double bonds, one in which the double bonds are concentrated in one fatty

Table 4
k' values for natural triacylglycerols from olive oil, sunflower oil and linseed oil

Triacylglycerols[a]	k'	k'_{TG}/k'_{PPO}
SSM	0.95	1.0
SMM	10.6	11.2
SSD	19.5	20.6
MMM	30.2	31.9
SMD	61.4	64.8
MMD	139.6	147.2
MDD	403.3	425.4
SDD + SST	209.9	221.5
SMT	425.4	448.7
MMT	619.1	653.0
DDD + SDT	796.7	840.4
MDT	1154	1217
STT	1764	1861
DDT	1913	2018
MTT	2543	2683
DTT	4301	4538
TTT	9681	10212

[a] For the abbreviations see the footnote to Table 2.

acid moiety is held more strongly. Thus, SSD is held more than twice as strongly as SMM, and SMD more than twice as strongly as MMM, while the k' of SST is about seven times greater than that of MMM.

In the light of earlier findings [5], it seems probable that one silver ion can interact with two double bonds in different acyl moieties of one triacylglycerol at the same time, although the extent of this interaction may be limited by steric constraints. Whether double bonds in different acyl residues of one triacylglycerol molecule can interact with more than one silver atom simultaneously is not known. Neither is anything known of the nature of the surface of the stationary phase, the topology of silver ions and the conformation of the triacylglycerol molecule, so it is not possible to estimate what type of interaction is more probable. It seems likely that by increasing the number of double bonds leading to a different spatial position of the molecule, the number of single and separate complexation interactions with silver ions increases. The result is that the molecule spends a longer time on the stationary phase.

The greatest relative increase in k' value was between PPO and POO where the replacement of one saturated moiety with one monoenoic increased the k' value 10 times. This may indicate that chelate-type complexes are formed within the molecule. With an increasing number of double bonds, however, the relative rate of increase in the k' values tended to decrease, perhaps because the formation of chelate-type complexes is hindered by stereochemical factors. For example, the spatial arrangement of carbon atoms in different acyl chains may be such that double bonds are held too far apart to interact with a single silver ion simultaneously.

It is of interest to compare the data in Tables 3 and 4 from a practical point of view. The retention factor, k', is related to the selectivity of the separation. It was not possible to find conditions for isocratic elution that would provide reliable results in a reasonable time, and gradient elution seems essential. Critical pairs of triacylglycerols occur and these always have more than four double bonds. Of course, the selectivity of resolution is governed by other factors, and it may yet prove possible to select a mobile phase and gradient to solve these problems. Isocratic elution with acetone–acetonitrile (100:0.2, v/v) enabled successful resolution of the critical pair MDD–SMT. With increasing unsaturation, the difficulties become greater, although some useful separations have been achieved even with fish oils [7,14,15]. Acetonitrile is an essential component of the system, as it complexes strongly with silver ions displacing even polyunsaturated eluents. A more drastic change in the nature of the mobile phase will have profound influences on the order of elution as was observed, for example, in silver ion supercritical fluid chromatography [16].

The silver ion HPLC column has a rather low content of silver (less than 80 mg silver nitrate) [2], and this must be held as a mono-molecular layer at some distance from the silica surface (by the propylbenzenesulphonate spacer). The layer may not be uniform because of repulsion effects of the sulphonate residues. When operated isocratically, peak widths and shapes for unsaturated molecules are far from ideal and measurements of column efficiency indicated that there were only about 170 theoretical plates, although this is rather dependent on sample load. That the column works so well in practise, especially under gradient elution conditions, is undoubtedly due to the strength of the interaction between the silver ion and double bonds and the remarkable differences in the strengths of the interactions with molecules of different degrees of unsaturation, shown in Table 4.

4. Conclusion

The results therefore provide further evidence for the formation of chelate-type pi-complexes between silver ions and double bonds, with participation of the carbonyl oxygen in the complexation as a secondary effect. It is the strengths of these complexes, rather than column efficiency, which explain the high separating power of such columns.

Acknowledgements

This research was supported by the Karlshamns Research Board, Sweden, the Scottish Office Agriculture and Fisheries Department and the Bulgarian National Research Foundation.

References

[1] W.W. Christie, *High Performance Liquid Chromatography and Lipids*, Pergamon Press, Oxford, 1987.
[2] W.W. Christie, *J. High Resolut. Chromatogr. Chromatogr. Commun.*, 10 (1987) 148.
[3] B. Nikolova-Damyanova, in W.W. Christie (Editor), *Advances in Lipid Methodology - One*, The Oily Press, Ayr, 1992, pp. 181-237.
[4] B. Nikolova-Damyanova, B.G. Herslöf and W.W. Christie, *J. Chromatogr.*, 609 (1992) 133.
[5] W.W. Christie, *J. Chromatogr.*, 454 (1988) 273.
[6] B. Nikolova-Damyanova, W.W. Christie and B. Herslof, *J. Am. Oil Chem. Soc.*, 67 (1990) 503.
[7] P. Laakso and W.W. Christie, *J. Am. Oil Chem. Soc.*, 68 (1991) 213.
[8] P. Laakso and H. Kallio, *J. Am. Oil Chem. Soc.*, 70 (1993) 1161.
[9] P. Laakso, V.V. Nurmela and D.R. Homer, *J. Agric. Food Chem.*, 40 (1992) 2472.
[10] C.H. Winter, E.B. Hoving and F.A.J. Muskiet, *J. Chromatogr.*, 616 (1993) 9.
[11] L. Bruhl, E. Schulte and H.-P. Thier, *Fat Sci. Technol.*, 95 (1993) 370.
[12] F.H. Mattson and R.A. Volpenhein, *J. Lipid Res.*, 4 (1963) 392.
[13] *Gmelin Handbuch der Anorganischen Chemie*, Vol. 61, Teil B5, Springer, Berlin, 1975.
[14] P. Laakso, W.W. Christie and B. Pettersen, *Lipids*, 25 (1990) 284.
[15] A.S. McGill and C.F. Moffat, *Lipids*, 27 (1992) 360.
[16] L.G. Blomberg, M. Demirbuker and P.E. Andersson, *J. Am. Oil Chem. Soc.*, 70 (1993) 939.

ELSEVIER

Journal of Chromatography A, 694 (1995) 381–389

JOURNAL OF CHROMATOGRAPHY A

Separation and quantification of the triacylglycerols in evening primrose and borage oils by reversed-phase high-performance liquid chromatography

Peter R. Redden[a,*], Yung-Sheng Huang[b], Xiaorong Lin[a], David F. Horrobin[a]

[a]*Efamol Research Institute, Kentville, Nova Scotia, B4N 4H8, Canada*

[b]*Medical Nutritional R and D, Ross Products Division, Abbott Laboratories, 625 Cleveland Avenue, Columbus, OH 43215, USA*

First received 20 September 1994; revised manuscript received 18 November 1994

Abstract

Evening primrose and borage oil are used frequently in nutritional and clinical studies where an impaired Δ^6-desaturase enzyme activity may be bypassed by supplementation with γ-linolenic acid (GLA, 18:3$n-6$). The separation and quantification of the triglycerides of borage oil and evening primrose oil has been carried out using reversed-phase HPLC with UV detection. Borage oil was found to have 34 UV-detectable fractions and evening primrose 22. The TG fractions were collected manually, their fatty acid composition determined and quantified with an internal standard. The probable identity of the individual TG fractions was deduced using the fatty acid composition of the TG fractions, calculated theoretical carbon numbers (TCN) for the various TG species and the predicted probability of occurrence. Correction factors, U_i, for GLA (18:3$n-6$), gadoleic acid (20:1$n-9$), erucic acid (22:1$n-9$) and nervonic acid (24:1$n-9$) were estimated to be 0.3–0.4, 0.6, 0.4 and 0.3, respectively, and are used along with other known U_i correction factors for unsaturated fatty acids to calculate TCN values for all the TG species. These U_i values represent the loss in affinity of the unsaturated fatty acid for the reversed-phase C-18 stationary phase. The reversed-phase HPLC trace of borage oil is much more complex compared to evening primrose oil. Apart from differences in the total fatty acid composition there are substantial differences in the quantity of individual TG species present in the two oils. The clinically important fatty acid, γ-linolenic acid, is distributed much more widely throughout the TG species of borage oil compared to evening primrose oil. Over 90% of the GLA present in evening primrose occurs in the first 9 eluting TG species whereas only about 65% is found in these TG species of borage oil.

1. Introduction

Clinical evidence has shown that diseases possibly associated with an impaired Δ^6-desaturase activity as indicated by deficits of linoleic acid metabolites, may be alleviated by dietary supplementation of γ-linolenic acid (GLA, 18:3$n-6$), an intermediate Δ^6-desaturation product of linoleic acid (LA, 18:2$n-6$) [1–5]. In human and animal tissues, GLA levels are generally low because GLA is rapidly metabolized to 20:3$n-6$ and subsequently to 20:4$n-6$ [6]. However, significant levels of GLA, mainly in

* Corresponding author.

0021-9673/95/$09.50
SSDI 0021-9673(94)01148-6

the triacylglycerol (TG) form, have been found in evening primrose oil (EPO, *Oenothera biennis*), borage oil (BO, *Borago officinalis*), black currant seed oil (*Ribes nigrum*) and fungal oils (e.g. *Mucor javanicus*) [7,8]. Among these, EPO and BO are used most frequently in nutritional and clinical studies. However, the biological potency of these two oils appears to be quite different [9–15]. Thus BO and EPO do not have equivalent effects explicable on the basis of the GLA content of the oils.

There are several possible explanations for this. Apart from GLA there are substantial differences in the overall fatty acid compositions of the two oils (Tables 1 and 2). There may be minor non-triglyceride components of the oils which exert pharmacological effects. Alternatively, the association of GLA with other fatty acids in the TG molecules may modulate GLA potency in exerting its beneficial effects. Additionally, fats with similar fatty acid composition but different TG structures exert different biological activities [16–18]. For example peanut oil in its native state is relatively atherogenic, however, when peanut oil is randomized it loses its atherogenicity [16,17]. In this article we were interested in comparing the identification and quantitation of the individual TG species between the two oils.

The HPLC separation of the TG species of natural fats and oils has been carried out by numerous workers with a wide variety of solvents and methods of detection [19–24]. Although the separations in most cases was good, the identification of the individual TG fractions was made solely on the basis of their retention times; consequently the assignments were incomplete and in some cases incorrect. Here we describe the separation, identification and distribution of the TG species in EPO and in borage oil using highly efficient reversed-phase HPLC columns. The individual TG fractions as they elute from the HPLC column were collected, their fatty acid composition determined and quantitated by GC using an internal standard. In addition, a comparison of the TG species was made between quantification with an internal standard and integration of the areas of the TG species obtained with an evaporative light-scattering detector.

2. Experimental

HPLC grade isopropanol, chloroform, and acetonitrile were purchased from BDH (Toronto, Ont., Canada). BF_3-methanol was supplied by Pierce Chemical Co. (St. Louis, MO, USA). The TG standards tri-γ-linolenin (GGG) and trilinolein (LLL) were purchased from Nu-Chek Prep (Elysian, MN, USA) Pure di-γ-linoleneoyl-monolinolein (LGG), and dilinoleoyl-mono-γ-linolenin (LGL) were purified by semi-prep HPLC as outlined below from a sample of EPO enriched in unsaturated TG species (Callanish, Breasclete, Scotland). Note that the abbreviations used for TG's are meant to mean all positional isomers of a particular TG and according to a rule often used in reversed-phase HPLC are named with the shortest or most saturated fatty acid chain first and most highly unsaturated fatty acid chain in the middle. The triacylglycerol components in cold pressed olive oil, evening primrose oil (Efamol, Guildford, U.K.) and borage oil (Callanish) were purified by silica gel column chromatography using 3% diethyl ether in hexane.

HPLC analysis was carried out using a Beckman System Gold solvent module 126, autosampler Model 507 and variable UV wavelength detector Model 166. The following column, conditions and solvent system were used for the purification of LGG and LGL from the enriched unsaturated TG EPO sample. The column used was a μ-Bondapak C-18 radial-pak 10 cm × 25 mm, 6 μm (Millipore Corp., Milford, MA, USA). The solvent system was acetonitrile–2-propanol (65:35 v/v) at a flow rate of 10 ml/min with UV detection at 218 nm. The following columns, conditions and solvent system were used for the separation of the TG species of the various oils. A reversed-phase Supelcosil LC-18 column (25 cm × 4.6 mm, 5 μm, Supelco, Bellefonte, PA, USA), was used for the separation and analysis. The purified oils were dissolved in chloroform (200 mg/ml) and eluted with

Table 1
Fatty acid composition (area % of the total fatty acids) of the TG fractions of borage oil separated by reversed-phase HPLC

Fraction no.	16:0	18:0	18:1 $n-9$	18:1 $n-7$	18:2 $n-6$	18:3 $n-6$	20:1 $n-9$	22:1 $n-9$	24:1 $n-9$	Other
Total oil	11.3	3.9	18.9	0.1	37.6	20.6	3.5	1.8	0.8	1.5
1						99.9				0.1
2	2.1	1.1	3.5		33.1	59.1				1.1
3	0.8	0.4	0.8		64.7	32.4				1.0
4	3.2	2.2	26.8	2.8	9.3	55.8				
5	29.0	1.7	2.5		3.1	62.9				
6	1.7	1.0	1.3		93.8	1.7				0.5
7	0.7	0.4	30.9	1.4	33.8	31.7	0.3			0.8
8	27.3	0.5	2.2		32.9	34.8	1.7			0.6
9	15.4	20.4	7.9		11.9	38.1				6.3
10	0.7	0.7	31.6	1.2	64.1	0.9	0.5			0.4
11	14.7	0.5	15.5	0.6	43.6	15.4	8.6	0.4		0.7
12	16.3	13.7	19.1	0.8	16.8	32.2	0.5	0.6		
13	51.8	3.1	3.8		4.9	36.3				
14	2.4	1.2	7.3	1.4	55.0	1.6	29.9			1.2
15	1.4	1.7	39.8	1.1	29.4	9.1	2.3	9.2	1.5	3.1
16	17.4	9.0	24.3	0.8	40.7	3.9	3.0	0.9		
17	31.6	9.7	10.5	0.5	17.9	18.8	8.8			1.8
18	27.4	30.7	5.4		8.9	27.7				
19	1.7	2.1	6.1		52.1		7.0	31.0		
20	3.0	3.0	28.7		32.8		32.4			
21	1.8	0.8	53.2	1.1	11.7	11.2	4.9	2.9	10.3	2.1
22	9.9	6.8	9.6		30.2	3.1	31.9	4.6		4.0
23	12.0	18.1	41.7	1.2	21.9		3.8			1.3
24	19.6	8.8	36.2		6.5	12.6	4.7	11.6		
25	38.1	22.5	16.7		20.8	1.8				
26	13.7	37.7				20.3			28.3	
27			8.8		41.5		5.5	12.8	25.7	5.7
28			35.7		19.6		14.7	25.5		4.4
29	11.1	6.2	22.1		16.7	3.5	19.7	13.8	3.4	3.2
30	8.5	21.2	37.8		2.9	10.2	4.5	4.0	9.4	1.5
31	19.7	43.0	25.6		11.7					
32	6.0	3.8	32.5		13.4	2.3	6.7	17.2	15.7	2.4
33	17.6	8.8	12.4		22.4		3.2	18.5	17.1	
34	9.7	17.3	26.1		9.0	5.9	10.5	7.0		14.5
Total recom.	10.9	5.2	18.7	1.0	34.8	19.3	4.4	2.9	1.4	

The total recombined fatty acid composition was determined by computation using an internal standard.

acetonitrile–2-propanol (65:35 v/v) at a flow of 1 ml/min and UV detection at 210 nm. The eluting TG species emerging from the UV detector were collected manually for fatty acid analysis by GC. When the evaporative light-scattering detector (ACS Model 740/14, Applied Chromatography System, Macclesfield, England) was used the settings were as follows: attenuation range, 16; photomultiplier sensitivity, 5; time constant, 5 s; evaporator set, 40 and internal air pressure, 187 kPa. The output signal analysis and integration were performed with an IBM PS/2 computer using the System Gold software (version 3.1).

GC analysis was carried out using a Hewlett-

Table 2
Fatty acid composition (area % of the total fatty acids) of the TG fractions of EPO separated by reversed-phase HPLC

Fraction no.	16:0	16:1 $n-7$	18:0	18:1 $n-9$	18:1 $n-7$	18:2 $n-6$	18:3 $n-6$	Other
Total oil	5.3	0.1	1.0	6.4	0.6	75.1	11.3	0.4
1							tr	
2	7.3	1.1	1.9	6.3		37.6	43.9	1.8
3	1.0		0.2	1.1		65.7	31.4	0.5
4	10.7		7.5	20.7		32.6	28.5	
5	24.4		8.8	11.6		20.4	34.8	
6	0.2	0.1	0.1	0.2		99.4	0.1	
7	2.3		1.3	26.9	2.6	39.0	27.2	0.7
8	28.8	1.4	1.3	2.0		35.3	30.6	0.5
9	20.1		24.3			33.5	22.2	0.6
10	1.2	0.7	0.4	30.1	2.6	64.4		
11	28.8			2.0		68.2	1.0	
12	10.7		24.1	10.4		28.7	26.1	
13	33.2		10.4	8.5		29.7	18.1	
14	17.2	5.5	8.4	14.7		54.3		
15	2.7	0.8	1.6	57.9	3.4	33.6		
16	14.0		18.6	15.3	1.0	51.1		
17	44.7		6.7	5.9		34.6	8.1	
18	20.8		20.2			32.7	26.3	
19	11.7		7.7	55.2		25.4		
20	11.9	4.2	16.3	23.9		38.0		5.7
21	31.9		28.3	8.5		28.1	3.2	
22	13.7	2.7	7.8	6.0		66.6	1.6	1.5
Total recom.	7.0	0.3	2.4	8.6	0.5	72.3	8.9	

The total recombined fatty acid composition was determined by computation using an internal standard.

Packard Model 5890 chromatograph equipped with a flame ionization detector [25]. The column was a fused capillary Omegawax column (30 m × 0.32 mm, 0.25 μm film thickness, Supelco) at a split ratio of 1:25, injection port temperature of 200°C, detector temperature of 220°C and an oven temperature programmed at 165°C for 2 min then 6°C/min to 180°C and then held at 180°C for 13 min. The individual TG species collected after evaporation of the solvent were methylated along with an internal standard (heptadecanoic acid) in 2 ml of toluene and 2 ml of 14% BF_3-methanol at 90°C for 30 min, cooled, 2 ml of 0.9% saline added and the required methyl esters extracted with hexane (5 ml).

3. Results and discussion

The reversed-phase HPLC traces of borage oil and EPO with UV detection at 210 nm are given in Fig. 1. Broadly speaking the TG profile of borage oil is more complex than EPO: EPO was found to have 22 UV detectable TG fractions and borage oil 34. The fatty acid profiles of the individual TG fractions for borage oil and EPO are given in Tables 1 and 2, respectively. The analysis and separation of TG's by reversed-phase HPLC is sometimes difficult as both the degree of unsaturation and chain length of the fatty acyl groups are important. One of these difficulties is the formation of "critical pairs"

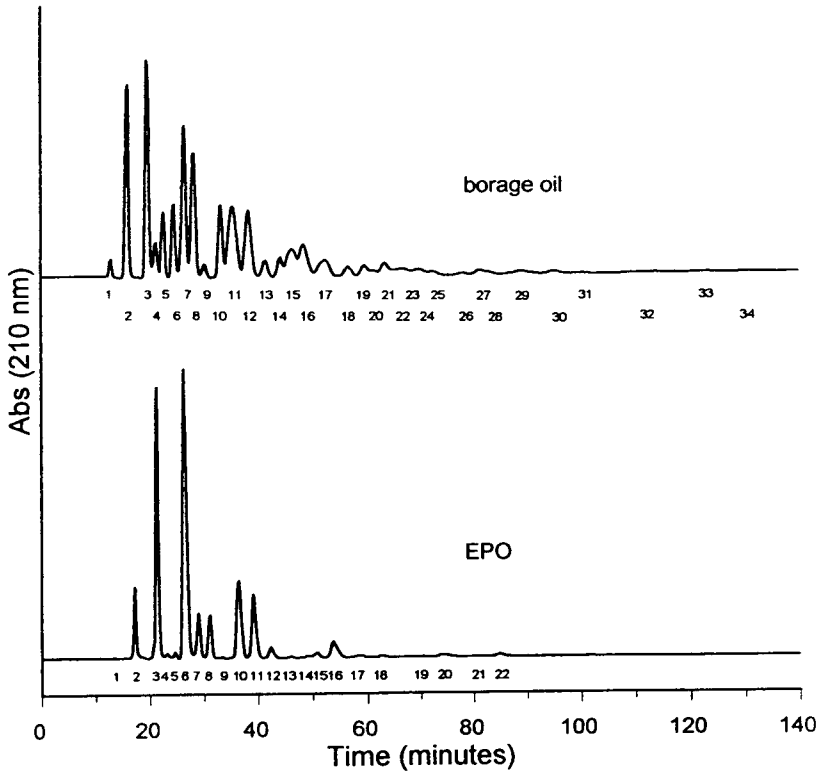

Fig. 1. Reversed-phase HPLC profile of the triglycerides of EPO and borage oil using a Supelcosil LC-18 column (250 × 4.6 mm I.D., 5 μm) with isopropanol–acetonitrile (35:65, v/v) at a flow rate of 1 ml/min and detection by UV absorption at 210 nm. The fractions collected for GC analysis are shown above the baseline.

which elute close to one another during reversed-phase chromatography in spite of differences in chain lengths and number of double bonds. Critical pairs are defined as structures with an equivalent carbon number (ECN),

$$ECN = CN - 2n$$

where CN equals the number of carbon atoms in the fatty acids and n equals the number of double bonds per molecule. It has, however, been demonstrated [22] that the reversed-phase HPLC retention times of TG's are in a positive logarithmic relationship to their theoretical carbon number, TCN, defined as

$$TCN = ECN - \sum U_i$$

where ECN is the equivalent chain length defined as above and U_i represents a correction factor summed for all three fatty acids of the TG. These U_i values are determined experimentally and were determined to be zero for saturated fatty acids, 0.6–0.65 for oleic acid and 0.7–0.8 for linoleic acid [21].

The U_i values for GLA found in borage oil and EPO and for gadoleic acid, 20:1$n-9$; erucic acid, 22:1$n-9$ and nervonic acid, 24:1$n-9$ found in borage oil have not been determined. However, a good estimation of the U_i value for GLA was determined by co-eluting isocratically a mixture of the pure TG's, GGG, LGG, LGL and LLL along with olive oil rich in OLL, OLO, PLO, PLP, OOO and SOO. By plotting the log

RRT for the olive oil TG species against their corresponding known TCN values and extrapolating the line through the observed log RRT values for the GLA-containing TG species it was possible to assess the TCN values for GGG, LGG and LGL to be 35.0, 36.5 and 38.0, respectively (Fig. 2). Relative Retention Time, RRT, values (relative to LLL) are used instead of retention times or capacity factors since the latter are subject to drifting during the analysis. Using the value of 0.8 for the U_i for L sets the U_i value for GLA at 0.3–0.4. Although it has been stated that the values of U_i vary with elution conditions we have assumed the values for linoleic acid and oleic acid to be the same or at least similar under our elution conditions [19].

Similarly an estimation of the U_i values for $20{:}1n-9$, abbreviated Ga; $22{:}1n-9$, abbreviated E; and $24{:}1n-9$, abbreviated N, can also be determined using Fig. 2. As given in Table 1 the 14th fraction of borage oil was found to be predominantly GaLL. This fraction was observed to have a TCN value of 44.0, corresponding to a U_i value for $20{:}1n-9$ of 0.6. Similarly fraction 19 of borage oil was determined to be mainly ELL and fraction 27 was determined to be predominantly NLL allowing calculation of a U_i value for $22{:}1n-9$ of 0.4 and a U_i value for $24{:}1n-9$ of 0.3. Using these estimated U_i values allows calculation of the TCN values for the various other TG species found in the two oils.

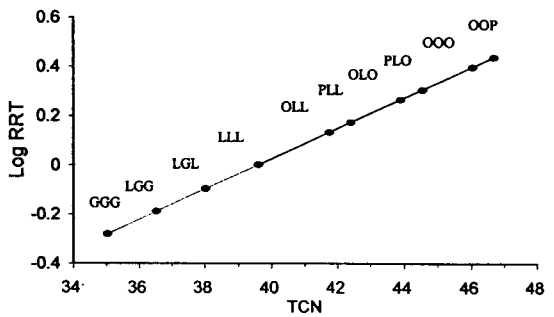

Fig. 2. Log RRT of triglyceride standards of olive oil versus their theoretical carbon number, (TCN), $r^2 = 0.9993$. The separation of the TG's was performed with the same conditions as described for Fig. 1. The TCN values for the GLA-containing TG's were estimated by extrapolating the plot through the observed log RRT values for the GLA-containing TG's.

To a first approximation there is general agreement that the distribution of fatty acids among the TG's of unsaturated vegetable oils follows a random distribution. Previously an algorithm has been devised which follows the random theory of distribution [26]. The proportion of each TG is then calculated from probability. The algorithm used is

$$\eta = n \cdot p$$

where η is the probability of occurrence of a given TG, n is a weighting factor for the number of times the same fatty acid occurs in the TG (n is either 1, 3 or 6 depending on whether a fatty acid occurs 3 times, 2 times or only once, respectively in the TG) and p is the percentage abundance of the fatty acid present in the fat. For the borage oil and EPO samples examined here the probability of the various TG species occurring in the oils are given in Tables 3 and 4, respectively, with TG species less than 0.05% being excluded.

Hence, using these probability values, along with the fatty acid composition of the TG fractions collected, and comparing the observed TCN values with calculated TCN values, the identity or probable identity of the TG species present in the fractions was deduced. These are shown in Tables 3 and 4 as well. Since the fatty acid composition of the individual TG fractions were determined and their retention times are related to their TCN values, reasonably reliable identification was possible. Certainly, if available, mass spectroscopy would provide verification of the assignments.

The individual TG fractions of both borage oil and EPO were quantitated using heptadecanoic acid as an internal standard. Of all the detection methods available for quantification, GC analysis of the fatty acid constituents of the TG species in the presence of an internal standard would be expected to give a high degree of precision [19]. These results are presented in Tables 3 and 4, respectively. With regards to quantification of the TG fractions, a check on the recovery of the fatty acids by computation (Total Recom. Tables

Table 3
Probable TG species, observed theoretical carbon number (TCN), calculated TCN, probability of occurrence and weight% distribution for the TG fractions of borage oil separated by reversed-phase HPLC

Fraction #	Prob. TG	Obs. TCN	Cal. TCN	Prob. (%)	Weight% (IS)	Weight% (ELS)
1	GGG	35.0	34.8	0.9	0.6	0.3
2	LGG	36.5	36.4	4.8	4.7	7.4
3	LGL	38.0	38.0	8.7	8.3	12.9
4	OGG	38.5	38.6	2.4	1.0	0.6
5	PGG	39.1	39.2	1.4	1.9	1.5
6	LLL	39.6	39.6	5.3	4.0	5.3
7	OGL	40.2	40.2	8.8	7.4	11.6
8	PGL, GaGG	40.6	40.6, 40.8	5.3, 0.4	6.1	9.2
9	SGG	41.3	41.2	0.5	1.0	0.1
10	OLL	41.8	41.8	8.0	5.1	9.6
11	GaGL, OGO	42.3	42.2, 42.3	1.6, 2.2	9.0	12.4
	PLL		42.4	4.8		
12	SGL, EGG	42.8	42.8, 42.8	1.8, 0.2	5.6	5.9
	PGO		43.0	2.7		
13	PGP	43.4	43.6	0.8	1.3	0.6
14	GaLL	43.8	43.8	1.5	2.3	1.5
15	OLO	44.2	43.9	4.9	5.8	5.4
16	SLL, OGGa	44.5	44.4, 44.4	1.7, 0.8	7.2	7.8
	EGL, PLO		44.4, 44.6	0.9, 4.8		
17	SGO, PGGa	45.1	45.0, 45.0	0.9, 0.5	3.4	1.8
	PLP		45.2	1.4		
18	PGS	45.6	45.6	0.6	1.1	0.2
19	ELL	46.0	46.0	0.8	1.8	0.6
20	OLGa	46.1	46.0	3.2	1.1	0.4
21	OOO, GaGGa	46.4	46.1, 46.4	0.7, 0.1	3.1	1.6
	NGL		46.5	0.4		
22	PLGa, SLO	46.7	46.6, 46.6	0.9, 1.7	1.2	nd
	OGE		46.6	0.4		
23	POO	46.8	46.7	1.2	2.6	2.6
24	SGGa, PGE	47.0	47.0, 47.2	0.2, 0.3	2.2	nd
25	PLS, POP	47.4	47.2, 47.4	1.0, 0.7	1.6	0.4
26	SGS, PPP	47.9	47.6, 48.0	0.1, 0.2	0.4	nd
27	GaLGa, NLL	48.1	48.0, 48.1	0.1, 0.3	1.6	0.1
28	OOGa, OLE	48.3	48.1, 48.2	0.4, 0.8	0.7	nd
29	SLGa, GaGE	48.8	48.6, 48.6	0.3, 0.1	2.4	nd
	OGN, SOO		48.7, 48.7	0.2, 0.4		
	POGa, PLE		48.8, 48.8	0.4, 0.5		
30	SLS, SGE	49.3	49.2, 49.2	0.2, 0.1	1.7	0.3
	PGN, PGaP		49.3, 49.4	0.1, 0.1		
31	POS	49.6	49.4	0.5	0.8	nd
32	PSP, OGaGa	50.5	50.0, 50.2	0.2, 0.1	1.5	nd
	GaLE, OOE		50.2, 50.3	0.1, 0.2		
	OLN, OGaE		50.3, 50.4	0.4, 0.1		
33	SOGa, PLN	51.0	50.8, 50.9	0.2, 0.2	0.9	0.04
	SLE, POE		50.9, 51.0	0.2, 0.2		
34	PGaS, PEP	51.5	51.4, 51.6	0.1, 0.1	0.6	nd

Abbreviations: nd, not detected; P, Palmitic; Po, Palmitoleic; S, Stearic; O, oleic; L, linoleic; G, γ-linolenic; Ga, Gadoleic; E, erucic; N, nervonic acids; IS, internal standard quantitation with heptadecanoic acid and ELS, quantitation based on integration of the TG peaks using an evaporative light-scattering detector.

Table 4
Probable TG Species, observed theoretical carbon number (TCN), calculated TCN, probability of occurrence and weight% distribution for the TG fractions of EPO separated by reversed-phase HPLC

Fraction #	Prob. TG	Obs. TCN	Cal. TCN	Prob. (%)	Weight% (IS)	Weight% (ELS)
1	GGG	35.3	34.8	0.1	nd	nd
2	LGG	36.9	36.4	2.9	2.7	1.2
3	LGL	38.3	38.0	19.0	14.7	20.8
4	OGG	38.9	38.6	0.3	0.5	nd
5	PGG	39.3	39.2	0.2	0.4	nd
6	LLL	39.6	39.6	42.3	38.0	48.3
7	OGL	40.4	40.2	3.5	3.3	1.7
8	PGL	40.9	40.8	2.7	3.2	1.6
9	SGG	41.4	41.2	0.04	0.3	nd
10	OLL	41.9	41.8	11.8	12.3	14.6
11	OGO, PLL	42.4	42.3, 42.4	0.2, 8.9	10.9	9.2
12	SGL, PGO	43.0	42.8, 43.0	0.5, 0.3	1.5	nd
13	PGP	43.6	43.6	0.09	0.3	nd
14	PoLL	44.0	–	–	0.5	nd
15	OLO	44.3	43.9	1.1	2.1	0.7
16	SLL, PLO	44.6	44.4, 44.6	1.7, 1.7	5.1	1.9
17	SGO, PLP	45.3	45.0, 45.2	0.05, 0.6	1.1	nd
18	PGS	45.7	45.6	0.04	0.4	nd
19	OOO, SLO	46.5	46.1, 46.6	0.03, 0.3	0.4	nd
20	POO	46.9	46.7	0.08	1.5	nd
21	PLS, POP	47.5	47.2, 47.4	0.24, 0.06	0.5	nd
22	PPP	47.5	48.0	0.01	0.5	nd

Abbreviations as described for Table 3.

1 and 2) confirms that recoveries were nearly quantitative using an internal standard. Overall, there is partial agreement between the ELS detector and internal standard quantification; however, the ELS results tend to be higher for the major fractions and lower for minor fractions. In fact, in most cases the minor TG's were not detected with the ELS detector. It is known that the response of the ELS detector with respect to mass is sigmoidal for TG standards [19]. This means that it is necessary to calibrate the ELS detector with a wide range of TG standards before quantification can be determined with an ELS detector.

The triglyceride structure of borage oil is clearly much more complex than that of EPO and some empirical observations can be noted. From a comparison of Tables 3 and 4, three fractions, LGG, LLL and LGL account for only 17.0% by weight of borage oil whereas they account for 55.4% by weight of EPO. Over 75% of EPO is accounted for by four fractions, whereas the most abundant four fractions of borage oil account for only 32.9% of the oil. Moreover, over 90% of the GLA present in EPO can be accounted for in the first 9 eluting TG species whereas only about 65% can be accounted for in these species in borage oil.

The predicted probability of a TG species occurring in the two oils agrees well with the values quantitated using an internal standard. This experimental observation agrees with that previously seen for other polyunsaturated oils [26]. However, this does not mean that, within a particular TG species, the fatty acids are distributed evenly: the positional isomeric composition of a particular TG species must be determined experimentally. Further studies determining which positional isomers of a particular TG species, in particular the GLA containing TG species, and to what extent each occurs in the two oils are in progress.

References

[1] S. Wright and J.L. Burton, *Lancet II*, (1982) 1120.
[2] J. Chaintreuil, L. Monnier, C. Colette, P. Crastes de Paulet, A. Orsetti, D. Speilmann, F. Mendy and A. Craste de Paulet, *Hum. Nutr. Clin. Nutr.*, 38C (1984) 121.
[3] J.K. Pye, R.E. Mansel and L.E. Hughes, *Lancet II*, (1985) 373.
[4] J. Poulakka, L. Makarainen, L. Viinikka and O. Ylikorkala, *J. Reprod. Med.*, 30 (1985) 149.
[5] D.F. Horrobin, *Rev. Contemp. Pharmacother.*, 1 (1990) 1.
[6] H. Sprecher, *Progr. Lipid Res.*, 20 (1981) 13.
[7] B.J.F. Hudson, *Hum. Nutr. Food Sci. Nutr.*, 41F (1987) 1.
[8] Horrobin, D.F. in G. Galli and A.P. Simopoulos (Editors), *Dietary ω3 and ω6 Fatty Acids*, Plenum Publishing Corp., New York, 1989, p. 297.
[9] D.K. Jenkins, J.C. Mitchell, M.S. Manku and D.F. Horrobin, *Med. Sci. Res.*, 16 (1988) 525.
[10] L.D. Lawson and B.G. Hughes, *Lipids*, 23 (1988) 313.
[11] Y.-Y Fan and R.S. Chapkin, *J. Nutr.*, 122 (1992) 1600.
[12] M.M. Engler, *Prostaglandins, Leukotrienes and Essential Fatty Acids*, 49 (1993) 809.
[13] D.E. Barre, B.J. Holub and R.S. Chapkin, *Nutr. Res.*, 13 (1993) 739.
[14] L. Monner, S. El Boustani, A. Crastes de Paulet, B. Descomps and F. Mendy, *Corps. Gras*, in press.
[15] N.E. Cameron, M.A. Cotter, K.C. Dines, S. Robertson and D. Cox, *Br. J. Pharmacol.*, 109 (1993) 972.
[16] D. Kritchevsky, *Arch. Pathol. Lab. Med.*, 112 (1988) 1041.
[17] D. Kritchevsky, S.A. Tepper, D. Vesselinovitch and R.W. Wissler, *Atheroscler.*, 17 (1973) 225.
[18] M.M. Jensen, M.S. Christensen and C.-E. Hoy, *Ann. Nutr. Metab.*, 38 (1994) 104.
[19] W.W. Christie, *HPLC and Lipids, A Practical Guide*, Pergamon, Oxford, 1987.
[20] W.M.N. Ratnayake, D.G. Matthews and R.G. Ackman, *J. Am. Oil Chem. Soc.*, 66 (1989) 966.
[21] W.W. Christie, *Fat. Sci. Tech.*, 93 (1991) 65.
[22] A.H. El-Hamdy and E.G. Perkins, *J. Am. Oil Chem. Soc.*, 58 (1981) 867.
[23] J.L. Perrin, A. Prevot, H. Traitler and U. Bracco, *Rev. Franc. Corps Gras.*, 34(4) (1987) 221-223.
[24] K. Aitzetmuller and M. Gronheim, *J. High Resolut. Chromatogr.*, 15 (1992) 219.
[25] Y.-S. Huang, R. Smith, P.R. Redden, R.C. Cantrill and D.F. Horrobin, *Biochem. Biophys. Acta.*, 1082 (1991) 319.
[26] C. Merritt, Jr., M. Vajdi, S.G. Kayser, J.W. Halliday and M.L. Bazinet, *J. Am. Oil Chem. Soc.*, 59 (1982) 422.

ELSEVIER

Journal of Chromatography A, 694 (1995) 391–398

JOURNAL OF CHROMATOGRAPHY A

Pulsed electrochemical detection of alkanolamines separated by multimodal high-performance liquid chromatography

David A. Dobberpuhl[1], Dennis C. Johnson*

Department of Chemistry, Iowa State University, Ames, IA 50011, USA

First received 19 August 1994; revised manuscript received 3 November 1994; accepted 8 November 1994

Abstract

Pulsed electrochemical detection (PED) is applied to alkanolamines separated by high-performance liquid chromatography (HPLC). A multimodal HPLC column with both cation-exchange and reversed-phase retention modes is used with an acidic mobile phase to assure alkanolamines are in their cationic form. Baseline resolution of alkanolamines, including positional isomers, is possible. Detector response for a representative alkanolamine, tris(hydroxymethyl)aminomethane (Tris), is shown to be linear over a concentration range of more than three decades. The limit of detection for Tris is 20 n*M* (500 fmol in a 25-μl injection) and the standard deviation of the PED response for 10 μM Tris is better than 0.4%. HPLC–PED is demonstrated to permit the sensitive and precise determination of alkanolamines in a biological sample (blood) and a commercial formulation (shaving gel) with minimal sample preparation.

1. Introduction

Alkanolamines are used extensively by chemical and pharmaceutical industries as lubricants, corrosion inhibitors, emulsifying agents, and as ingredients of various pharmaceutical preparations. Furthermore, they are often utilized for metal surface finishing, gas purification, and as additives and dyes in cleaning solutions [1,2]. Because alkanolamines are used in many ways, and since they have been identified as pollutants in certain waste water effluents [3], there is a strong need to quantify alkanolamines with high sensitivity and accuracy, and without extensive sample manipulation.

Methods used to determine alkanolamines have included wet chemical techniques, gas chromatography, thin-layer chromatography, and high-performance liquid and ion chromatography (HPLC, HPIC) coupled with spectrometric, electrochemical or conductivity detection. Wet chemical techniques generally are more precise than instrumental methods; however, their application to complex real-life matrices is made difficult by the need to isolate the analytes from the sample matrix. Gas chromatography is possible [4–8], but the high polarity of alkanolamines makes them difficult to analyze in this manner. Thin-layer chromatography with photometric detection has been demonstrated for the determination of β-alkanolamines [9]. However, because of the absence of natural chromophores and/or fluorophores, photometric detection of alkanolamines requires they be

* Corresponding author.

[1] Present address: Department of Chemistry, Creighton University, Omaha, NE 68178, USA.

0021-9673/95/$09.50
SSDI 0021-9673(94)01094-3

derivatized with a spectrometrically active adduct. The same is true for the HPLC techniques utilizing photometric detection [10–14]. Derivatization techniques can be time-consuming, and quantitation sometimes made difficult because the alkanolamines are derivatized with varying efficiencies in different sample matrices. Therefore, direct detection is preferable whenever possible. Conductivity detection has been used for the direct detection of alkanolamines separated by HPIC [15–17]; however, the sensitivity of conductivity detection is generally not as good as that of most other chromatographic detection methods.

Recently, pulsed electrochemical detection (PED) coupled with HPLC has been shown to be a viable method for the determination of alkanolamines. LaCourse et al. [18] demonstrated the separation of mono-, di- and trialkanolamines using a dodecanesulfonate ion-pair reagent and a silica-based C_{18} reversed-phase column. Although determination of alkanolamines was possible at the ppb level, relatively long chromatographic runs (1–2 h) were necessary to obtain reasonable separation. Campbell et al. [2] also determined alkanolamines via HPLC–PED, employing the reversed-phase characteristics of a polymer-based column (Dionex PAX-500) to separate diethanolamine (DEA) and triethanolamine (TEA) in an aluminum etching bath. However, use of the same column in our laboratory indicated that the smaller and more hydrophilic alkanolamines were not strongly retained, and often were unresolved from each other and from the solvent peak.

Because of the hydrophilic nature of aliphatic alkanolamines, HPIC seemed to hold greater promise than reversed-phase HPLC as a separation technique for these compounds. However, a column that combines both cation-exchange and reversed-phase retention properties (Dionex PCX-500) might be expected to hold advantages for alkanolamine separations. A preliminary demonstration of HPLC–PED using this type of column was included in a recent review [19]. Herein we provide a more complete description of alkanolamine retention on a so-called "multimodal" column. The separation of alkanolamines is studied as a function of mobile phase composition, with retention measured versus both the counter cation (Na^+) and organic modifier (acetonitrile, ACN) concentration in the eluent. Using optimized isocratic conditions, baseline resolution is shown for a mixture of alkanolamines, including positional isomers. The method is also demonstrated for the determination of alkanolamines in a commercial formulation and a biological sample.

2. Experimental

2.1. Reagents

All chemicals used in preparation of chromatographic eluents were reagent grade or better and used as received. Sodium acetate (Fisher) was obtained in either anhydrous or trihydrate form. Glacial acetic acid (Fisher) and acetonitrile (Fisher) were HPLC grade. All mobile phases were filtered through a 0.2-μm nylon filter (Whatman) prior to use. The 0.30 *M* solution of NaOH mixed with the chromatographic effluent stream was prepared by dilution of a commercially available 50% (w/w) solution (Fisher).

Ethanolamine (Fisher) and all other alkanolamines (Aldrich) were of the best grade available. Perchloric acid (Fisher) used for dilution of biological samples was reagent grade. Water for all solutions was purified by passing tap water through two D-45 deionizing tanks (Culligan) and a Milli-Q system (Millipore).

2.2. Voltammetric apparatus and procedures

Pulsed voltammetry was performed at the gold disk of an AFMT28AUAU rotating ring-disk electrode (RRDE, Pine Instruments). Rotation of the electrode was provided by an AFMSR rotator (Pine). The counter electrode for the electrochemical cell was provided by a coiled platinum wire. Potentials are reported versus a saturated calomel electrode (SCE, Fisher). The electrochemical cell was made of Pyrex, and had porous glass frits separating the compartments for the working, reference and counter elec-

trodes. Potential control was maintained with an AFRDE4 bi-potentiostat (Pine) interfaced to a personal computer (PC, Jameco) via a DT2801-A data acquisition board (Data Translation). Potential–time waveforms were generated by the PC using programs written in ASYST 4.0 software (Keithley/Asyst). Electrolyte solutions were deaerated by dispersed nitrogen gas.

2.3. Chromatographic apparatus and procedures

Unless noted otherwise, all chromatographic equipment was from Dionex. Separations utilized either a full-sized (250 × 4 mm) or guard (50 × 4 mm) version of the PCX-500 column. Sample injection was provided by a pneumatically activated injector equipped with a 25-μl sample loop. A GPM gradient pump and pulsed electrochemical detector were interfaced to a Zenith PC through an AI-450 chromatography automation system.

The Dionex PED system provides the options of obtaining an output signal corresponding to: (i) the time-integral of electrode current over the integration period of the waveform ($\int i\partial t$, C) or (ii) the average current with the integration period ($\int i\partial t/t_{INT}$, C s^{-1}). The first option was selected in this research. PED was performed in a flow-through cell consisting of a 1.4-mm diameter Au working electrode and a Ag/AgCl reference electrode. The counter electrode was provided by the upper half of the detection cell, which was made of stainless steel. A solution of 0.30 *M* NaOH was added post-column through a mixing tee, with constant flow maintained by a post-column pneumatic controller. The post-column eluent had a final pH of ca. 13, providing the alkaline environment necessary for alkanolamine detection at the Au working electrode.

3. Results and discussion

3.1. Voltammetry of alkanolamines

Selection of the optimal detection potential for use in HPLC–PED was based on current–potential (i–E) curves obtained by pulsed voltammetry. Typical results are shown in Fig. 1 for tris(hydroxymethyl)aminomethane (Tris). Use of pulsed voltammetry for optimization of PED waveforms has been described [20]. The data in Fig. 1 were obtained by positive scan of the detection potential (E_{DET}) according to a staircase waveform consisting of 10-mV step increments, while maintaining the oxidative cleaning potential (E_{OXD}) and reductive regeneration potential (E_{RED}) at constant value of +0.80 V and −0.80 V, respectively. Values of electrode current shown in Fig. 1 correspond to average values for an integration period (t_{INT}) of 50 ms following a delay period (t_{DEL}) of 250 ms during the detection period ($t_{DET} = t_{DEL} + t_{INT}$) for each application of the PED waveform.

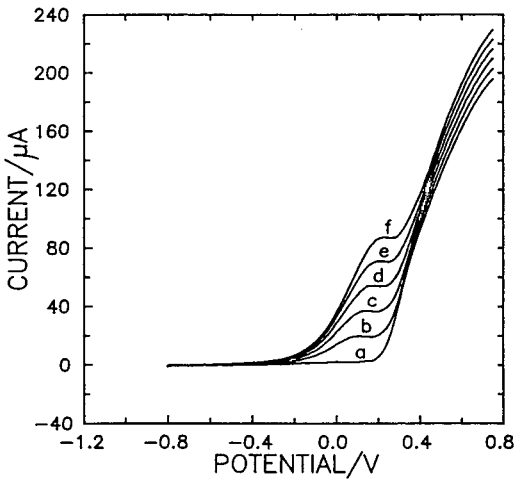

Fig. 1. Pulsed voltammetric response of Tris at a Au RDE in 0.1 *M* NaOH. Rotation rate: 400 rpm. Potential waveform: E_{DET} in the PED waveform is scanned from −0.80 V to 0.75 V according to a staircase waveform using 10-mV step increments (t_{DET} = 300 ms, t_{DEL} = 250 ms); E_{OXD} = 0.80 V (t_{OXD} = 120 ms); E_{RED} = −0.80 V (t_{RED} = 380 ms). Curves: a = 0 μM; b = 20 μM; c = 40 μM; d = 60 μM; e = 80 μM; f = 100 μM Tris.

In the absence of Tris (curve a), most of the current generated by pulsed voltammetry at the Au working electrode is the result of formation of surface oxide (AuO) at $E_{DET} > 0.2$ V. Anodic response for Tris (curves b–f) is obtained for $E_{DET} >$ ca. −0.2 V with a plateau signal for $E_{DET} = 0.0$ to 0.2 V (e.g., curve b) at low concentrations and 0.1 to 0.2 V at high con-

centrations (e.g., curve f). In this plateau region, the PED response to Tris appears to be a linear function of concentration, which is indicative of a mass-transport limited reaction. A similar response was obtained for all other alkanolamines studied, including 2-amino-1-ethanol (ETH), 3-amino-1-propanol (PRO), 4-amino-1-butanol (BUT) and 5-amino-1-pentanol (PEN). Based on these results the maximum signal-to-background ratio (S/B) is obtained for E_{DET} in the range 0.0 to 0.1 V.

3.2. Optimization of HPLC conditions

A preliminary separation of five alkanolamines is shown in Fig. 2 for the PCX-500 (250 × 4 mm) column. The mobile phase consisted of an acetate buffer (pH ≈ 5) which is sufficiently acidic to ensure protonation of the amine group, thereby producing the cationic form of the alkanolamines necessary for retention on the multimodal column. Because alkanolamines are not oxidized at Au electrodes in acidic media, post-column addition of NaOH was used to provide the alkaline environment necessary to obtain PED response. Sodium acetate (NaOAc) in the eluent provided Na^+ as the counter ("pusher") ion necessary to elute the alkanolamines from the cation-exchange portion of multimodal column. In general, retention time increases as a function of decreasing hydrophilicity of the cationic alkanolamines. Tris, with three alcohol groups, is the most hydrophilic and, therefore, exhibits the least retention. With the exception of ETH and PRO, baseline resolution was possible for the terminal amino alcohols under the conditions used for Fig. 2. The small peak at ca. 2 min is the result of O_2 dissolved in the sample which is reduced to H_2O_2 at E_{RED} and subsequently detected anodically by oxidation to H_2O at E_{DET}.

Fig. 3 shows the retention factors (k) for five alkanolamines plotted versus the concentration of ACN in the acetate mobile phase. It is evident that the retention factors for the larger and more hydrophobic alkanolamines, e.g., BUT (d) and PEN (e), are most affected by the amount of ACN in the mobile phase. This is to be expected

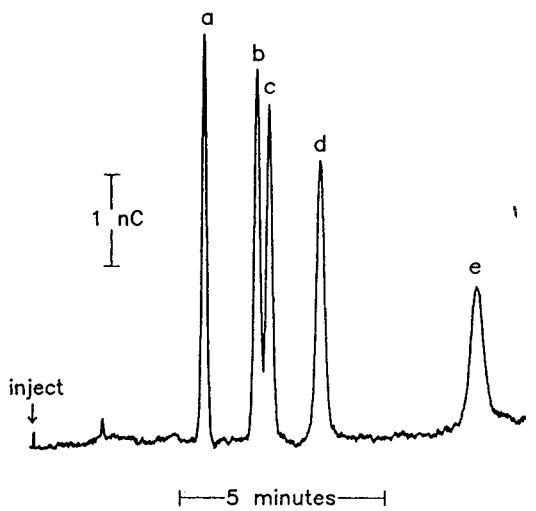

Fig. 2. HPLC–PED of five alkanolamines. Column: Dionex PCX-500 (250 × 4 mm). Injection: 25 μl. Eluent: 20 mM HOAc/60 mM NaOAc at 1.0 ml min^{-1}. Post-column addition: 0.30 M NaOH at 0.6 ml min^{-1}. PED waveform: E_{DET} = 0.05 V (t_{DET} = 300 ms, t_{DEL} = 250 ms); E_{OXD} = 0.80 V (t_{OXD} = 120 ms); E_{RED} = −0.40 V (t_{RED} = 180 ms). Peaks: a = 4 μM Tris; b = 10 μM ETH; c = 10 μM PRO; d = 10 μM BUT; e = 10 μM PEN.

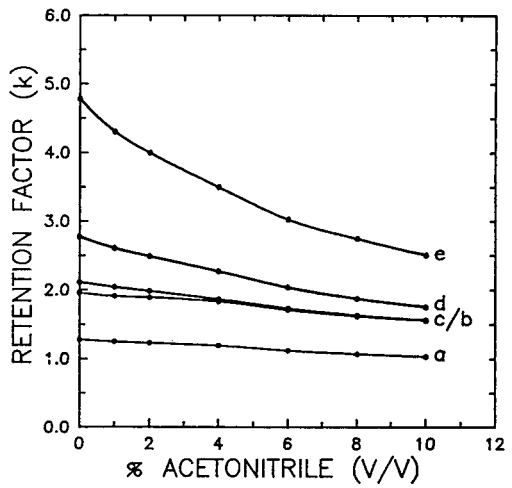

Fig. 3. Retention factors (k) plotted versus eluent acetonitrile (ACN) content. Column: Dionex PCX-500 (250 × 4 mm). Eluent: 20 mM HOAc/60 mM NaOAc–variable ACN at 1.0 ml min^{-1}. Post-column addition: 0.30 M NaOH at 0.6 ml min^{-1}. PED waveform as in Fig. 2. Curves: a = Tris; b = ETH; c = PRO; d = BUT; e = PEN.

for a retention mechanism having a significant reversed-phase component. The ACN concentration, while not having a strong influence on the retention of the smaller alkanolamines, is critical to the separation of ETH and PRO (b and c). For ACN concentrations larger than 2% (v/v), the retention factors for ETH and PRO are virtually identical. Hence, the best separation of these two compounds is obtained without ACN present in the eluent. Although literature supplied with the column indicates that the use of mobile phases containing no organic solvent may damage the column, we saw no indication of column deterioration over several months of operation. Larger alkanolamines ($>C_6$) also can be eluted using this separation strategy. However, as the hydrophobicity of the alkanolamine increases, there is an increasing need for the addition of organic modifier to the mobile phase. For example, to obtain reasonable elution times for the C_6–C_8 alkanolamines on the 250- mm column, a mobile phase containing between 5–15% ACN is suggested.

Fig. 4 shows values of the retention factors for alkanolamines versus the concentration of Na^+, added as NaOAc, in the mobile phase without the presence of ACN. These results demonstrate a significant decrease in k with increasing Na^+ concentration, indicating a strong cation-exchange component for the retention of alkanolamines on the multimodal column. The optimum separation of alkanolamines is realized at NaOAc eluent concentrations in the range 40–100 mM. Variation of the acetic acid (HOAc) concentration in the mobile phase had little effect on alkanolamine retention, providing there was sufficient HOAc (>10 mM) to assure protonation of the amine functional groups.

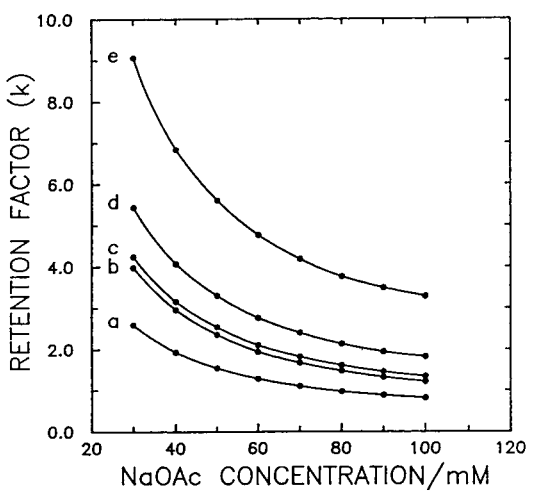

Fig. 4. Retention factors (k) plotted versus eluent NaOAc content. Column: Dionex PCX-500 (250 × 4 mm). Eluent: 20 mM HOAc/variable NaOAC at 1.0 ml min^{-1}. Post-column addition: 0.30 M NaOH at 0.6 ml min^{-1}. PED waveform as in Fig. 2. Curves: a = Tris; b = ETH; c = PRO; d = BUT; e = PEN.

3.3. Detection limits, linearity and reproducibility

The linear dynamic range of the HPLC–PED response for alkanolamines was determined using Tris as a representative compound. Response was linear within the range 50 nM to 100 μM, as indicated by the following regression statistics: slope = 1.57 nC μM^{-1}, intercept = 0.17 nC, and correlation coefficient (R^2) = 0.9997 ($n = 11$). The limit of detection ($S/N = 3$) for 25-μl injections of Tris is estimated to be 20 nM (500 fmol). Negative deviations from linear response were observed beginning at concentrations greater than 200 μM and, for concentrations above 2000 μM, the PED signal changed only slightly with increased concentration. These calibration data were obtained using $E_{DET} = 0.0$ V to minimize the background signal and obtained the lowest possible detection limit. Examination of the pulsed voltammetric data in Fig. 1 reveals that this detection potential does not correspond to the plateau response for high concentrations of Tris. Therefore, choice of $E_{DET} = 0.1$ V is recommended to achieve maximum linearity of calibration curves, albeit with some sacrifice of detectability.

Fig. 5 shows HPLC–PED results for ten consecutive injections of 10 μM Tris. The relative standard deviation (R.S.D.) of these peak heights is ca. 0.4%. This indicates that HPLC–PED provides a very reproducible response for alkanolamines.

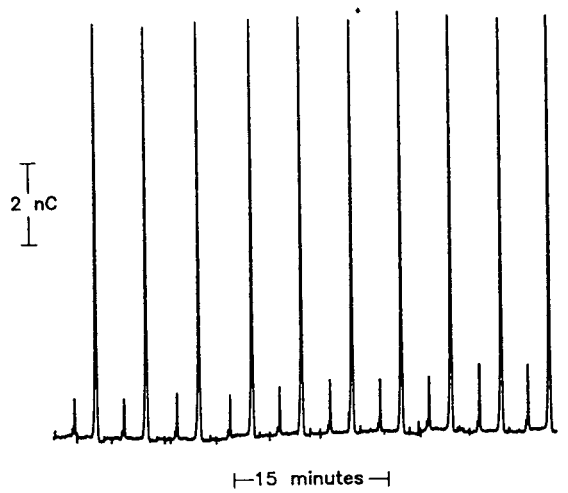

Fig. 5. Reproducibility of HPLC response. Column: Dionex PCX-500 (250 × 4 mm). Injections: 25 μl of 10 μM Tris. Eluent: 20 mM HOAc/60 mM NaOAc at 1.0 ml min^{-1}. Post-column addition: 0.30 M NaOH at 0.6 ml min^{-1}. PED waveform as in Fig. 2.

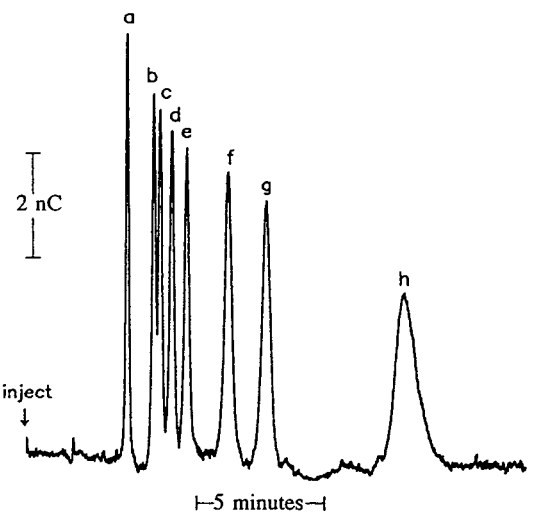

Fig. 6. HPLC–PED of alkanolamine isomers. Column: Dionex PCX-500 (250 × 4 mm). Injection: 25 μl. Eluent: 20 mM HOAc/70 mM NaOAc at 1.0 ml min^{-1}. Post-column addition: 0.30 M NaOH at 0.6 ml min^{-1}. PED waveform as in Fig. 2. Peaks: a = 8 μM Tris; b = 20 μM ETH; c = 20 μM PRO; d = 20 μM 2-amino-1-propanol; e = 40 μM BUT; f = 40 μM 2-amino-1-butanol; g = 40 μM PEN; h = 80 μM 2-amino-1-pentanol.

3.4. Isomeric separation and other applications

The separation of several alkanolamine positional isomers is demonstrated in Fig. 6. Compare peaks c and d for PRO and 2-amino-1-propanol, respectively; peaks e and f for BUT and 2-amino-1-butanol, respectively; and peaks g and h for PEN and 2-amino-1-pentanol, respectively. It is apparent that alkanolamine isomers with terminal amine groups are eluted before their β-amino analogues. This order of elution is explained on the basis of the relative positions of the functional groups. β-Alkanolamines have both the amine and the alcohol functional groups near one end of the molecule. As a result, a larger portion of the molecular structure is hydrophobic, resulting in stronger retention on the reversed-phase portion of the multimodal column. Furthermore, variation of the acetonitrile concentration in the mobile phase had a greater effect on the retention of the β-amino alcohols than the retention of the terminal-amino alcohols, which supports the conclusion that the β-alkanolamines are more hydrophobic.

Application of the HPLC–PED system for the determination of an alkanolamine in a commercial shaving gel using a 50 × 4 mm column is shown in Fig. 7. Minimal sample preparation was required, consisting of dilution (1:10 000, w/v) of a small portion of the sample with deionized water before injection. The resulting chromatogram exhibits only two peaks, and its simplicity is largely attributable to the choice of E_{DET} in the PED waveform. At E_{DET} = 0.05 V, PED is fairly selective for organic compounds with the alcohol moiety. Thus, many possible interferents show no response at the Au working electrode. The first peak is from sorbitol, an ingredient in the shaving gel. The second peak corresponds to TEA. The relative standard deviation for five determinations of TEA was better than 1.0%, thus indicating that even with very little sample preparation, good precision is possible. The shoulder on peak b for TEA suggest an overlap of two unresolved peaks. However, a second compound was never resolved from TEA using this column or the longer analytical column

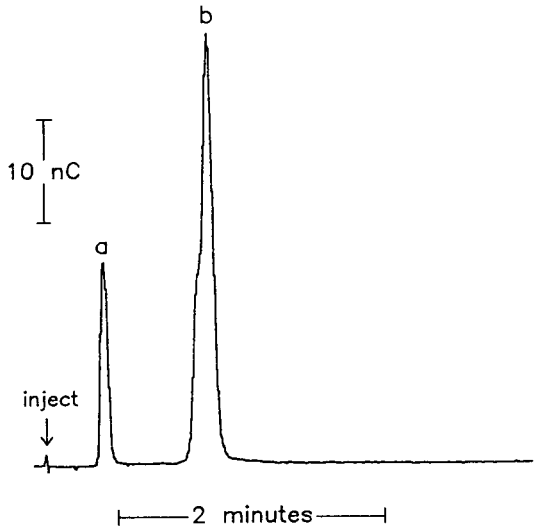

Fig. 7. HPLC–PED of commercial shaving gel. Column: Dionex PCX-500 (50 × 4 mm). Injection: 25 μl. Eluent: 20 m*M* HOAc/60 m*M* NaOAc at 1.0 ml min^{-1}. Post-column addition: 0.30 *M* NaOH at 0.6 ml min^{-1}. PED waveform as in Fig. 2. Peaks: a = sorbitol; b = TEA.

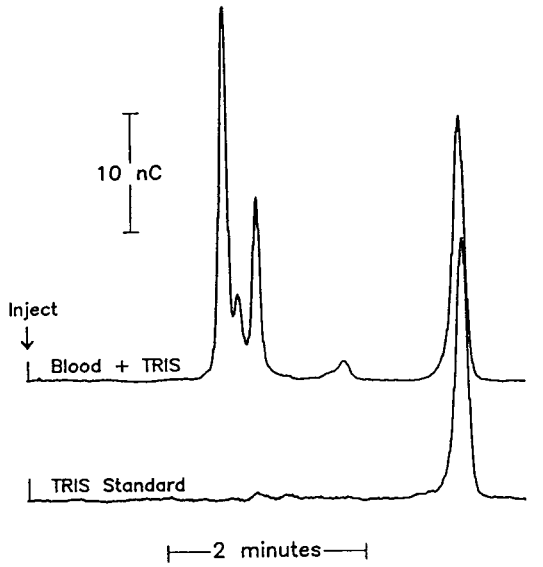

Fig. 8. HPLC–PED of Tris in blood serum. Column: Dionex PCX-500 (250 × 4 mm). Injections: 25 μl. Eluent: 20 m*M* HOAc/60 m*M* NaOAc at 1.0 ml min^{-1}. Post-column addition: 0.30 *M* NaOH at 0.6 ml min^{-1}. PED waveform as in Fig. 2. Upper chromatogram: serum from human blood spiked with Tris and diluted with deionized water to a final concentration of 20 μ*M*. Lower chromatogram: 20 μ*M* Tris standard.

(250 × 4 mm). The cause of the anomalous peak shape in Fig. 7 is unknown at the present time.

The HPLC–PED system was tested for determination of Tris in human blood serum. Tris is known clinically as Tromethamine and is used as a blood buffering agent [21]. Furthermore, Arispe et al. [22] recently reported that Tris has possible therapeutic value in the treatment of Alzheimer's disease. Therefore, the clinical determination of Tris in blood might be of some interest. Artificial samples of Tris in blood were prepared as follows: 100-μl aliquots of human blood were added to 100-μl aliquots of 2.00 m*M* Tris. These mixtures then were diluted to 10.0 ml either with deionized water or with 1.0 *M* $HClO_4$ to give a final Tris concentration of 20.0 μ*M*. The solutions were mixed thoroughly, centrifuged, and filtered through a 0.22-μm syringe filter (Whatman) to remove red blood cells prior to injection.

The HPLC–PED results obtained for the blood samples containing 20.0 μ*M* Tris are adequately represented by the upper chromatogram in Fig. 8 for a sample diluted with water. The lower chromatogram represents the response for a 20.0 μ*M* Tris standard in water. The recovery efficiency for Tris in blood was dependent upon the sample diluent. When samples were diluted with deionized water, recovery efficiency was 81.6 ± 3.1% ($n = 4$). When 1.0 *M* perchloric acid was the diluent, the recovery efficiency was 102.0 ± 2.3% ($n = 4$). We speculate that the lower recovery efficiency for samples diluted with water is the result of complexation of Tris by blood proteins resulting in a decreased concentration of free Tris. Dilution of samples with acid caused the proteins to be ionized, thus releasing the bound Tris and allowing complete recovery. Another benefit of using acid as the blood diluent relates to sample stability. Injections could be made several days after sample dilution by acid without any discernible decrease in the recovery efficiency. Other peaks in the upper chromatogram have

not been identified, with the exception of the first peak that corresponds to normal levels of blood sugar (glucose).

4. Conclusions

The separation of alkanolamines was demonstrate using HPLC. The separation relies upon both cation-exchange and reversed-phase retention mechanisms of a multimodal column, and the strategy provides baseline resolution of positional isomers of several alkanolamines using isocratic elution. When coupled with PED, the determination of alkanolamines was shown to be sensitive and reproducible. Detection limits in the nanomolar region were possible, and the linear dynamic range was greater than three decades. The method has the advantage of being rugged, with minimal sample preparation required to successfully analyze alkanolamines in both commercial and biological samples.

Acknowledgement

This work was supported by a grant from Dionex Corporation.

References

[1] *The Merck Index*, Merck, Rahway, NJ, 11th ed.,1991, pp. 588, 1521, 1536–1537.
[2] D.L. Campbell, S. Carson and D. Van Bramer, *J. Chromatogr.*, 546 (1991) 381.
[3] R.B. Butwell, D.J. Kubek and P.W. Sigmund, *Hydrocarbon Processing*, Gulf Publishing Co., 1982, pp. 108–116.
[4] O.F. Dawodu and A. Meisen, *J. Chromatogr.*, 629 (1993) 297.
[5] O.F. Dawodu and A. Meisen, *J. Chromatogr.*, 587 (1991) 237.
[6] N.C. Saha, S.K. Jain and R.K. Dua, *Chromatographia*, 10 (1977) 368.
[7] S. Boneva and N. Dimov, *Chromatographia*, 14 (1981) 601.
[8] G. Vincent, M. Desage, F. Comet, J.L. Brazier and D. LeCompte, *J. Chromatogr.*, 295 (1984) 248.
[9] M. Nishikata, *J. Chromatogr.*, 408 (1987) 449.
[10] N.P.J. Price, J.L. Firmin and D.O. Gray, *J. Chromatogr.*, 598 (1992) 51.
[11] J.A. Grunau and J. M Swiader, *J. Chromatogr.*, 594 (1992) 165.
[12] A.J. Bourque and I.S. Krull, *J. Chromatogr.*, 537 (1991) 123.
[13] J.F. Davey and R.S. Ersser, *J. Chromatogr.*, 528 (1990) 9.
[14] A.R. Hayman, D.O. Gray and S.V. Evans, *J. Chromatogr.*, 325 (1985) 462.
[15] J. Krol, P.G. Alden, J. Morawski and P.E. Jackson, *J. Chromatogr.*, 626 (1992) 165.
[16] J. Gorham, *J. Chromatogr.*, 362 (1986) 243.
[17] H. Small, T.S. Stevens and W.C. Bauman, *Anal. Chem.*, 47 (1975) 1801.
[18] W.R. LaCourse, W.A. Jackson and D.C. Johnson, *Anal. Chem.*, 61 (1989) 2466.
[19] D.C. Johnson and W.R. LaCourse, *Electroanalysis*, 4 (1992) 367.
[20] W.R. LaCourse and D.C. Johnson, *Anal. Chem.*, 65 (1993) 50.
[21] G.G. Nahas, *Pharmacol. Rev.*, 14 (1962) 447.
[22] N. Arispe, E. Rojas and H.B. Pollard, *Proc. Natl. Acad. Sci. U.S.A.*, 90 (1993) 567.

ELSEVIER

Journal of Chromatography A, 694 (1995) 399–406

JOURNAL OF CHROMATOGRAPHY A

Directly coupled sample treatment–high-performance liquid chromatography for on-line automatic determination of liposoluble vitamins in milk

M.M. Delgado-Zamarreño*, A. Sanchez-Perez, M.C. Gomez-Perez, J. Hernandez-Mendez

Department of Analytical Chemistry, Nutrition and Food Science, Faculty of Chemistry, University of Salamanca, 37008 Salamanca, Spain.

First received 20 July 1994; revised manuscript received 8 November 1994; accepted 15 November 1994

Abstract

We developed an on-line system for the determination of liposoluble vitamins A, D_3 and E in milk, both liquid and in powder form, using an automated sample treatment system coupled to chromatographic determination. For this, C_{18} cartridges were used because of the strong capacity of this material for the extraction and preconcentration of such vitamins, its ease in handling and the possibility of coupling it with automatic analysis systems.

Alkaline hydrolysis of the samples was performed in an on-line system comprising two confluent channels through which the sample solution and alcoholic sodium hydroxide plus ascorbic acid flowed for a given period of time. A third channel merged with the other two to neutralize the solution before it arrived at the C_{18} cartridge. The latter, inserted into a loop with a six-port injection valve, retained the soluble vitamins. The vitamins were eluted with a stream of methanol and the eluate was automatically injected into the chromatographic system. Variables affecting the on-line system were optimized: sample size, flow-rate, preconcentration, washing and elution times, etc. The recoveries for powdered and liquid milk for the three vitamins assayed ranged between 80 and 105% ($n = 10$). Additionally, a day-to-day precision (10 days) of the method of 4.5% was obtained for the different vitamins.

1. Introduction

The determination of microconstituents of samples includes a sample preparation step that usually is laborious and time-consuming. The aim of sample preparation is to extract the analytes from the matrix to be analyzed and to concentrate them, if needed, to obtain a measurable response in a chromatographic or any other type of system. Whereas the actual analytical procedure may only take a few minutes, the sample preparation step may take several hours.

Currently, chromatographers are searching for better sample preparation techniques to improve the speed and precision of analysis. An additional goal is to obtain more cost-effective, easy to use, and mostly automated methods.

The interest aroused by solid–liquid extraction

* Corresponding author.

0021-9673/95/$09.50
SSDI 0021-9673(94)01142-7

(solid-phase extraction, SPE) has increased not only because it affords results similar to liquid–liquid extraction but also because it requires smaller amounts of solvent, is faster and gives cleaner solutions because there is an inherent filtration. Another important aspect is the possibility of using cartridges in which SPE is used in continuous set-ups.

For the determination of liposoluble vitamins in milk, sample treatment is slow and tedious. It consists of alkaline hydrolysis of the sample followed by extraction of the vitamins from the non-saponifiable matter, evaporation of the solvent and injection into the chromatographic system. Although attempts to minimize the treatment by direct extraction of the vitamins from the sample [1–3] have been described, some authors had to perform fractionation steps and clean-up of the extracts prior to quantification [4–7]. However, it was observed previously [8] that the classic treatment should be used for milk samples because the results obtained after direct extraction are too low.

There are numerous reports on the determination of different liposoluble vitamins in milk using HPLC in normal-phase [9–15] and reversed-phase [16–20] modes, usually with UV or fluorimetric [15] and amperometric detection for vitamins A and E [20]. A method has also been proposed for the simultaneous determination of vitamins A, D_3 and E in milk samples without the need of any clean-up step for the detection of vitamin D_3 [8].

The aim of the present work was to design an on-line sample treatment system with a chromatographic system for the simultaneous determination of liposoluble vitamins in liquid and powdered milk samples. No automated method for the determination of liposoluble vitamins in this kind of sample has been found in the literature consulted.

2. Experimental

2.1. Apparatus

A Spectra-Physics SP 8800 ternary pump equipped with a Spectra System AS1000 automatic injector with a 100-μl loop was used. The detectors were a Spectra-Physics SP8450 UV detector and electrochemical detector EG and PAR Model 400, with a glassy carbon working electrode. Peak areas were measured by a Spectra-Physics SP 4290 integrator.

The on-line system consisted of commercially available Sep-Pak Plus C_{18} cartridges (Millipore) placed in the sample loop of a Rheodyne Model 5020 six-port injection valve; a Gilson 231-401 microprocessor; a Gilson Minipuls-3 peristaltic pump with Isoversinic pump tubes; PTFE tubing (0.50 mm I.D.) for the rest of the channels, including the knotted reactor of 5 m of length.

Chromatographic columns: precolumn RP18 15×3.2 mm, 7 μm (Brownlee Labs.) and column OD-224 RP18 220×4.6 mm, 5 μm (Brownlee Labs.).

2.2. Reagents

All-*trans*-retinol (vitamin A) was from Sigma, cholecalciferol (vitamin D_3) from Fluka, α-tocopherol (vitamin E) from Aldrich, Ascorbic acid and NaOH (analytical-reagent grade) from Panreac and methanol (LC grade) from Carlo Erba. Water was purified in a Elga-Stat water-purification system.

The alcoholic sodium hydroxide solution consisted of 50 ml ethanol and 15 ml of 60% aqueous NaOH solution and 5 ml of 10% ascorbic acid.

The washing solution was water–methanol (60:40). The elution solvent was methanol. The mobile phase was a solution of acetic acid–sodium acetate 2.5 m*M* in methanol–water (99:1, v/v).

3. Results and discussion

Determination of liposoluble vitamins in milk samples usually includes saponification of the fat material, extraction of the vitamins from the non-saponifiable material and clean-up of the extracts before injection into the chromatographic system. In the present work, a flow system coupled to the chromatographic system is proposed which performs these steps automatically.

The set-up is shown schematically in Fig. 1. Alkaline hydrolysis of the samples is performed in the two-channel system through which the sample and alcoholic sodium hydroxide with ascorbic acid (to avoid oxidation of the vitamins) are passed for a given time (preconcentration time). Hydrolysis occurs in the reactor. A third channel merges with the former ones to neutralize the solutions before the C_{18} cartridge is reached. This cartridge, inserted into the loop of an injection valve, retains the liposoluble vitamins. Later, the washing solution is passed through the cartridge followed by a stream of methanol, which elutes the vitamins. The eluate is automatically injected into the chromatographic system. The two injection valves together with the integrator are controlled by a microprocessor, thus automating the process.

Fig. 1A shows the whole process in detail; initially, the two valves are set at the load position such that the hydrolyzed and neutralized sample reaches the C_{18} cartridge where the vitamins are retained, while the washing solution flows through the second valve.

After a suitable preconcentration time, the first valve is switched to the injection position, the second valve remaining unchanged (Fig. 1B). In this way the cartridge is washed with the water–methanol mixture. When the washing time has been completed, methanol is introduced through the same channel to elute the vitamins from the cartridge, thereby filling the loop of the second valve (Fig. 1C). When the loop contains the greatest amount of vitamins eluted (elution time) the second valve turns automatically, injecting the 100 μl directly into the chromatographic column where the vitamins are separated for later detection. Fig. 2 shows a diagram of the whole set-up; electrochemical and UV (280 nm) detectors were used.

The results obtained spectrophotometrically were similar to those obtained using electrochemical detection except that in some cases certain problems arose regarding spectrophotometric quantification of vitamins A and E, which were not detected. In the UV detection a 280 nm wavelength was chosen as a compromise wavelength for the detection of vitamins A, D_3 and E. UV detection is less sensitive than amperometric detection [8]. The present work only reports the data obtained by electrochemical detection.

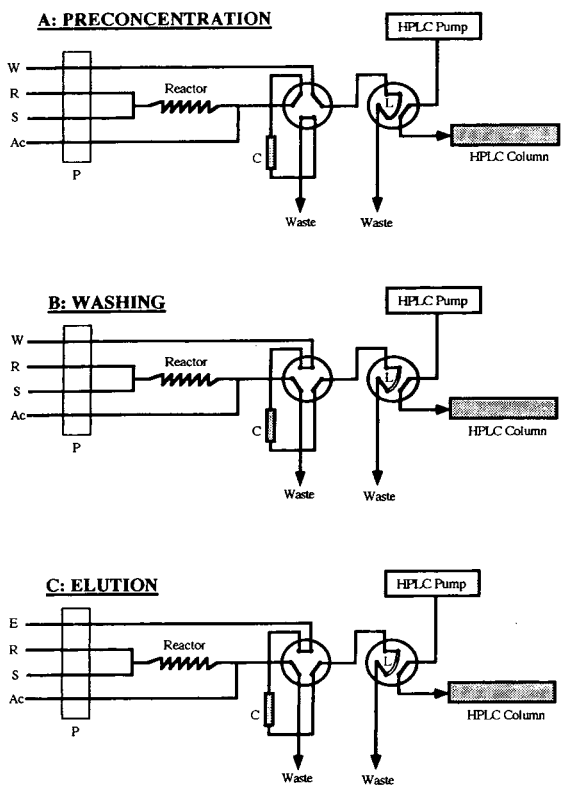

Fig. 1. Schematic diagram of the on-line hydrolysis and elution with HPLC system. P = Peristaltic pump; R = hydrolysis reagent; S = sample; Ac = acetic acid; W = washing; E = elution; C = C_{18} cartridge; L = 100-μl loop.

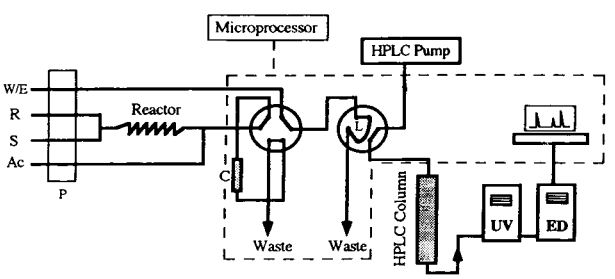

Fig. 2. Diagram of coupled on-line sample treatment–HPLC for determination of liposoluble vitamins. P = Peristaltic pump; R = hydrolysis reagent; S = sample; Ac = acetic acid; W = washing; E = elution; C = C_{18} cartridge; L = 100-μl loop. HPLC conditions: mobile phase: methanol–water (99:1), 0.0025 *M* HAcO–NaAcO; flow-rate: 1.0 ml/min; UV detection at 280 nm; electrochemical detection at + 1300 mV.

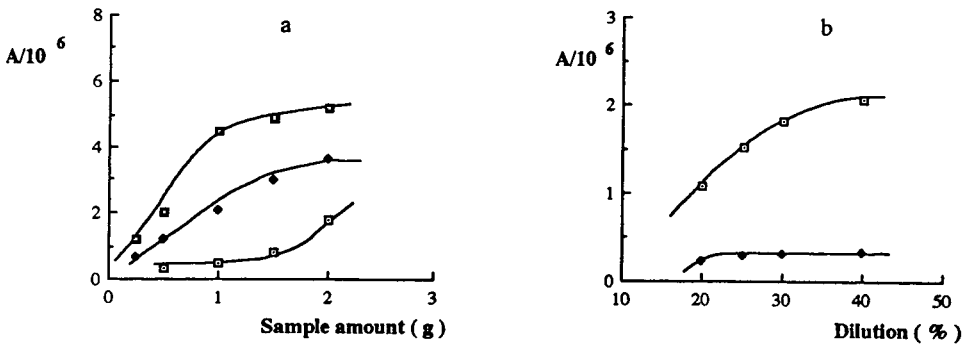

Fig. 3. Influence of sample amount. (a) Milk powder; □ = Vitamin A; ◆ = vitamin D_3; ■ = vitamin E. (b) Liquid milk; □ = Vitamin A; ◆ = vitamin E.

3.1. Optimization of variables

To automate the process, it is necessary to optimize some of the variables affecting the different steps of the system. These are:

Amount of sample: In the case of powdered milk, solutions containing 0.5–2 g were prepared in 25 ml of water, while liquid milk samples were diluted with water from 10 to 50%. The results obtained are shown in Fig. 3. For the working conditions employed, samples of powdered milk of 2 g and liquid milk diluted at 30% were chosen. The fat content of the milk powder is lower than the fat content of the liquid milk. Accordingly, larger amounts of milk powder produce a higher signal for the three vitamins. However, problems of C_{18} cartridge obstruction arose when the amount of the samples was large. In the case of liquid milk two effects are present: a larger dilution should give a smaller signal; however, alkaline hydrolysis is more complete for a larger dilution and the signal is higher, probably because vitamin-fat bonds are broken without difficulty; furthermore, no obstruction of the C_{18} cartridges is produced.

Concentration of acetic acid: The strongly alkaline hydrolysis reagent should be neutralized before it arrives at the cartridge or it will destroy the C_{18} packing. In this way, possible corrosion of the stainless-steel tubes of the injection valves of the system is also avoided. To achieve this, a third channel was introduced through which a solution of acetic acid was passed. Experiments were performed with concentrations of acetic acid ranging from 1 to 3 *M* in order to reach pH values close to 7. As can be seen in Fig. 4, for concentrations of acetic acid ranging from 2.4 to 2.8 *M* the pH of the resulting solution was around 6. Acetic acid of 2.5 *M* was chosen as the working concentration.

Flow-rate: Flow-rate affects the hydrolysis of the fat material since a contact time between the sample and the hydrolysis reagent is required; it also affects the retention of the vitamins in the C_{18} cartridge. Different flow-rates in the 0.5–2.0 ml/min range were tried. As can be seen in Fig. 5, the best results were obtained for flow-rates of 1.25 ml/min, and hence, this was used as the optimum value.

Washing mixture and washing time: The mixture employed for washing was methanol–water.

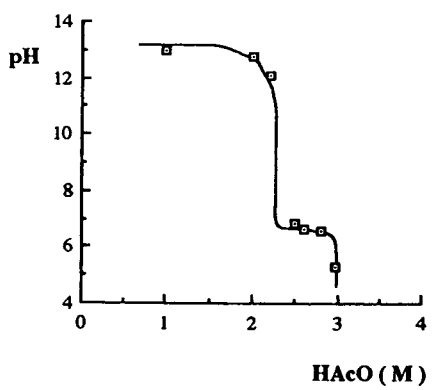

Fig. 4. Influence of acetic acid concentration on neutralization of the hydrolyzate.

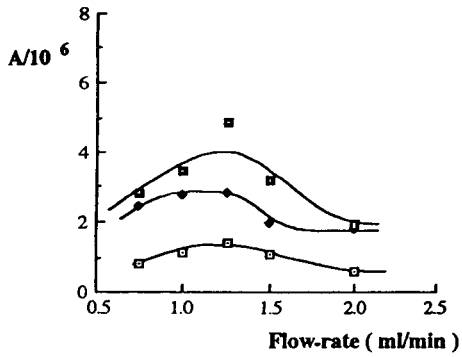

Fig. 5. Influence of flow-rate. □ = Vitamin A; ◆ = vitamin D_3; ◘ = vitamin E.

The composition of this mixture and the washing time are important variables to be controlled since if a mixture whose composition in methanol is too high is used, the vitamins may elute in the washing step. Mixtures of water–methanol ranging between 50:50 and 0:100 and washing times between 2 and 5 min were tried (Fig. 6). The best results were obtained with a water–methanol (60:40) washing mixture and a washing time of 4.0 min.

Preconcentration time: Extraction of the vitamins from the non-saponifiable material of the hydrolyzate is performed by the SPE cartridge inserted in the injection loop, at the same time performing a preconcentration of the analytes. It is therefore important to control the time during which the hydrolyzate passes through the cartridge, the preconcentration time, since the amount of vitamins extracted will be proportional to this time. Preconcentration times ranging from 1.0 to 6.0 min were investigated, as can be seen in Fig. 7. For times above 5 min, the analytical signal remained almost constant. Moreover, times above 6 min led to obstructions in the cartridge. Accordingly, a time of 5.0 min was chosen as the most suitable preconcentration time.

Elution time: The vitamins are eluted with methanol and are transported by the flow system to the loop of the injection valve of the chromatograph automatically. It is therefore important to control the time of elution since on one hand the liposoluble vitamins must be eluted and, on the other, the richest fraction should fill the 100 μl of the loop to be injected. Elution of the vitamins is a function of their polarity; first vitamin A is eluted and then D_3 and E, which are less polar. So, optimal elution of all three vitamins had to be determined. As can be seen in Fig. 8, a maximum in the signal for vitamins D_3 and E occurred at around 4.2 min while the maximum for vitamin A appeared before this time. However, other substances retained by the cartridge also eluted before vitamin A, potentially overlapping partly with this vitamin (Fig. 9). The optimum elution time chosen was 4.0 min.

Optimization of chromatographic variables: In a previous work [8] a systematic study of the variables affecting the chromatographic system was described. The mobile phase was water–

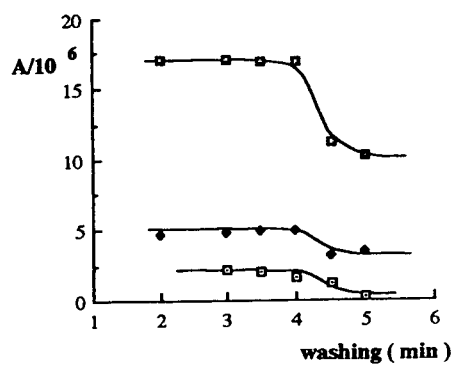

Fig. 6. Influence of washing time. □ = Vitamin A; ◆ = vitamin D_3; ◘ = vitamin E.

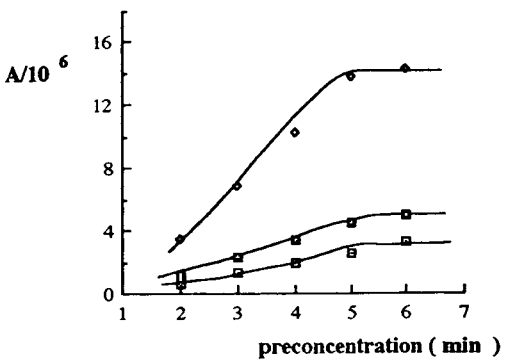

Fig. 7. Preconcentration time. □ = Vitamin A; ◇ = vitamin D_3; ◘ = vitamin E.

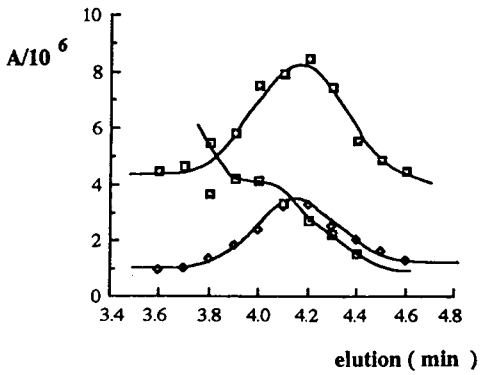

Fig. 8. Elution time. □ = Vitamin A; ◇ = vitamin D_3; ◘ = vitamin E.

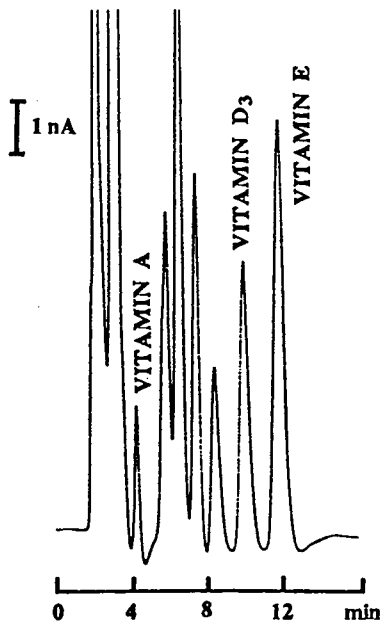

Fig. 9. Chromatogram obtained after application of the proposed method to a sample of milk powder.

methanol (1:99) with 2.5 m*M* acetic acid–sodium acetate, at a flow rate of 1.0 ml/min.

3.2. Analytical application

With the proposed system we obtained the corresponding calibration curves for samples containing the three vitamins at amounts similar to those contained in the milk samples. The calibration curves are shown in Table 1.

The detection limits (signal-to-noise ratio 3) obtained under the proposed working conditions were the following: $3.49 \cdot 10^{-8}$, $1.77 \cdot 10^{-6}$ and $3.11 \cdot 10^{-7}$ *M* (0.10, 6.8 and 1.34 ng injected) for vitamins A, D_3 and E, respectively.

The precisions of the method obtained with 10

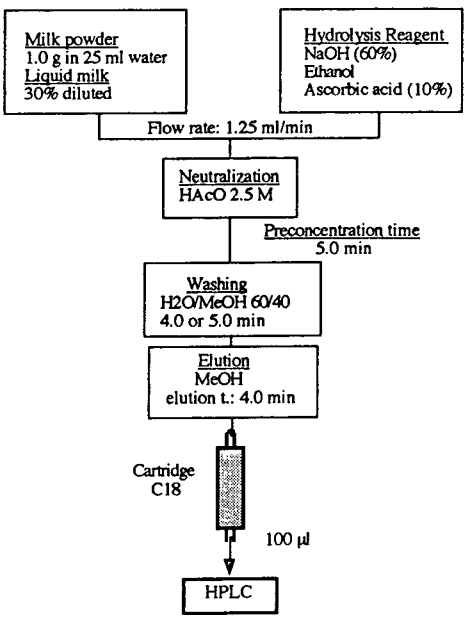

Fig. 10. Scheme of proposed procedure.

Table 1
Calibration fits: area (units) = $a + bC$, where C is concentration in *M*

Vitamin	*a*	*b*	Correlation coefficient
Vitamin A	$(2.90 \pm 3.2) \cdot 10^{5}$	$(8.73 \pm 0.13) \cdot 10^{12}$	0.9997 ($n = 7$)
Vitamin D_3	$(5.62 \pm 4.96) \cdot 10^{4}$	$(4.32 \pm 0.08) \cdot 10^{11}$	0.9995 ($n = 7$)
Vitamin E	$(1.92 \pm 0.95) \cdot 10^{4}$	$(6.19 \pm 0.14) \cdot 10^{11}$	0.9992 ($n = 7$)

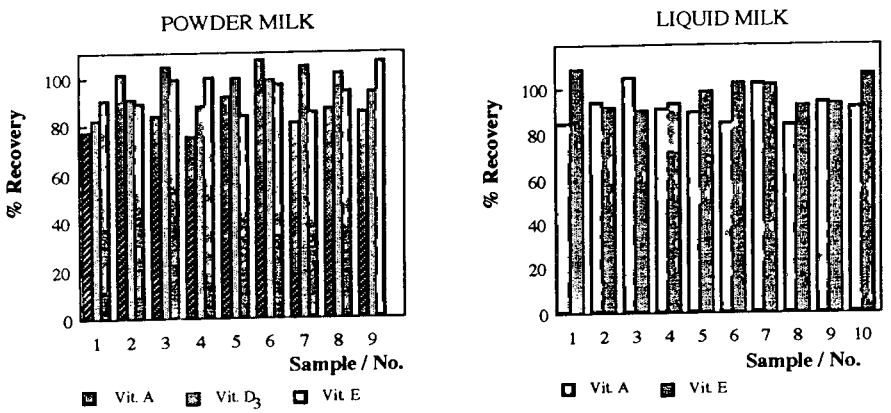

Fig. 11. Recoveries of the proposed method for samples of milk.

samples containing $1.18 \cdot 10^{-6}$ *M* of vitamin A, $3.85 \cdot 10^{-6}$ *M* vitamin D_3 and $3.10 \cdot 10^{-6}$ *M* of vitamin E were 3.8, 5.0 and 3.7%, respectively.

3.3. Analysis of milk samples

The procedure proposed for automatic determination of vitamins A, D_3 and E is shown in Fig. 10. Fig. 10 also specifies the conditions for the analysis of milk samples. The proposed method was applied to nine samples of infant formula milk and ten samples of liquid cow's milk. An example of the chromatograms obtained is shown in Fig. 9. Application of this procedure affords recoveries in the 88–105% range (Fig. 11), vitamins D_3 and E being those having the best recovery factors. The results obtained regarding the contents of the corresponding vitamins are shown in Tables 2 and 3.

The vitamin contents obtained in the powdered milk can be compared with those quoted by the manufacturer although it was not possible to do the same with the liquid milk samples because this value was not available for the commercial products.

The day-to-day precision was obtained by replicate analyses ($n = 10$) of powdered milk and liquid milk, the values found being (R.S.D., %):

Table 2
Determination of vitamins A, D_3 and E in different powdered milk samples (results from three replicate analyses)

Sample No.	Vitamin A (μg/100 g)		Vitamin D_3 (μg/100 g)		Vitamin E (mg/100 g)	
	Found	Quoted by supplier	Found	Quoted by supplier	Found	Quoted by supplier
1	394 ± 4	450	10.4 ± 0.3	10	3.0 ± 0.1	2.7
2	458 ± 3	450	13.6 ± 0.7	10	2.8 ± 0.2	2.7
3	412 ± 7	450	2.3 ± 0.9	3	4.7 ± 0.8	4.4
4	503 ± 3	550	8.7 ± 0.3	7.5	4.5 ± 1.7	5.5
5	409 ± 5	450	8.2 ± 0.2	10	3.5 ± 0.2	3.5
6	481 ± 4	465	8.5 ± 1.5	7.7	4.2 ± 0.8	5.7
7	421 ± 7	453	8.3 ± 1.4	7.5	5.3 ± 0.8	6
8	440 ± 2	456	6.1 ± 0.8	7.6	8.9 ± 0.7	8.6
9	479 ± 6	450	12.4 ± 2.3	10	4.0 ± 0.3	4

Table 3
Determination of vitamins A, D_3[a] and E in different liquid milk samples (results from three replicate analyses)

Sample	Vitamin A (μg/100 ml)	Vitamin E (μg/100 ml)
1	24.9 ± 0.3	67.8 ± 3.4
2	48.8 ± 0.7	93.4 ± 0.9
3	31.8 ± 0.2	170 ± 0.7
4	49.1 ± 0.3	145 ± 2.0
5	50.9 ± 0.4	141 ± 8.5
6	42.9 ± 0.7	193 ± 2.5
7	37.8 ± 3.3	118 ± 0.8
8	36.2 ± 0.8	125 ± 7.5
9	55.0 ± 0.9	165 ± 3.4
10	80.9 ± 0.3	91.4 ± 0.9

[a] Vitamin D_3 was not detected in samples of liquid cow's milk because of the low amounts present.

powdered milk: vitamin A, 3.9; vitamin D_3, 6.8; vitamin E, 5.4; liquid milk: vitamin A, 5.1; vitamin E, 1.2.

In all instances, good reproducibility of the analyses and acceptable relative standard deviations were found.

4. Conclusions

A method has been set up for the automatization of the analysis of liposoluble vitamins in milk; the method includes sample treatment and HPLC determination. In this way, sample treatment is very rapid; a sample takes some 25 min since its introduction into the system until evaluation of the corresponding chromatogram. The reproducibility of the method is very acceptable, as may be deduced from the values obtained in the day-to-day precision. The automatization of the method and its precision make it suitable for routine milk (liquid and powdered) analysis.

Acknowledgement

Financial assistance from the DGICYT (Ali 93-1164) is gratefully acknowledged.

References

[1] R.S. Mills, *J. Assoc. Off. Anal. Chem.*, 68 (1985) 56.
[2] S.F. O'Keefe and P.A. Murphy, *J. Chromatogr.*, 445 (1988) 305–309.
[3] A. Takeuchi, T. Okano and N. Tsugama, *J. Micronutr. Anal.*, 4 (1988) 193.
[4] W.O. Landen, *J. Assoc. Off. Anal. Chem.*, 68 (1985) 183.
[5] W.O. Landen, D.M. Hines, T.W. Hamill, J.I. Martin, E.R. Young, R.R. Eitenmiller and A.M. Soliman, *J. Assoc. Off. Anal. Chem.*, 68 (1985) 509.
[6] M.L. Grace and R.A. Bernhard, *J. Dairy Sci.*, 67 (1984) 1646.
[7] W. Ye, L. Liu and H. Li, *Sepu*, 10 (1992) 2240.
[8] M.M. Delgado Zamarreño, A. Sanchez Perez, C. Gomez Perez and J. Hernandez Mendez, *J. Chromatogr.*, 623 (1992) 69.
[9] E.J. de Vries and B. Borsje, *J. Assoc. Off. Anal. Chem.*, 65 (1982) 1228.
[10] D.C. Sertl and B.E. Molitor, *J. Assoc. Off. Anal. Chem.*, 68 (1985) 177.
[11] X. LI, L. Zhang and J. Zuo, *Yingyang Xuebabo*, 5 (1983) 103; *C.A.*, 99 (1983) 103811p.
[12] H. Johnsson and H. Hessel, *Int. J. Vitam. Nutr. Res.*, 57 (1987) 357.
[13] V.K. Agarwal, *J. Assoc. Off. Anal. Chem.*, 71 (1988) 19.
[14] C.J. Lammi-Keefe, *J. Pediatr. Gastrenterol. Nutr.*, 5 (1986) 934.
[15] W. Knifel, F. Ulbert and U. Winkler-Macheiner, *Dtsch. Lebensm-Rundsch.*, 83 (1987) 137; *C.A.*, 107 (1987) 95416c.
[16] S.L. Reynolds and H. Judd, *Analyst*, 109 (1984) 489.
[17] A.F. Wickroski and L.A. Mc Lean, *J. Assoc. Off. Anal. Chem.*, 67 (1984) 62.
[18] J. Ballester, E. Cortes, M. Moya and M.J. Campello, *Clin. Chem.*, 33 (1987) 796.
[19] H. Johnsson, B. Halen, H. Hessel and A. Nyman, *Int. J. Vitam. Nutr. Res.*, 59 (1989) 262.
[20] C. Bauer, J. Mattusch, B. Vorger and G. Werner, *Lebensmittelchemie*, 45 (1991) 110; *Anal. Abstr.*, 55 (1993) 6H195.

ELSEVIER

Journal of Chromatography A, 694 (1995) 407–413

JOURNAL OF CHROMATOGRAPHY A

Sensitive fluorescence detection of robenidine by derivatization with dansyl chloride and high-performance liquid chromatography

Huguette Cohen*, Fred Armstrong, Harold Campbell

Laboratory Services Division, Food Production and Inspection Branch, Agriculture Canada, Building No. 22, C.E.F., Ottawa, Ontario K1A 0C6, Canada

First received 17 June 1994; revised manuscript received 7 November 1994; accepted 8 November 1994

Abstract

A normal-phase high-performance liquid chromatographic procedure is presented for the determination of robenidine following derivatization with dansyl chloride. The derivatization, separation and detection conditions were optimized. The dansyl derivative is first purified on a silica gel cartridge followed by HPLC analysis on a silica gel column. The eluate is monitored by fluorescence detection at 320 nm excitation and 485 nm emission wavelength. The lower limit of detection of robenidine is 0.4 μg/ml.

1. Introduction

Medicated animal feedstuffs play an important role in intensive livestock production systems throughout the world. In the European community the use of these substances in feedstuffs is controlled by Council Directive [1] which has been amended many times over the last few years. The latest consolidated version of the annexes in this directive was published as a Commission Directive [2] and contains a list of 21 coccidiostats including robenidine. Robenidine hydrochloride, 1,3-bis(*p*-chlorobenzylideneamino)guanidine hydrochloride, is the active ingredient in American Cyanamid's Robenz, used in chicken feeds and supplements [3]. In Canada, robenidine is used as an aid in prevention of coccidiosis in chickens, turkeys and rabbits at doses of 33 or 50 mg/kg for poultry and rabbit feeds respectively. The absorption, excretion, and metabolism of ^{14}C-labelled robenidine hydrochloride was studied in rats [4] to assess the safety of robenidine in poultry products [5,6].

Very few analytical methods have been developed for detection of robenidine. The thin-layer chromatography method [7] uses a colorimetric sodium hydroxide in dimethyl formamide, and absorbance measured at 373 nm, whereas a HPLC method with detection at 280 nm shows a poor sensitivity (52.68 μg/ml) [8,9].

Robenidine does not have native fluorescence, however this difficulty has been overcome in the present work by introducing a highly fluorescent moiety into the robenidine. Such an approach has found application in the field of amino acid and peptide chemistry and also in pesticide residue analysis [10–13]. The reagent most often

* Corresponding author.

0021-9673/95/$09.50
SSDI 0021-9673(94)01096-X

utilized in such labelling techniques is 5-(dimethylamino)naphthalene-1-sulfonyl chloride (dansyl chloride, Dns-Cl) which reacts with primary and secondary amino groups and phenolic hydroxy groups to form highly fluorescent derivatives.

The present work details the use of Dns-Cl as fluorogenic labelling reagent for determination of robenidine. The technique can detect robenidine at 0.4 μg/ml.

2. Experimental

2.1. Chemicals and materials

Dns-Cl and 4-dimethylaminopyridine were obtained from Aldrich (Milwaukee, WI, USA). Robenidine was donated by Cyanamid (Gosport, Hants, UK). Water was purified using a Millipore Milli-Q system. All other solvents were purchased from J.T. Baker (Phillipsburg, NJ, USA) and were HPLC grade. Chloroform did not contain alcohol, but was stabilized with a non-polar hydrocarbon. Tetrahydrofuran was not stabilized against peroxide formation. Sep-Pak VAC/3cc silica cartridges were obtained from Waters/Millipore (Milford, MA, USA). Silica gel 60 was 70–230 mesh, from EM Science (Gibbstown, NJ, USA).

2.2. Apparatus

Reactions were carried out in Pyrex (100 × 13 mm I.D.) test tubes closed with PTFE-lined screw caps. An aluminum block heater with wells was used to heat the tubes. Silica cartridges were eluted using a vacuum manifold equipped with Luer-Loc adapters (Supelco, Oakville, Canada), set to maintain a slight pressure.

The HPLC system consisted of a Beckman 110A pump, a Waters U6K injector, a Perkin-Elmer LS-4 fluorescence detector and a Spectra-Physics 4270 integrator. A mobile phase of chloroform–hexane–tetrahydrofuran–methanol (50:50:2:1) was pumped at 2 ml/min through a Zorbax Sil (5 μm silica, 25 cm × 4.6 mm I.D.) column protected by a Brownlee (7 μm silica, 15 cm × 3.2 mm I.D.) guard column. The detector was set for excitation at 320 nm and emission at 485 nm.

^{1}H and ^{13}C NMR spectra were recorded on a Bruker AM 500 MHz NMR spectrometer at 500 and 125.28 MHz, respectively. Chemicals shifts are referenced with respect to [$^{2}H_6$]dimethyl sulfoxide (DMSO-d_6) at 2.49 ppm (^{1}H) and 39.5 ppm (^{13}C) and are reported relative to tetramethylsilane.

Chemical shift assignments were made via ^{1}H/^{13}C heteronuclear correlation and homonuclear decoupling experiments and by consideration of substituents effect.

Mass spectrometry was performed on a Finnigan-MAT-90. Samples were introduced by direct probe heated from 30 to 350°C and held at 350°C. Electron impact (EI) spectra were recorded from 200 to 600 u at 1 scan/s.

2.3. Preparation of solutions

Robenidine (20 mg) was weighed into a volumetric flask (100 ml) and dissolved with a solution of dichloromethane–methanol (90:10) to obtain a concentration of 0.2 mg/ml. The flask was shaken and then left overnight or until dissolution was complete.

Dns-Cl and dimethylaminopyridine (DMAP) were dissolved in dichloromethane to give solutions of 2 and 4 mg/ml, respectively. Solutions were stored in low actinic glass at 4°C.

2.4. Derivatization conditions

Robenidine solution was evaporated to dryness under a slow stream of nitrogen by heating on a water bath at 60°C to remove traces of methanol that could react with Dns-Cl. The residue was dissolved in 1.0 ml DMAP solution and 1.0 ml Dns-Cl solution was added. The tube was capped tightly, and heated for 60 min at 80°C. The mixture was then cooled on ice. During derivatization the reaction tube was wrapped in aluminium foil since dansyl derivatives are known to be photosensitive.

2.5. Purification of the reaction mixture for HPLC analysis

The cooled reaction mixture was transferred from the reaction tube to a silica gel cartridge. The tube was washed with 5.0 ml of dichloromethane, and this was applied to the silica gel cartridge. The dichloromethane eluate was discarded. The cartridge was then eluted with 5 ml of ethyl acetate to collect the reaction product. Ethyl acetate was evaporated to dryness under a gentle stream of nitrogen in a water bath at 60°C. The residue was taken up in 2.0 ml of HPLC mobile phase mixture, and 20 μl were injected into the HPLC system. Chromatograms are shown in Fig 2: (A) without a clean-up and (B) after clean-up.

2.6. Preparation of a quantity of the derivative for NMR and MS studies

A solution of 750 mg robenidine, 1500 mg Dns-Cl and 1500 mg DMAP in 500 ml dichloromethane was heated at 60°C for 2 h in a 2-l round-bottom flask equipped with a condenser. The reaction was protected from atmospheric moisture with a calcium chloride filled tube fitted on the condenser.

Preliminary clean-up of the reaction mixture was done using a 15 cm chromatography column (5 cm I.D.) filled to 5 cm with silica gel 60 slurried in dichloromethane. Half the reaction mixture (250 ml) was added and the column was washed with 2 × 100 ml of dichloromethane. The product was eluted in 200 ml ethyl acetate, and solvent removed on a rotary evaporator to dryness and the residues were taken up in few ml of dichloromethane.

Further purification was done on a 20 cm column of 2% water-deactivated silica gel 60 packed in dichloromethane in a 3 cm I.D. chromatography column. The column was prewashed with 100 ml 2% ethyl acetate in dichloromethane and the product of the previous column was added. The column was then washed with 600 ml of 2% ethyl acetate in dichloromethane, while the progress of the green fluorescent product band was followed by illumination with a 366 nm UV lamp. The band was eluted with 250 ml of 5% ethyl acetate in dichloromethane and evaporated to dryness on a rotary evaporator using methanol to drive off water. The residue was taken up in dichloromethane and recrystallized from methanol–dichloromethane (1:1) as yellow-green needles. These were dried in a vacuum drying pistol at 60°C for 16 h. The crystalline product showed a sharp melting point at 221°C.

2.7. Reaction conditions studies

Temperature

Time series run at 60 and 80°C with solvent and reagent concentrations as described under *Derivatization conditions* show that the reaction proceeds more quickly at 80°C than 60°C. A temperature of 80°C is the practical limit for the solvent, tubes and heater used.

Dns-Cl concentration

Reactions were run with 0.1 mg/ml robenidine in dichloromethane and Dns-Cl concentrations were varied from 0.03 to 1 mg/ml. The concentration of DMAP was twice that of Dns-Cl in each case. Increasing the Dns-Cl concentration was found to increase product yield. The limiting factor is the solubility of Dns-Cl in dichloromethane. The highest practical concentration for a stock solution is 2 mg/ml, equivalent to 1 mg/ml in the reaction mix.

Catalyst concentration

A series of reactions run at various concentration ratios (DMAP/Dns-Cl) with robenidine at 1.0 mg and 0.1 mg/ml show that the optimum concentration of DMAP varies with the concentration of Dns-Cl but not with the level of robenidine. The optimum was found at a concentration ratio of 2 mg/ml DMAP/1 mg/ml Dns-Cl.

Time

Time studies were carried out to a maximum of 3 h. The reactions were run at 80°C with a concentration of robenidine of 0.1 mg/ml, Dns-Cl 1 mg/ml and DMAP 2 mg/ml. The study

Table 1

Solvents	Bases, at a concentration of 1 mg/ml					
	DMAP	DMAP–K_2CO_3	DMAP–NaOH	K_2CO_3	K_2CO_3–18-crown-6 ether	NaOH
Acetone	++	+ +	++	+	–	–
Acetone–acetonitrile (1:1)				+	+	
Acetone–tetrahydrofuran (1:1)	++					
Acetone–water (1:1)				–		++
Acetonitrile	+	–		+	–	–
Acetonitrile–water (1:1)				+		
Chlorobenzene	+					
Chloroform	++			–		
Dichloromethane	+++	+++	–	–		

Fluorescence of product on TLC: – = none; + = weak; ++ = medium; +++ = strong.

shows the optimum time is 60 min with the product amount decreasing afterward.

Thin-layer chromatography (TLC)

Normal- and reversed-phase systems were used.

On silica gel plate (Whatman) LK6 (normal phase), the migration solvent used is ethyl acetate–heptane (90:10). The R_F of the product is 0.5. Using a reversed-phase system of acetonitrile–water (80:20) on silica gel LKC_{18} (C_{18} bonded to silica) the R_F of the product is 0.3.

Solvents/bases

The reaction was tested in a series of solvents with different bases in order to find the best system. Robenidine was present at 0.2 mg/ml and Dns-Cl and bases were each added at 1.0 mg/ml. The mixture was heated at 80°C for 1 h. The amount of the product was determined visually on TLC plates. Results are recorded in Table 1.

3. Results and discussion

Because robenidine has no native fluorescence, the technique of spectrofluorometry has not been previously applied to its determination. This difficulty has been overcome in the present work by introducing a highly fluorescent moiety into the molecule of robenidine. The reagent most often used in such labelling techniques is Dns-Cl which reacts with primary and secondary amino groups and also phenolic hydroxy groups to form highly fluorescent derivatives. The robenidine molecule contains three possible reaction sites for dansylation, all on the nitrogens attached to C_8 (Fig. 1). The possibility of obtain-

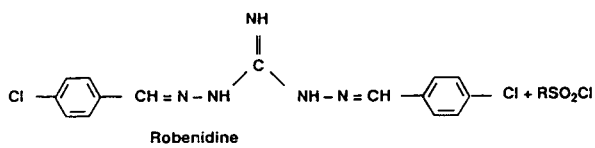

Robenidine

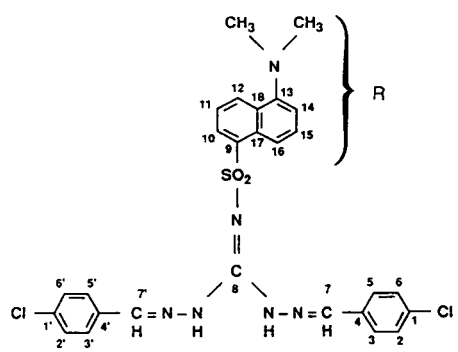

Dansyl Chloride Derivative of Robenidine

Fig. 1. Structures of robenidine and the Dns-Cl derivative of robenidine.

ing a mixture of isomers was eliminated by preparing the derivative and analyzing the structure by MS and NMR. The results from spectral data have clearly indicated that only one derivative is obtained.

The derivative, yellow green needles, exhibited a molecular ion at m/z 566 (10%) and a two chlorine isotopic peak at 568 (7%) with fragmentation ions at m/z 414 (25%), 412 (75%), 301 (100%, the base peak), 237 (55%) and 210 (24%). The ^{1}H and ^{13}C NMR shifts of the derivative are recorded in Table 2. The data indicate that robenidine's symmetry with respect to C_8 is retained in the derivative since a single resonance is obtained for both C_7 and $C_{7'}$ (Table 2). In the absence of symmetry, these two carbons should have exhibited two different signals. This retention of plan of symmetry shows that Dns-Cl reacts only with the imine at C_8. The mass spectrum of the derivative shows a mass of 566^{+}, which corresponds to the robenidine basic structure that has a symmetrical plan in relation to the C_8–NH.

In all applications using Dns-Cl as reagent for amino acids, peptides and proteins the derivatization occurs in aqueous media and at alkaline pH. In our case even though robenidine is soluble mainly in water (the standard solution), the water is evaporated with methanol to dryness, and the derivatization reaction proceeds in dichloromethane, with DMAP (an organic base). In this regard this is a new way to use this derivatization reaction in anhydrous conditions.

The parameters investigated included the yield of reaction product as a function of time. Reactions were performed at 80°C in capped tubes with the same concentrations of robenidine, Dns-Cl and DMAP in all. Tubes were withdrawn at different time intervals, cooled and the reaction mixture analyzed by HPLC.

Several systems of base/solvent were studied (Table 1), the best mixture was chosen for

Table 2
^{1}H NMR and ^{13}C NMR signal for dansylated robenidine derivative

Position	^{13}C (δ ppm)[a]	^{1}H (δ ppm)[b]	J (Hz)[c]
1,1′	132.7 (*132.2*)		
2,2′	128.8 (*128.7*)	7.50 (*7.95*)	d, 12.5 (*d, 8.5*)
3,3′	129.0 (*129.5*)	7.78 (*7.49*)	d, 7.8 (*d, 8.4*)
4,4′	134.8 (*135.2*)		
5,5′	129.0 (*129.5*)	7.78 (*7.49*)	d, 7.8 (*d, 8.4*)
6,6′	128.8 (*128.7*)	7.50 (*7.95*)	d, 12.5 (*d, 8.5*)
7,7′	146.6 (*147.6*)	8.40 (*8.45*)	
8	151.0 (*152.8*)		
9	140.1		
10	125.8	8.24	d, 7.9
11	123.4	7.57	dd, 8.5, 7.9
12	128.4	8.38	d, 8.5
13	149.2		
14	114.9	7.23	d, 7.5
15	127.1	7.60	dd, 8.6, 7.5
16	120.9	8.59	d, 8.6
17	129.4		
18	129.1		
$N(CH_3)_2$	45.1	2.80	
–NH		8.59	

[a] Chemical shift ^{13}C (in ppm).
[b] J values in Hz and chemical shifts in δ units (downfield of tetramethylsilane).
[c] J of robenidine deplacement/coupling; italic numbers between parentheses are for underivatized robenidine.

further optimization and the conditions were as follows: robenidine was 0.2 mg/ml, Dns-Cl was 1 mg/ml, base at concentration 1 mg/ml and the reaction time 1 h at 80°C. The use of DMAP and dichloromethane was found to be the best system.

A series of five concentration of robenidine (6.4, 3.2, 1.6, 0.8 and 0.4 μg/ml) were taken and derivatized as described above and purified with silica gel cartridge prior to injection to HPLC.

Application of the formula $y = a + bx$ using peak areas gave a very good linearity with correlation coefficient of 0.9990 with intercept $a = -1136$ and slope $b = 62539$.

The procedure reported clearly established that the minimum level of detection of robenidine was 0.4 μg/ml or 8 ng in a 20-μl injection at S/N of 3.

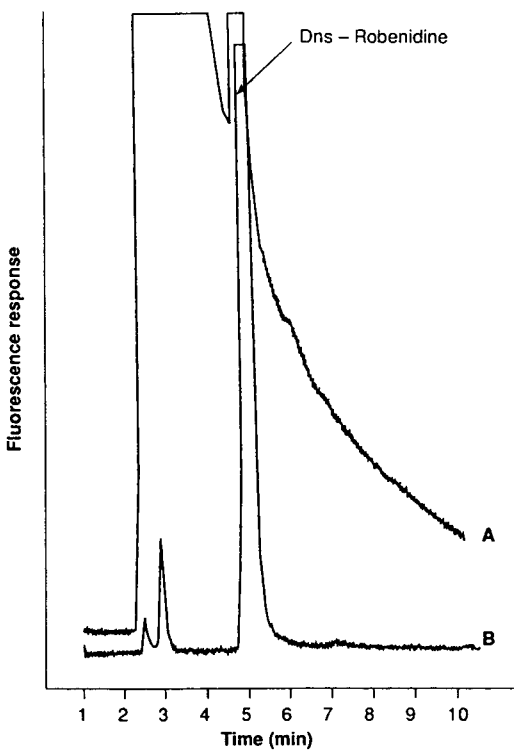

Fig. 2. Chromatograms of robenidine: A = without cleanup, 12.8 μg/ml; B = after silica gel cartridge cleanup, 12.8 μg/ml. HPLC conditions given in the text.

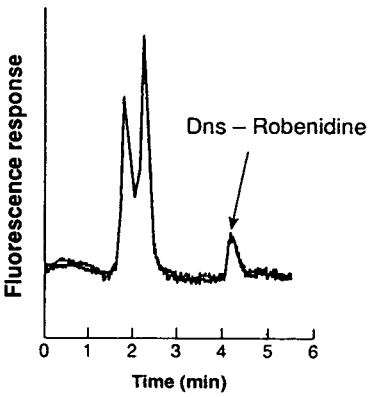

Fig. 3. HPLC of robenidine 0.4 μg/ml. Conditions given in the text.

A normal-phase chromatogram (Fig. 2) shows the separation of Dns-robenidine prior to and after silica column clean up and Fig. 3 shows the minimum detectable amount of robenidine.

In the catalyst concentration studies (0.1 and 1.0 mg/ml), the latter concentration of 1 mg/ml was selected because of the poor solubility of robenidine at higher concentration in the reaction solvent (dichloromethane–methanol, 90:10). Data showed that at these levels the maximum yield of the derivative was obtained when the ratio of Dns-Cl and DMAP was 1 to 2. DMAP acted both as a catalyst and a scavenger of H^+ (HCl). It was observed that cleanup improved the quality of the chromatogram as seen in Fig. 2 which records the chromatograms of the reaction mixture before (A) and after (B) cleanup on a silica gel cartridge. The recovery of the derivative was done through the Sep-Pak clean up step. Using peak areas the recovery was at 96.6% and the relative standard deviation 1.26% ($n = 4$).

4. Conclusions

The detection method has a detection limit superior to others reported using HPLC. The detection limit is improved by two orders of magnitude. The specific solubility of the derivative in dichloromethane allows its purification with a silica gel column. We are currently inves-

tigating the technique to determine robenidine in both spiked and actual samples.

Acknowledgements

The authors thank J. Nikiforuk (Research Branch, Agriculture Canada) for the NMR spectra and analysis and also N. Snider for MS spectra (Laboratory Services Division, Agriculture Canada).

References

[1] *Off. J. European Communities, Special Edition*, 8 (1973) 4.
[2] *Off. J. European Communities*, L245 (1985).
[3] H.D. Chapman, *Parasitol. Today*, 9 (1993) 159.
[4] J. Zulalian and P.E. Gatterman, *J. Agr. Food Chem.*, 21 (1973) 794.
[5] K. Al-Shawabkeh, *Disarat Ser. B, Pure Appl. Sci.*, 17 (1990) 86.
[6] M.Q. Xie, T. Fukata, J.M. Gilbert and L.R. MacDougald, *Parasitol. Res.*, 77 (1991).
[7] G.F. Bories, *Analyst*, 100 (1975) 567.
[8] M.K. Cody, G.B. Clark, B.O.B. Conway and N.T. Crosby, *Analyst*, 115 (1990) 1.
[9] J.B. Zagar, P.O. Ascione and G.P. Chrekian, *J. Assoc. Off. Anal. Chem.*, 58 (1975) 822.
[10] F. Garcia Sanchez and C. Cruse Blanco, *Analyst*, 116 (1991) 851.
[11] D.W. Fink, *Trends Anal. Chem.*, 1 (1982) 254.
[12] W.R. Seitz, *CRC Crit. Rev. Anal. Chem.*, 8 (1980) 367.
[13] N.P.J. Price, J.L. Firmin and D.O. Gray, *J. Chromatogr.*, 598 (1992) 51.

ELSEVIER

Journal of Chromatography A, 694 (1995) 415–423

JOURNAL OF CHROMATOGRAPHY A

High-temperature reversed-phase high-performance liquid chromatographic analysis of a synthetic copolymer on a non-porous support

John Bullock

Sterling-Winthrop Pharmaceuticals Research Division, Collegeville, PA 19426, USA

First received 7 September 1994; revised manuscript received 11 October 1994; accepted 11 October 1994

Abstract

High-temperature HPLC using a non-porous microparticulate reversed-phase column was evaluated for characterizing an exploratory magnetic resonance imaging polymeric contrast agent. High-efficiency separations were achieved allowing resolution of over 50 individual oligomers. Separations were optimized with respect to temperature and addition of neutral salt. Results were compared to those obtained with a traditional porous HPLC support as well as a macroporous perfusion-type column. Separation efficiencies were highest with the non-porous support followed in order by the macroporous and traditional porous packing. The utility of this technique for characterizing degradation of the polymer under stress conditions was demonstrated.

1. Introduction

The application of reversed-phase (RP) HPLC to characterize oligomeric and polymeric materials has been well documented [1–7]. For high-molecular-mass polymers, where the total number of species is very large and the differences in the chromatographic properties of different sized chains is negligible, resolution of individual polymer species is not feasible. In this case RP-HPLC has been restricted to purity determination for residual monomers or other low-molecular-mass impurities or assessment of chemical composition [5,8,9] for certain types of copolymers. However, the chromatographic properties of low-molecular-mass polymers are sometimes distinct enough to allow chromatographic resolution of the polymer into its constituent oligomers. This allows for a more detailed characterization of the chemical species composing the polymer in terms of molecular mass distribution and structural properties.

Examples of HPLC separations of oligomeric materials include polyethers [4–7,10], polystyrene [2], ethoxylated alkyl alcohols and carboxylic acids [11], polyethoxylated octylphenols [12,13] and various copolymers [14–16]. These separations have typically been conducted on traditional bonded phase porous silica packings in either the RP or, in the case of diol and amino bonded phases or bare silica columns, in the normal-phase mode. The advantages of elevated temperatures was noted in some RP-HPLC applications to improve resolution for poly-

0021-9673/95/$09.50
SSDI 0021-9673(94)00974-0

ethers [8] due to improvement in overall chromatographic efficiency in addition to a favorable conformational change in the polymer.

In the field of bioanalytical chemistry, there have been a number of improvements in chromatographic supports in recent years which have resulted in higher chromatographic efficiency and recovery for proteins and oligonucleotides. Of note are the development of small-particle non-porous or micropellicular supports [17–21] operated in either the RP or ion-exchange modes. These supports were designed to have improved mass transfer properties for these large biopolymers which translates in many instances into improved chromatographic efficiencies and recoveries. As with traditional HPLC packings, chromatographic efficiency is expected to increase with increasing temperature for these alternative HPLC supports. However, the instability of these biopolymers to heat has limited the use of these columns at elevated temperatures. Numerous types of wide-pore or macroporous HPLC supports have also been developed for biopolymer separations. Wide-pore columns were designed to allow greater access of the biopolymers to the bonded phase and eliminate the potential for any sizing effects. In the case of the macroporous supports, a second objective is to reduce band spreading as a result of slow diffusion through a porous matrix.

In this work, the application of non-porous and macroporous supports operated at elevated temperatures (up to 100°C) was investigated for characterizing a synthetic, copolymeric, exploratory magnetic resonance imaging (MRI) contrast agent. This agent was designed to have an extended in vivo half-life in the vascular compartment for certain types of diagnostic applications [22]. The samples examined in this work have average molecular masses ranging from 10 000 to over 30 000. The combination of the non-porous packing along with the elevated temperatures was investigated for examining the oligomeric distribution of different molecular mass samples as well as stressed samples of the polymer.

2. Experimental

2.1. Materials

Water was purified by a Barnstead water-purification system (Barnstead/Thermolyne). HPLC-grade acetonitrile was from J.T. Baker and HPLC-grade $NaClO_4$ was purchased from Fisher Scientific. All other chemicals were of reagent grade and from J.T. Baker.

Polymer samples were synthesized as depicted in Fig. 1. Details of the synthesis can be found elsewhere [22]. Molecular mass analysis of the samples was performed by aqueous size-exclusion chromatography. Samples of the polymer were degraded by heating at 80°C in either 0.1 *M* NaOH or 0.1 *M* HCl and neutralized prior to analysis.

2.2. HPLC instrumentation

All separations were conducted on a Hewlett-Packard (HP) 1090M liquid chromatograph controlled by a HP Vectra DOS-based personal computer work station. A 3 cm × 4.6 mm Hytach

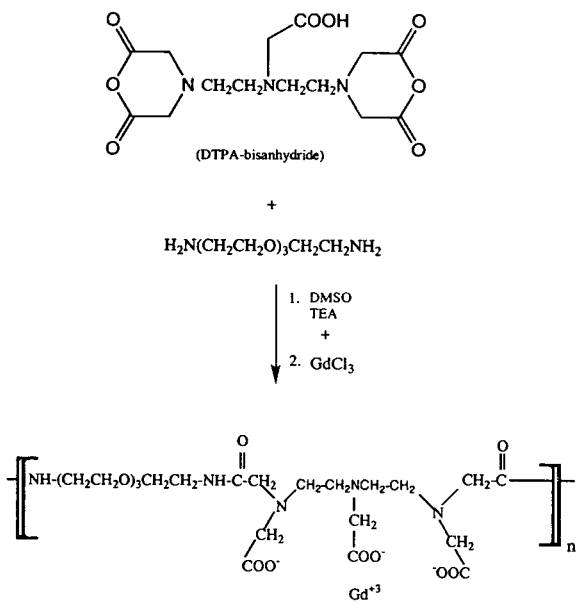

Fig. 1. Synthetic scheme for producing the MRI polymer.

C_{18} column based on a 2-μm non-porous silica support was purchased from Glycotech (Hamden, CT, USA). A 3 cm × 4.6 mm Poros R/H column based on a macroporous perfusion type support was obtained from Perseptive Biosystems (Cambridge, MA, USA). A Capcell PAK C_{18} SG, 120 Å, 15 cm × 4.6 mm column was obtained from Dychrom (Sunnyvale, CA, USA). Unless otherwise noted, solvent A was 400 m*M* $NaClO_4$ and solvent B was 400 m*M* $NaClO_4$ in a mixture of acetonitrile–water (20:80). The flow-rate was 1 ml/min and detection was accomplished at 200 nm. Polymer samples were prepared in the A solvent at 6 mg/ml. Injection volumes of 3 μl were used corresponding to 18 μg of polymer. The column temperatures and gradient profiles used are indicated in the text.

3. Results

3.1. Influence of temperature on efficiency and resolution

Fig. 2 displays a set of chromatograms obtained at different temperatures using the non-porous RP-HPLC column on a synthetic polymer sample of average molecular mass 30 000. A linear gradient from 0 to 100% B over 60 min was used in each case. A significant improvement in resolution and efficiency accompanied by decreasing retention is observed with increasing temperature. At the highest temperature, partial resolution of up to the first 50 or so oligomers is achieved. The characteristic pattern of peaks observed in these chromatograms is

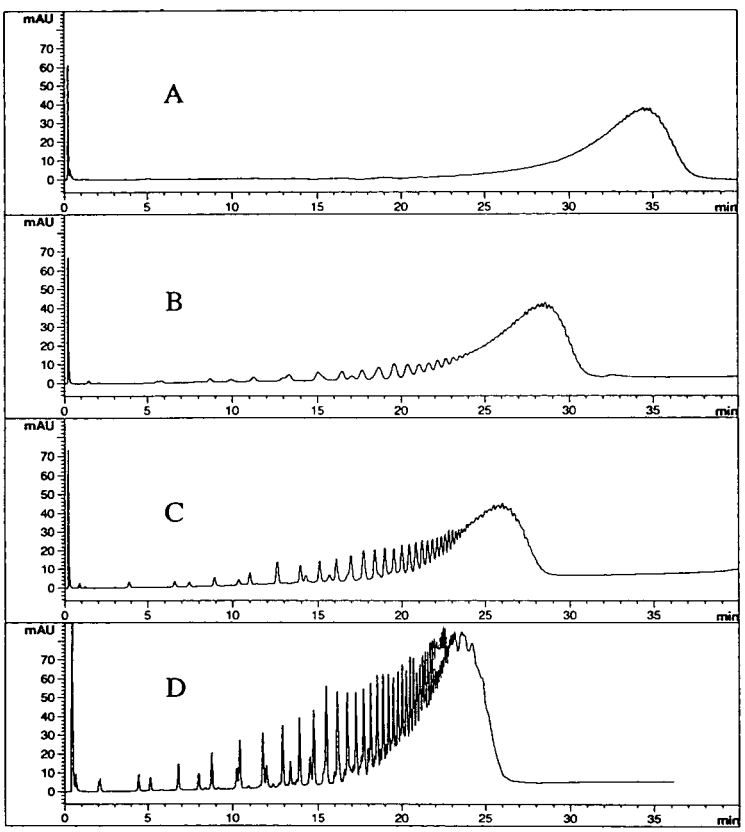

Fig. 2. Separations of a polymer of average molecular mass 30 000 at different operating temperatures: (A) 25°C, (B) 60°C, (C) 80°C and (D) 100°C. Gradient profile from 0 to 100% B in 60 min. Refer to Experimental section for other conditions.

interpreted to result from the distribution in molecular mass as well as the variability in the composition of end groups on each polymer chain which is anticipated for this condensation copolymer. This pattern was highly reproducible from analysis to analysis. In addition, the stability of the polymer at neutral pH values up to 121°C for at least 1 h has been established ruling out any type of on-column chemical degradation of the polymer.

3.2. Effect of neutral salt on retention

Fig. 3 contains chromatograms obtained under the identical conditions used in Fig. 2 except for the level of salt, $NaClO_4$, used in the mobile phase. This particular salt was chosen because of its high solubility in acetonitrile in addition to its low UV absorbance at the low wavelengths used in this work. In general, addition of salt increased retention of the polymer. This phenomenon can probably be explained by a "salting in" effect with the addition of increasing amounts of $NaClO_4$. An increase in the number of oligomers separated was observed in going from no salt to 400 m*M* salt. No significant improvement in resolution was attained at levels above 400 m*M* $NaClO_4$. In addition, this salt was also beneficial in minimizing any secondary ionic or silanophilic interactions between the silica support and the ionic termini or polar regions of the polymer. In the absence of any salt, the high-molecular-mass end of the polymer distribution tailed off slowly and did not return to baseline until about 45

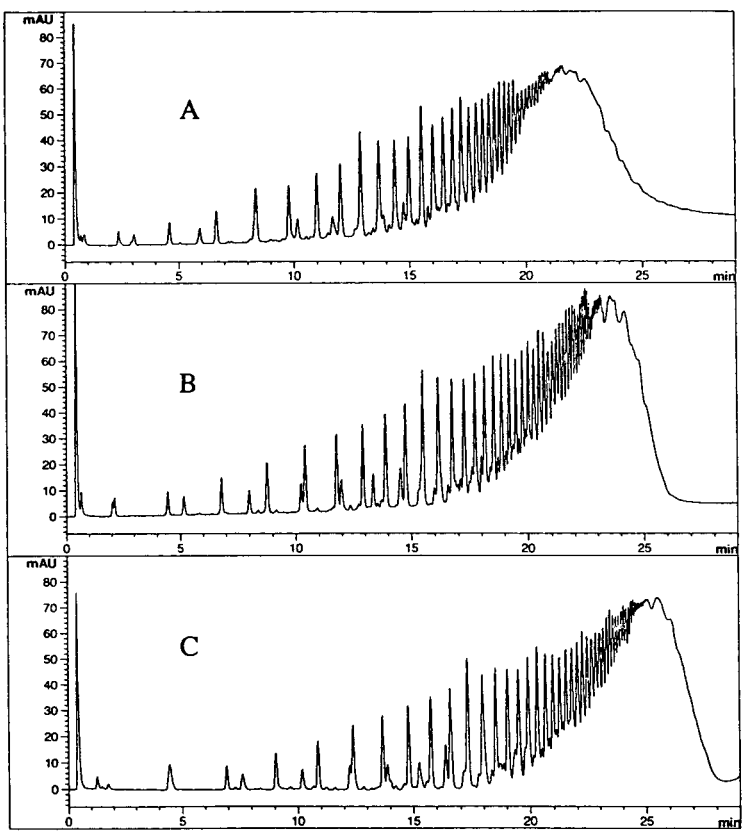

Fig. 3. Separations of a polymer of average molecular mass 30 000 at 100°C with different concentrations of $NaClO_4$: (A) no salt, (B) 400 m*M* and (C) 1000 m*M*. Other conditions as given in Fig. 2.

min. In the presence of salt, the high-molecular-mass portion of the polymer peak displayed no significant tailing.

3.3. Comparison of results on different types of packings

Fig. 4 compares the separation obtained at 100°C on the non-porous HPLC column to that obtained on a traditional porous C_{18} silica (120 Å) as well as a reversed-phase perfusion type (Poros) of packing. The Poros column contains a packing material composed of macropores of two size ranges: 800–1500 Å and 6000–8000 Å [23]. In terms of resolution and efficiency, a clear-cut advantage is observed with the non-porous packing material compared to the traditional porous column. The results with the Poros column were intermediate between the other two columns but, in general, this column showed significant improvement in resolution compared with the traditional C_{18} RP column. The lower retention of the polymer on the traditional pore size column compared to the macroporous column may indicate that the sample cannot fully penetrate the small pores of the former column. However, the retentive surface of these columns is different (C_{18} derivatized silica versus aromatic derivatized polystyrene resin) and, therefore, the inherent difference in hydrophobicities and capacities of these columns may account for the difference in polymer retention. Both the

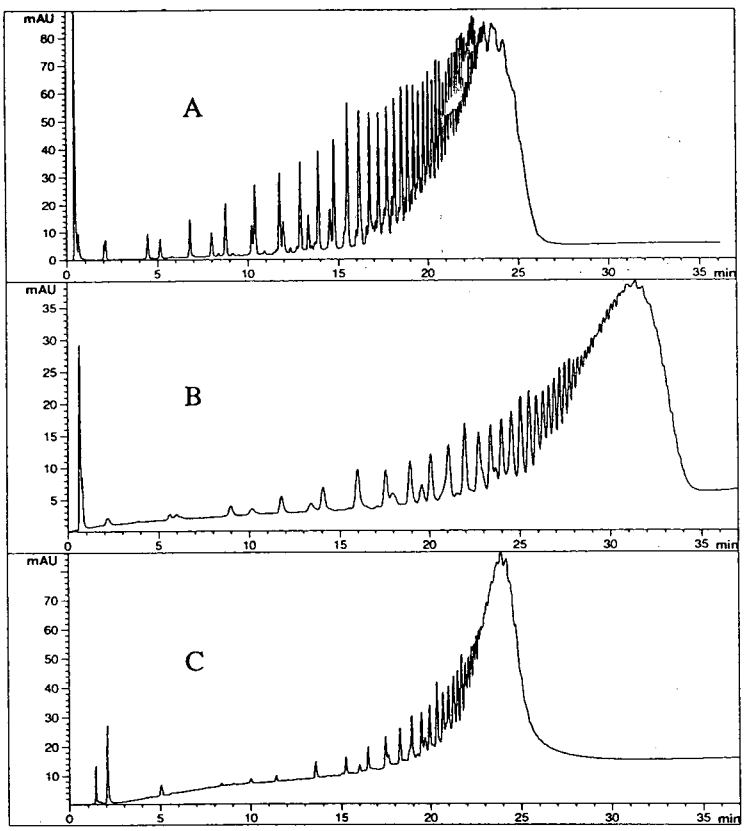

Fig. 4. Separations of a polymer of average molecular mass 30 000 on three different types of columns: (A) non-porous, (B) macroporous and (C) traditional porous RP-HPLC column. Operating temperature of 100°C and gradient profile of 0 to 100% B in 60 min. Other conditions as given in the Experimental section.

Poros and traditional C_{18} columns demonstrated an improvement in resolution with increasing temperature (data not shown) as was observed with the non-porous column.

Of concern in this work was the stability of the columns to high temperature. The manufacturer of the Poros column recommends an upper temperature limit of 80°C and so this column was used at elevated temperatures for only short periods. The other two manufacturers do not explicitly specify temperature limits. While the long-term stability of the non-porous column at 100°C has not been determined, daily use at these elevated temperatures for several weeks did not result in any noticeable deterioration in column performance.

3.4. Analysis of different molecular mass samples

The dependency of retention on molecular mass is substantiated based on analysis of polymer samples of different molecular mass. Fig. 5 depicts the chromatograms obtained on three different samples of average molecular masses 30 000, 15 000 and 8000 using the non-porous column at 100°C. These results demonstrate that for low-molecular-mass polymers (less than approximately 15 000) almost the entire distribution of polymeric species can be at least partially resolved. For higher-molecular-mass polymers, this technique is still useful for examining the lower-molecular-mass range of the distribution in

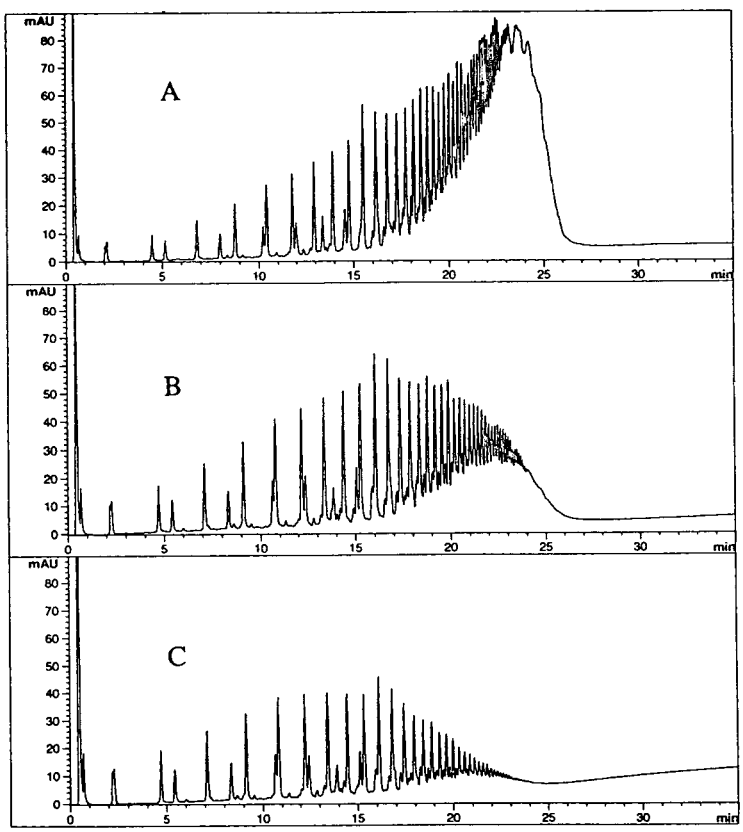

Fig. 5. Separations of polymers of average molecular mass (A) 30 000, (B) 15 000 and (C) 8000 on the non-porous RP-HPLC column operated at 100°C with a gradient of 0 to 100% B in 60 min.

addition to potential degradation products (see below).

3.5. Characterization of degradation products in stressed polymer samples

One of the potential uses of this methodology is to analyze for potential degradation products of the polymer as well as other low-molecular-mass by-products and residual starting materials. Polymer samples that were subjected to hydrolysis in acid or base at elevated temperatures were analyzed on the non-porous column at 100°C. Fig. 6 contains chromatograms of the base stressed polymer obtained at different time points. Substantially the same chromatograms in terms of oligomer profiles were obtained in the acid stressed samples although the rate of hydrolysis was slower in acid. With increasing hydrolysis time the oligomeric distribution in these stressed samples shifts to lower molecular masses. A distinct pattern of peaks is observed in these chromatograms and, in general, the pattern of low-molecular-mass oligomers formed on stressing differs somewhat from that originally present in the polymer. It is probable that degradation occurs primarily through hydrolysis of the amide linkages in the polymer, although other modes of degradation cannot be ruled out. In this case, one would expect to obtain a different compositional distribution in terms of end groups on individual polymer chains which

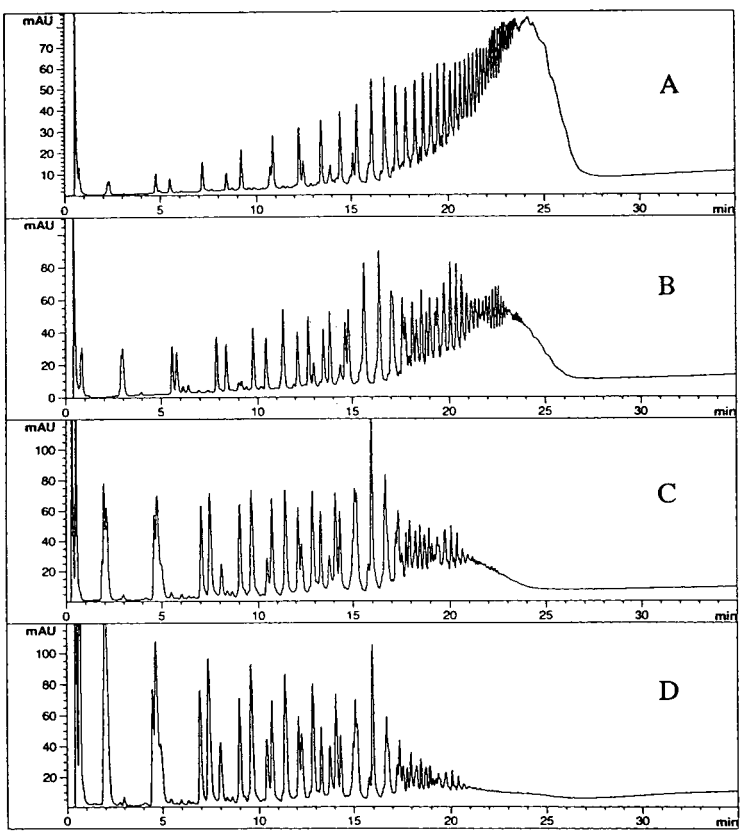

Fig. 6. Separations of a polymer of average molecular mass 30 000 stressed in 0.1 *M* NaOH at 80°C for (A) 0 min, (B) 5 min, (C) 15 min and (D) 30 min. Conditions as in Fig. 4 for the non-porous RP-HPLC column.

would change the pattern of peaks compared with the unstressed polymer.

4. Discussion

The high efficiency and resolution achieved here for individual oligomers in this polymer results from the combination of the small particle non-porous packing material in conjunction with high operating temperatures. The small particle size of the non-porous packing (2 μm) is expected to contribute some degree to the improved efficiency. The non-porous morphology of the particles should lend itself to an additional level of improvement in efficiency as a result of lowering the resistance to mass transfer. Finally, molecular diffusivity and sorption kinetics should increase with increasing temperature adding to the overall improvement in efficiency. These points are supported by the experiments documented here. In fact, the benefits of elevated temperatures when used in conjunction with non-porous supports has been predicted by Antia and Horváth [24] for the reasons enumerated here. In particular, their theoretical treatment of this subject matter highlighted these advantages for high-mass materials. Studies involving biopolymer separations on non-porous supports with temperatures as high as 80°C have been reported but in general the instability of these compounds to heat has limited the upper temperature used. The improvement in resolution obtained with the macroporous perfusion-type column compared to the traditional porous column is probably due to the superior mass transport through the macroporous support.

The use of high temperatures up to 80°C in conjunction with traditional porous supports has been reported for polyether-type oligomer separations [8]. In this case higher resolution with increasing temperature was concluded to result from the improvement in overall chromatographic efficiency with increasing temperature in addition to a favorable structural conformational change in the oligomers which resulted in better interaction of the oligomers with the bonded phase. Studies are ongoing to assess possible temperature induced conformational changes in the MRI polymer which might be contributing to the improved chromatographic efficiency and resolution observed in this work. However, preliminary differential scanning calorimetry studies could not substantiate any structural changes in the polymer with increasing temperature.

5. Conclusions

Oligomer separations for a synthetic copolymer with average molecular masses in the range 8000–30 000 have been achieved using a non-porous RP-HPLC column operated at elevated temperatures. The combination of the unique morphology of this type of column packing material in conjunction with high operating temperatures was shown to be necessary to achieve high-resolution separations of individual oligomers.

Acknowledgements

D. Ladd, R. Hollister, G. Wu and X. Peng of the Department of Medicinal Chemistry at Sterling-Winthrop are thanked for the preparation of the polymer samples.

References

[1] C.G. Smith, P.B. Smith, A.J. Pasztor, M.L. McKelvy, D.M. Meunier, S.W. Froelicher and A.S. Ellaboudy, *Anal. Chem.*, 96 (1993) 217R.
[2] P. Jandera, *J. Chromatogr.*, 449 (1988) 361.
[3] T.C. Schunk, *J. Chromatogr. A*, 656 (1993) 591.
[4] G. Barka and P. Hoffmann, *J. Chromatogr.*, 389 (1987) 273.
[5] G. Glockner, *J. Appl. Polym. Sci.*, 51 (1992) 45.
[6] K. Rissler, U. Fuchslueger and H.J. Grether, *J. Chromatogr. A*, 654 (1993) 309.
[7] L.R. Snyder and J.J. Kirkland, *Introduction To Modern Liquid Chromatography*, Wiley-Interscience, New York, 2nd ed., 1979, pp. 317, 359.
[8] S. Teramachi, A. Hasegawa, T. Matsumoto, Y. Tsukahara and Y. Yamashita, *Macromolecules*, 25 (1992) 4025.

[9] T.C. Schunk, *J. Chromatogr. A*, 661 (1994) 215.
[10] R.E.A. Escott and N. Mortimer, *J. Chromatogr.*, 553 (1991) 423.
[11] Y. Mengerink, H.C.J. de Man and Sj. van der Wal, *J. Chromatogr.*, 552 (1991) 593.
[12] Z. Wang and M. Fingas, *J. Chromatogr.*, 637 (1993) 145.
[13] W.R. Melander and Cs. Horváth, *J. Chromatogr.*, 185 (1979) 129.
[14] S. Mori and M. Mouri, *Anal. Chem.*, 61 (1989) 2171.
[15] H.S. Sato, K. Ogino, S. Maruo and M. Sasaki, *J. Polym. Sci., Polym. Phys.*, 29 (1991) 1073.
[16] S. Mori, *J. Appl. Polym. Sci., Polym. Symp.*, 48 (1991) 133.
[17] T. Hashimoto, *J. Chromatogr.*, 544 (1991) 257.
[18] K.K. Unger, G. Jilge, J.N. Kinkel and M.T.W. Hearn, *J. Chromatogr.*, 359 (1986) 61.
[19] K. Kalghatgi, *J. Chromatogr.*, 499 (1990) 267.
[20] Y.F. Maa and Cs. Horváth, *J. Chromatogr.*, 445 (1988) 71.
[21] D.C. Lommen and L.R. Snyder, *LC·GC*, 11 (1993) 222.
[22] R.A. Snow, D.L. Ladd, J.L. Toner and K.R. Hollister, *US Pat. Appl.*, 93 09766 (1993).
[23] F.E. Regnier, *Nature*, 350 (1991) 634.
[24] F.D. Antia and Cs. Horváth, *J. Chromatogr.*, 435 (1988) 1.

ELSEVIER

Journal of Chromatography A, 694 (1995) 425–431

JOURNAL OF CHROMATOGRAPHY A

Arsenic speciation by micellar liquid chromatography with inductively coupled plasma mass spectrometric detection ☆

Hong Ding, Jiansheng Wang, John G. Dorsey, Joseph A. Caruso*

Department of Chemistry, University of Cincinnati, Cincinnati, OH 45221-0172, USA

First received 15 June 1994; revised manuscript received 2 November 1994; accepted 8 November 1994

Abstract

Four environmentally and biologically important arsenic species, dimethylarsenic acid (DMA), monomethylarsonic acid (MMA), As(III) and As(V) are separated by micellar liquid chromatography. Linear dynamic ranges for the four species are three orders of magnitude and detection limits are in the picogram range with inductively coupled plasma mass spectrometric (ICP-MS) detection. This paper discusses in detail the development of the chromatographic conditions. The micellar mobile phase, which consisted of 0.05 *M* cetyltrimethylammonium bromide, 10% propanol and 0.02 *M* borate buffer, showed good compatibility with ICP-MS. This method allowed direct injection of urine samples onto the chromatographic system without extensive pretreatment and presented no interference from chlorine in the matrix. Detection limits are comparable with other LC–ICP-MS studies. An SRM urine sample was used to demonstrate the applicability of this technique to "real-life" situations. Results indicated that DMA, MMA and As(V) were present in the urine sample.

1. Introduction

Micellar liquid chromatography (MLC) refers to the type of chromatography that uses surfactants in aqueous solutions well above their critical micelle concentrations (CMC), as alternative mobile phases for reversed-phase liquid chromatography (RPLC). Armstrong and Henry [1] were the first to demonstrate the usefulness of MLC and there have been excellent reviews of this unique technique [2,3]. In addition to the number of compounds with a wide range of polarities amenable to separations by RPLC, MLC extends the analyte candidates to almost all hydrophobic and many hydrophilic compounds providing they can partition to the micelles. Other advantages MLC offers over RPLC, such as simultaneous separation of both ionic and non-ionic compounds, faster analysis times and improved detection sensitivity and selectivity [4], stem from its unique three-way equilibrium mechanism [5] where micelles act as a pseudo phase in addition to the mobile and stationary phases.

Elemental speciation is becoming more and more important since the environmental toxicity and biological importance of many elements depend on their different chemical forms and oxidation states. Inductively coupled plasma

* Corresponding author.

☆ Presented in part at the *20th FACSS Meeting, Detroit, IL, October 1993*, paper 338, and at the *Winter Conference on Plasma Spectrochemistry, San Diego, CA, January 1994*, paper TP32.

0021-9673/95/$09.50
SSDI 0021-9673(94)01085-4

mass spectrometry (ICP-MS) is the dominant detection method used in elemental analysis due to its elemental specificity and trace level detection limits. By combining the separation power of chromatography and the element-selective detection of ICP-MS, HPLC–ICP-MS becomes an excellent technique in trace level speciation [6,7].

Arsenic has found wide use in pesticides, herbicides, wood preservatives, desiccants, etc., and arsenic exposure occurs in many circumstances including occupations (coal mines, smelters), air and food [8]. The toxicity of arsenic varies widely with the different chemical forms. The inorganic arsenics are more toxic than the organoarsenicals, while trivalent arsenic compounds are more toxic than their pentavalent counterparts [8]. Monomethylarsonic acid (MMA) and dimethylarsenic acid (DMA) are the two main metabolites found to be toxic. The four arsenic compounds, As(III), As(V), DMA and MMA investigated in this work are the arsenic species studied most in the literature. The speciation of these four compounds by chromatography have mainly focused on ion-exchange [9–15] and ion-pairing techniques [10,16,17]. HPLC–ICP-atomic emission spectrometry (AES) for arsenic speciation was first discussed in 1981 [9]. Since then the detection limits have been greatly improved over the optical work with the use of ICP-MS [10–17].

The main focus of this work was to investigate the use of MLC for direct injection of "dirty samples" and better compatibility with ICP-MS. With conventional hydro–organic mobile phases, "dirty samples" such as body fluids, usually have to be deproteinized before chromatography to prevent protein precipitation in the column. However, the unique micelle aggregates in MLC should dissolve proteins in the sample and cause them to elute with the void volume without plugging the column. The possibility of direct sample introduction should greatly simplifies sample treatment and improves accuracy. In addition, MLC should give better compatibility to ICP-MS than RPLC. This is because MLC uses no or low concentrations of organic solvents, while the high organic content in RPLC usually leads to plasma instability, increased background and carbon deposition on the sampling cone of the ICP.

2. Experimental

A VG PlasmaQuad PQII + turbo (VG Elemental, Winsford, UK) ICP-MS system was used with a nickel sampler and skimmer, both of 1.0 mm diameter orifice. The sample introduction system consisted of a C-1 type concentric nebulizer (Precision Glassblowing, Parker, CO, USA) and a double-pass spray chamber cooled to 5°C with a Neslab (Portsmouth, NH, USA) Endocal refrigerated chiller.

The HPLC system was a Dionex AI-450 metal-free model (Dionex, Sunnyvale, CA, USA) with a Rheodyne Model 9125 injector (Cotati, CA, USA) and a laboratory-built 100-μl injection loop. A Hamilton (Reno, NV, USA) PRP-1 column (15 cm × 4.1 mm), with a guard column made of the same material was used.

LC was operated isocratically with a flow-rate of 1.0 ml/min. The outlet of the analytical column was connected to the nebulizer through a piece of polyether ether ketone (PEEK) (25 cm × 0.10 mm) and then PTFE capillary tubing (25 cm × 0.12 mm), with a total volume of approximately 4.8 μl which would have a minimum effect on extra-column peak broadening.

For preliminary work, an Alltech RP metal-free column (15 cm × 4.6 mm) (Deerfield, IL, USA) and a guard column of the same material were coupled to ICP-AES (PlasmaTherm, Kresson, NJ, USA). The early HPLC system consisted an ISCO Model 2350 pump and 2360 programmer (Lincoln, NE, USA), and a Rheodyne 7010 injector with a 100-μl sample loop.

Void volumes were measured by the injection of water.

2.1. Standards and reagents

Chemicals used were reagent grade, and obtained from Fisher Scientific (Fair Lawn, NJ, USA) except when otherwise indicated.

The mobile phase used was prepared from

cetyltrimethylammonium bromide (CTAB) and distilled deionized water, with a resistance of 18 MΩ (Barnstead, Boston, MA, USA). The buffer was made from boric acid and the pH of solutions was adjusted with sodium hydroxide. *n*-Propanol was added as the mobile phase modifier. Stock solutions (1000 ppm as arsenic) of DMA, As(III) and As(V) in mobile phase, were prepared from cacodylic acid, sodium arsenite and sodium arsenate, respectively. MMA stock solution (from Dr. John S. Thayer, Department of Chemistry, University of Cincinnati) was used as received.

Freeze-dried urine SRM 2670, elevated level, was obtained from National Institute of Standards and Technology (NIST, Gaithersburg, MD, USA). It was reconstituted according to instructions and filtered once with a 0.45-μm syringe filter (Alltech).

3. Results and discussion

3.1. Mobile phase compositions

The preliminary optimization of the chromatography was carried out with the ISCO HPLC system and ICP-AES.

In aqueous solvents, these arsenic species dissociate to give anions, thus CTAB became the surfactant of choice since the cationic CTAB would allow better partitioning of solutes into the micelles due to electrostatic interactions. Fig. 1 shows that the capacity factor, k', of arsenic compounds, decreased with increasing mobile phase concentrations, and resulted in reasonable retention times with CTAB concentrations ≥ 0.05 *M*. However, for ICP operations, it is important to note that salt (CTAB) content should be kept as low as possible to minimize clogging problems. With 0.1 *M* CTAB, deposition of salt at the nebulizer, spray chamber and torch injector tip occurred. Therefore 0.05 *M* is a practical compromise. For As(V), no data were plotted for CTAB concentrations below 0.1 *M*, because at mobile phase concentrations below 0.1 *M*, As(V) eluted at very long times ($k' > 15$) with very broad peaks.

In order to decrease the retention time of As(V), and improve the peak shape, the *n*-propanol concentration was varied. It has been reported that 3% propanol as the mobile phase additive is essential to enhance column efficiency in MLC [18] by improving slow mass transfer. Fig. 2 shows that with increased propanol concentration, k' of all four arsenic compounds decreased, giving shorter retention times (within 15 min). Signal-to-background ratios improved dramatically from 5 to 10% propanol in the mobile phase, as seen in Fig. 3. This is because increased propanol concentration improved the chromatography while having negligible degradation on plasma stability or analyte sensitivity. This improvement resulted in better peak shapes and thus better signal-to-background ratios as calculated from peak heights. A 10% propanol concentration was chosen because the signal-to-background ratios at 10% propanol were com-

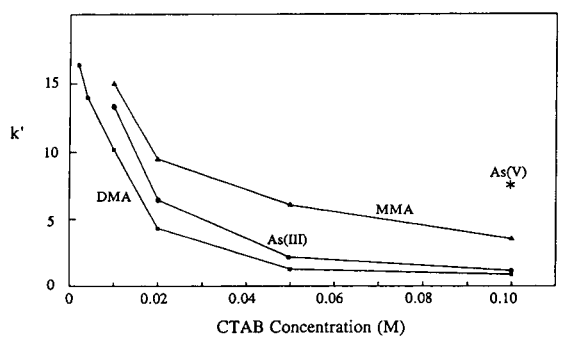

Fig. 1. Effect of CTAB concentration on k' with 5% propanol and pH 10.

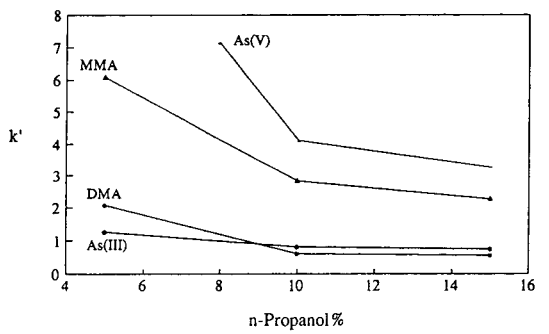

Fig. 2. Effect of percentage of propanol on k' at 0.05 *M* CTAB and pH 10.

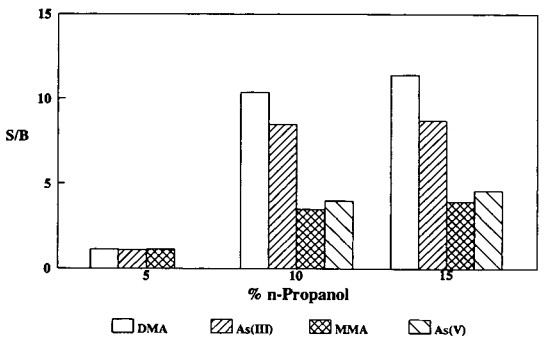

Fig. 3. Effect of propanol concentration on sensitivity at 0.05 *M* CTAB and pH 10.

parable to those obtained at 15% and the organic solvent should be kept as low as possible to favor micelle formation.

In order to improve the resolution between DMA and As(III), the pH of the mobile phase was studied. Although the chromatography used here was not an ion-exchange mode, the pH of the mobile phase had an important effect on retention. This is mainly because arsenic compounds are more anionic under more basic conditions, [for As(V), $pK_{a1} = 2.25$, $pK_{a2} = 6.77$ and $pK_{a3} = 11.6$; $pK_a = 9.23$ for As(III); $pK_a = 6.19$ for DMA; pK_a for MMA is not available), thus giving more interaction with the cationic micelles. As expected, longer retention of arsenic species was observed with increasing pH of the mobile phase. As can be seen from Fig. 4, a mobile phase of pH 12 would give the best separation between DMA and As(III). However, pH 12 was not practical because the large amount of NaOH needed to reach pH 12 caused severe salt deposition in the torch, and on the sampler and skimmer of the ICP. A pH value of 10.2 provided the best compromise, giving a baseline resolution ($R_s = 8$) between the two peaks while maintaining reasonable analysis times. The sudden change of k' (evident in Fig. 4), as a function of mobile phase pH values higher than pH 12, might be caused by changes in the stationary phase. The polystyrene–divinylbenzene beads were believed to swell and shrink with extreme mobile phase pH, causing changes in the active sites responsible for retention.

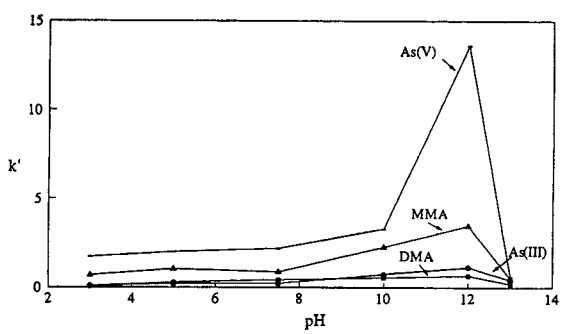

Fig. 4. pH effect on k' at 0.05 *M* CTAB and 15% propanol.

In summary, 0.05 *M* CTAB, 10% propanol, 0.02 *M* borate buffer and 40°C column temperature were used for mobile phase conditions.

3.2. HPLC–ICP-MS

After the preliminary study, the Dionex HPLC system was interfaced to ICP-MS to carry out calibration and sample analysis. Parameters for ICP-MS were optimized based on signal-to-background ratios and are summarized in Table 1. The spray chamber was cooled to minimize solvent vapor loading to the plasma. However, temperatures below 5°C were not advisable due to precipitation of CTAB. (Other surfactants such as cetyltrimethylammonium chloride, could be used should lower temperatures be needed). A separation of the four arsenic standards with good resolution is shown in Fig. 5 and figures of merit are illustrated in Table 2. For the arsenic standards, concentrations of 5 ppb, 10 ppb, 100 ppb and 1 ppm were used. The response (based on peak height) of this technique was linear over

Table 1
ICP-MS conditions

Forward power	1.35 kW
Reflected power	2 W
Nebulizer flow	0.74 l/min
Auxiliary flow	1.0 l/min
Coolant flow	12 l/min
Spray chamber temperature	5°C

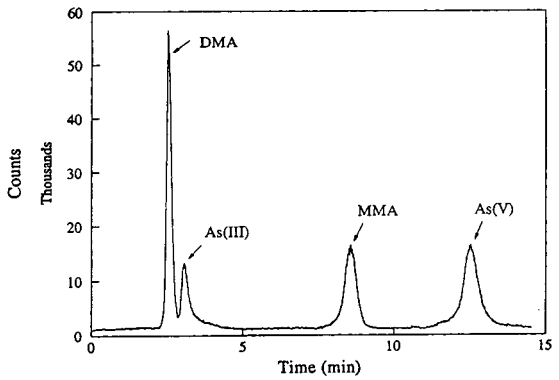

Fig. 5. Chromatogram of mixture of four arsenic standards. Hamilton PRP-1 column. Chromatographic conditions: 0.05 *M* CTAB, 10% propanol, pH 10.2, column temperature 40°C. $m/z = 75$.

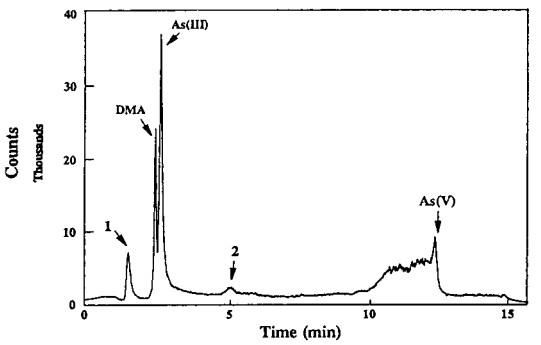

Fig. 6. Chromatogram arsenic speciation in urine. Hamilton PRP-1 column. Chromatographic conditions as in Fig. 5. $m/z = 75$. Peaks 1 and 2 are different forms of Cl^-.

three orders of magnitude. Detection limits were 90 pg for DMA, and 300 pg for As(III), MMA and As(V). Reproducibilities were determined by eight injections of a 100 ppb test mixture, and relative standard deviations were less than or equal to 5%. The better detection limit for DMA, compared to the other three compounds, is primarily due to the better peak shape.

Detection limits of this work compare favorably with those of ion-pairing chromatography (from 50 to ca. 300 pg) [10]. However, they are higher than the results obtained with an ion-exchange technique (from 20 to ca. 91 pg) [12]. This can be ascribed to the larger peak volumes [19] in this work, and possibly the complex mobile phase content, especially the Na^+ ions (coming from the buffer), which might have caused suppression of the ionization of arsenic, resulting in decreased signal sensitivity.

3.3. Analysis of urine

Urine samples were filtered prior to injection, and were then injected directly onto the column without any further treatment. Fig. 6 shows that DMA, As(III) and AS(V) were found with concentrations listed in Table 3. Total arsenic found was 0.52 ± 0.02 ppm, which is in agreement with the certified value of 0.48 ± 0.10 ppm. The last peak was, however, very broad and may represent more than one arsenic species. Spiking a 30 ppb standard in urine confirmed the presence of As(V), however, to this point we do not have a positive identification of the hump before the peak of As(V).

Table 2
Analytical figures of merit for arsenic speciation

	DMA	As(III)	MMA	As(V)
Linear dynamic range (orders of magnitude)	3	3	3	3
R^2	0.9990	0.9797	0.9880	0.9856
R.S.D. (%)[a]	3.4	4.7	4.9	5.0
Slope of log–log plot	0.99	0.93	0.92	0.91
Detection limit (pg)[b]	90	300	300	300

[a] R.S.D. of peak height for 8 replicate injections of 10 ng arsenic analyte.
[b] Detection limit defined by 3 × standard deviation of background/slope of calibration curves.

Table 3
Speciation of arsenic in urine

	Urine	Certified value
DMA	0.07 ± 0.01 ppm	
As(III)	0.40 ± 0.01 ppm	
As(V)	0.05 ± 0.01 ppm	
Total	0.52 ± 0.02 ppm	0.48 ± 0.10 ppm

3.4. Chlorine interference

A chloride interference ($^{40}Ar^{35}Cl^+$, the polyatomic ion formed in the plasma at $m/z = 75$) with arsenic can be severe in chloride-containing matrices, particularly in biological samples. In other studies, elimination of the $ArCl^+$ was investigated using hydride generation [17] and by chromatographically separating Cl^- from arsenics using an ion-exchange column with appropriate sample dilution [13]. In this method, however, the Cl^- interference did not pose a problem. Figs. 6 and 7 show two Cl^--containing complexes eluting from the column (confirmed by monitoring at $m/z = 77$, $^{40}Ar^{37}Cl$ where monoisotopic arsenic is not present). One of the two complexes may be in the form of hyperchloride containing species (some Cl^- may be converted to hyperchloride under the very basic conditions of the mobile phase). Nevertheless, they did not co-elute with any of the four arsenic compounds. Some Cl^- was found to be retained on the column after 30 to 40 injections of pure 0.15 *M* NaCl solution (human urine is about 0.15 *M* in NaCl [20]), as observed by the high background at $m/z = 77$. This can be explained by the electrostatic attraction between Cl^- and some of the cationic CTAB adsorbed on the column. However, the retained Cl^- was readily removed by flushing the column with methanol–water.

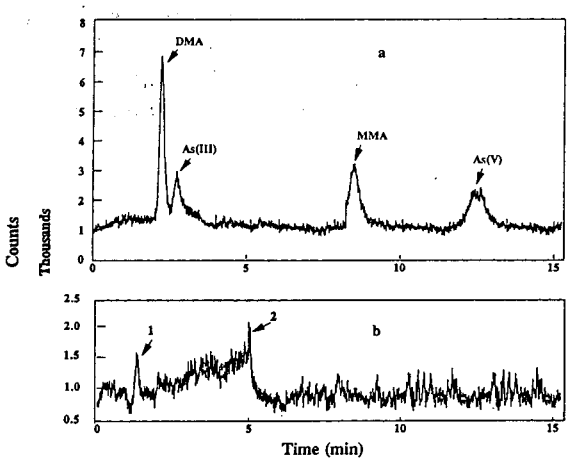

Fig. 7. Comparison of retention of arsenic standards and NaCl. $m/z = 75$. (a) Injection of 10 ppb standard, (b) injection of 0.15 *M* NaCl. Peaks 1 and 2 in chromatogram b are different forms of Cl^-.

4. Conclusions

MLC is compatible with ICP-MS and provides comparable figures of merit with other LC–ICP-MS methods. No O_2 addition to the nebulizer gas was necessary as is usually the case with methanol–or acetonitrile–water mobile phases. This reduces instrumental complexity, and prolongs the life-time of the sampling cone. No serious salt deposition was observed if periodically, a short rinse with 3% HNO_3 solution was carried out. Urine samples were filtered only before injection and no pressure build-up was observed, illustrating the capability for direct introduction of "dirty samples" onto the chromatographic system. The many advantages of MLC demonstrated by this work, clearly indicates that it is worthy of further investigation as an alternative chromatographic mode for ICP-MS detection.

Acknowledgements

The authors would like to thank National Institute of Environmental Health Sciences, through grant numbers ES-03221 and ES-04908 for financial support, and the Environmental Protection Agency for assisting in the purchase of the VG PlasmaQuad PQII instrument through grant number CR818301-02. We are also grateful to the Electric Power Research Institute for support by grant number 2485-26. H.D. is par-

ticularly grateful to Dr. Lisa K. Olson for correcting the manuscript.

References

[1] D.W. Armstrong and S.J. Henry, *J. Liq. Chromatogr.*, 3 (1980) 657.
[2] D.W. Armstrong, *Sep. Purif. Methods*, 14 (1985) 213.
[3] J.G. Dorsey, *Adv. Chromatogr.*, 27 (1987) Ch. 5.
[4] D.W. Armstrong and F. Nome, *Anal. Chem.*, 53 (1981) 1662.
[5] M.G. Khaledi, *Trends Anal. Chem.*, 7 (1988) 293.
[6] J.J. Thompson and R.S. Houk, *Anal. Chem.*, 58 (1988) 2541.
[7] N.P. Vela, L.K. Olson and J.A. Caruso, *Anal. Chem.*, 65 (1993) 585A.
[8] B.A. Fowler, *Biological and Environmental Effect of Arsenic*, Elsevier, Amsterdam, New York, 1983.
[9] M. Morita, T. Uehiro and K. Fuwa, *Anal. Chem.*, 53 (1981) 1806.
[10] D. Beauchemin, K.W.M. Siu, J.W. McLaren and S.S. Berman, *J. Anal. At. Spec.*, 4 (1989) 285.
[11] B.S. Sheppard, J.A. Caruso, D.T. Heitkemper and K.A. Wolnik, *Analyst*, 117 (1992) 971.
[12] D.T. Heitkemper, J. Creed, J.A. Caruso and F.L. Fricke, *J. Anal. At. Spec.*, 4 (1989) 279.
[13] B.S. Sheppard, W. Shen, J.A. Caruso, D.T. Heitkemper and F.L. Fricke, *J. Anal. At. Spec.*, 5 (1990) 431.
[14] E.H. Larsen, G. Pritzl and S.H. Hansen, *J. Anal. At. Spec.* 8 (1993) 557.
[15] S. Branch, L. Ebdon and B. O'Neill, *J. Anal. At. Spec.*, 9 (1994) 33.
[16] D. Beauchemin, M.E. Bednas, S.S. Berman, J.W. McLaren, K.W.M. Siu and R.E. Sturgeon, *Anal. Chem.*, 60 (1988) 2209.
[17] W.C. Story, J.A. Caruso, D.T. Heitkemper and L. Perkins, *J. Chromatogr. Sci.*, 30 (1992) 427.
[18] J.G. Dorsey, M.T. DeEchegaray and J.S. Landy, *Anal. Chem.*, 55 (1983) 924.
[19] J.P. Foley and J.G. Dorsey, *Chromatographia*, 18 (1984) 503.
[20] G.K.C. Low, G.E. Bately and S.J. Buchanan, *Chromatographia*, 22 (1986) 292.

ELSEVIER

Journal of Chromatography A, 694 (1995) 433–440

JOURNAL OF CHROMATOGRAPHY A

Quenching-free reactive-flow photometry☆

Kevin B. Thurbide, Walter A. Aue*

Department of Chemistry, Dalhousie University, Halifax, Nova Scotia B3H 4J3, Canada

First received 21 June 1994; revised manuscript received 27 October 1994; accepted 27 October 1994

Abstract

The reactive-flow detector (RFD) behaves in many aspects like the typical flame photometric detector (FPD) for gas chromatography, thereby strongly suggesting that it, too, may be subject to severe, analytically deleterious quenching effects by hydrocarbons. However, tests carried out with compounds of the prominent FPD analytes sulfur, phosphorus, tin and manganese demonstrate —for *all* their emitting species— that the quenching of chemiluminescence by hydrocarbons does *not* occur in the RFD. A mechanistic hypothesis involving the oxygen atom is put forth in an attempt to rationalize this important difference between conventional flame and reactive flow.

1. Introduction

The reactive-flow detector (RFD) is a simple device that monitors the chemiluminescence of gas chromatographic peaks containing sulfur or phosphorus in a glowing column ("reactive flow") of premixed hydrogen–air gas [1]. The reactive flow is tolerant of solvent peaks, stable vis-a-vis moderate changes in composition, and persistent over any desired length of time. Interestingly, though, it is not self-sustaining: the reactive flow must have continuous access to a conventional flame. Reactive flows are easily generated inside borosilicate or quartz capillaries of various lengths and diameters.

The properties of the RFD, as far as investigated, suggest that it is a close cousin in behaviour and performance to the popular flame photometric detector (FPD) [2–26]. This is certainly true of its response to S and P, in particular its sensitivity, selectivity, and linearity (or non-linearity). The only pronounced difference found so far between the two detectors relates to their behavior vis-a-vis two test hydrocarbons: the RFD responds with roughly equal intensity to naphthalene and *n*-dodecane; the FPD, as is well known, responds much stronger to aromatics than to aliphatics.

A second possible difference, also relating to carbon behavior, may have manifested itself in our earlier pursuit of detection limits: in an attempt to elute sulfur and phosphorus peaks as early and as sharp as possible, we allowed them to ride up on the solvent tail (Fig. 3 in Ref. [1]). This is a practice ill suited to the FPD: there, the solvent tail can severely quench analyte response.

Quenching by co-eluting hydrocarbons is one —if not the— major drawback of the FPD [2–26]. Given the prominence and importance of this detector, it is not surprising that many

* Corresponding author.

☆ Part of doctoral thesis of K.B.T.

0021-9673/95/$09.50
SSDI 0021-9673(94)00883-3

attempts should have been made to elucidate and, more importantly, to eliminate its quenching behavior. Not all such efforts have been entirely successful. Perhaps this was not solely the fault of the FPD: quenching effects are known to affect even typical high-energy, thermal emission sources —although less so than they do affect typical low-energy, chemiluminescent systems. The quenching effect, e.g. that of carbon on phosphorus, has been known for more than a century: as P.T. Gilbert relays it in his labor-of-love monograph, E. Mulder found in the 1860s "that a single drop of ether in the hydrogen generator quenches the green (i.e. HPO) spectrum" [27].

Clearly, if the RFD is to have any chance of being accepted by the *analytical* community, it must be less, not more, susceptible to quenching than the FPD. The FPD has so far been shown to respond in an analytically interesting manner to some twenty elements. The ones whose behavior vis-a-vis co-eluting hydrocarbons has been checked (S, Fe, Sn, P, Mn and Cr) were all quenched to a fairly similar degree. This was taken to suggest "that hydrocarbons may quench the exciting flame rather than the excited analyte" [23].

(Note that, to our knowledge, only the *analytically* interesting quenchers have so far been investigated: this means carbon compounds in GC–FPD and carbon and nitrogen compounds in LC–FPD [25,26]. Also, the tin luminescence on quartz can be quenched by phosphorus or by large amounts of tin itself [28].)

Presuming, perhaps wrongly so, that hydrocarbonaceous quenching mechanisms are similar or identical [23] for most or all of the FPD-active elements, we decided to select only a few examples for testing in the RFD. Our selection considered both the analytical relevance and the spectroscopic variety of the emitting species.

Sulfur and phosphorus are obvious candidates for the test, given their history [20] as well as their industrial, environmental and biochemical importance. Both are prominent analytes in present-day analytical laboratories; both produce *molecular* emitters (and perhaps some underlying, very feeble continua). The green HPO* yields a linear calibration curve, the blue S_2^* a roughly quadratic one [2,3,21,29]. Sulfur response can also be linear if the red HSO* [30,31] is sampled. Tin, a main-group metal, is the most sensitive element in the FPD in the form of its blue surface luminescence, i.e. a *continuum* of spectroscopically unknown origin [32,33]; its weaker emitters are the greenish SnOH* and the red SnH*. Organotins are often monitored by the FPD in the residue analysis of fungicides, antifouling compounds, polymer stabilizers, etc. [34]. The transition metal manganese produces, in addition to a somewhat less prominent continuum, strong *atomic* Mn* emission. Its FPD response can be used to determine the common gasoline antiknock additive MMT ([35], cf. [36,37]).

The four elements S, P, Sn and Mn thus represent a good cross-section of chemically important, spectrally disparate, and analytically meaningful test species. Suitably volatile and stable compounds of these elements (the "analytes") will therefore be co-chromatographed with hydrocarbons of a similar retention time (the "quenchers"), in a technique familiar from the literature. The hydrocarbon concentration is to be varied, up to the point where it will temporarily expel the reactive flow from the capillary [1]. The constancy of the analyte's peak height —over several orders of quencher concentration— will then offer a highly sensitive and analytically relevant measure of the detector's resistance to quenching.

2. Experimental

The RFD has been described in Ref. [1]. Briefly, this simple detector, built on the remains of an old Tracor 550 flame ionization detector (FID), monitors the emission of a luminescent, H_2-rich premixed hydrogen–air column, which is enveloped by a glass capillary carrying a regular air-rich hydrogen flame on top. The glowing column in this first prototype is of 3.5 cm length and 1.8 mm diameter; its central section is sampled by a 1/4 in. (1 in. = 2.54 cm) diameter glass image conduit (Edmund Scientific, 101 E.

Gloucester Pike, Barrington, NJ 08007-1368, USA; item 38307) and a Hamamatsu (360 Foothill Road, Bridgewater, NJ 08807-0910, USA) R-268 or R-374 photomultiplier tube of nominal range 300 to 650 nm, or 185 to 850 nm, respectively.

The typical flows are 12 ml/min nitrogen through the 2 m × 1.8 mm I.D. borosilicate column packed with 10% Apiezon L on Chromosorb W, 45–60 mesh (roughly 350–250 μm in particle diameter) used to separate the compounds; ca. 40 ml/min hydrogen and 60 ml/min air premixed to establish the hydrogen-rich reactive flow; and approximately 150 ml/min air introduced into the detector housing to maintain the air-rich, FID-type flame on top of the capillary. Other conditions are similarly conventional and/or conform to precedent [1].

3. Results and discussion

By fortunate circumstance and low chromatographic resolution, pairs of analyte and quencher that would co-elute on the existing Apiezon L column [1] were not hard to find. The pairs used were thianaphthene and naphthalene for sulfur, tris(pentafluorophenyl) phosphine and *n*-hexadecane for phosphorus, tetra-*n*-butyl stannane and *n*-hexadecane for tin, and methylcyclopentadienylmanganese tricarbonyl and *n*-dodecane for manganese. Fig. 1 shows the reassuringly consistent results, which are expressed there as fractional analyte response versus the (logarithmic amount of) quencher. Clearly, the co-eluting quencher exerts no influence on the analyte's response in any of the four cases.

Experimentally, the quenchers were also chromatographed by and for themselves; their quencher-without-analyte signals serving as background checks on the measured quencher-with-analyte peaks. This was done to ascertain that the peak of the quencher (i.e. its own luminescence) was indeed small enough not to interfere with that of the "quenched" analyte. (For one data point of Fig. 1, the quencher peak did indeed turn out a bit too large and had to be deducted.) Quencher amounts between about 10

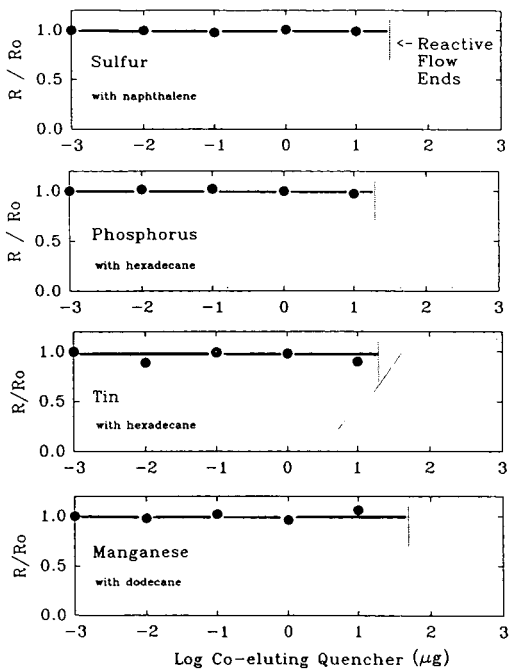

Fig. 1. RFD response in the presence of co-eluting hydrocarbons as indicated. Analytes: 50 ng thianaphthene (benzo[*b*]thiophene), 500 ng tris(pentafluorophenyl) phosphorus, 1 ng tetra-*n*-butyl tin and 500 ng methylcyclopentadienylmanganese tricarbonyl (MMT).

and 100 μg —and above, of course— cause the luminescent column of the reactive flow to temporarily abandon the capillary (i.e. withdraw from purview of the image conduit): this event therefore defines the upper limit of the RFD's operational range.

In the absence of optical filters, the peak heights of Fig. 1 may represent more than one major emitting species per element (the likely numbers are 1 for P, 2 for S and Mn, and 3 for Sn). To check separately for each one of these (and perhaps for some as yet unrecognized ones) would be a difficult and daunting task. Fortunately it proved unnecessary. With the usual FPD interference filter removed, all emissions within optical range of image conduit and photomultiplier tube are being recorded —and with it the quenching of any emitting species. Since no peak was ever quenched, it is safe to assume that

all emitting species of *each* particular element are indeed immune to quenching in the RFD.

It would be surprising if the clear result of Fig. 1 —no quenching anytime in the RFD— were not to hold for other elements and quenchers as well. We refrain, therefore, from extending the series of tested elements beyond the prominent FPD foursome of S, P, Sn and Mn. Yet there remains one aspect that, though subject to prediction by analogy, still needs verification by experiment. It concerns the analyte concentration.

The four analytes whose behavior is depicted in Fig. 1 were for obvious reasons injected in large and constant amounts. If this had been the FPD, the fact that the amounts were large and constant would not have made any difference: fractional quenching in the FPD depends only on the concentration of the quencher, not on the concentration of the analyte (cf. [23,24] and references cited therein). Since the RFD has shown itself to differ from the FPD's quenching behavior, however, similarity in regard to analyte concentration can not be presumed. Rather, it must be established.

Experimentally that calls for investigating the behavior of *small* amounts of analyte. Yet this is difficult to achieve within the framework of Fig. 1, since the peak of the quencher is then likely to overpower the peak of the analyte. For this reason we resort here to a type of FPD experiment —often carried out unwittingly, rarely carried out deliberately [7]— in which a small analyte peak rides on the tail of a large quencher (solvent) peak. Obviously, the more prominent the tail the more pronounced the quenching.

Fig. 2 shows one typical experiment from a series of tests that comprise various elements but produce invariably the same result. The amount of analyte is now much closer to the detection limit. As suggested by the earlier Fig. 1, the solvent tail exerts no visible influence on the analyte peak: the latter retains its normal height. We are therefore pleased to conclude that quenching does *not* occur in the RFD to any significant extent, no matter what the analyte (or quencher) concentration.

From an analytical viewpoint that conclusion is

Fig. 2. RFD response of a trace sulfur peak on and off the solvent tail. The amount of injected analyte (1 ng thianaphthene) is precisely the same; however, the amount of solvent (acetone) has been increased 12 times for the second chromatogram by drawing additional acetone into the syringe prior to injection. The enhanced dip preceding the second solvent peak is due to the increased pressure surge caused by the sudden evaporation of a larger amount of acetone.

welcome indeed. Quenching has presented a major problem for the FPD, particularly since this detector is often used to determine trace analytes contained in hydrocarbonaceous matrices. The most typical cases involve sulfur compounds in natural gas and oil; however, thiophosphate pesticides, organotin biocides or polymer additives, and a variety of other heteroorganic species found in environmental or biological systems have (or might yet be) proven important as well.

While the RFD does not appear to be subject to quenching, it should be noted that its operating range is shorter than that of the FPD: A large amount of hydrocarbon, just like the usual solvent peak, will temporarily expel the reactive flow from the capillary. This occurs in the prototype RFD with amounts of 10 to 100 μg. On the other hand, this much quencher hardly if ever flows from a capillary column: if contained in a single peak it would represent the 1 to 10% component of a 1-μl injection! Furthermore, the glowing column invariably recovers —faster with higher flows, slower with lower ones. Whether different dimensions of the reactive flow —i.e. of the capillary that houses it— would change its operating limit has not been investigated.

A direct comparison of RFD and FPD quenching behavior is difficult because the latter strongly depends on detector construction and operation. Farwell and Barinaga's review [3] mentions that "several tens of nanograms of carbon per second are necessary before hydrocarbons will produce significant reduction in the sulfur response". In our old Shimadzu Model 4 FPD, quenching effects (by a constant stream of methane) became noticeable at roughly 1 μg C/s [23,24]. Quenching is significantly reduced when the column effluent is carried to the detector by the air or oxygen (rather than by the hydrogen) stream (e.g. [13]). There are also differences between different detectors depending on whether their flame is a "pure" diffusion flame or whether, by jet wear or design, their gas streams premix to some degree while ascending toward the reaction zone.

From a mechanistic point of view, the fact that quenching does *not* occur in the reactive flow is certainly interesting. A variety of scenarios may offer plausible causes. We shall describe here only one of these —for the general purpose of citing the literature and starting the discussion; for the particular purpose of justifying its use as our working hypothesis. It should be understood, however, that a kinetic scenario at this early stage of the RFD's development stems from pure imagination, not experiment.

The reactive flow regime may be compositionally related to the well-studied region between the second and third explosion limits of hydrogen–oxygen mixtures, where peroxide chemistry plays a decisive role [38]. If so, it is likely that a radical like the oxygen atom —which characteristically functions as a chain-branching agent— should be nigh absent in the RFD.

Let us for now assume, therefore, that quenching in the FPD is indeed, as has been suggested, a quenching "of the exciting flame rather than of the excited analyte" [23]; and that such quenching occurs via the reaction (or reactions) of the oxygen atom and a simple carbon species (or a pool of simple carbon species) —say reactions like the chemiionization process that is usually considered responsible for the response of the flame ionization detector [39]:

$$CH + O \rightarrow CHO^+ + e^-$$

Such reactions would tend to diminish chain branching, i.e. they would reduce the concentration of those free radicals (H, OH) whose recombination is believed to provide the energy for many of the chemiluminescent processes monitored in the FPD (e.g. [20,40,41]). It is perhaps worthy of note that propane added to H_2–O_2 mixtures depresses the second explosion limit proportional to the oxygen atom concentration (although the authors attributed the effect to the reaction of the hydrocarbon with hydrogen atoms [42]).

In some (unrelated) studies by our group, hydrocarbons introduced into the FPD flame did indeed quench the radical-driven OH emission (experimentally: the $0 \rightarrow 0$ bands at 306–309 nm); and there also appeared to exist some correlation between the quenching of the OH bands and the quenching of several FPD-active elements in the same, methane-doped flame [43]. In contrast, the strong 306+ nm OH emission from the RFD showed no (or only negligible) quenching by one-microgram amounts of typical quenchers and analytes.

A variety of reactions have been considered responsible for the appearance of the OH bands under various conditions [40], e.g.

$$H + OH + OH \rightarrow H_2O + OH^*$$

and

$$O + H \rightarrow OH^*$$

and it thus seems permissible to link the quenching of FPD response by hydrocarbons to a quenching of the radical chain mechanism driving the hydrogen–air *flame*. Whether it is really the oxygen atom that serves as the primary target of carbon species is open to debate: too little is known about the FPD flame (or, for that matter, the RFD glow).

But let us assume —for sake of a model argument— that the crucial link is indeed the oxygen atom. This would explain why the presence of hydrocarbons has little or no influence on the reactive flow: in the RFD that crucial link must be largely missing. (If the reactive flow would increase its rate of oxygen atom formation, it would use the oxygen atom for branched-chain propagation and could thus no longer remain a glowing column. Rather, it would revert to a premixed hydrogen-rich, small flame burning at the bottom of the capillary. Incidentally, such a flame is easy to produce by increasing the air content of the supply gases: once the flame ignites at the bottom, the glow above it *vanishes* [1]. See "Note added in proof".)

It is, of course, also possible to imagine scenarios of a different kind. For instance, there could perhaps exist one type of hydrocarbon species that, while responsible for quenching in the FPD, is not formed in the RFD. (This species would again play the role of a missing link, though this time on the quencher side). While we do not give much credence to this particular scenario, it might still be of interest to collect, analyze and compare organic effluents from doped RFD-type glows vs. FPD-type flames (see the extended discussion of glow and flame "reactor" systems in Ref. [1]).

Indeed, most of the above speculations could be easily confirmed or denied by subjecting the technically accommodating RFD system to some fairly obvious and —at least from our point of view— quite promising experiments. Such experiments would, however, exceed the simple chromatographic and analytical objectives of the current study.

It was designed solely to determine whether or not quenching occurs within the operating range of the RFD. The obvious and clear conclusion is that it does not —at least not for the conditions, analytes and quenchers used. This welcome finding removes one of the major impediments to the analysis of photometrically responsive elements in hydrocarbonaceous matrices.

4. Note added in proof

During the setting of this manuscript we happened to investigate, very roughly, the optical emission and analyte quenching properties of the lower part of what may be called a "separated", "double" or "split" flame (compare [1,20] and references cited therein). This system was produced in the RFD by increasing the air supply to an existing reactive flow, thereby collapsing its luminescent column into a hydrogen-rich, premixed flame burning at the bottom (restriction) of the capillary. One result of this investigation happens to be of particular relevance to the present manuscript. Similar to the reactive flow, this lower part of the split flame failed to show any clear evidence of anlyte quenching. When exposed to *exorbitant* concentrations of hydrocarbons, it —again like the reactive flow— withdrew temporarily from the capillary (and left only the upper, air-rich flame burning).

This interesting result does not alter the conclusions and speculations of the main manuscript. It does, however, allow us to consider the RFD's immunity to quenching from an additional viewpoint. First, note that the lower flame, while clearly of the hydrogen-rich variety, contains *more* air than the typical FPD flame (or, for that matter, the reactive flow). It is also *premixed*. Such conditions can, in other systems, drastically lower the extent of analyte quenching (compare, e.g., Ref. [13]).

Second, the expulsion from the capillary of the reactive flow or the lower flame can be considered mechanistically identical or at least chemically analogous to such flow or flame being terminally "quenched", i.e. being extinguished, by the hydrocarbon. This analogy is important

here because, for the FPD, we had earlier suggested, "oversimplified, that *hydrocarbons may quench the exciting flame rather than the excited analyte*" [23]. For spatially and kinetically restricted excitation regimes —that is, for regimes operating within a limited range of conditions as in the RFD capillary— the (imaginary) onset of quenching of the analyte may be preceded and hence pre-empted by the terminal quenching of the reactive flow or the lower flame itself.

(Interestingly, a *regular* hydrogen-rich premixed flame —established for comparison purposes with the same flows as the lower split flame, but made to burn on *top* of a capillary of smaller diameter— *did* show clear quenching effects. This free-burning flame was, however, extinguished by approximately the same load of quencher that would expell the reactive flow or the lower flame from the capillary, i.e. by peaks containing roughly 50 to 80 μg of hydrocarbon.)

The expulsion/extinction of the RFD's excitation medium defines, of course, the end of the detector's operating range. The reactive flow and the lower flame could hence be considered systems that, by their composition and circumstance, are highly resistant to analyte quenching in the first place. If exposed to *overwhelming* loads of organics, however, they simply self-extinguish (and later re-ignite) —thus preventing any quenching of analyte response from ever taking place.

This scenario suggests a correlation between the spatial stability of a reactive flow and its experimental immunity to analyte quenching. Whether this correlation subsumes all kinetics and encompasses all conditions possible in the RFD capillary would still have to be investigated.

An investigation of this sort may also shed further light on the validity of the (here imported) mechanistic premise that, in the typical FPD quenching process, a reduction of the analyte's chemi-excitation rate is caused primarily by a reduction in the concentration of flame-sustaining radicals such as H, OH, etc., whose energy of recombination powers the chemiluminescence. In simpler terms, this premise —which is consistent with, and supported by, the present study— suggests that most if not all response quenching is caused by a general quenching of the *flame* chemistry —here to the point of pre-emptive extinction/expulsion— rather than by processes like collisional deactivation of the excited state, chemical scavenging of its precursor(s), etc., that could be considered a specific quenching of the *analyte* chemistry (cf. [3,23] and references cited therein).

Acknowledgements

This study was supported by NSERC research grant A-9604. The continued [1] faithful assistance of J. Müller (glassblowing), B. Millier (electronics) and C.G. Eisener (machining) is gratefully acknowledged.

References

[1] K.B. Thurbide and W.A. Aue, *J. Chromatogr.*, 684 (1994) 259.
[2] M. Dressler, *Selective Gas Chromatographic Detectors* (*Journal of Chromatography Library*, Vol. 36), Elsevier, Amsterdam, 1986, pp. 152–156.
[3] S.O. Farwell and C.J. Barinaga, *J. Chromatogr. Sci.*, 24 (1986) 483.
[4] T. Sugiyama, Y. Suzuki and T. Takeuchi, *J. Chromatogr.*, 80 (1973) 61.
[5] S.-A. Fredriksson and A. Cedergren, *Anal. Chim. Acta*, 100 (1978) 429.
[6] M. Dressler, *J. Chromatogr.*, 270 (1983) 145.
[7] P.L. Patterson, *Anal. Chem.*, 50 (1978) 345.
[8] B.J. Ehrlich, R.C. Hall, R.J. Anderson and H.G. Cox, *J. Chromatogr. Sci.*, 19 (1981) 245.
[9] G.H. Liu and P.R. Fu, *Chromatographia*, 27 (1989) 159.
[10] M. Maruyama and M. Kakemoto, *J. Chromatogr. Sci.*, 16 (1978) 1.
[11] S.V. Olesik, L.A. Pekay and E. Paliwoda, *Anal. Chem.*, 61 (1989) 58.
[12] W.E. Rupprecht and T.R. Phillips, *Anal. Chim. Acta*, 47 (1969) 439.
[13] S.-A. Fredriksson and A. Cedergren, *Anal. Chem.*, 53 (1981) 614.
[14] E.R. Adlard, *CRC Crit. Rev. Anal. Chem.*, 5 (1975) 13.
[15] J.F. Karnicky, L.T. Zitelli and S. van der Wal, *Anal. Chem.*, 59 (1987) 327.
[16] M.T. Shabbeer and R.M. Harrison, in R.M. Harrison and S. Rapsomanikis (Editors), *Environmental Analysis*

using Chromatography Interfaced with Atomic Spectroscopy, Ellis Horwood, Chichester, 1989, Ch. 12.
[17] S. Kapila, K.O. Duebelbeis, S.E. Manahan and T.E. Clevenger, in R.M. Harrison and S. Rapsomanikis (Editors), *Environmental Analysis using Chromatography Interfaced with Atomic Spectroscopy*, Ellis Horwood, Chichester, 1989, Ch. 3.
[18] R.S. Hutte and J.D. Ray, in H.H. Hill and D.G. McMinn (Editors), *Detectors for Capillary Chromatography*, Wiley-Interscience, New York, 1992, Ch. 9.
[19] V.A. Joonson and E.P. Loog, *J. Chromatogr.*, 120 (1976) 285.
[20] P.T. Gilbert, in R. Mavrodineanu (Editor), *Analytical Flame Spectroscopy*, Philips Technical Library/Macmillan, London, 1969.
[21] A.R.L. Moss, *Scan (Cambridge, U.K.)*, No. 4 (1974) 5.
[22] S. Cheskis, E. Atar and A. Amirav, *Anal. Chem.*, 65 (1993) 539.
[23] W.A. Aue and X.-Y. Sun, *J. Chromatogr.*, 641 (1993) 291.
[24] X.-Y. Sun and W.A. Aue, *J. Chromatogr. A*, 667 (1994) 191.
[25] T.L. Chester, *Anal. Chem.*, 52 (1980) 638.
[26] V.L. McGuffin and M. Novotny, *Anal. Chem.*, 53 (1981) 946.
[27] E. Mulder, *Bull. Soc. Chim. Fr.*, 1 (1864) 453; *J. Prakt. Chem.*, 91 (1864) 111; as cited by P.T. Gilbert, in R. Mavrodineanu (Editor), *Analytical Flame Spectroscopy*, Philips Technical Library/Macmillan, London, 1970.
[28] C.G. Flinn and W.A. Aue, *Can. J. Spectr.*, 25 (1980) 141.
[29] W.A. Aue and C.G. Flinn, *J. Chromatogr.*, 158 (1978) 161.
[30] U. Schurath, M. Weber and K.H. Becker, *J. Chem. Phys.*, 67 (1977) 110.
[31] W.A. Aue and X.-Y. Sun, *J. Chromatogr.* 633 (1993) 151.
[32] G.B. Jiang, P.S. Maxwell, K.W.M. Siu, V.T. Luong and S.S. Berman, *Anal. Chem.*, 63 (1991) 1506.
[33] W.A. Aue, B.J. Flinn, C.G. Flinn, V. Paramasigamani and K.A. Russell, *Can. J. Chem.*, 67 (1989) 402.
[34] R.J. Maguire, *Water Poll. Res. J. Can.*, 26 (1991) 243.
[35] W.A. Aue, B. Millier and X.-Y. Sun, *Anal. Chem.*, 62 (1990) 2453.
[36] V.S. Gaind, K. Vohra and F. Chai, *Analyst*, 117 (1992) 161.
[37] M.D. DuPuis and H.H. Hill, Jr., *Anal. Chem.*, 51 (1979) 292.
[38] B. Lewis and G. von Elbe, *Combustion, Flames and Explosions of Gases*, Academic Press, Orlando, FL, 3rd ed., 1987, e.g. p. 38.
[39] H.H. Hill and D.G. McMinn (Editors), *Detectors for Capillary Chromatography*, Wiley-Interscience, New York, 1992, Ch. 2.
[40] A.G. Gaydon and H.G. Wolfhard, *Flames*, Chapman & Hall, London, 3rd revised ed., 1970.
[41] C.T.J. Alkemade, T. Hollander, W. Snelleman and P.J.T. Zeegers, *Metal Vapours in Flames*, Pergamon, Oxford, 1982.
[42] R.R. Baldwin, N.S. Corney and R.M. Precious, *Nature*, 169 (1952) 201.
[43] X.-Y. Sun and W.A. Aue, unpublished results, 1993.

ELSEVIER

Journal of Chromatography A, 694 (1995) 441–451

JOURNAL OF CHROMATOGRAPHY A

Determination of trifluoroacetylated glycosides by gas chromatography coupled to methane negative chemical ionization mass spectrometry

David Chassagne[a], Jean Crouzet[a,*], Raymond L. Baumes[b], Jean-Paul Lepoutre[b], Claude L. Bayonove[b]

[a]*Laboratoire de Génie Biologique et Sciences des Aliments, Unité de Microbiologie et Biochimie Industrielles, Associée à l'INRA, Université de Montpellier II, 34095 Montpellier Cedex 05, France*

[b]*Laboratoire des Arômes et des Substances Naturelles, Institut des Produits de la Vigne, INRA, 2 Place Viala, 34060 Montpellier Cedex 01, France*

First received 7 July 1994; revised manuscript received 8 November 1994; accepted 11 November 1994

Abstract

Gas chromatography coupled to methane chemical ionization mass spectrometry was used for qualitative determination of trifluoroacetylated plant glycosides. The mass spectra obtained exhibited characteristic fragment ions of the sugar moiety and molecular or pseudo-molecular ions. The pattern of these chemical ionization spectra was influenced by source temperature. This method was applied to the structural determination of glycosides from purple passion fruit and muscat wine (Muscat of Frontignan) extracts obtained by adsorption on Amberlite XAD-2.

1. Introduction

The occurrence of glycosidically bound volatile components such as monoterpenic, aromatic and aliphatic alcohols, phenols, C-13 norisoprenoids or polyols in fruits such as grape [1,2], papaya [3] and passion fruit [4,5] has been reported. Several methods for the extraction and determination of these non-volatile components have been described, but their qualitative determination involved time-consuming and laborious steps [1,6–8]. Recently, a method for the direct analysis of glycosidic extracts by gas chromatography (GC) coupled to mass spectrometry (MS) after derivatization was reported [9,10]. Trifluoroacetylated (TFA) derivatization proved most suitable for qualitative and quantitative analysis of monoterpenyl glycosides in electron impact (EI) MS, but chemical ionization (CI) in the positive ion mode gave unsatisfactory results, except for some terpenyl and aryl monoglucosides. The high electron affinity of polyhalogenated organic compounds, as the TFA derivatives, made negative ion CI-MS (NCI-MS) very attractive to analyse directly TFA glycosides [11]. Thus, this paper reports the GC–NCI-MS analysis of TFA derivatives of glycosides previously synthesized [12], and its application to the qualitative analysis of glycosides from passion fruit and muscat wine extracts.

* Corresponding author.

0021-9673/95/$09.50
SSDI 0021-9673(94)01118-4

2. Experimental

2.1. Reagents and reference samples

Analytical-reagent grade solvents were further purified by distillation before use. Amberlite XAD-2 resin from Röhm and Haas was purified according to the procedure of Günata et al. [6]. The trifluoroacetylating reagent N-methylbis-(trifluoroacetamide), phenyl and octyl β-D-glucopyranoside were obtained from Sigma. Standard glycosides were synthesized as reported [12].

2.2. Plant material

Mature purple passion fruits (*Passiflora edulis* Sims) from Zimbabwe were purchased in France (Rungis) and stored at 4°C until processing. The wine was made from Muscat of Frontignan grapes grown at the vineyard of the wine experimental station in Pech-Rouge (South of France) by standard wine processing.

2.3. Isolation of natural glycosidic components

Passion fruit was cut, and the seeds were removed by filtration through a gaze. The juice and the pulp were centrifuged (30 min, 10 000 *g*) at 4°C. The clear juice obtained was kept at −18°C until analysis. Muscat wine and passion fruit juice were fractionated on XAD-2 resin as described by Günata et al. [6]. A 50-ml volume of pentane–dichloromethane (2:1, v/v) was used for the elution of free aroma fractions and those were discarded. A 50-ml volume of methanol was used for the elution of the bound fraction from passion fruit whereas this fraction was obtained using 50 ml of ethyl acetate in the case of muscat wine. The bound fractions were dried over anhydrous sodium sulfate.

2.4. Trifluoroacetylation

The bound fraction obtained from 1 ml of passion fruit juice, 20 ml of muscat wine or a mixture of synthetic glycosides was concentrated to dryness, in a small screw-capped vial at 60°C under nitrogen and derivatized according to the method of Voirin et al. [9].

2.5. Direct GC–NCI-MS analysis of the bound fractions

NCI-MS spectra were recorded for the TFA derivatives by coupling a Hewlett-Packard (HP) 5890 gas chromatography equipped with a DB-5 fused-silica capillary column (30 m × 0.32 mm I.D.; 0.25 μm bonded phase; J & W Scientific), to a HP 5889A mass spectrometer. The transfer line was heated at 290°C. Injections of about 1 μl were on column: the injector temperature was programmed at 60°C/min from 110 to 260°C then held at this temperature for 55 min. The column temperature was programmed at 3°C/min from 125 to 290°C with helium as carrier gas at 1.1 ml/min.

For NCI-MS, the operating conditions were as follow; emission current: 350 μA; energy of the electrons: 200 eV; the temperatures of the source and quadrupole were 200 and 120°C, respectively; methane was used as the reactant gas at 80 Pa, as measured at the source ion gauge. The ion source tuning was carried out in the positive ion mode by using perfluorotributylamine. Mass spectra were scanned in the range m/z 100–1400 at 500 ms intervals with a repeller potential of 7 V. The mass spectra reported were recorded when the abundance of pseudo-molecular ions maximized.

3. Results and discussion

In a first step, the TFA derivatives of commercial or synthesized glycosides were studied by GC–NCI-MS with methane as moderating gas. Methane was chosen because it is the most popular CI reagent: as the obtained results were satisfactory, no other gas was investigated.

3.1. Capillary GC–NCI-MS

A representative reconstructed total ion current (TIC) chromatogram from the GC–NCI-MS analysis of standard glycosides is shown in Fig. 1.

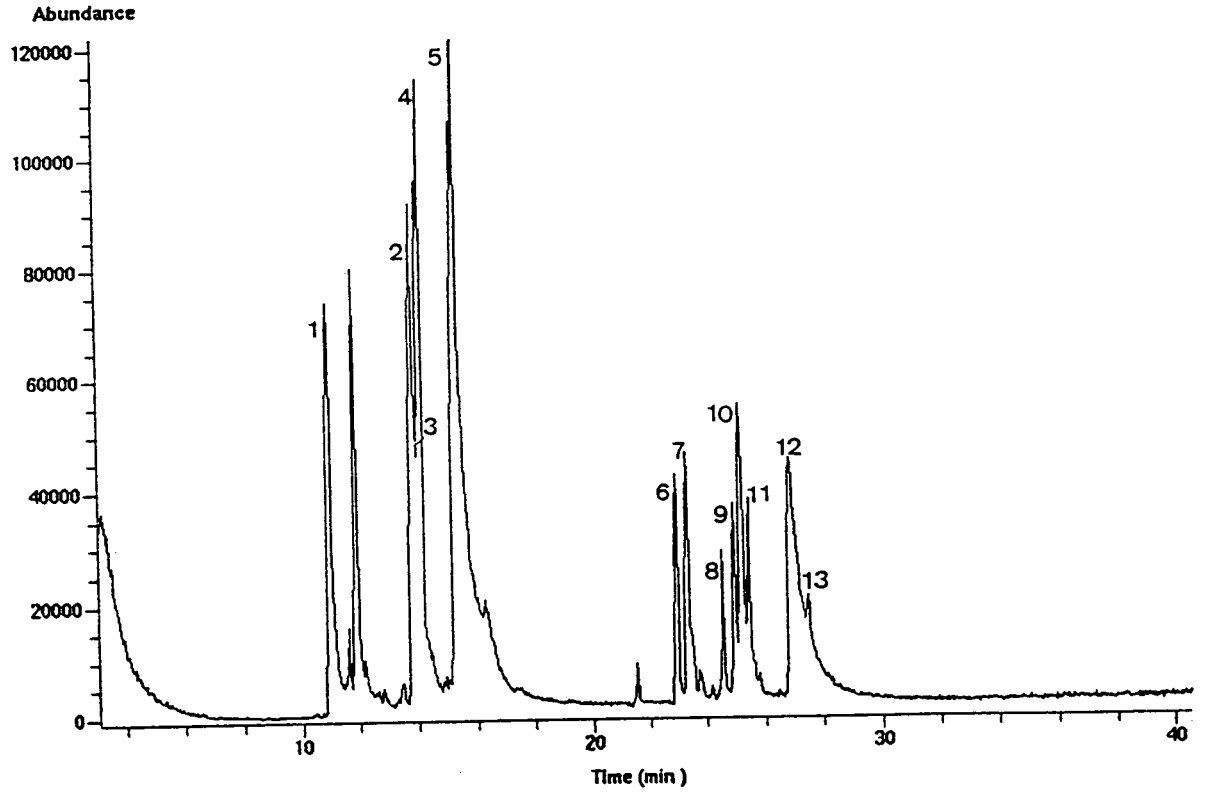

Fig. 1. Total ion chromatogram of TFA derivatives of standard glycosides. This sample was analysed by using methane negative ionization. Peaks: 1 = phenyl, 2 = octyl, 3 = (*R*)-linalyl, 4 = (*S*)-linalyl, 5 = 2-phenylethyl glucosides; 6 = (*R*)-linalyl, 7 = (*S*)-linalyl, 10 = 2-phenylethyl rutinosides; 8 = (*R*)-linalyl, 9 = (*S*)-linalyl, 12 = 2-phenylethyl arabinosylglucosides; 11 = linalyl, 13 = 2-phenylethyl apiosylglucosides.

GC–NCI-MS displayed the same degree of resolution of glycosides as that reported under EI analytical conditions by Voirin et al. [9] for the same mixture, allowing easy comparison of the obtained chromatograms.

3.2. Characteristic fragment ions

The operational parameters (see below) were determined to obtain high relative abundance of analyte specific ions which might give structural information for both glucosides and diglycosides studied. The NCI-MS spectra of TFA derivatives of linalyl β-D-glucopyranoside and β-rutinoside are shown in Fig. 2 as characteristic examples. The two most abundant ions of low mass in these spectra were characteristic of the derivatizing group (TFA): These ions at *m/z* 113 and 227 would correspond to $[TFAO]^-$ and $[2TFAOH - H]^-$ ions, respectively, formed by dissociative electron capture of the sample [13].

However, spectra obtained in the negative ion mode are generally characterized by the presence of ions specific of the analyte, i.e. molecular or pseudo-molecular ions [11]. Under the experimental conditions used, molecular ions M^- for glycosides were observed, pointing out an ionization by electron-capture reaction. The TFA group is known to increase the electron-capture probability, either in GC–electron-capture detection (ECD) or GC–NCI-MS, as already observed for the TFA derivatives of chlorophenols and chloroanilines with methane as moderating gas [13]. For all the glycosides

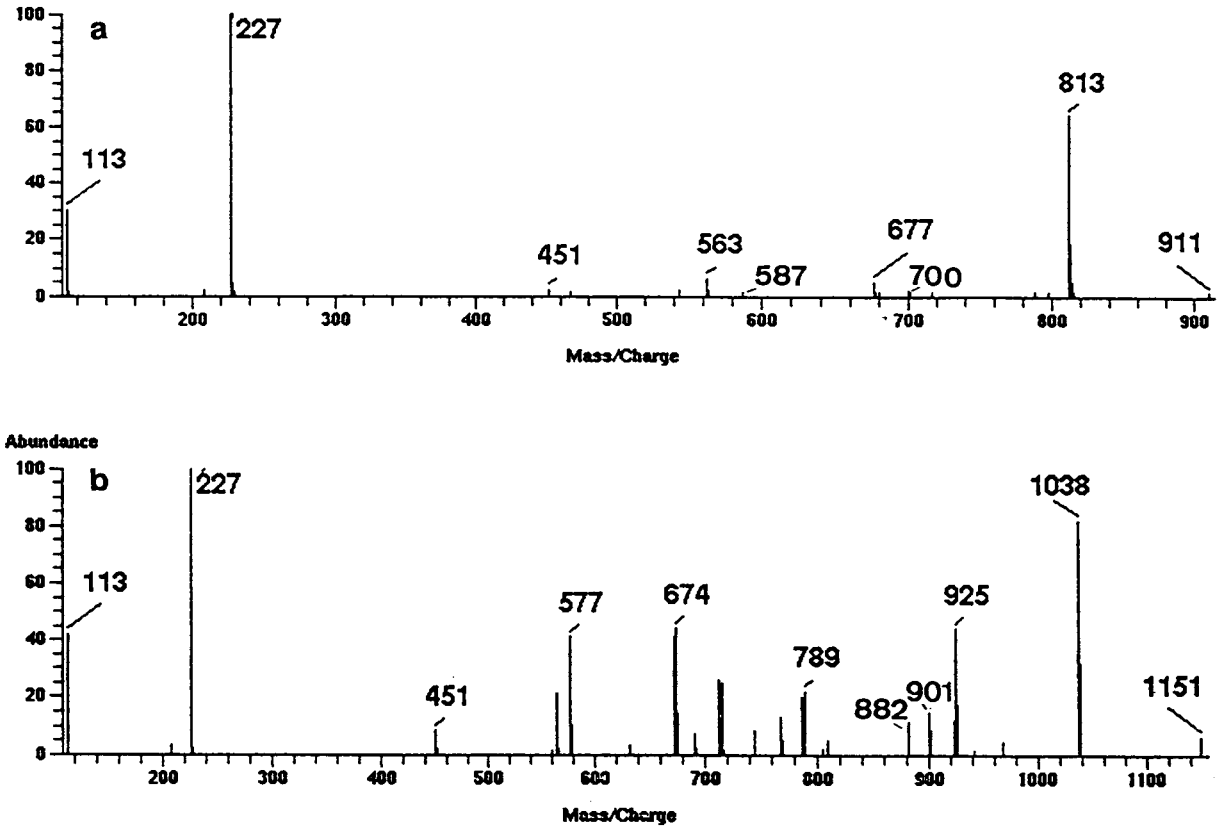

Fig. 2. NCI-MS spectra of TFA derivatives of (a) linalyl glucopyranoside and (b) linalyl β-D-rutinoside.

studied, an adduct ion $[M + TFAO]^-$ was observed at an m/z value corresponding to [M + 113] with much higher abundance for glucosides than for diglycosides. This adduct ion would be formed by TFAO, produced by dissociative electron capture of the sample, which would associate with additional sample [14]. No other artifacts such as alkylated adduct ions, sometimes observed when CH_4 was used as the moderating gas, were observed [15]. Moreover a fragment ion $[M - TFAO]^-$ was obtained by dissociative electron capture of each glycoside studied. Thus, the presence of the specific ions M^-, $[M - TFAO]^-$ and $[M + TFAO]^-$ in our conditions allowed the unequivocal determination of the molecular mass for each glycoside (Table 1).

On the other hand, NCI-MS of glycosides gave some information concerning the sugar moiety. Indeed, the ions at m/z 563, 887 and 901 are fragment ions specific of TFA sugar units corresponding respectively to $[GlcTFA \sim O]^-$, $[AraTFA \sim GlcTFA \sim O]^-$ and $[RutTFA \sim O]^-$ ions (where ~ indicates that a bond is present),

Table 1
Molecular, adduct and fragment ions observed in NCI-MS spectra of TFA derivatives of glycosidic standards

Derivatives (peaks in Fig. 1)	M^-	$[M + OTFA]^-$	$[M - OTFA]^-$
1	640	753	527
2	676	789	563
3, 4	700	813	587
5	668	781	555
6, 7	1038	1151	925
10	1006	1119	893
8, 9, 11	1024	1137	911
12, 13	992	1105	879

formed by loss of the aglycone fragment. This observed fragmentation was similar to that reported by König et al. [16] for EI-MS of trifluoroacetylated sugars. Other characteristic fragment ions of osidic moieties were observed and were summarized in Table 2. Therefore, sequence information was directly available from the spectra due to the successive cleavages, e.g. the molecular ion M^- (m/z 1038) and the fragment ions characteristic of TFA rutinose (m/z 901) and of TFA rhamnose (m/z 451) in the mass spectrum of linalyl rutinoside (Fig. 2). However, 6-O-β-D-apiofuranosyl and 6-O-α-L-arabinofuranosyl glucopyranosides could not be distinguished on the basis of the relative abundances of ions characteristic of the sugar moiety.

Structural information on the aglycone moiety was minimal except for molecular mass, which was calculated by difference between the molecular mass of glycosides and that of the sugar moiety which were both available. However, EI-MS of these TFA glycosides were shown to give valuable structural information on the aglycone moiety [9,10]. To our knowledge, overall results

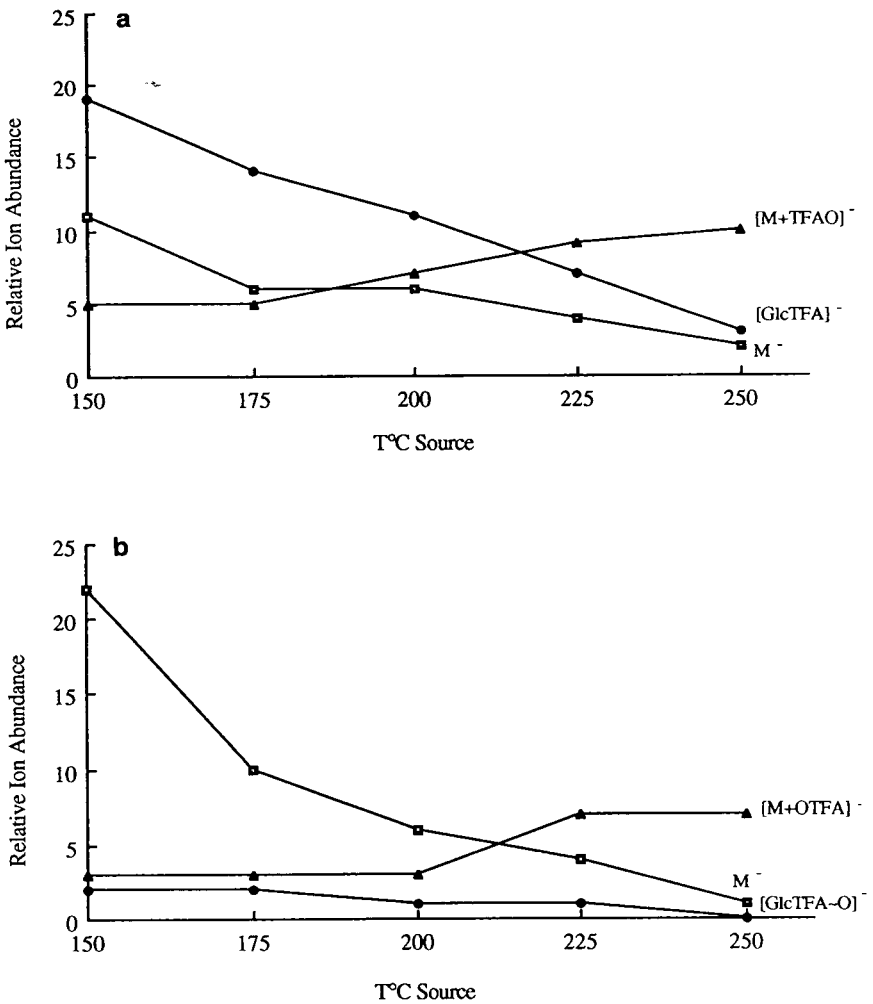

Fig. 3. Variation of ionic abundances of TFA derivatives of (a) phenyl β-D-glucoside and (b) octyl β-D-glucoside with source temperature.

Table 2
Interpretation of characteristic fragment ions of the sugar moiety

Glucoside		Apiosyl and arabinosyl glucosides		Rutinoside	
m/z	Fragment ions	*m/z*	Fragment ions	*m/z*	Fragment ions
563	$[GlcTFA \sim O]^-$	887	$[(Ara \sim Glc)TFA \sim O]^-$	901	$[RutTFA \sim O]^-$
677	$[GlcTFA \sim O + TFAOH]^-$	868	$[(Ara \sim Glc)TFA \sim O - F]^-$	882	$[RutTFA \sim O - F]^-$
544	$[GlcTFA \sim O - F]^-$	775	$[(Ara \sim Glc)TFA \sim O - (-H + TFAO)]^-$	789	$[RutTFA \sim O - (-H + TFAO)]^-$
451	$[GlcTFA \sim O - (-H + TFAO)]^-$	660	$[(Ara \sim Glc)TFA \sim O - [TFAO + TFAOH)]^-$	674	$[RutTFA \sim O - (TFAO + TFAOH)]^-$
		437	$[AraTFA \sim O]^-$	451	$[RhaTFA \sim O]^-$

afford valuable information for tentative identification of natural glycosides.

3.3. NCI-MS parameters effects

For a given moderating gas, the pattern of a CI spectrum can be strongly influenced by operational parameters such as ionization energy, source pressure and temperature [11,14,15]. Thus, the influence of these parameters on the relative abundances and the ionic current profiles of the M^- and $[M+TFAO]^-$ ions and of the $[GlcTFA]^-$ or $[GlcTFA\sim O]^-$ ions of TFA derivatives of phenyl and octyl glucosides were examined. The more significant parameter was the source temperature. When the source temperature increased, the relative abundances of the M^- ion and of the $[GlcTFA]^-$ or $[GlcTFA\sim O]^-$ ions decreased, while the relative abundance of the adduct ion increased (Fig. 3). Furthermore, the molecular ion displayed the broadest chromatographic profile at the lowest source temperature (150°C) and at the highest pressure (186 Pa), which was ineffective to obtain a good reconstructed ion chromatogram. From these results, the operating conditions were chosen as follows: temperature and pressure of the source respectively at 200°C and 80 Pa; ionization energy at 200 eV.

3.4. Application to natural glycosides from passion fruit juice and muscat wine

Several papers have reported the occurrence of glycosides as flavor precursors in the juice of the purple passion fruit from analysis of the

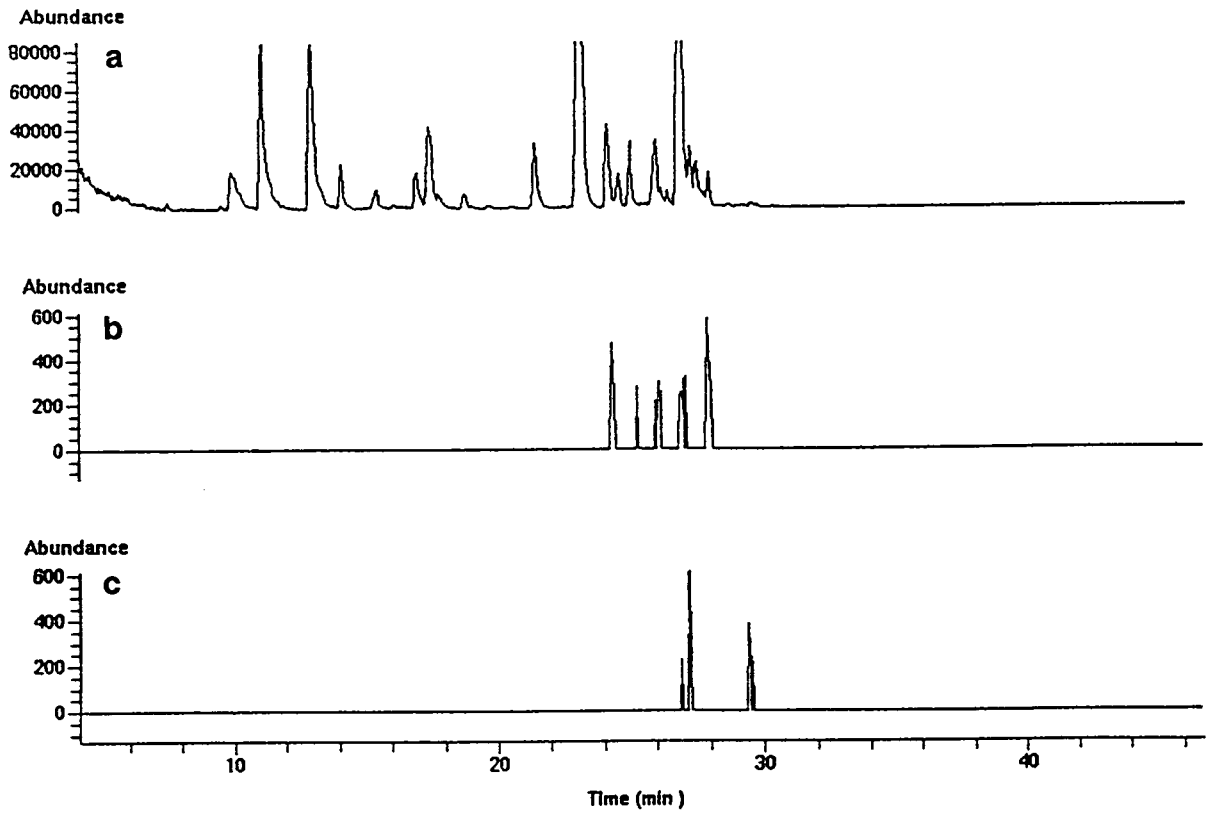

Fig. 4. GC–NCI-MS of a passion fruit glycosidic extract (TFA): (a) Total ion chromatogram, (b) reconstructed mass chromatogram at m/z 754 and (c) reconstructed mass chromatogram at m/z 770.

sugars and the aglycones liberated by acid or enzymatic hydrolysis of glycosidic extracts [4,5,17]. Some aglycones such as monoterpenoids with various oxidation states, benzyl alcohol, 2-phenyl ethanol and C-13 norisoprenoids were identified. However, there is some information about the nature of the sugars constitutive of the glycosidic moiety and their sequence is scarce. In contrast to passion fruit, glycosides of *Vitis vinifera* grape, as well as aglycones and sugar moieties, have been extensively investigated [1,2,6–10,18].

Thus, TFA derivatives of glycosides from passion fruit and muscat wine were analysed using GC–NCI-MS to obtain complementary informations to those reported by Voirin et al. [10] and Baumes et al. [18] from EI-MS of the TFA derivatives of grape and wine glycosidic extracts. The total ion current chromatograms (Figs. 4a and 5a) in the NCI mode of the TFA derivatives of the two fractions showed the same profiles as those obtained when the EI mode was used. Most of the glycosides detected in the chromatograms showed molecular ions at m/z 813, 1024 and 1038, which corresponded to glycosides of monoterpenols (M_r 154). Comparisons of spectra in the NCI and EI modes of the derivatives of the synthetic compounds allowed the positive identification of the corresponding natural glycosides. Furthermore, they allowed to obtain NCI-MS data for other natural glycosides. The cyanogenic glucoside, prunasin [2(*R*)-(β-D-

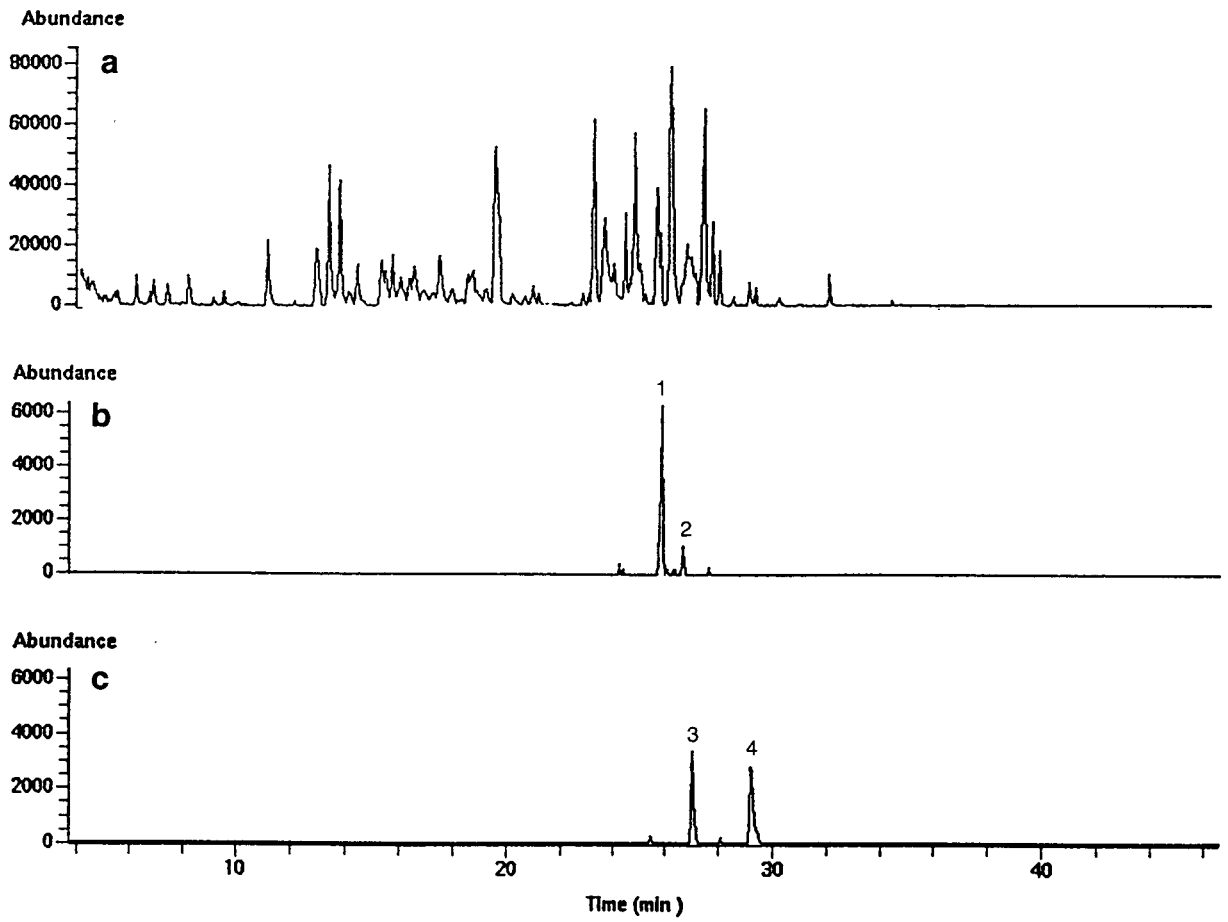

Fig. 5. GC–NCI-MS of a muscat wine glycosidic extract (TFA): (a) Total ion chromatogram, (b) reconstructed mass chromatogram at m/z 754 and (c) reconstructed mass chromatogram at m/z 770.

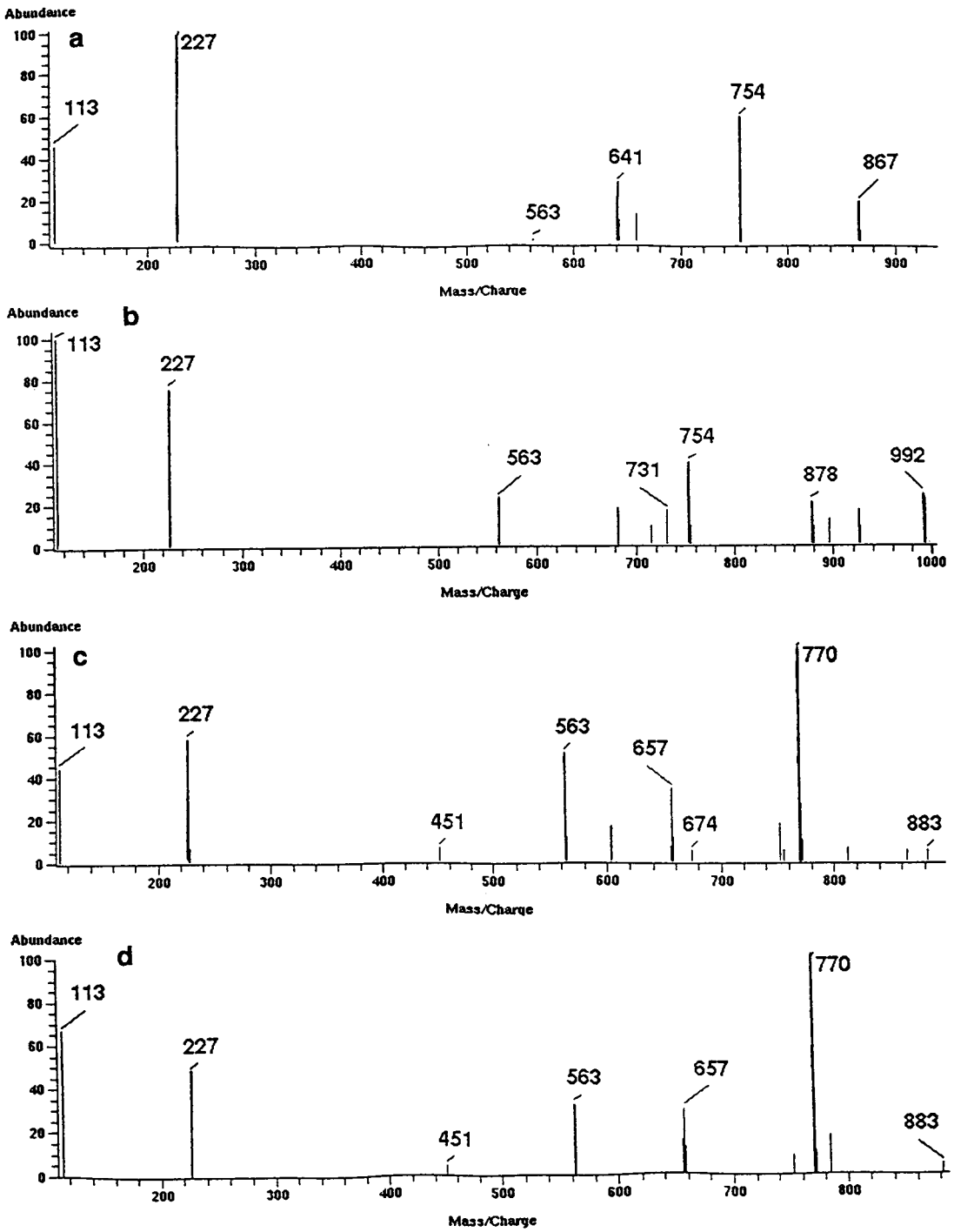

Fig. 6. NCI-MS spectra of TFA derivatives of four different C-13 norisoprenoïds of glucosides detected in muscat wine extract (a), (b) *m/z* 754 (peaks 1 and 2, Fig. 5b) and (c, d) *m/z* 770 (peaks 3 and 4, Fig. 5c).

glucopyranosyloxy)-2-phenylacetonitrile], identified in the purple passion fruit by Spencer et Seigler [19], gave some characteristic ions: M^- (m/z 679), $[M+TFAO]^-$ (m/z 792) and $[GlcTFA\sim O]^-$ (m/z 563). β-D-Glucopyranosides, β-D-rutinosides, α-L-arabinofuranosyl β-D-glucopyranosides of linalool oxides from the muscat wine extracts gave molecular ions at m/z 716, 1054 and 1040, respectively.

The detection of coeluted compounds was easier in NCI mode than in EI mode. As a lot of C-13 norisoprenoid aglycones of grape and passion fruit glycosides have been recently identified [18,20–22], we focused our attention on minor compounds as C-13 norisoprenoid glycosides. These compounds were difficult to detect because they were eluted in the range of the chromatogram corresponding to the most abundant monoterpene diglycosides. The peaks of the reconstructed mass chromatograms at m/z 754 (Figs. 4b and 5b) and at m/z 770 (Figs. 4c and 5c) for the passion fruit extract (Fig. 4) and the wine extract (Fig. 5) were highly indicative of C-13 norisoprenoid glucosides with aglycone molecular masses of 208 and 224, respectively. Indeed the ions m/z 754 and 770 correspond to the molecular ions M^- of the TFA derivatives of C-13 norisoprenoid glucosides at the oxidation level of hydroxy megastigmadienone and oxygenated hydroxy megastigmadienone, respectively. For the muscat wine extract, the spectra obtained for the two derivatives selected from the ion m/z 754 were very similar (Fig. 6a and b), as well as those for the two derivatives selected from the ion m/z 770 (Fig. 6c and d). These spectra exhibited characteristic fragmentation of TFA derivatives: ions at m/z 563 and 451 allowing to identify the osidic part, in this case glucose. Other adduct and fragment ions were also significantly present. In fact, the derivatized glucosides detected at m/z 754 were assigned to glucosides of 3-hydroxy-β-damascone (Fig. 6a) and 3-oxo-α-ionol (Fig. 6b), already identified by Baumes et al. [18]. However, the second one was coeluted with a phenylethyl diglycoside giving the ions m/z 992 (M^-), 879 ($[M-OTFA]^-$) and 683 ($[M-OTFA-HOTFA]^-$) in the spectrum shown in Fig. 6b.

For the passion fruit extract, four peaks were detected in the reconstructed mass chromatogram at m/z 754 and two peaks at m/z 770, but their abundances were lower than that obtained for the muscat wine extract. All these trace compounds, except the last eluted one, were coeluted with glycosidic compounds much more abundant (see the difference in the abundances of the peaks shown in Fig. 4a and Fig. 4b or c) so that the spectra obtained were very polluted. However the two peaks detected at m/z 770, as well as the second and the third eluted ones detected at m/z 754, had the same retention times as those detected in the wine extract. Thus, it may be assumed that these compounds are identical, which could be checked by detecting ion current at a few characteristic mass values by GC–EI-MS with selected ion monitoring of their TFA derivatives. These last results will be published in a forthcoming paper on glycosidic precursors of passion fruit.

4. Conclusions

We have shown that NCI mass spectra of the TFA derivatives of synthetic and natural glycosides of volatile compounds provided complementary useful informations for their structural determination. In contrast to EI-MS, NCI-MS allowed to obtain the molecular mass and the carbohydrate sequence of these glycosides. A good optimization of the source temperature was crucial for the direct observation of molecular ions. Thus GC–EI- and–NCI-MS are very suitable for on-line analysis of naturally occurring mono- and diglycosides of volatile compounds and could be used as screening techniques for these compounds.

References

[1] C.R. Strauss, B. Wilson, P.R. Gooley and P.J. Williams, in T.H. Parliment and R. Croteau (Editors), *Biogeneration of Aromas* (*ACS Symposium Series*, Vol. 317), American Chemical Society, Washington, DC, 1986, p. 222; and references cited therein.

[2] P.J. Williams, M.A. Sefton and I.L. Francis, in R. Teranishi, G.R. Takeoka and M. Güntert (Editors), *Flavors Precursors-Thermal and Enzymatic Conversions* (*ACS Symposium Series*, No. 490), American Chemical Society, Washington, DC, 1992, p. 74; and references cited therein.
[3] J. Heidlas, M. Lehr, H. Idstein and P. Schreier, *J. Agric. Food Chem.*, 32 (1984) 1020.
[4] K.H. Engel and R. Tressl, *J. Agric. Food Chem.*, 31 (1983) 998.
[5] P. Winterhalter, *J. Agric. Food Chem.*, 38 (1990) 452.
[6] Y.Z. Günata, C. Bayonove, R.L. Baumes and R. Cordonnier, *J. Chromatogr.*, 331 (1985) 83.
[7] C.R. Strauss, P.R. Gooley, B. Wilson and P.J. Williams, *J. Agric. Food Chem.*, 35 (1987) 519.
[8] C. Salles, J.C. Jallageas and J. Crouzet, *J. Chromatogr.*, 522 (1990) 255.
[9] S.G. Voirin, R.L. Baumes, Z.Y. Günata, S.M. Bitteur, C.L. Bayonove and C. Tapiero, *J. Chromatogr.*, 590 (1992) 313.
[10] S.G. Voirin, R.L. Baumes, J.C. Sapis and C.L. Bayonove, *J. Chromatogr.*, 595 (1992) 269.
[11] H. Budzikiewicz, *Mass Spectrom. Rev.*, 5 (1986) 345.
[12] S.G. Voirin, R.L. Baumes, J.C. Sapis and C.L. Bayonove, *Carbohydr. Res.*, 207 (1990) 39.
[13] T.M. Trainor and P. Vouros, *Anal. Chem.*, 59 (1987) 601.
[14] W.C. Brumley and J.A. Sphon, in H. Gilbert (Editor), *Application of Mass Spectrometry in Food Science*, Elsevier Applied Science, London, 1987, Ch. 3, p. 141.
[15] M.J. Incorvia Mattina and L.Q. Huang, *Anal. Chem.*, 62 (1990) 602.
[16] W.A. König, H. Bauer, W. Voelter and E. Bayer, *Chem. Ber.*, 106 (1973) 1905.
[17] M.J. Fontvielle and J. Crouzet, *Riv. Ital. EPPOS*, (1991) 691.
[18] R. Baumes, I. Dugelay, Y.Z. Günata, C.Tapiero, S. Bitteur and C. Bayonove, in C. Bayonove, J. Crouzet, C. Flanzy, J.C. Martin and J.C. Sapis (Editors), *Connaissance Aromatique des Cépages et Qualité des Vins*, Actes du Symposium International, Montpellier, 1993, p. 90.
[19] K.C. Spencer and D.S. Seigler, *J. Agric. Food Chem.*, 31 (1983) 794.
[20] M.A. Sefton, G.K. Skouroumounis, R.A. Massy-Westropp and P.J. Williams, *Aust. J. Chem.*, 42 (1989) 2071.
[21] P. Winterhalter in R. Teranishi, G.R. Takeoka and M. Güntert (Editors), *Flavors Precursors-Thermal and Enzymatic Conversions* (*ACS Symposium Series*, No. 490), American Chemical Society, Washington, DC, 1992, p. 98.
[22] A. Razungles, Z.Y. Günata, S. Pinatel, R. Baumes and C. Bayonove, *Sci. Aliments*, 13 (1993) 59.

ELSEVIER

Journal of Chromatography A, 694 (1995) 453–461

JOURNAL OF CHROMATOGRAPHY A

Rapid micro liquid–liquid extraction method for trace analysis of organic contaminants in drinking water

Andreas Zapf, Regine Heyer, Hans-Jürgen Stan*

Institute of Food Chemistry, Technical University of Berlin, Gustav-Meyer-Allee 25, 13355 Berlin, Germany

First received 19 August 1994; revised manuscript received 2 December 1994; accepted 2 December 1994

Abstract

The applicability and performance of a micro liquid–liquid extraction method for trace analysis of organic compounds in drinking water is reported. Tap water samples of 400 ml are saturated with sodium chloride and extracted once with 500 μl of toluene. Extracts are analyzed directly without further treatment by gas chromatography using simultaneous electron-capture and nitrogen–phosphorus detection. Recoveries of 82 organic compounds, including organochlorine and organophosphorus insecticides, triazine and acetanilide pesticides, chlorinated anilines and phenols from tap water samples spiked at 50 to 500 ng/l were determined and relative standard deviations were calculated. For 68 compounds the recoveries were higher than 50%. The mean relative standard deviations at spiking levels of 50, 100 and 500 ng/l were 7.9, 6.6 and 5.2%, respectively. The extraction method proved to be rapid, simple and inexpensive. In most cases compounds were reproducibly detected well below the European Union maximum tolerance level for pesticide residues in drinking water of 100 ng/l.

1. Introduction

In recent years, many man-made organic compounds, mainly pesticides, have been found as contaminants in ground and surface water. Maximum tolerance levels were set as in the European Union (EU) guideline for drinking water [1], which establishes a maximum tolerance level for individual pesticides of 100 ng/l. This so-called "zero tolerance" level represents the performance standard of current trace analysis methods as well as being a benchmark for new procedures.

Trace analysis of organic compounds in water is carried out by several methods. The traditional liquid–liquid extraction with large volumes of organic solvent followed by clean up and concentration steps is known as an effective procedure regarding accuracy and sensitivity. However, interferences from solvents used, their toxicological relevance and possible cross-contaminations favoured the development of solid-phase extraction, which is relatively simple in use and needs only small amounts of solvents. But even in this case, interferences from solid-phase materials may occur [2].

As a simple and inexpensive but exact and sensitive method, micro liquid–liquid extraction (mLLE) combined with gas chromatography (GC) has been successfully applied to analysis of organic compounds in water [3–6]. In a field study, we determined alachlor and two degradation products in ground water saturated with sodium chloride by extracting 400-ml samples

* Corresponding author.

0021-9673/95/$09.50
SSDI 0021-9673(94)01199-0

with 500 μl of toluene. The extracts were analyzed without further treatment with GC using nitrogen–phosphorus detection (NPD) and mass-selective detection [7]. A solid-phase extraction procedure first applied was lengthy and not suitable for the analysis of the volatile metabolite 2,6-diethylaniline [7,8]. Since results of the micro liquid–liquid extraction were found to be satisfactory with respect to speed, accuracy and sensitivity, the applicability of this extraction method to the analysis of other environmental contaminants usually dealt with in our laboratory was tested. Substances from important pesticide classes were selected, including organochlorine, organophosphorus, triazine and acetanilide pesticides together with a few degradation products. Chlorinated phenols and anilines which represent common water pollutants from industry as well as metabolites of phenyl urea, acylanilide and carbamate pesticides were also investigated. To obtain an overview of the applicability of mLLE to the investigated contaminant classes, only those substances were chosen which could be determined by GC with electron-capture detection (ECD) and/or NPD without the need of derivatization or mass-selective detection techniques.

2. Procedure

2.1. Materials

Standard substances were of analytical purity, purchased from Promochem (Wesel, Germany), or of Pestanal quality, from Riedel de Haën (Seelze, Germany). Sample vials, screw caps and septa were purchased from Zinsser (Frankfurt, Germany) and 200-μl inserts for the sample vials were obtained from CS-Chromatographie Service (Langerwehe, Germany). Narrow-necked bottles used for extraction were obtained from H. Jürgens & Co. (Bremen, Germany) and PTFE-faced seals were purchased from Schott (Mainz, Germany).

Stock solutions of all compounds were prepared in toluene or methanol. Standards and samples were finally dissolved in toluene. All solvents were Pestanal products from Riedel de Haën. Sodium chloride, trisodium citrate dihydrate and citric acid were purchased from Merck (Darmstadt, Germany).

As a buffering mixture trisodium citrate dihydrate–citric acid monohydrate (40:1, w/w) (pH 6.5–7.0) was used.

2.2. Instrumentation

Shaker

A KL2 shaker from Edmund Bühler (Bodelshausen, Germany) was used.

GC–ECD and GC–NPD

An HP 5890 gas chromatograph with electron-capture and nitrogen–phosphorus detectors, an HP 7673 autosampler and a split–splitless injector for capillary columns was employed. Nelson analytical software 2600, V 4.1 was used for data acquisition.

A fused-silica column (25 m × 0.32 mm I.D.), coated with SE-54 material with a film thickness of 0.17 μm, was used with helium as carrier gas. The effluent was split into equal parts by means of a Y press fit connector. The temperatures of the injection port, the electron-capture detector and the nitrogen–phosphorus detector were set at 210, 300 and 280°C, respectively. The column temperature program was started with 1 min at 100°C, increased at 30°C/min to 150°C, held for 2 min, then increased at 3°C/min to 205°C and at 10°C/min to 260°C, held at 260°C for 20 min. A 2-μl volume of sample was injected with the autosampler using hot splitless injection with the split closed for 1 min.

2.3. Micro liquid–liquid extraction

A 400-ml tap water sample in a 500-ml narrow-necked bottle was saturated with 150 g NaCl and buffered to pH 6.5–7.0 by addition of 6 g of the buffering mixture. The water sample was spiked with analyte mixtures in 100 μl methanol to achieve concentrations of 50, 100 and 500 ng/l. After addition of 500 μl toluene, the bottle was sealed and shaken for 20 min at 420 rpm. Screw caps with PTFE-faced silicone rubber

seals were used. After phase separation, the solvent layer was brought up to the bottleneck by addition of a saturated NaCl solution using a Pasteur pipette connected to a separating funnel as demonstrated in Fig. 1. About 150 μl of the toluene phase were transferred into sample vials of 200 μl volume by means of another Pasteur pipette. 2 μl were injected into the GC–ECD/NPD system.

2.4. Calibration

Extraction rates were determined by external standard calibration. Concentrations of standard solutions were 25, 50, 100, 250 and 500 pg/μl in toluene. Calibration curves were calculated by linear least-squares regression using peak areas.

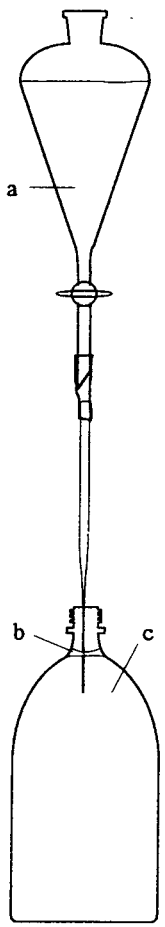

Fig. 1. Simple equipment to bring the toluene phase up to the bottle neck. a = Separating funnel filled with saturated NaCl solution; b = solvent layer; c = sample.

3. Results and discussion

Recovery experiments with a variety of pesticides and other environmental pollutants from spiked tap water samples were carried out at concentration levels of 50, 100 and 500 ng/l. At each concentration level, five analyses were performed.

Illustrating the results compiled in Table 1, chromatograms obtained from extracts of samples containing 100 ng/l of each compound are shown in Figs. 2–5. This concentration level represents the EU guideline maximum tolerance level for pesticides in drinking water.

Best peak sizes were obtained from analytes exhibiting high ECD response factors. All chlorinated pesticides investigated (Fig. 2), a number of organophosphorus pesticides (Fig. 3), the chlorophenols with the exception of the relatively low chlorinated 2,4-dichlorophenol (Fig. 5), the higher chlorinated anilines and 4-chloro-2-nitroaniline produced peak sizes indicating that these compounds should be easily detectable at concentrations well below the 100 ng/l level shown in the chromatograms.

NPD signals of all organophosphorus pesticides except the last eluting compound dialifos and most of the nitrogen-containing pesticides were found to be high enough for reliable screening at the 100 ng/l level (Figs. 3 and 4). According to their low nitrogen content, the investigated anilines exhibit low NPD response factors. However, peak heights were clearly above a signal-to-noise ratio of 3 which is commonly set as the detection limit, thus enabling their detection at the 100 ng/l concentration level in screening analyses.

Many of the analytes investigated show sufficient response to both detectors used enabling their identification by the presence of peaks in both detector traces at the same retention time and with the expected response ratio. These compounds include the majority of the organo-

Table 1
Recovery of various organic compounds from tap water samples spiked with 50, 100 and 500 ng/l

Compound	50 ng/l		100 ng/l		500 ng/l		Det.
	Recovery (%)	R.S.D. (%)	Recovery (%)	R.S.D. (%)	Recovery (%)	R.S.D. (%)	
Chlorinated insecticides							
Aldrin	46	8.0	52	11	61	7.6	ECD
Chlorfenson	61	13	67	6.8	80	13	ECD
o,p-DDD	66	3.5	71	1.8	71	3.4	ECD
o,p-DDE	53	17	62	3.4	71	3.6	ECD
p,p-DDT	68	3.7	69	2.0	76	4.7	ECD
Dichlobenil	70	6.1	70	3.5	65	4.5	NPD
Dieldrin	66	4.1	68	2.1	70	6.3	ECD
α-HCH	70	1.4	66	3.3	68	3.5	ECD
β-HCH	50	8.0	61	3.6	67	2.4	ECD
Heptachlor	70	10	69	9.5	73	5.1	ECD
Heptachlor epoxide, *trans*	61	6.8	66	2.9	70	3.3	ECD
Hexachlorobenzene	35	12	52	12	64	7.6	ECD
Lindane	65	4.3	62	3.2	65	2.4	ECD
Methoxychlor	80	14	81	4.0	81	3.7	ECD
Mirex	49	18	64	2.0	66	3.4	ECD
Pentachlorobenzene	+		41	14	56	11	ECD
Quintozene	60	4.2	62	3.6	64	4.7	ECD
Triazine and acetanilide herbicides							
Ametryn	76	3.9	73	3.2	74	2.9	NPD
Atraton	70	4.3	62	2.4	61	3.6	NPD
Atrazine	67	2.1	64	5.3	64	3.4	NPD
Desethylatrazine	n.d.		n.d.		n.d.		NPD
Desisopropylatrazine	n.d.		n.d.		n.d.		NPD
Desmetryn	105	19	79	14	74	2.9	NPD
Metazachlor	79	1.5	75	2.1	71	3.4	NPD
Methoprotryn	93	4.0	84	2.7	82	3.3	NPD
Metolachlor	73	10.2	68	4.3	69	2.3	NPD
Metribuzin	53	6.2	41	19	41	3.5	NPD
Prometon	76	5.1	72	3.1	73	3.4	NPD
Prometryn	74	2.6	72	2.6	72	2.9	NPD
Propazine	72	4.9	72	6.5	72	3.2	NPD
Sebuthylazine	71	4.2	73	8.5	69	3.4	NPD
Simazine	49	3.5	35	4.0	30	4.1	NPD
Terbutryn	76	3.0	73	2.0	72	2.9	NPD
Terbutylazine	76	12	72	5.5	70	3.5	NPD
Triadimefon	89	3.8	83	1.8	77	2.5	NPD
Organophosphorus insecticides							
Acephate	n.d.		n.d.		n.d.		NPD
Azinphos-ethyl	112	8.7	114	13	116	8.3	ECD
Bromophos-ethyl	69	5.3	66	10	76	7.7	NPD
Bromophos-methyl	70	6.4	64	10	74	8.4	NPD
Chlorpyrifos-methyl	89	4.7	77	8.7	82	9.6	NPD
Chlorthion	90	2.7	84	3.3	75	3.2	NPD
Demeton-S-methyl	85	3.1	63	3.3	44	5.0	NPD
Demeton-S-methyl sulfone	81	9.8	71	9.7	77	13	NPD
Dialifos	64	9.6	64	11	74	6.8	ECD

Table 1 *(Continued)*

Compound	50 ng/l		100 ng/l		500 ng/l		Det.
	Recovery (%)	R.S.D. (%)	Recovery (%)	R.S.D. (%)	Recovery (%)	R.S.D. (%)	
Diazinon	76	7.9	64	12	70	9.4	NPD
Chlorfenvinphos	104	6.7	98	12	107	6.2	ECD
Dichlofenthion	73	4.7	70	5.0	62	4.5	NPD
Dichlorvos	47	2.9	38	1.6	34	4.5	ECD
Dicrotophos	97	2.4	72	6.6	56	4.1	NPD
Ditalimfos	92	18	65	6.1	69	5.5	NPD
Ethoprophos	62	5.8	63	8.9	68	4.3	ECD
Etrimfos	73	11	58	8.4	71	11	NPD
Isofenphos	69	9.4	78	5.8	76	4.2	ECD
Malathion	83	4.9	74	11	82	12	NPD
Methamidophos	n.d.		n.d.		n.d.		ECD/NPD
Parathion-ethyl	55	10	72	12	77	4.9	ECD
Parathion-methyl	65	10	85	18	83	5.4	ECD
Phosalone	104	7.7	105	14	111	8.7	ECD
Tetrachlorvinphos	126	2.5	112	11	111	7.8	ECD
Tolclofos-methyl	78	10	72	4.8	70	3.2	ECD
Anilines							
2-Chloroaniline	46	6.0	40	4.5	39	5.0	NPD
3-Chloroaniline	47	9.9	36	3.4	31	4.4	NPD
4-Chloro-2-nitroaniline	42	6.0	46	2.5	51	5.7	ECD
2,3-Dichloroaniline	77	7.8	65	3.5	64	4.9	NPD
2,4-Dichloroaniline	44	21	60	9.0	66	6.6	NPD
2,6-Dichloroaniline	96	8.9	76	11	68	4.9	NPD
3,4-Dichloroaniline	66	15	65	12	66	7.8	NPD
3,5-Dichloroaniline	82	11	68	7.7	69	4.1	NPD
2,6-Diethylaniline	59	12	73	4.0	70	2.8	NPD
2,6-Dimethylaniline	52	3.1	47	4.7	46	5.8	NPD
2,4-Dinitroaniline	n.d.		n.d.		n.d.		ECD/NPD
3-Nitroaniline	n.d.		n.d.		n.d.		ECD/NPD
2,3,4,5-Tetrachloroaniline	68	2.2	69	3.1	63	2.8	ECD
2,3,5,6-Tetrachloroaniline	56	6.5	67	12	75	4.0	NPD
3,4,5-Trichloroaniline	74	10	71	3.8	76	6.1	ECD
Phenols							
2,4-Dichlorophenol	59	32	55	10	54	7.3	ECD
2-Nitrophenol	n.d.		n.d.		n.d.		ECD/NPD
Pentachlorophenol	85	5.4	75	5.3	66	6.2	ECD
2,3,4,5-Tetrachlorophenol	92	8.6	88	4.8	90	3.6	ECD
2,3,5-Trichlorophenol	72	10	71	5.0	74	4.1	ECD
2,3,6-Trichlorophenol	71	8.9	70	4.6	75	4.3	ECD
2,4,5-Trichlorophenol	70	11	71	4.8	77	4.4	ECD

Mean recoveries and relative standard deviations (R.S.D.s) given in percent. Det. = Detection method used for quantification; n.d. = not detected after extraction; + = detected, but below limit of determination.

phosphorus pesticides investigated, the acetanilide herbicides metolachlor and metazachlor, the triazine herbicide metribuzin and the azol fungicide triadimefon as can be seen in Figs. 3 and 4.

Contaminants of tap water responding to ECD

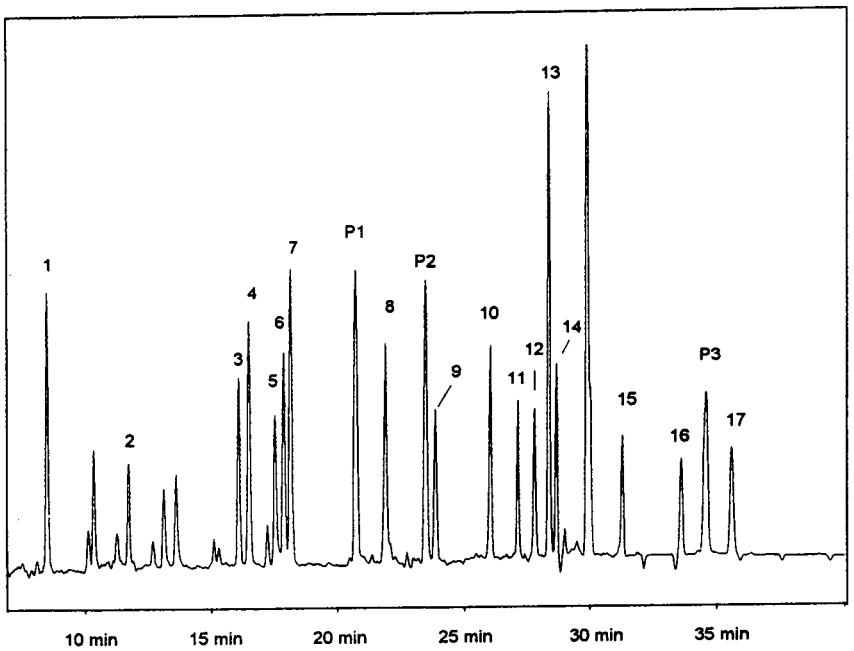

Fig. 2. GC–ECD of a mLLE extract of a tap water sample spiked with chlorinated insecticides (100 ng/l of each compound). Peaks: 1 = dichlobenil; 2 = pentachlorobenzene; 3 = α-HCH; 4 = hexachlorobenzene; 5 = β-HCH; 6 = lindane; 7 = quintozene; 8 = heptachlor; 9 = aldrin; 10 = heptachlor epoxide (*trans*-); 11 = *o,p*-DDE; 12 = chlorfenson; 13 = dieldrin; 14 = *o,p*-DDD; 15 = *p,p*-DDT; 16 = methoxychlor; 17 = mirex; P1 = dibutylphthalate; P2 = diisobutylphthalate; P3 = di-2-ethylhexylphthalate.

and NPD were found in all extracts. Three peaks in the ECD trace were identified as phthalate plasticizers, namely dibutyl, diisobutyl and di-2-ethylhexyl phthalates (P1, P2, P3). One large peak in the NPD trace was found to be tributyl phosphate (T). The identity of these contaminants was confirmed by GC–MS.

3.1. Recovery at three concentration levels

mLLE as described works with an extreme ratio of extracting solvent and extracted liquid of 1:800 and relies on one single extraction step. Only analytes with a very favourable partition ratio can be expected to be extracted sufficiently. On the other hand the simplicity of the procedure could compensate for lower recoveries if these are reproducible. To achieve high reproducibility, extraction was carried out using a mechanical mixing device. Samples were citrate buffered and saturated with NaCl, this ensuring a reproducible near-neutral pH and constant high ionic strength of the aqueous phase. NaCl saturation of the sample proved to be necessary not only to produce a salting out effect shifting the partition ratio of most analytes in favour of the organic solvent, but to minimize solubility of toluene in water and allow sufficient recovery of the small solvent amount applied. Solvent recoveries were estimated by removing the solvent layer completely by means of a scaled 0.5-ml pipette. A recovery of 325 to 350 μl or 65–70% was found as the range of 10 experiments with a mean of 68%. This demonstrates the ruggedness of the method.

The results of the recovery experiments of 82 target compounds at three concentration levels, namely at 50, 100 and 500 ng/l are compiled in Table 1. At each concentration level, five determinations were carried out from which the standard deviations were calculated. Out of the 82 target compounds, 68 were recovered in the range of 50 to 115% with a single extraction step. From the pesticides, only the two polar

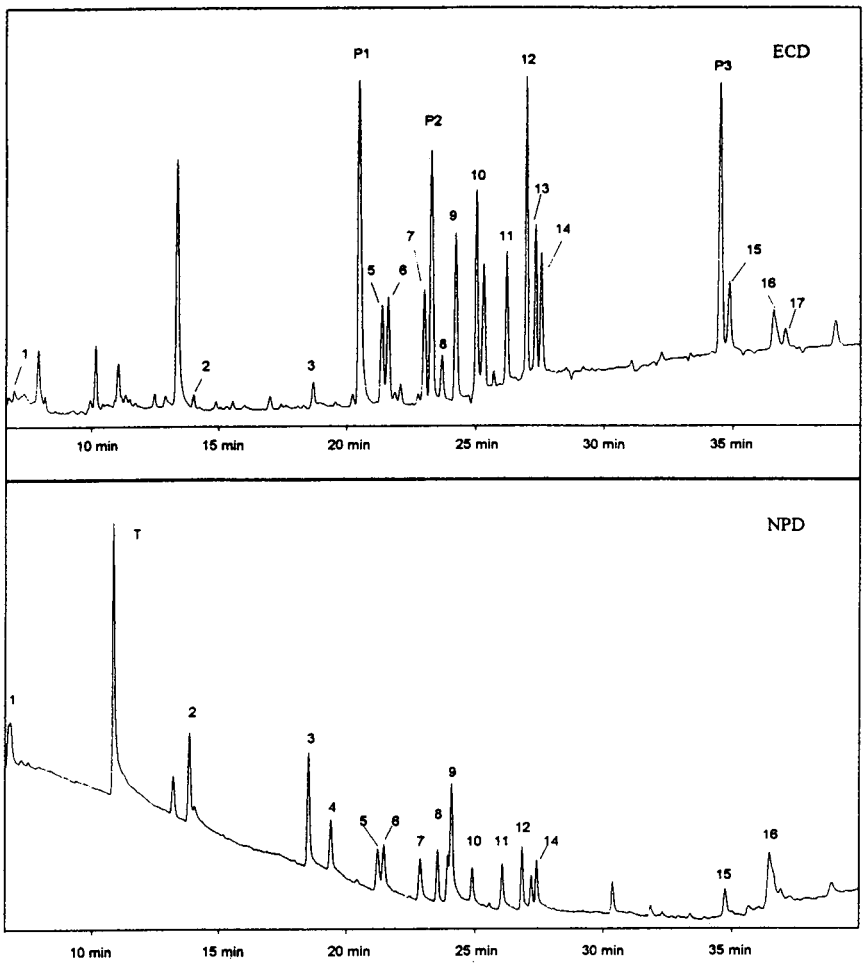

Fig. 3. GC–ECD and GC–NPD of a mLLE extract of a tap water sample spiked with organophosphorus pesticides (100 ng/l of each compound). Peaks: 1 = dichlorvos; 2 = ethoprophos; 3 = diazinon; 4 = etrimfos; 5 = parathion-methyl; 6 = tolclofos-methyl; 7 = demeton-S-methyl sulfone; 8 = malathion; 9 = parathion-ethyl; 10 = bromophos-methyl; 11 = chlorfenvinphos; 12 = bromophos-ethyl; 13 = tetrachlorvinphos; 14 = ditalimfos; 15 = phosalone; 16 = azinphos-ethyl; 17 = dialifos; T = tributylphosphate; P1, P2, P3 as in Fig. 2.

organophosphates with good water solubility, acephate and methamidophos, could not be recovered. The same holds true for the two nitroanilines, 2-nitrophenol and the two desalkyl triazines which both are known to give low recoveries in many extraction procedures. Lower recoveries than 50% were observed with demeton-S-methyl, dichlorvos, metribuzine and simazine as well as some anilines. All recoveries for the target compounds were calculated with the mean recovery of the solvent of 68% mentioned above.

Summarizing, most of the pesticides and pollutants under investigation were found to be recovered to an extent that makes their detection in drinking water samples possible at the 100 ng/l concentration level and below applying GC with simultaneous parallel detection by ECD and NPD for screening analysis. In addition, the injected amount of target analytes of 100 pg or

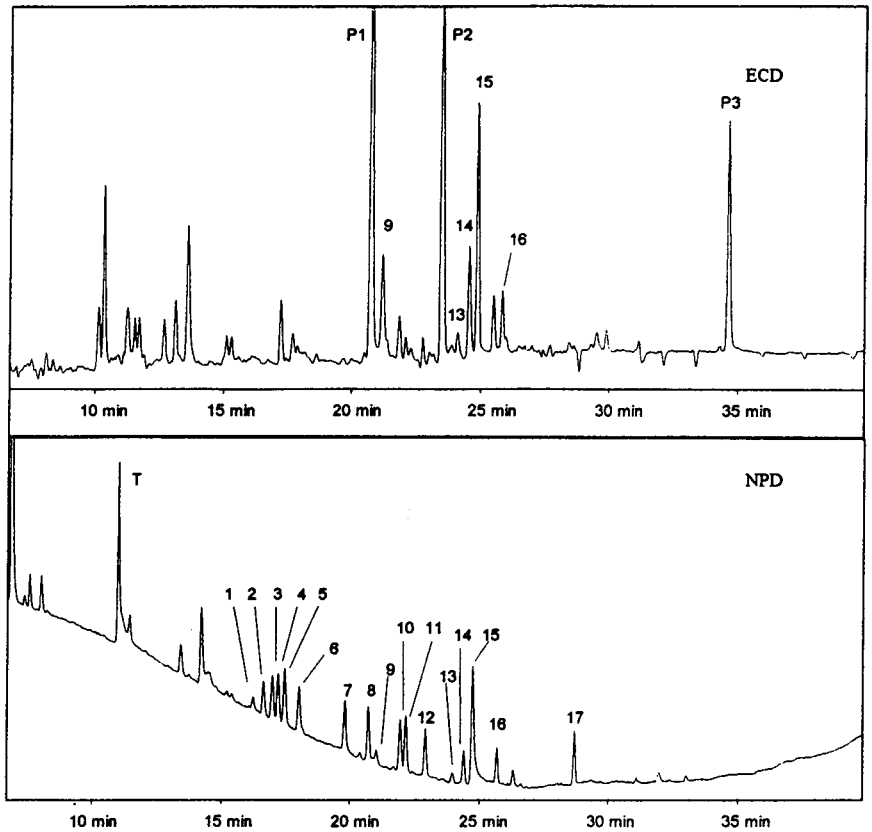

Fig. 4. GC–ECD and GC–NPD of a mLLE extract of a tap water sample spiked with triazines and other nitrogen-containing pesticides (100 ng/l of each compound). Peaks: 1 = simazine; 2 = atraton; 3 = prometon; 4 = atrazine; 5 = propazin; 6 = terbuthylazin; 7 = sebuthylazin; 8 = desmetryn; 9 = metribuzin; 10 = ametryn; 11 = prometryn; 12 = terbutryn; 13 = metolachlor; 14 = triadimefon; 15 = chlorthion; 16 = metazachlor; 17 = methoprotryn; T as in Fig. 3; P1, P2, P3 as in Fig. 2.

more is sufficient for confirmatory analysis by GC–MS in the selected ion monitoring (SIM) mode.

The reproducibility of an analytical procedure usually is characterized by standard deviations. In the analytical method described, these standard deviations reflect not only the variation of the extraction process but also the reproducibility of the GC separation and the detector response. Many target compounds can be determined with both detectors, the peak areas with the lower standard deviations are reported together with the detector trace used in Table 1. Most of the standard deviations reported in the table are clear below 10% at all three concentration levels. The mean of all standard deviations of all target compounds was calculated at the spike level of 50 ng/l with 7.9%, 100 ng/l with 6.6% and 500 ng/l with 5.2%.

Summarizing the recovery data the mLLE method described can be considered as a simple and reliable method for the screening of drinking water samples for a variety of pesticide residues at the concentration level necessary to meet the requirement of the drinking water guidelines of the EU. The reliability of the results will certainly be enhanced by combination with more selective determination methods such as capillary GC with atomic emission detection or mass spectrometric detection. When analyzing a limited

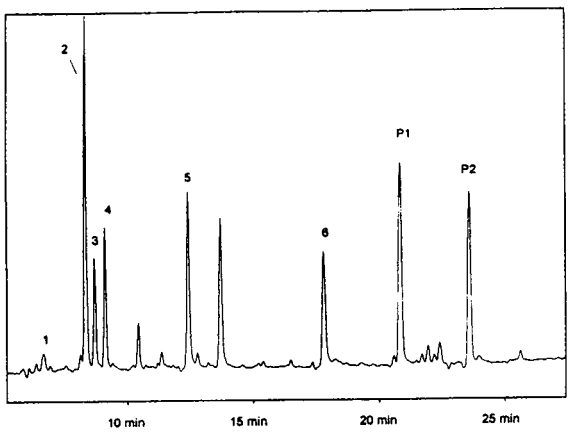

Fig. 5. GC–ECD of a mLLE extract of a tap water sample spiked with chlorinated phenols (100 ng/l of each compound). Peaks: 1 = 2,4-dichlorophenol; 2 = 2,3,5-trichlorophenol; 3 = 2,4,5-trichlorophenol; 4 = 2,3,6-trichlorophenol; 5 = 2,3,4,5-tetrachlorophenol; 6 = pentachlorophenol; P1, P2 as in Fig. 2.

number of related target compounds, for example triazine herbicides, the addition of a suitable surrogate standard will further add to the reliability of quantitative results. Furthermore, such a surrogate standard is an important indicator of the performance of the whole method, when applied to numerous different matrices.

4. Conclusions and outlook

The method presented is found to be suitable for the analysis of a wide range of organic trace compounds in drinking water. It can be easily performed in any GC laboratory with basic equipment and low manpower. Interferences from large solvent volumes or solid phase extraction materials are avoided. Results obtained with a special application of this method to ground water in a field study on leaching of alachlor and its metabolites [7] indicate that the method should be suitable also for this matrix. During this study, one analyst could process up to 50 ground water samples per day. A modification of the method was successfully applied in another field study on leaching of the phenoxycarbonic acid mecoprop and its metabolite 2-methyl-4-chlorophenol. The analytes were extracted from acidified ground water samples and determined by GC after pentafluorobenzylation [9]. An extension of the latter procedure to the determination of further acidic herbicides has been completed [10].

Modifications e.g. of pH or solvent composition may improve results for still poorly extracted compounds and make the procedure applicable to further substance classes.

References

[1] *EEC Drinking Water Guideline, 80/779/EEC, EEC No. L229/11-29*, European Economic Community, Brussels, 30 August 1980.
[2] G.A. Junk and J.J. Richard, *Anal. Chem.*, 60 (1988) 451–455.
[3] D.A. Murray, *J. Chromatogr.*, 177 (1979) 135–140.
[4] P.-F. Blanchet, *J. Chromatogr.*, 179 (1979) 123–129.
[5] D.R. Thielen, G. Olsen and A. Davis, *J. Chromatogr. Sci.*, 25 (1987) 12–16.
[6] T.L. Potter, T. Carpenter, R. Putnam, K. Reddy and J.M. Clark, *J. Agric. Food Chem.*, 39 (1991) 2184–2187.
[7] R. Heyer and H.-J. Stan, *Int. J. Environ. Anal. Chem.*, in press.
[8] R. Heyer, A. Zapf and H.-J. Stan, *Fresenius' J. Anal. Chem.*, in press.
[9] R. Heyer and H.-J. Stan, *Pestic. Sci.*, submitted for publication.
[10] R. Heyer and H.-J. Stan, in preparation.

ELSEVIER

Journal of Chromatography A, 694 (1995) 463–469

JOURNAL OF CHROMATOGRAPHY A

Ion-exchange electrokinetic capillary chromatography with Starburst (pamam) dendrimers: a route towards high-performance electrokinetic capillary chromatography

M. Castagnola[a,c,*], L. Cassiano[b], A. Lupi[c], I. Messana[b,c], M. Patamia[c], R. Rabino[b], D.V. Rossetti[b], B. Giardina[b,c]

[a]*Dipartimento di Medicina Sperimentale e Scienze Biochimiche, Università di Roma "Tor Vergata", Rome, Italy*
[b]*Istituto di Chimica e Chimica Clinica, Facoltà di Medicina "A. Gemelli", Università Cattolica del S.C., Rome, Italy*
[c]*Centro di Studio per la Chimica dei Recettori e delle Molecole Biologicamente Attive, CNR, Rome, Italy*

First received 16 August 1994; revised manuscript received 18 October 1994; accepted 19 October 1994

Abstract

The use of different generations of Starburst (pamam) dendrimers provides a new opportunity for ion-exchange electrokinetic capillary chromatography. The uniform surface charge density and the structural homogeneity of these macroelectrolytes provide a decrease of plate height in comparison with micellar electrokinetic capillary chromatography with cationic surfactants. In addition, the use of different dendrimer generations allows the separation selectivity to be modulated.

1. Introduction

The presence of electroosmotic flow (f_{eo}) in capillary electrophoresis (CE) is the basis for a class of relatively new separation techniques collectively termed electrokinetic chromatography. The f_{eo} acts as a chromatographic eluent and the analytes are separated on the basis of their different interaction either with an electrolyte that migrates counterflow to the f_{eo} or with different stationary phases that are linked to the inner surface of the capillary. The best studied electrokinetic chromatography is micellar electrokinetic capillary chromatography (MEKC), originally developed by Terabe and co-workers [1,2]. In this case an anionic detergent [usually sodium dodecyl sulphate (SDS)] is added in the electrophoretic solution at a concentration greater than its critical micellar concentration (CMC); the negatively charged micelles migrate counterflow towards the anodic terminal of the capillary, such as a pseudo-stationary chromatographic phase. Another option for electrokinetic separations is the use of soluble polymer ions that migrate counterflow to f_{eo} [3]; in this instance the technique is termed ion-exchange electrokinetic chromatography (IEEKC).

Even though the separative potential of electrokinetic chromatography is impressive, the separation depends on many parameters which are difficult to optimize [4]. The counterflow electrolyte concentration, the pH of the solution,

* Corresponding author. Address for correspondence: Centro di Studio per la Chimica dei Recettori e delle Molecole Biologicamente Attive, c/o Istituto di Chimica e Chimica Clinica, Facoltà di Medicina e Chirurgia, Università Cattolica, Largo F. Vito 1, 00168 Rome, Italy.

0021-9673/95/$09.50
SSDI 0021-9673(94)01015-3

the polarity and the percentage of organic solvents, the temperature and the applied voltage are important parameters that are mutually connected in the modulation of the selectivity and of the performance of the separation. In fact, the band broadening can be described, as for any chromatographic system, in term of plate height, which depends on several terms [5,6]; one of the most relevant is linked to the microheterogeneity of the counterflow electrolyte [4].

In order to modulate this microheterogeneity, recently the use of double-chain surfactants [7] or the modification of MEKC in microemulsion electrokinetic chromatography has been suggested [8]. In close comparison with chromatographic systems, one of the main reasons for the progress from conventional to high-performance separations was the availability of small, stable, uniform stationary phases; thus the availability of uniformly sized polyelectrolytes can contribute to obtaining electrokinetic separations characterized by high performance.

For this purpose, novel interesting dendritic molecules are available. They are obtained by "cascade" synthesis starting from an initiator core of a branched building block [9]. As a function of the starting block these substances were divided into several classes [10]; some of them were named arborols, silvanols, micellanes (or unimolecular micelles); recently, different generations of cascade dendrimers obtained from an initiation core of ethylenediamine became commercially available (Aldrich); they were collectively termed Starburst [poly(amidoamine); pamam] dendrimers (SPD). They are characterized by a surface with a uniform charge density. Tanaka et al. (11) reported that these substances can be utilized as good carriers for electrokinetic chromatography.

This study was aimed at establishing if the use of these compounds in electrokinetic chromatography provides a general increase in the separation performance. As the Starburst dendrimers utilized have terminal positive charges, the separations were carried out with an inverted electroosmotic flow with respect to the usual direction (anodic instead of cathodic electroosmotic flow) [12].

2. Experimental

2.1. Chemicals

Starburst (pamam) dendrimers of different generations were purchased from Aldrich (Milwaukee, WI, USA). Dodecyltrimethylammonium bromide (DTAB) was obtained from Sigma-Chemie (Deisenhofen, Germany), triethylamine of Sequanal grade from Pierce (Rockford, IL, USA), acetanilide and methanol of HPLC grade from Carlo Erba (Milan, Italy) and dansylamino acids from Sigma (St. Louis, MO, USA). Other common reagents were of analytical-reagent grade from Merck (Darmstadt, Germany) and were used as received.

2.2. Instrumentation and method

The MEKC separations were performed with a P/ACE System 2100 (Beckman, Palo Alto, CA, USA), equipped with GOLD software (Beckman); the capillary was of bare silica, 56.5 cm in length (50.0 cm at the detection window) × 75 μm I.D., with the injection terminal corresponding to the cathodic solution. The applied voltage was 15 kV and the temperature of the separation was 25°C (unless indicated otherwise). The electrophoretic buffer was 40 mmol/l phosphoric acid – 43 mmol/l triethylamine adjusted pH 8.3 with HCl (or NaOH in the case of DTAB solution) and mixed with methanol (80:20) to obtain a final concentration 4.0% (w/v) of cationic detergent. This concentration corresponds to 30.0, 12.3 and 5.8 mmol/l for SPD of generations 1, 2 and 3, respectively, and to 130 mmol/l for DTAB (considerably greater than its critical micellar concentration [13]). The samples were prepared at a concentration 0.3 mmol/l in a buffer obtained by diluting the separation buffer (without the cationic surfactant) in the ratio 1:9 with ultrapure water. The injection time was 1.0 s, corresponding to about 4 nl of sample solution and to about 10 fmol of sample injected. Detection was performed at a wavelength of 254 nm. The capillary, before each run, was rinsed with 1.0 mol/l NaOH for 5 min, washed with ultrapure

water for 5 min and equilibrated with the separation buffer for 2 min.

3. Results and discussion

Starburst (pamam) dendrimers (SPD) are a class of branched molecules, usually starting from an initial core of ethylenediamine. The first synthetic step in their production involves Michael addition of methyl acrylate to the nucleophilic core; after a reaction with an excess of ethylenediamine, a nucleophilic surface of generation 0 is obtained. Repetition of these two steps leads to the following generations, which are characterized by a number of repeat units or degree of polymerization (N_{ru}), number of surface groups (Z_S) and molecular mass (M_r) as a function of the initiator core multiplicity ($N_c = 4$) and its molecular mass ($M_c = 60.1$), branch cell multiplicity ($N_b = 2$) and repeat unit molecular mass (M_{ru}), according to recurrent equations described by Tomalia [14]. The values of N_{ru}, M_r, Z_s and total charge (Z_t) for the dendrimers of generation 0 to 3, are reported in Table 1, where several other properties of the dendrimers are also shown, such as the values of the ratio between their total charge and the molecular mass to the power 1/3 (which can be assumed to be approximately proportional to the dendrimer radius) and the values of the ratio between their surface charge and the molecular mass to the power 2/3 (which can be assumed to be approximately proportional to the dendrimer surface area). The first ratio should be related to the dendrimer mobility and the second should be proportional to the surface charge density and should be related to the interaction with other electrolytes.

As dendrimers can be considered to be polymer solutes with a uniformly charged surface, the electrokinetic separation should be considered as ion-exchange electrokinetic chromatography, although further interactions might contribute to the solute retention [11]. When higher SPD generations become available, this definition could be reconsidered as the thermodynamic properties of a solution containing a macromolecule uniformly charged on the surface should be established and compared with micellar solutions.

In order to produce a counterflow migration of the positively charged SPD, an anionic f_{eo} is necessary; this can be achieved by the use in the separation solution of a high concentration of triethylamine [12]; in addition, the presence of a cationic surfactant such as SPD itself contributes to the generation of anodic electroosmotic flow [13].

After testing several substances, acetanilide was chosen as a marker of the f_{eo} mobility (μ_{eo}). In fact, its migration always coincided with a small disturbance on the baseline (if present) due to a sample plug. The mobility of f_{eo} and the mobilities of several standard dansylamino acids are plotted as a function of the surface charge density of the dendrimer multiplied by its concentration (Fig. 1); μ_{eo} increases as a function of the SPD generation and decreases as a function of the product of the surface charge density and the concentration. Hence the concentration of the dendrimer (over a limiting value) is not relevant for the generation of μ_{eo}, while the most relevant parameter should be related to the dimensions of the SPD. A dendrimer of higher

Table 1
Properties of Starburst (pamam) dendrimers as a function of their generation

Generation	N_{ru}	M_r	Total Z (Z_t)	Surface Z (Z_s)	$Z_t/(M_r)^{1/3}$	$Z_s/(M_r)^{2/3}$
0	4	516	6	4	0.75	0.062
1	12	1430	16	8	1.42	0.063
2	28	3256	32	16	2.16	0.073
3	60	6909	64	32	3.36	0.088

For explanation of the symbols, see the text.

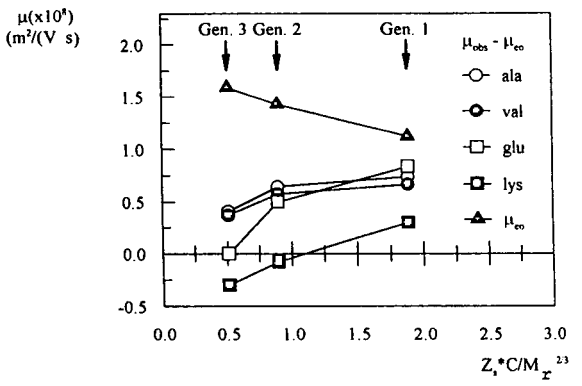

Fig. 1. Mobility of the electroosmotic flow (μ_{eo}) and intrinsic mobility [$\mu_{obs} - \mu_{eo}$ (Eq. 1)] of several dansyl-amino acids as a function of the product of the surface charge density and concentration for different SPD generations. The IEEKC conditions are given in Section 2.2.

generation has a greater effect on the inversion of the surface ζ potential, which is probably connected to the higher positive charge presented towards the solution by the higher dendrimer bound to the inner capillary wall.

As outlined by Terabe and Isemura [3], the observed mobility (μ_{obs}) in IEEKC is given by

$$\mu_{obs} = \mu_{eo} + x_f\mu_f + (1 - x_f)\mu_p$$
$$= \mu_{eo} + \frac{1}{1 + K[P]} \cdot \mu_f + \frac{K[P]}{1 + K[P]} \cdot \mu_p \qquad (1)$$

where μ_f and x_f are the mobility and the molar fraction of the analyte ion free from the polymer ion, respectively, μ_p is the mobility of the polymer ion, [P] its concentration and K the ion-pair association constant. It must be noted that μ_f and μ_p have opposite signs. This equation assumes that μ_p does not change significantly on interaction. Further, Eq. 1 does not account for any other interaction and it assumes that μ_{eo} does not change significantly as a function of [P]. As previously outlined, with the use of SPD this condition is approximately respected.

The results reported in Fig. 1 indicate that the intrinsic mobilities ($\mu_{obs} - \mu_{eo}$) of several standard dansylamino acids (Ala, Val, Glu, Lys) generally decrease as a function of the dendrimer generation (or increase as a function of the product between the surface charge density and the concentration). This observation indicates that the last term of Eq. 1 increases as a function of SPD generation, either for a large increase in the ion-pair association constant and/or an increase in μ_p as a function of the SPD generation (see Table 1). This is particularly evident for the intrinsic mobility of dansyl-Glu, which in the case of SPD of generation 1 is the highest measured, owing to its negative charge, whereas in the case of SPD of generations 2 and 3 it is lower than the mobility measured for dansyl-Ala and dansyl-Val as a consequence of a strong increase in its ion-pair association constant as a function of dendrimer generation. The intrinsic mobility of dansyl-Lys is the lowest, obviously owing to its positive charge. Further, the modification of its mobility as a function of the SPD generation indicates that the interaction increases according to SPD dimensions more for dansyl-Lys than for dansyl-Ala and dansyl-Val. Thus mechanisms different from simple ion-pair interaction operate, as already observed by Tanaka et al. [11].

The uniformity of SPD chemical structure can contribute to a higher performance of the electrokinetic separation. The band broadening in MEKC [5,6] can be expressed in terms of several factors contributing to the overall plate height (H_{tot}), similarly to the common Van Deemter equation for chromatographic separations. The principal factors are the plate heights generated by longitudinal diffusion (H_{ld}), sorption–desorption kinetics in micellar solubilization (H_{mc}), intermicelle mass transfer in the aqueous phase (H_{aq}), radial temperature gradient effect on the electrophoretic velocity of the micelles (H_{tm}) and dispersion of electrophoretic mobilities of the micelles (H_{ep}). Among these factors, H_{ld}, H_{mc} and H_{ep} are those which, in MEKC, have the greatest effect on H_{tot}. In particular, H_{ep} is connected with the differences in mobilities of the micelles and, as a consequence, is linked to the microheterogeneity of the micellar phase. A similar treatment for IEEKC was not described. Nevertheless, the principal factors in IEEKC should be H_{ld} and H_{ep}, while the others can be considered negligible or unsuitable, e.g., H_{mc}

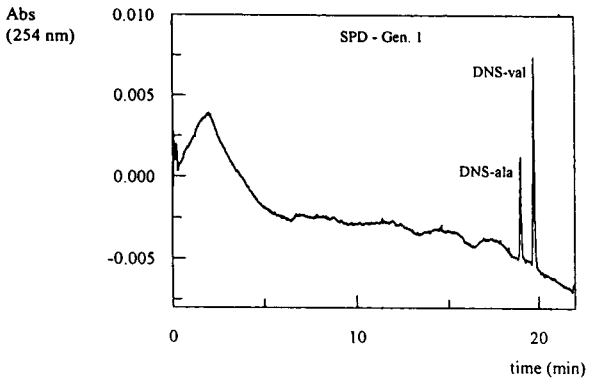

Fig. 2. Separation of dansyl-Ala and dansyl-Val in the presence of SPD of generation 1. The IEEKC conditions are given in Section 2.2.

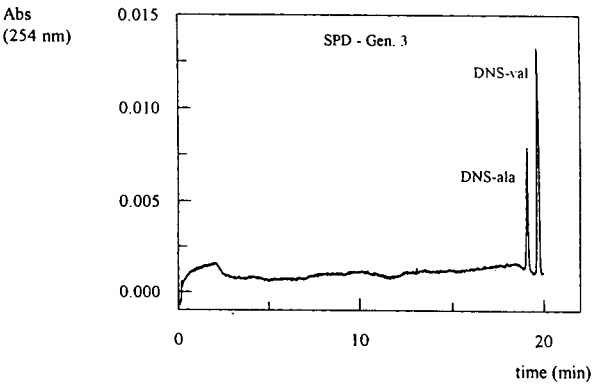

Fig. 4. Separation of dansyl-Ala and dansyl-Val in the presence of SPD of generation 3. The IEEKC conditions are given in Section 2.2.

should be described as a factor linked to the sorption–desorption kinetics of interaction of the analytes with the dendrimer (H_{ki}).

In Figs. 2–4, separations of dansyl-Ala and dansyl-Val in the presence of SPD of generations 1–3 are shown. In Fig. 5, for comparison, the separation of the same pair in the presence of DTAB at a concentration greater than its CMC is presented. This comparison is not completely pertinent since the electrokinetic DTAB separation is under micellar conditions, but, in the absence of an appropriate reference, is the best that can be proposed. In Table 2 the performance of these separations in terms of mean

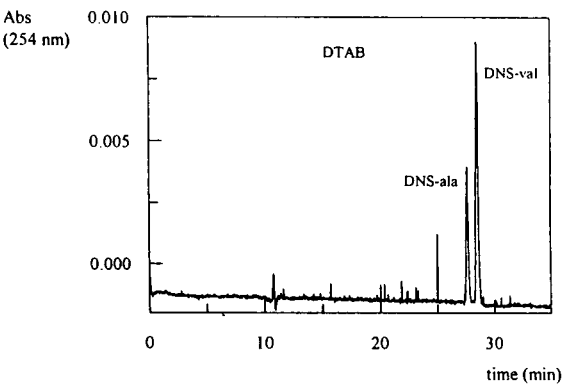

Fig. 5. Separation of dansyl-Ala and dansyl-Val in the presence of DTAB. The IEEKC conditions are given in Section 2.2.

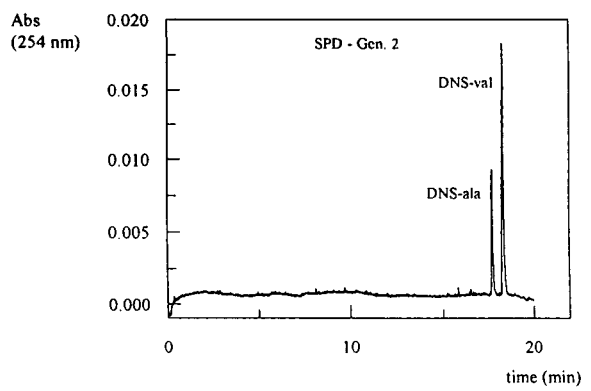

Fig. 3. Separation of dansyl-Ala and dansyl-Val in the presence of SPD of generation 2. The IEEKC conditions are given in Section 2.2.

theoretical plates, plate height and resolution is reported. Their values were calculated according to the usual relationships:

Table 2
Performance of IEEKC separation of dansyl-Ala and dansyl-Val by Starburst (pamam) dendrimers (SPD) of different generations

SPD generation	N	H (μm)	R
1	614 000	0.81	7.5
2	586 000	0.85	5.9
3	463 000	1.08	5.0
DTAB	277 000	1.81	4.0

$$N = 16(t_m/w)^2 \quad (2)$$

$$H = L/N \quad (3)$$

$$R = 2\,\Delta t/(w_1 + w_2) \quad (4)$$

where w is the peak width at the peak base, t_m is the migration time and L is the length from the injection-point to the detection window of the capillary. As expected, the performance of the separations in the presence of SPD is about twice as good as that with DTAB. This can be linked to a strong decrease in H_{ep} due to the SPD microhomogeneity. The plate height increases with increase in generation. This can derive from a slight increase in H_{ep} as a function of SPD generation since, from the last term of Eq. 1, either multiple interactions of dansylamino acids can contribute to a greater dispersion of the mobility of the counterflow SPD polymer or greater molecular flexibility of the lateral chain in the SPD of higher generation can generate a variability of the ion-pair association constants.

Fig. 6 shows the dependence of the plate height on temperature. The separations in the presence of SPD of generations 1 and 2 showed a slight decrease in performance as a function of temperature increase; this is easily ascribed to an increase in H_{ld} and/or H_{tm}. The separation in the presence of SPD of generation 3 and in the presence of DTAB showed a minimum in the plate height at 30°C that suggested a complex contribution of temperature to the performance of the separation; in DTAB separations the increase in performance as a function of increase in temperature is probably linked to stabilization of the micellar phase [4].

The greater complexity of MEKC with DTAB compared with IEEKC with SPD is evidenced by the performance of the separations as a function of the applied voltage (Fig. 7); in IEEKC with SPD the plate height decreased linearly when the voltage increased, according to the usual electrophoretic properties; in MEKC separation a strong increase in plate height was noted. With SPD of generation 1 and DTAB, the applied voltage was not set above 18 kV owing to the too strong current increase. As with generation 1 SPD the increase in voltage is linked to an increase in the separation performance, the decrease in performance observed with the use of DTAB cannot be ascribed only to a Joule effect.

In conclusion, IEEKC in the presence of SPD seems to be governed by general properties simpler than those observed in MEKC separations. The uniformity of their structure seems to provide an improvement in the separation performance. In addition, the different ion-pair interactions of the analytes as a function of SPD generation offer a new option for modification of the separation selectivity.

The future availability of SPD of generation

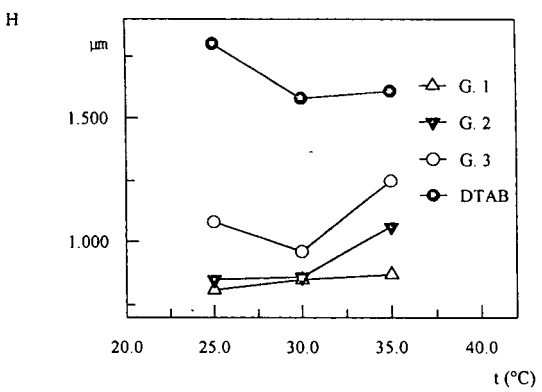

Fig. 6. Dependence of the plate height on temperature using different SPD generations and DTAB. The other IEEKC conditions are given in Section 2.2.

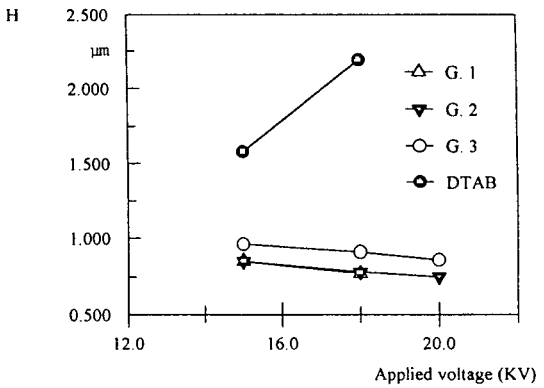

Fig. 7. Dependence of the plate height on applied voltage using different SPD generations and DTAB. The other IEEKC conditions are given in Section 2.2.

higher than 3 will permit the observations to be extended to a wider range and the thermodynamic properties of macrosolutes with a uniformly charged surface to be established.

References

[1] S. Terabe, K. Otsuka, K. Ichikawa, A. Tsuchiya and T. Ando, *Anal. Chem.*, 56 (1984) 111.
[2] S. Terabe, K. Otsuka and T. Ando, *Anal. Chem.*, 57 (1985) 834.
[3] S. Terabe, T. Isemura, *Anal. Chem.*, 62 (1990) 650.
[4] M. Castagnola, D.V. Rossetti, L. Cassiano, R. Rabino, G. Nocca and B. Giardina, *J. Chromatogr.*, 638 (1993) 327.
[5] M.J. Sepaniak and R.O. Cole, *Anal. Chem.*, 59 (1987) 472.
[6] S. Terabe, K. Otsuka and T. Ando, *Anal. Chem.*, 61 (1989) 251.
[7] M. Tanaka, T. Ishida, T. Araki, A. Masuyama, Y. Nakatsuji, M. Okahara and S. Terabe, *J. Chromatogr.*, 648 (1993) 469.
[8] S. Terabe, N. Matsubara, Y. Ishihama and Y. Okada, *J. Chromatogr.*, 608 (1992) 23.
[9] G.R. Newkome, Z.Q. Yao, G.R. Baker and V.K. Gupta, *J. Org. Chem.*, 50 (1985) 2003.
[10] D.A. Tomalia, A.M. Naylor and W.A. Goddard, III, *Angew. Chem.*, 102 (1990) 119.
[11] N. Tanaka, T. Tanigawa, K. Hosoya, K. Kimata, T. Araki and S. Terabe, *Chem. Lett.*, (1992) 959.
[12] D. Corradini, A. Rhomberg and C. Corradini, *J. Chromatogr. A*, 661 (1994) 305.
[13] D. Crosby and Z. El Rassi, *J. Liq. Chromatogr.*, 16 (1993) 2161.
[14] D.A. Tomalia, *Aldrichim. Acta*, 26 (1993) 91.

ELSEVIER

Journal of Chromatography A, 694 (1995) 471–479

JOURNAL OF CHROMATOGRAPHY A

Application of micellar electrokinetic chromatography and indirect UV detection for the analysis of fatty acids

F.B. Erim*, X. Xu, J.C. Kraak

Laboratory for Analytical Chemistry, University of Amsterdam, Nieuwe Achtergracht 166, 1018 WV Amsterdam, Netherlands

Received 12 September 1994; accepted 11 November 1994

Abstract

A micellar electrokinetic chromatographic system using indirect UV detection was developed for the analysis of saturated fatty acids. Sodium dodecyl benzenesulfonate (SDBS) was used as micellar surfactant as well as chromophore for the indirect detection. The effects of the addition of acetonitrile and Brij on the migration and solubility of the fatty acids was investigated. With a mixture of 10 m*M* SDBS + 50% acetonitrile + 30 m*M* Brij, a complete separation of the C_8–C_{20} fatty acids was obtained. The applicability of the developed system for the analysis of fatty acids in butter is demonstrated.

1. Introduction

Fatty acids are defined as all saturated and unsaturated aliphatic carboxylic acids with a carbon chain length in the range C_6–C_{24}. In nature many fatty acids are present, but only the C_8–C_{22} carboxylic acids are of commercial importance [1]. These relevant compounds can be either isolated from animals and vegetables or synthesized. The determination of the individual fatty acids provides important information about the composition of natural fats and oils produced from animals and vegetables [2]. This necessitates the use of advanced and fast analysis techniques. Gas and liquid chromatography have found to be very suited for the analysis of fatty acids [3–5]. Both techniques are widely applied but there is still a need to speed up the analysis because of the innumerable applications in life. An attractive alternative separation technique might be capillary electrophoresis [6] and in particular micellar electrokinetic chromatography (MEKC) as introduced by Terabe et al. [7]. The last technique combines electrophoresis and chromatography and can be used to separate neutral solutes as well as ionic compounds [8,9]. An additional advantage of micellar systems is the fact that compounds which are insoluble or slightly soluble in aqueous phases can be solubilized. The solubility of fatty acids in aqueous solutions decreases rapidly with increasing alkyl chain and therefore MEKC seems to be an attractive separation technique for these compounds. However, the absence of a chromophoric or fluorophoric group in the fatty acids excludes direct UV or fluorometric detection and therefore indirect detection has to be used [10].

In this paper we report the results of an investigation to develop a MEKC system for the

* Corresponding author.

0021-9673/95/$09.50
SSDI 0021-9673(94)01114-1

separation of 13 fatty acids using indirect UV detection. The applicability of the developed MEKC system will be demonstrated with analysis of real samples.

2. Experimental

2.1. Apparatus

A commercial capillary zone electrophoresis (CZE) injection system (Prince; Lauer Labs., Emmen, Netherlands) in combination with on-column UV detection (Linear 200; Linear Inst., Fremont, CA, USA) was used. The wavelength was set at 198 nm. Unless otherwise stated, the analysis voltage was 20 kV. Sample injection was carried out with pressure (40 mbar, 0.06 min) at the anodic side. A 60 cm × 50 μm I.D. fused-silica capillary (Polymicro Technologies, Phoenix, AZ, USA) was used. The distance to the detection window was 45 cm. The measurements were performed at room temperature (23 ± 2°C).

2.2. Chemicals

Sodium dodecyl benzenesulfonate (SDBS) was purchased from Fluka (Bornem, Belgium). Brij 35 was obtained from Merck (Darmstadt, Germany) and acetonitrile from Janssen Chimica (Beerse, Belgium). The fatty acids with alkyl chains of C_8–C_{20} were obtained from different sources: C_8, C_9, C_{10}, C_{12}, C_{14}, C_{16} and C_{18} from Merck; C_{11}, C_{17} and C_{20} from Sigma (Bornem, Belgium) and C_{13}, C_{15} and C_{19} from Fluka.

2.3. Procedures

During the night the capillaries were stored in 0.1 *M* NaOH.

Prior to use, the capillary was flushed for 10 min with water and the actual buffer solution successively. Before each measurement, the capillary was flushed for 2 min with the actual buffer solution.

The actual buffer solutions were prepared by mixing stock solutions of Tris buffer (adjusted with HCl to pH 8.5), surfactants and acetonitrile and adjusting the final volume with water. Doubly distilled water was used for all solutions. All buffer solutions were filtered prior to use through a 0.1-μm Millipore (Bedford, MA, USA) filter (type Millex-VV).

Stock solutions of fatty acids were prepared in methanol or acetonitrile. Sample solutions were prepared by mixing measured quantities of stock solutions of fatty acids, buffer, surfactants and organic solvents and adjusting the final volume with water. In this way the composition of the sample can be kept similar to that of the buffer solution. The electroosmotic flow was determined from the residence time of the solvent peak or with methanol. In some cases sudan was used to determine the residence time of an analyte totally incorporated into the micelle.

3. Results

The electrophoretic mobility of the fatty acids decreases with increasing alkyl chains. The C_8–C_{11} fatty acids can be separated by zone electrophoresis but not the C_{11}–C_{20} fatty acids because the difference in electrophoretic mobility becomes too small. Moreover, the solubility of the fatty acids decreases dramatically with increasing alkyl chain which causes serious detection problems. By adding micelles to the back ground electrolyte, fatty acids will be differentially solubilized in the micelle and this opens the possibility to separate the fatty acids according to their hydrophobicities e.g. length of the alkyl chain. In order to determine the optimum conditions for the separation of the fatty acids the effects of two surfactants, SDBS and Brij were studied including the effect of the addition of acetonitrile. The selection of SDBS was based on the result reported by Sandra et al. [9] who separated some smaller alkylcarboxylic acids using the same surfactant as chromophore for indirect UV detection.

3.1. Migration behaviour of fatty acids with SDBS

The effect of the SDBS concentration on the migration behaviour of fatty acids was studied

with C_{11}–C_{13}, using 5 m*M* Tris pH 8.5 as buffer. The critical micellar concentration (CMC) of SDBS has been reported to be around 2 m*M* [11]. In the range of 0.5–2 m*M* SDBS the solutes gave a negative peak all having about the same migration time. This indicates that no micelles are formed in this concentration range as expected on basis of the CMC. When increasing the SDBS concentration to 4 m*M*, the elution order changed into $C_{11} = C_{12} < C_{13}$. When further increasing the concentration to 10 m*M* SDBS the elution order became $C_{11} < C_{12} < C_{13}$ and the three solutes can be completely separated. This elution order is the reverse as expected in zone electrophoresis and demonstrates the micellar effect of SDBS. It can be noted that the baseline stability becomes significantly worse with increasing SDBS and resulted in disturbed and small peaks in particular for the C_{13} acid. Also it was not possible to dissolve the longer fatty acids even in 20 m*M* SDBS. In order to enlarge the solubility of the larger fatty acids the SDBS was mixed with sodium dodecyl sulfate (SDS) or the non-ionic surfactant Brij and with alcohols or acetonitrile. Mixing of SDBS with SDS caused a tremendous increase of the background noise signal. The addition of alcohols had very little effect on the solubility but the migration times increased due to a decrease of the electroosmotic flow. With the addition of Brij and acetonitrile the solubilities of the fatty acids increased significantly. Therefore the effect of the addition of Brij and acetonitrile on the migration behaviour of the fatty acids was studied more extensively. This will be discussed in the next sections.

3.2. Migration behaviour of fatty acids in SDBS–acetonitrile mixtures

The effect of the addition of acetonitrile to the SDBS system on the migration behaviour was studied with the C_{11}, C_{12} and C_{13} fatty acids as test solutes. Fig. 1 shows the effect of the addition of acetonitrile on the mobility of the fatty acids using 10 m*M* SDBS. As can be seen the electroosmotic flow decreases and the migration times of the fatty acids increases with increasing acetonitrile percentage. For up to

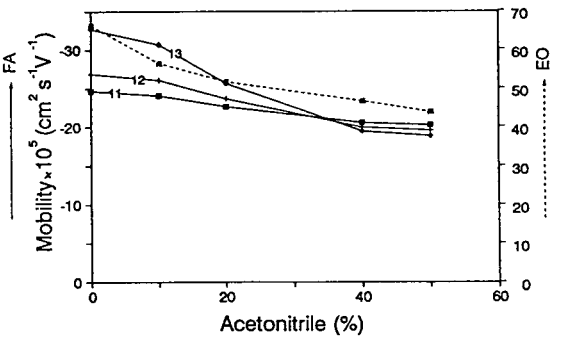

Fig. 1. Effect of the addition of acetonitrile on the electrophoretic mobility of C_{11}–C_{13} fatty acids (FA, solid lines) and electroosmotic flow (EO, dashed line) in a 10 m*M* SDBS micellar solution.

20% acetonitrile the elution order is the same but the baseline stability appeared to be worse. Surprisingly at 40% acetonitrile the elution order reverses and the baseline stability improved considerably as is illustrated in Fig. 2. The improvement of the baseline stability at larger organic solvent concentrations was found earlier by Gorse et al. [12]. In 40% acetonitrile the larger fatty acids dissolve considerably better and under these conditions C_8–C_{17} fatty acids (0.1–0.25 m*M* of each) could be completely separated except the C_{16} and C_{17} acids which coelute. By increasing the acetonitrile content to 50%, a separation of all the C_8–C_{19} fatty acids was obtained. However, the solubility of the largest fatty acids was still not sufficient to detect the solutes adequately. Moreover, sometimes bloc-

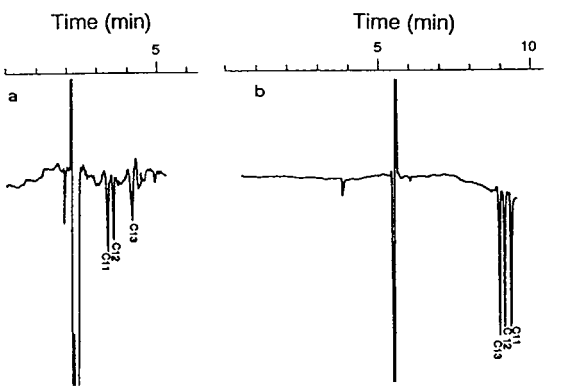

Fig. 2. Background signal obtained with (a) 10 m*M* SDBS and (b) 10 m*M* SDBS + 40% (v/v) acetonitrile.

kage of the capillary occurred arising from precipitates. In order to improve the solubility of the mixture, the acetonitrile content was increased up to 75%. However, this caused a dramatic increase of the background noise.

The effect of the SDBS concentration in 40% acetonitrile on the mobility of the fatty acids is shown in Fig. 3. As can be seen the mobility is hardly influenced by the SDBS concentration.

3.3. Migration behaviour of fatty acids with SDBS–Brij mixtures

The addition of the non-ionic surfactant Brij to an ionic surfactant in MEKC has found to bring about changes in the migration window and selectivity [13]. It is assumed that the changes are the result of the formation of mixed micelles. The effect of the addition of Brij to the SDBS system on the migration of C_{11}–C_{15} fatty acids was studied by varying the Brij concentration in the range 0.5–10 m*M*, keeping the SDBS concentration constant (10 m*M*). The CMC of Brij has been reported to be about 0.1 m*M* and thus at all used concentrations Brij micelles will be formed. The migration behaviour of the fatty acids as function of the Brij concentration is shown in Fig. 4. With 0.5 m*M* Brij C_{11}–C_{13} fatty acids migrate in the order $C_{11} < C_{12} < C_{13}$ but C_{14} and C_{15} could not be detected. With 1 m*M* Brij, C_{14} and C_{15} appeared in the electropherogram but as very small and

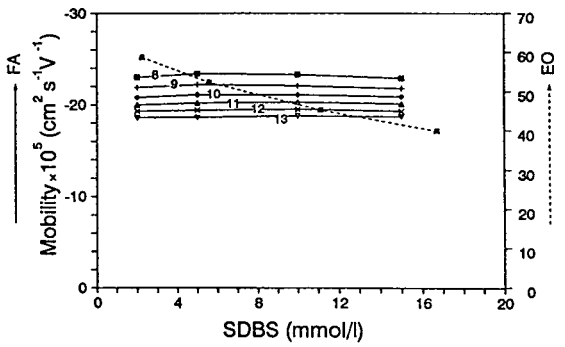

Fig. 3. Effect of the SDBS concentration on the electrophoretic mobility of some fatty acids (FA, solid lines) and electroosmotic flow (EO, dashed line) in the presence of 40% (v/v) acetonitrile.

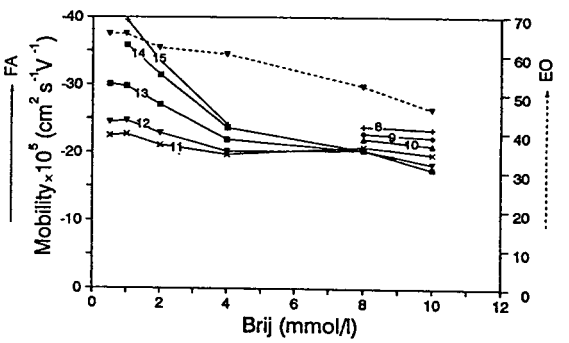

Fig. 4. Effect of the addition of Brij on the electrophoretic mobility of fatty acids (FA, solid lines) and electroosmotic flow (EO, dashed line) in a 10 m*M* SDBS micellar solution.

distorted peaks. When further increasing the Brij concentration to 2–4 m*M*, the electroosmotic flow decreases gradually. The migration time of C_{11} stays almost constant but that of the larger fatty acids decreases and they migrate close together. Surprisingly with 8 m*M* Brij a complete reversal of the elution order of the fatty acids occurs: the C_{12}–C_{15} fatty acids elute close together in front of the smaller ones! With 10 m*M* Brij the C_8–C_{13} fatty acids could be separated as shown in Fig. 5. Increasing the Brij concentration >10 m*M* resulted in more resolution between the solutes but in particular the peaks of the smaller fatty acids become distorted. The solubility of the larger acids increase considerably but no improvement of the resolution between the C_{13}–C_{15} acids occurred. It can be noted that the baseline stability improved

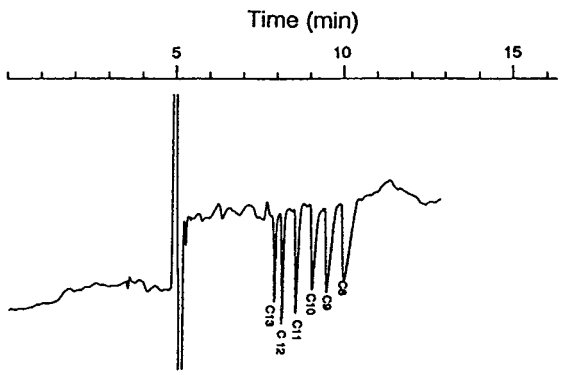

Fig. 5. Electropherogram of fatty acids using 10 m*M* SDBS + 10 m*M* Brij as background electrolyte.

with increasing Brij concentration. Further in all electropherograms a system peak was observed which always migrated at the same position of the C_{15} acid. Injection of sudan resulted in a peak with the same migration time as the system peak.

3.4. Migration behaviour of fatty acids with SDBS–Brij–acetonitrile mixtures

With SDBS–acetonitrile all the fatty acids could be separated but the solubility of the C_{18}–C_{20} acids is too small to detect them well. With SDBS–Brij mixtures the solubility of all acids is good but only the C_8–C_{13} could be separated while the larger fatty acids migrated together. On basis of these findings it was decided to combine the favourable selectivity of acetonitrile with the good solvation ability of Brij. For that purpose the migration of the fatty acids with various mixtures of SDBS–acetonitrile–Brij was investigated. Fig. 6 shows the effect of the Brij concentration on the migration of the fatty acids with 50% acetonitrile and 10 m*M* SDBS. From this figure it can be seen that by addition of 20 m*M* of Brij the speciation of all the fatty acids improves significantly and a complete separation of the C_8–C_{20} fatty acids can be obtained. Increasing the Brij concentration to 30 and 50 m*M* improves the resolution somewhat but at the cost of the separation time due to a gradual decrease of the electroosmotic flow. In particular

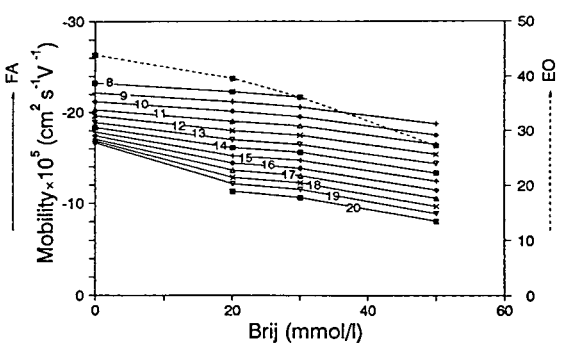

Fig. 6. Effect of the addition of Brij on the electrophoretic mobility of C_8–C_{20} fatty acids (FA, solid lines) and electroosmotic flow (EO, dashed line) using 10 m*M* SDBS + 50% (v/v) acetonitrile.

with 50 m*M* Brij the long migration times causes broader peaks of the C_8 and C_9 fatty acids. A concentration of 30 m*M* of Brij appears to be a good compromise between solubility, migration time, resolution and peak shapes. An electropherogram of all C_8–C_{20} fatty acids under these conditions is shown in Fig. 7.

In order to determine the effect of the acetonitrile content and SDBS concentration with 30 m*M* Brij, some addition experiments were performed. Fig. 8 shows the effect of acetonitrile with 10 m*M* SDBS and 30 m*M* Brij. It shows that acetonitrile affects considerably the electrophoretic mobilities and a complete separation of all fatty acids can only be realized at a high percentage of acetonitrile.

Fig. 9 shows the effect of the SDBS concentration on the migration using 30 m*M* Brij and 50% acetonitrile. As can be seen, the effect on the electrophoretic mobilities is very small. However, from the point of view of detection sensitivity the use of 10 m*M* SDBS appeared to be favourable. Under these conditions the concentration detection limit of the individual fatty acids was determined to be about 10^{-5} *M*.

The applicability of the developed separation system is illustrated in Fig. 10 showing the electropherograms of an extract of a dairy-fresh butter (Fig. 10a) and of a butter rich in unsaturated fatty acids (Becel) (Fig. 10b). Prior to analyses the butter was first saponified under alkaline conditions in ethanol. Then the ethanol was removed by evaporation and the residue dissolved in the buffer electrolyte and injected.

Although no attempts were undertaken to optimize the sample pretreatment of the butter, the electropherograms clearly show the usefulness of the developed CE technique for the determination of the fatty acids content in real samples. A complication occurring with the simple pretreatment is the presence of the unsaturated fatty acids in the extract. These compounds show a quite similar migration behaviour and therefore interfere in the electropherogram (the peaks indicated with asterisks). Attempts are now undertaken to shift the migration of the unsaturated fatty acids selectively towards free spaces in the electropherogram. It can be noted

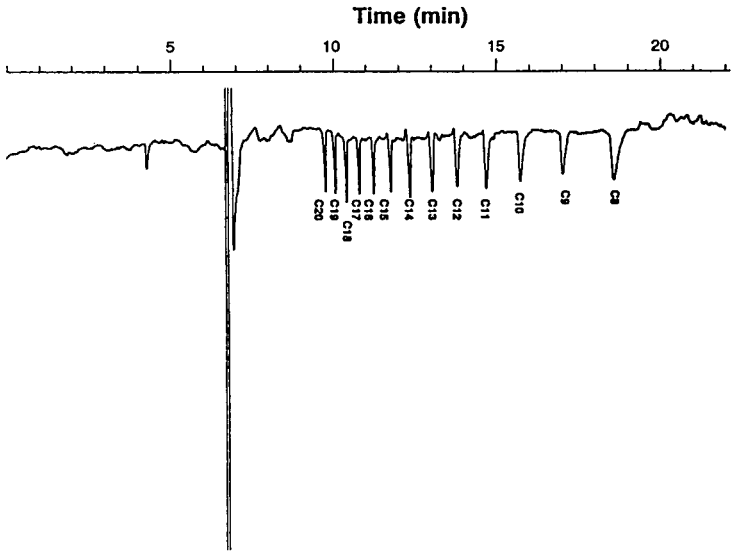

Fig. 7. Electropherogram of the C_8–C_{20} fatty acids using 10 m*M* SDBS + 50% acetonitrile + 30 m*M* Brij as background electrolyte.

that for the unsaturated fatty acids it is not necessary to apply indirect detection since these compounds show native UV absorption.

4. Discussion

The electrophoretic mobility, μ_{FA}, of the C_1–C_{10} acids are known from literature [14]. The μ values appear to decrease gradually from −56.6 for the C_1 acid to −22.1 for the C_{10} acid. The decrease of μ with increasing length of the alkyl chain in the acid have been also found with C_1–C_{12} alkyl sulfonates [14]. It is therefore likely to suppose that the same decrease in μ continues with the C_8–C_{20} fatty acids. This means that in the CZE mode with electroosmotic flow the apparent mobility of the larger fatty acids, μ^*_{FA}, will be larger than the smaller ones, resulting in an expected elution order of $C_{20} < C_{19} \ldots < C_8$.

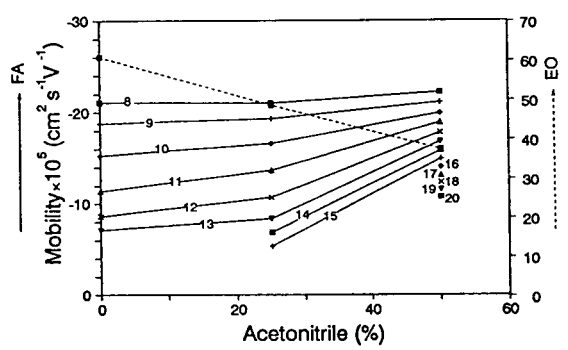

Fig. 8. Effect of the percentage acetonitrile on the electrophoretic mobility of fatty acids (FA, solid lines) and electroosmotic flow (EO, dashed line) using 10 m*M* SDBS + 30 m*M* Brij.

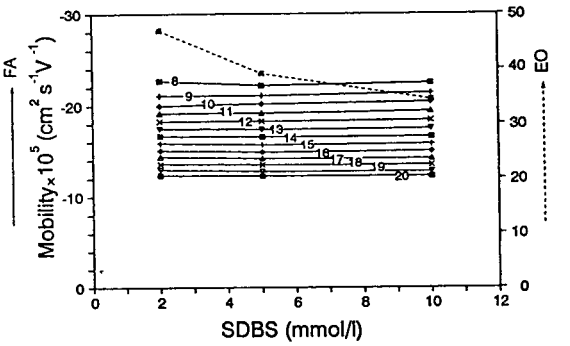

Fig. 9. Effect of the SDBS concentration on the electrophoretic mobility of fatty acids (FA, solid lines) and electroosmotic flow (EO, dashed line) using 50% (v/v) acetonitrile + 30 m*M* Brij as background electrolyte.

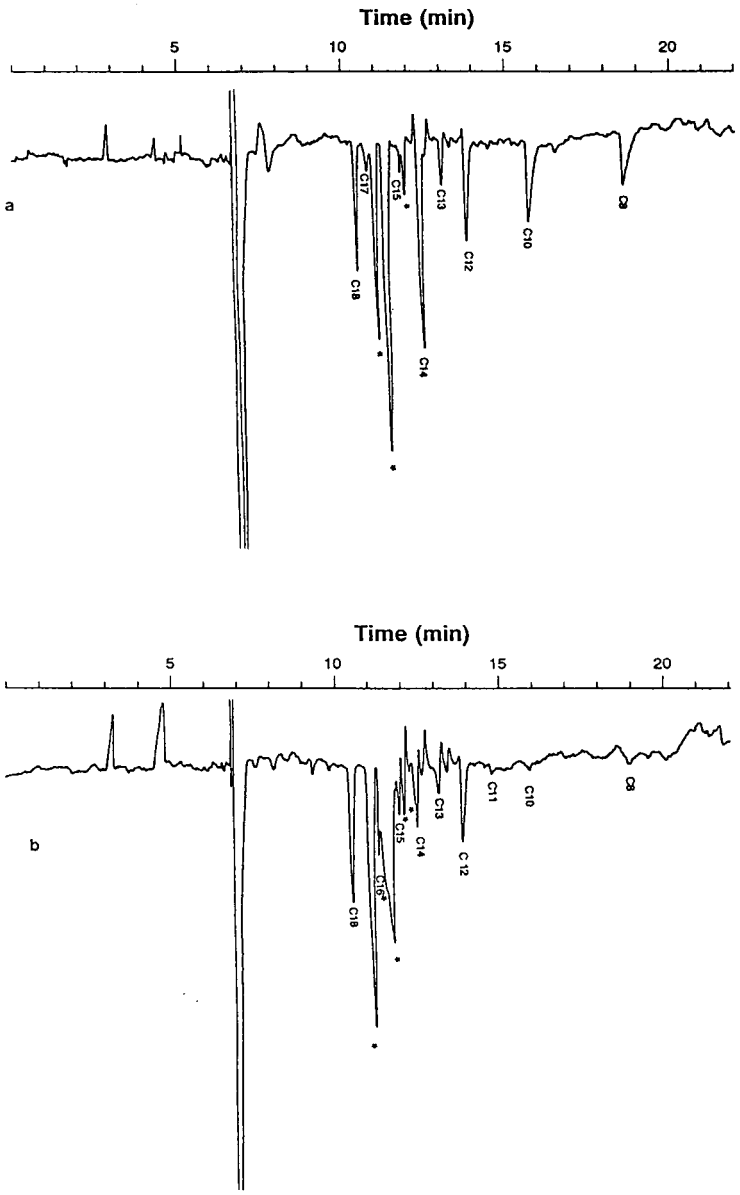

Fig. 10. Electropherograms of (a) an extract of a dairy-fresh butter and (b) a butter rich in unsaturated fatty acids (Becel).

In reality this order can only be verified with smaller fatty acids because the solubility of the larger fatty acids in the applied aqueous solutions in CZE is too small.

4.1. *Effect of SDBS*

When adding the negatively charged surfactant SDBS to the buffer, micelles are formed and migrate with a net velocity which is smaller that of the electroosmotic flow. The fatty acids will be distributed between the micelle and the surrounding electrolyte. Since the interior of the micelle is hydrophobic, the partition of the fatty acids towards the micellar phase will increase with increasing length of the alkyl chain. As a

result the larger fatty acids will spent more time in the micellar phase than the smaller ones and therefore will migrate slower. In other words an elution order of $C_8 < C_9 \ldots C_{20}$ can be expected and this is indeed found in this study as can be seen in Fig. 2a.

4.2. Effect of organic solvent

The effect of addition of organic solvents, like methanol and acetonitrile, to micellar systems has been studied before [12]. These studies showed that the addition of organic solvent (up to 20%) changes the partition of solutes (e.g. the capacity factors) between the micelles and surrounding liquid. It was suggested that the changes can partly be attributed to a reduction of the size of the micelles and of the surface charge density at the micelle-surrounding liquid interface with increasing solvent content. The addition of an organic solvent usually reduces the electroosmotic flow and thereby extends the separation window. The change was found to be significantly larger with methanol than with acetonitrile. In our study the behaviour of acetonitrile on the migration agrees, up to 20% of acetonitrile, with the findings as mentioned in Ref. [12]. The elution order of $C_8 < C_9 \ldots < C_{20}$ indicates that still micelles are present (see Fig. 1). However, at larger percentages of acetonitrile the elution order reverses completely into $C_{20} < C_{19} \ldots < C_8$, the expected order under CZE conditions. This indicates that either the micelles are largely disintegrated or the fatty acids migrate after the micelles (e.g. migrate close to t_0). Whether still micelles are present at larger acetonitrile content could not yet be answered by us because the neutral solute sudan, usually used to measure migration time of the micelle (t_{mc}), did not give any detector response.

4.3. Effect of Brij

The addition of a neutral surfactant like Brij to the solution with the charged SDBS micelles results in the formation of mixed micelles. The charge density of the mixed micelles will be smaller than without Brij. As a consequence of this, the electrophoretic mobility of the mixed micelle decreases which results in a decrease of the t_{mc} (e.g. the separation window becomes smaller) [13]. Ultimately at very large Brij concentrations, the electrophoretic mobility of the mixed micelle will approach that of the electroosmotic mobility (t_0). The migration behaviour of the fatty acids using Brij is in agreement with these expectations as can be seen in Fig. 4. At small Brij concentration the electrophoretic mobility of the mixed micelle is larger than that of the fatty acids and the elution order is $C_8 < C_9 \ldots < C_{15}$. At large Brij concentration the electrophoretic mobility of the mixed micelle is smaller than that of the fatty acids and an elution order of $C_{15} < C_{14} \ldots < C_8$ is found, the expected CZE order. This indicates that at larger Brij concentrations most probably the SDBS micelles are largely or completely disintegrated as found with larger acetonitrile contents. Although the occurrence of mixed micelles is likely, a definite answer can only given when the t_{mc} under the various conditions can be determined. In that respect it can be noted, that in all recorded electropherograms with SDBS–Brij systems, always a system peak appears just after the C_{15} peak. The migration time of sudan could be determined with larger Brij concentrations and its time coincides with that of the system peak. Therefore the system peak might be a marker for the mixed micelle migration time.

4.4. Effect of Brij + acetonitrile

The observed reversal of the migration order of the fatty acids when adding acetonitrile or Brij to SDBS cannot easily interpreted by the simple MEKC separation mechanism. It becomes even more complicated when both additives are used together. With both additives it seems that the SDBS micelle is largely disintegrated and that the SDBS molecules only act as a chromophore for the indirect detection. This finding is supported by the fact that with larger acetonitrile and Brij concentrations, the SDBS concentration has a minor effect on the migration behaviour of the fatty acids. From some preliminary experiments on the application of the developed sepa-

ration system to unsaturated fatty acids, which can also be detected directly with UV, it was found that the migration behaviour of the unsaturated fatty acids is not altered in the absence of SDBS.

5. Conclusions

MEKC combined with indirect UV detection using SDBS as chromophore can be used for the analysis of fatty acids. To create sufficient solubility and selectivity, the addition of 40–50% acetonitrile and 30 m*M* Brij to the background electrolyte is necessary. The system is in principle suited for the analysis of the unsaturated fatty acids using direct UV detection.

Whether the developed system for the separation of the fatty acids can be considered as a true MEKC system cannot yet be established.

References

[1] A. Thomas, *Ullmanns Encyclopedia of Industrial Chemistry*, Vol. A10, VCH, Weinheim, 1987, p. 173.
[2] E.H. Pryde (Editor), *Fatty Acids*, American Oil Chemists Society, Champaign, IL, 1979.
[3] M. Höckel, W. Dünges, A. Holzer, P. Brockerhoff and G.H. Rathgen, *J. Chromatogr.*, 221 (1980) 205.
[4] B. Schatowitz and G. Gercken, *J. Chromatogr.*, 425 (1988) 257.
[5] T. Hanis, M. Smrz, P. Klir, K. Macek, J. Klima, J. Base and Z. Deyl, *J. Chromatogr.*, 452 (1988) 443.
[6] J.W. Jörgenson and K.D. Lukacs, *Anal. Chem.*, 53 (1981) 1298.
[7] S. Terabe, K. Otsuka and T. Ando, *Anal. Chem.*, 57 (1985) 834.
[8] M.G. Khaledi, S.C. Smith and J.K. Strasters, *Anal. Chem.*, 63 (1991) 1820.
[9] J. Vindevogel and P. Sandra (Editors), *Introduction to Micellar Electrokinetic Chromatography*, Hüthig, Heidelberg, 1992.
[10] E.S. Yeung and W.G. Kuhr, *Anal. Chem.*, 63 (1991) 275A.
[11] N.M. van Os, J.R. Haak and L.A.M. Rupert, *Physico-Chemical Properties of Selected Anionic, Cationic and Nonionic Surfactants*, Elsevier, Amsterdam, 1993.
[12] J. Gorse, A.T. Balchunas, D.F. Swaileand and M.J. Sepeniak, *J. High Resolut. Chromatogr. Chromatogr. Commun.*, 11 (1988) 555.
[13] H.T. Rasmussen, A.T. Goebel and H.M. McNair, *J. High Resolut. Chromatogr.*, 14 (1991) 25.
[14] T. Hirokawa, M. Nishino, N. Aoki, Y. Kiso, Y. Sawamoto, T. Yagi and J.I. Akiyama, *J. Chromatogr.*, 271 (1983) D1–D106.

ELSEVIER

Journal of Chromatography A, 694 (1995) 480–485

JOURNAL OF CHROMATOGRAPHY A

Short communication

Stoichiometric mass-action ion-exchange model Explicit isotherms for mono-, di-, tri- and tetrameric ions

Costas S. Patrickios*, Evelthon S. Patrickios

27 Homer Street, Ayios Nicolaos, Limassol 252, Cyprus

First received 22 July 1994; revised manuscript received 11 October 1994; accepted 11 October 1994

Abstract

Analytical isotherms for the unhindered stoichiometric mass-action ion exchange of monomeric, dimeric, trimeric and tetrameric ions are derived. The linear increase in oligomer charge from 1 to 4 leads to an exponential increase in the affinity for the stationary phase which, in turn, results in a rapid change in the isotherm shape from hyperbolic to square. The utility of the developed explicit equations is not restricted by the limits imposed by the assumption for absence of steric hindrances because these analytical isotherms can facilitate the use of detailed numerical chromatographic models.

1. Introduction

The work of Brooks and Cramer [1,2] has recently led to the refinement of the stoichiometric mass-action model for polyelectrolyte ion exchange, originally proposed by Boardman and Partridge [3] and subsequently expanded by Regnier and co-workers [4,5] and Velayudhan and Horváth [6]. Two of Brooks and Cramer's contributions to the above theory are most important: first, the introduction of the steric factor defined as the number of column sites per adsorbed polyelectrolyte molecule which are inaccessible to the adsorbate due to steric hindrances; second, the formulation of the non-Langmuirian mass-action isotherm based on the requirement for electroneutrality on the stationary phase at all times. The concepts of the steric factor and the mass-action isotherm have been verified experimentally [7,8].

The developed mass-action isotherms are implicit in terms of the concentration of bound polyelectrolyte [1]. The purpose of this paper is to present the derivation of explicit forms of these isotherms in certain cases, namely, for the ion exchange of monomeric, dimeric, trimeric and tetrameric ions, in the absence of steric effects. The small size of the adsorbates dealt with in this study justifies the neglect of steric hindrances arising from adsorbate bulkiness as well as from inter-adsorbate electrostatic surface repulsion. Moreover, other steric effects can be avoided by using isotactic adsorbates (bearing charged side-groups with common orientation), and by choosing the appropriate stationary phase such that the charge spacing on the matrix is identical to that of the adsorbate. Isotactic oligo(methacrylic acid)s with degrees of poly-

* Corresponding author. Present address: School of Chemistry and Molecular Sciences, University of Sussex, Falmer, Brighton, E. Sussex BN1 9QJ, UK.

0021-9673/95/$09.50
SSDI 0021-9673(94)00975-9

merization ranging from 2 to 10 adsorbing on a methacrylate-based stationary phase will experience minimal steric hindrances and shall provide a good model system to test our theory. Despite the restrictions imposed by our assumption for absence of steric effects, the explicit isotherms presented below can facilitate the use of detailed numerical chromatographic models by providing time-saving initial values.

2. Theory

Although the analysis that follows deals with anion exchange, a very similar treatment can be performed for cation exchange.

Polyanion $P^{\nu-}$ comprises ν identical groups each bearing a single negative charge. All ν of the charges of the polyanion are assumed to be free of steric hindrances and be able to interact directly with the stationary phase; ν is called the characteristic charge of the polyanion. The exchange of $P^{\nu-}$ with the column counterion C^- can be described by the reaction:

$$\nu R^+C^- + P^{\nu-} \rightleftharpoons (R^+)_\nu P^{\nu-} + \nu C^- \quad (1)$$

where R^+ is the functional cationic group of the stationary phase and R^+C^- and $(R^+)_\nu P^{\nu-}$ represent the bound counterion and bound polyelectrolyte, respectively. In the following, $(R^+)_\nu P^{\nu-}$ will be written as $R_\nu^{\nu+}P^{\nu-}$. The mass-action equilibrium constant for the anion-exchange reaction, K, is then:

$$K = \beta[R_\nu^{\nu+}P^{\nu-}][C^-]^\nu/(\beta^\nu[R^+C^-]^\nu[P^{\nu-}]) \quad (2)$$

where β is the phase ratio (the ratio of the volumes of the stationary phase to the mobile phase), and where the brackets indicate molar concentrations; concentrations are used instead of activities under the assumption of ideal behavior both in the mobile phase and the stationary phase.

The free energy of ion exchange, ΔG, is:

$$\Delta G = -RT \ln K \quad (3)$$

Since all ν of the negatively charged groups of the polyelectrolyte are identical, Martin's additive theory (see [9]) suggests that the total free energy of ion exchange is equal to the product of the number of charged groups, ν, with the free energy of ion exchange of a single charged group, Δg:

$$\Delta G = \nu \Delta g \quad (4)$$

which implies that the ion-exchange constant of polyanion $P^{\nu-}$ is equal to the ion-exchange constant of the corresponding monomer, κ, raised to the polyanion characteristic charge, ν:

$$K = \kappa^\nu \quad (5)$$

Eq. 5 suggests that the adsorbate affinity for the stationary phase, as expressed by the ion-exchange constant K, increases exponentially with oligomer size.

Electroneutrality on the stationary phase requires that every functional group R^+ be bound by $P^{\nu-}$ or C^-, resulting in the stoichiometric condition:

$$\Lambda = [R^+C^-] + \nu[R_\nu^{\nu+}P^{\nu-}] \quad (6)$$

where Λ is the binding capacity of the column in monovalent anions, expressed in mol per volume of stationary phase.

Using Eq. 2, the concentration of bound polyanion $P^{\nu-}$, $[R_\nu^{\nu+}P^{\nu-}]$, can be expressed as:

$$[R_\nu^{\nu+}P^{\nu-}] = K\beta^{\nu-1}[R^+C^-]^\nu[P^{\nu-}]/[C^-]^\nu \quad (7)$$

Using Eq. 6, the concentration of bound counteranion C^-, $[R^+C^-]$, can be expressed as:

$$[R^+C^-] = \Lambda - \nu[R_\nu^{\nu+}P^{\nu-}] \quad (8)$$

Eq. 8 implies that at complete saturation of the column by $P^{\nu-}$ (which requires that $[R^+C^-] = 0$ and this is practically accomplished when $[P^{\nu-}]$ is very high) the limiting concentration of bound polyelectrolyte, $[R_\nu^{\nu+}P^{\nu-}]$, is:

$$[R_\nu^{\nu+}P^{\nu-}] = \Lambda/\nu \text{ for high } [P^{\nu-}] \quad (9)$$

Using Eq. 8 to eliminate $[R^+C^-]$ in Eq. 7, and substituting K from Eq. 5 leads to an expression which is implicit in $[R_\nu^{\nu+}P^{\nu-}]$:

$$[R_\nu^{\nu+}P^{\nu-}] = \kappa^\nu\beta^{\nu-1}(\Lambda - \nu[R_\nu^{\nu+}P^{\nu-}])^\nu[P^{\nu-}]/[C^-]^\nu \quad (10)$$

This is the stoichiometric mass-action anion-exchange isotherm for $R_\nu^{\nu+}P^{\nu-}$. This equation can be explicitly solved only for two types of limiting cases: for oligomeric anion-exchange, i.e. for $\nu = 1$, 2, 3 and 4, which is the subject of this work, and for the anion exchange of analytical amounts of anions, i.e. for $\nu[R_\nu^{\nu+}P^{\nu-}] << \Lambda$, which leads to [1]:

$$[R_\nu^{\nu+}P^{\nu-}] = \kappa^\nu \beta^{\nu-1}[P^{\nu-}]\Lambda^\nu/[C^-]^\nu \quad \text{for } \nu[R_\nu^{\nu+}P^{\nu-}] << \Lambda \tag{11}$$

We continue by solving Eq. 10 for monomeric ($\nu = 1$), dimeric ($\nu = 2$), trimeric ($\nu = 3$) and tetrameric ($\nu = 4$) anions. In the following, to illustrate better the composition of the oligomers by identical units, we represent them as A^-, $(A^-)_2$, $(A^-)_3$ and $(A^-)_4$ rather than P^-, P^{2-}, P^{3-} and P^{4-}.

In the case of the adsorption of monomeric anion A^- by exchange for C^-, ν is set equal to 1 in Eq. 10 and solving for $[R^+A^-]$ results in the isotherm:

$$[R^+A^-] = \frac{\Lambda}{1 + \frac{[C^-]}{\kappa[A^-]}} \tag{12}$$

It can be easily verified that in the cases of high and low concentrations of adsorbate A^-, Eq. 12 correctly yields the limiting expressions of Eqs. 9 and 11, respectively.

Adsorption isotherm 12 can be re-written in terms of the fractional saturation of the column by A^-, $\theta = [^+A^-]/\Lambda$:

$$\theta = \frac{1}{1 + \frac{[C^-]}{\kappa[A^-]}} \tag{13}$$

It should be reminded that this anion-exchange isotherm is derived for a system with two components, A^- and C^-, whose adsorption is dictated by the requirement for complete saturation of the stationary phase at all times [2]. It is interesting to note that in Langmuir adsorption, there is no requirement for complete saturation of the adsorbent [2]. It is worth comparing ion-exchange isotherm 13 with the one- and two-component Langmuir isotherms [10], in Eqs. 14 and 15, respectively:

$$\theta = \frac{1}{1 + \frac{1}{K_A[A]}} \tag{14}$$

$$\theta_A = \frac{1}{1 + \frac{1 + K_C[C]}{K_A[A]}} \tag{15}$$

where the negative valence superscripts have been dropped, and K_A and K_C represent the equilibrium binding constants for components A and C, respectively. It can be seen that Eq. 13 is intermediate to Eqs. 14 and 15, which can be understood considering the fact that the number of components in ion exchange is something between one and two: there are two adsorbing components and their adsorption is connected by the requirement that they completely saturate the stationary phase. In other words, the fact that Eq. 13 is equally similar to Eqs. 14 and 15 suggests that the mass-action theory does not ignore the presence of the second adsorbing component: the salt counterion.

In the case of the ion-exchange of dimeric anion A_2^{2-}, ν is set equal to 2 in Eq. 10 and rearranging terms results in the quadratic:

$$[R_2^{2+}A_2^{2-}]^2 - \left(\Lambda + \frac{[C^-]^2}{2^2\kappa^2[A_2^{2-}]\beta}\right) \cdot [R_2^{2+}A_2^{2-}] + \frac{\Lambda^2}{2^2} = 0 \tag{16}$$

which can be easily solved for $[R_2^{2+}A_2^{2-}]$ to give:

$$[R_2^{2+}A_2^{2-}] = \frac{\Lambda}{2} + \frac{[C^-]^2}{2^3\kappa^2[A_2^{2-}]\beta} \cdot \left(1 \pm \sqrt{1 + 2^3 \cdot \frac{\kappa^2[A_2^{2-}]\beta\Lambda}{[C^-]^2}}\right) \tag{17}$$

It is necessary now to determine which of the two solutions presented in Eq. 17 is acceptable. This will be done by using Eq. 17 to obtain the expressions for $[R_2^{2+}A_2^{2-}]$ at the high and low concentration limits and comparing the results with the predictions of Eqs. 9 and 11, respectively. At the limit of high concentration of A_2^{2-},

Eq. 17 yields the correct saturation capacity of $\Lambda/2$, as predicted by Eq. 9, for both the positive and the negative values of the square root term. At the low concentration limit of A_2^{2-}, however, calculated by expanding the square root and keeping the first three terms of the resulting polynomial, only the solution with the negative sign in front of the square root yields the expression predicted by Eq. 11. The accepted solution is therefore:

$$[R_2^{2+}A_2^{2-}] = \frac{\Lambda}{2} + \frac{[C^-]^2}{2^3\kappa^2[A_2^{2-}]\beta} \cdot \left(1 - \sqrt{1 + 2^3 \cdot \frac{\kappa^2[A_2^{2-}]\beta\Lambda}{[C^-]^2}}\right) \quad (18)$$

In the case of the ion-exchange of trimeric anion A_3^{3-}, ν is set equal to 3 in Eq. 10 and rearranging terms results in the equation:

$$[R_3^{3+}A_3^{3-}]^3 - \Lambda[R_3^{3+}A_3^{3-}]^2 + \left(\frac{\Lambda^2}{3} + \frac{[C^-]^3}{3^3\kappa^3[A_3^{3-}]\beta^2}\right) \cdot [R_3^{3+}A_3^{3-}] - \frac{\Lambda^3}{3^3} = 0 \quad (19)$$

Because the coefficients of the $[R_3^{3+}A_3^{3-}]$ terms in Eq. 19 are real and because the discriminant of Eq. 19 is positive, there is only one real root [11]. Using the formulas given by Spiegel [11] and performing the appropriate simplifications, the solution to Eq. 19 is:

$$[R_3^{3+}A_3^{3-}] = \frac{\Lambda}{3} - \frac{[C^-]}{3} \cdot \sqrt[3]{\frac{\Lambda}{6\kappa^3[A_3^{3-}]\beta^2}} \cdot \left(\sqrt[3]{1 + \sqrt{1 + \frac{2^2}{3^4} \cdot \frac{[C^-]^3}{\kappa^3[A_3^{3-}]\beta^2\Lambda^2}}} + \sqrt[3]{1 - \sqrt{1 + \frac{2^2}{3^4} \cdot \frac{[C^-]^3}{\kappa^3[A_3^{3-}]\beta^2\Lambda^2}}}\right) \quad (20)$$

It can be observed that in the case of high concentration of adsorbate A_3^{3-}, Eq. 20 correctly yields the saturation capacity of $\Lambda/3$, as predicted by Eq. 9. It can also be shown that at the low concentration limit of A_3^{3-}, calculated by successively expanding the square and cube roots, Eq. 20 behaves as predicted by Eq. 11.

For the ion exchange of tetrameric anion A_4^{4-}, ν is set equal to 4 in Eq. 10 and rearranging terms results in the equation:

$$[R_4^{4+}A_4^{4-}]^4 - \Lambda[R_4^{4+}A_4^{4-}]^3 + \frac{3\Lambda^2}{2^3} \cdot [R_4^{4+}A_4^{4-}]^2 - \left(\frac{\Lambda^3}{4^2} + \frac{[C^-]^4}{4^4\kappa^4[A_4^{4-}]\beta^3}\right) \cdot [R_4^{4+}A_4^{4-}] + \frac{\Lambda^4}{4^4} = 0 \quad (21)$$

which can be solved using the formulas given by Spiegel [11] to yield four roots for the concentration of bound tetramer, $[R_4^{4+}A_4^{4-}]$:

$$[R_4^{4+}A_4^{4-}] = \frac{\Lambda}{4} + \frac{\sqrt{\Xi}}{2} \cdot \left(1 \pm \sqrt{-1 \mp \frac{\Lambda}{\sqrt{\Xi}} + 2\sqrt{1 + \frac{\Lambda^2}{4\Xi}}}\right) \quad (22)$$

where Ξ is given by:

$$\Xi = \sqrt[3]{\frac{[C^-]^8}{2 \cdot 4^8\kappa^8[A_4^{4-}]^2\beta^6}} \cdot \left(\sqrt[3]{1 + \sqrt{1 + \frac{4^5}{3^3} \cdot \frac{\kappa^4[A_4^{4-}]\beta^3\Lambda^3}{[C^-]^4}}} + \sqrt[3]{1 - \sqrt{1 + \frac{4^5}{3^3} \cdot \frac{\kappa^4[A_4^{4-}]\beta^3\Lambda^3}{[C^-]^4}}}\right) \quad (23)$$

The only solution in Eq. 22 that behaves correctly at low adsorbate concentrations is the one with the negative big square root term and the positive $\Lambda/\Xi^{1/2}$ term leading to the acceptable form of the isotherm:

$$[R_4^{4+}A_4^{4-}] = \frac{\Lambda}{4} + \frac{\sqrt{\Xi}}{2} \cdot \left(1 - \sqrt{-1 + \frac{\Lambda}{\sqrt{\Xi}} + 2\sqrt{1 + \frac{\Lambda^2}{4\Xi}}}\right) \quad (24)$$

The developed stoichiometric mass-action isotherms shown in Eqs. 12, 18, 20 and 24 are plotted in Fig. 1 where both the mobile and stationary phase concentrations of the adsorbate are expressed in terms of concentration of monomer segments (equivalents). The concentration

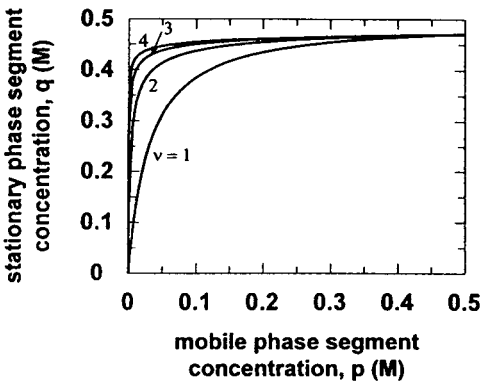

Fig. 1. Stoichiometric mass-action ion-exchange isotherms of monomeric, dimeric, trimeric and tetrameric ions on a stationary phase with a ligand density of 0.50 *M* and a phase ratio of 1, and a mobile phase uni-univalent salt concentration of 0.25 *M*. The equilibrium ion-exchange constant of the monomer is taken to be 8.341. The concentrations of the adsorbates in both the mobile and stationary phases are expressed in equivalents.

of monomer segments in the mobile phase, p, is calculated from:

$$p = 1[A^-] = 2[A_2^{2-}] = 3[A_3^{3-}] = 4[A_4^{4-}] = \nu[A_\nu^{\nu-}] \quad (25)$$

while the concentration of monomer segments on the stationary phase, q, is given by:

$$q = 1[R^+A^-] = 2[R_2^{2+}A_2^{2-}] = 3[R_3^{3+}A_3^{3-}] = 4[R_4^{4+}A_3^{3-}] = \nu[R_\nu^{\nu+}A_\nu^{\nu-}] \quad (26)$$

This transformation is useful because, as implied by Eqs. 9 and 26, it results in a saturation concentration of monomer segments on the stationary phase of Λ, which is independent of polyanion characteristic charge [9]. The values of the parameters utilized in the figure were $[C^-] = [Cl^-] = 0.25$ *M*, $\Lambda = 0.50$ *M*, $\kappa = 8.341$ and $\beta = 1$. The column capacity, Λ, of 500 m*M* was typical of a Waters Protein-Pak Q-8HR strong anion-exchange column [7]. The monomer anion-exchange constant was calculated as the 31st root of the anion-exchange constant of a dextran sulphate fraction with a characteristic charge of 31 [7], according to Eq. 5. The figure clearly shows that by increasing the number of negatively charged residues on the oligomers from 1 to 4, the isotherm shape rapidly changes from hyperbolic to square. This is a direct result of the exponential increase in the adsorbate affinity for the stationary phase with oligomer size as well as of the constant saturation capacity in terms of monomer segments.

3. Conclusions

Analytical expressions for the ion-exchange isotherms of monomeric, dimeric, trimeric and tetrameric ions, based on the stoichiometric mass-action model of Brooks and Cramer [1] in the absence of steric effects, were developed and presented. Owing to the exponential increase in oligomer affinity for the adsorbent with adsorbate size, the derived isotherms steepen abruptly by increasing the number of charged units from 1 to 4. The utility of the developed analytical isotherms extends beyond the limits set by the assumption for absence of steric hindrances because these explicit equations can provide time-saving initial values to detailed numerical chromatographic models.

Future work will focus on the experimental verification of Martin's additive theory for ion exchange by determining the anion-exchange free energies of a series of monodisperse oligo(methacrylic acid)s [12,13]. Drager and Regnier's [14] data on oligonucleotide anion exchange indicate that by increasing the number of groups per molecule from 5 to 14, the free energy of ion exchange per group gradually decreases, suggesting an increase in group affinity with oligomer size.

References

[1] C.A. Brooks and S.M. Cramer, *AIChE J.*, 38 (1992) 1969.
[2] C.A. Brooks, III, *Ph.D. Thesis*, Rensselaer Polytechnic Institute, Troy, NY, 1993, pp. 26–33.
[3] N.K. Boardman and S.M. Partridge, *Biochem. J.*, 59 (1955) 543.
[4] W. Kopaciewicz, M.A. Rounds, J. Fausnaugh and F.E. Regnier, *J. Chromatogr.*, 266 (1983) 3.

[5] M.A. Rounds and F.E. Regnier, *J. Chromatogr.*, 283 (1984) 37.
[6] A. Velayudhan and Cs. Horváth, *J. Chromatogr.*, 367 (1986) 160.
[7] S.D. Gadam, G. Jayaraman and S.M. Cramer, *J. Chromatogr.*, 630 (1993) 37.
[8] G. Jayaraman, S.D. Gadam and S.M. Cramer, *J. Chromatogr.*, 630 (1993) 53.
[9] S.C.D. Jen and N.G. Pinto, *Reactive Polym.*, 19 (1993) 145.
[10] G.W. Castellan, *Physical Chemistry*, Benjamin/Cummings, Menlo Park, CA, 3rd ed., 1983, pp. 426–427.
[11] M.R. Spiegel, *Mathematical Handbook of Formulas and Tables*, McGraw-Hill, New York, 1990, pp. 32–33.
[12] J. Mykytiuk, S.P. Armes and N.C. Billingham, *Polym. Bull.*, 29 (1992) 139.
[13] S.P. Rannard, N.C. Billingham, S.P. Armes and J. Mykytiuk, *Eur. Polym. J.*, 29 (1993) 407.
[14] R.R. Drager and F.E. Regnier, *J. Chromatogr.*, 359 (1986) 147.

ELSEVIER

Journal of Chromatography A, 694 (1995) 486–491

JOURNAL OF CHROMATOGRAPHY A

Short communication

Lead phosphate hydroxyapatite high-performance liquid chromatography

A. Benmoussa[a], M. Mikou[a], J.L. Lacout[b,*], A.M. Siouffi[c]

[a]*Laboratoire de Chimie Minérale Appliquée, Faculté des Sciences de Fès-Atlas, B.P. 1796, Fès, Maroc*

[b]*Laboratoire des Matériaux Physico-Chimie des Solides INP-ENSCT, URA CNRS 445, 38 Rue des 36 Ponts, 31400 Toulouse, France*

[c]*Laboratoire de Chimie Analytique Appliquée, Université Aix–Marseille, 3 Avenue Escadrille Normandie Niémen, 13397 Marseille Cedex 20, France*

First received 20 July 1994; revised manuscript received 2 December 1994; accepted 5 December 1994

Abstract

Spherical aggregates of lead phosphate hydroxyapatite (PbHA) have been developed as an adsorbent in high-performance liquid chromatography. There are effectively two types of crystal surface, a (or b) and c which appear on the crystal, analogous to the case of calcium phosphate hydroxyapatite. Basic proteins adsorb to the c surface, and can be eluted by chloride or phosphate salts. Acidic proteins adsorb to the a (or b) surface, and are eluted only by phosphate. All proteins were adsorbed at pH 6 and eluted at pH 8–10. The binding capacity of PbHA for bovine serum albumin was determined by frontal analysis; the shape of the adsorption isotherm is of the Langmuir type.

1. Introduction

The calcium phosphate hydroxyapatite (CaHA), crystal chemical composition $Ca_{10}(PO4)_6(OH)_2$, belongs to the space group $P6_{3/m}$; the crystal unit cell is characterized by the primitive vectors $\vec{a}$, $\vec{b}$ and $\vec{c}$ with $\vec{b}\Lambda\vec{b} = 120°$, $\vec{b}\Lambda\vec{c} = 90°$, $a = b = 9.420$ Å and $c = 6.882$ Å [1]. Column chromatography using CaHA as adsorbent was originally introduced by Tiselius et al. [2] for the separation and purification of biomolecules. It is stable over a wide pH range (5.5–10.0), heat-resistant, and allows for a high recovery of biomolecules with unaltered physico-chemical properties. A method has also been successfully utilized to separate nucleic acids such as native and denatured DNA, linear and circular DNA and RNA [3]. Studies on the structure, mode of action and applicability of CaHA by Bernardi and Giro [3–5] and others [6–9] have made this adsorbent especially popular. High-performance liquid chromatography (HPLC) using spherical aggregates (particle size 5–10 μm) of CaHA [10,11] and strontium phosphate hydroxyapatite (SrHA) micro-crystals [12] was recently developed.

CaHA is a particular type of a group of crystals, called apatite, that have a general chemical composition represented as $M_{10}(XO_4)_6Y_2$. The M (metal) and the XO_4 sites of the structure can, in general, be filled respec-

* Corresponding author.

0021-9673/95/$09.50
SSDI 0021-9673(94)01204-0

tively with mono- to trivalent cations and di- to tetravalent groups, and the Y site can be filled with substances with mono- to trivalent anions; the Y site and M can often be vacant [13]. Thus, the M site can be occupied by Ca, Pb, Cd, Sr, Ni, Na or vacancy; the XO_4 site by PO_4, ASO_4, VO_4, CrO_4, SiO_4, CO_3; and the Y site by OH, F, Cl, Br, I, O, N, CO_3, . . . or vacancy [13].

Lead phosphate hydroxyapatite (PbHA) is obtained by substituting Pb^{2+} for Ca^{2+}, thus yielding $Pb_{10}(PO_4)_6(OH)_2$ with a = b = 9.920 Å and c = 7.480 Å; in the PbHA structure, the M site is occupied by lead ions with a radius of 1.19 Å [14] as compared with the CaHA structure in which the M site is occupied by calcium ions with a smaller radius, 1.00 Å [14].

We have developed spherical aggregates (5–10 μm diameter) of microcrystalline PbHA to be packed into HPLC columns. This paper reports their preparation and their physico-chemical properties. Performances of HPLC columns packed with this material were evaluated with protein standards.

2. Materials and methods

PbHA micro-crystals (average particle size 0.1 μm) as starting materials were prepared by slowly dropping ammonium phosphate solution (0.186 *M*, 3 l) into a boiling lead nitrate solution (0.31 *M*, 3 l) in basic media for 3 h at 100°C; the precipitate was matured for 30 min. A small amount of the solution was picked up and characterized. After dilution at a convenient viscosity with deionised water, the moist precipitate was sprayed in a centrifugal spray-dry apparatus model (RAMM) with a flow-rate of 1.2–1.4 l/h at 200°C. The resulting sprayed drops were dried at 95°C into spherical aggregates with diameters of 2–30 μm. The 5–10 μm fraction (Fig. 1) was isolated by an elutriation method.

On the basis of both the X-ray diffraction analysis (Fig. 2) and elemental analysis, it was confirmed that the PbHA aggregates are pure apatite (a = b = 9.920 Å and c = 7.480 Å) with a chemical composition represented as $Pb_{10}(PO_4)_6(OH)_2$ and a Pb/P molar ratio equal to one of a stoichiometric apatite, 1.67. The total surface area (15 m^2/g) was determined by the Brunauer–Emmet–Teller (BET) method with a mixture of nitrogen–helium (30:70) on a Quantasorb II apparatus (Quantachrome).

The proteins used in the present work were albumin (from bovine serum), lysozyme (from chicken egg) and cytochrome *c* (from horse heart) purchased from Sigma (Saint-Quentin, France).

The spherical PbHA aggregates (5–10 μm) were packed in a stainless-steel column (75 mm × 4.6 mm I.D.) using the slurry packing procedure. PbHA microparticles (2 g) were dispersed in CCl4 (20 ml) and then sonicated for 5 min. The resulting slurry was packed with a Haskel Model MCP-110 pump using ethanol as

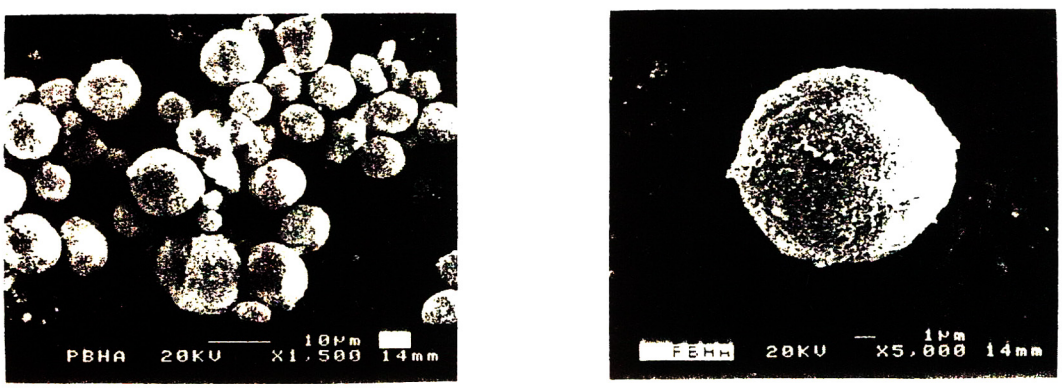

Fig. 1. Scanning electron micrograph of spherical PbHA with an average diameter of ca. 7 μm.

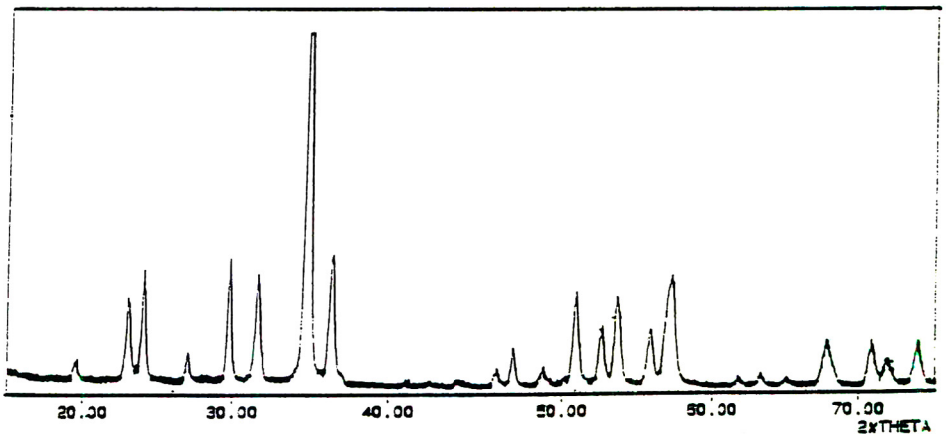

Fig. 2. X-Ray diffraction patterns of PbHA.

pressurizing agent under pressure (100 bar). All chromatographic measurements were carried out at room temperature with a system consisting of a Model 112 (Beckman) HPLC pump equipped with a Model 165 variable-wavelength UV detector (Beckman). Samples were eluted using a molarity gradient of potassium phosphate buffer at pH 6.8 (i.e., an equimolar mixture of K_2HPO_4 and KH_2PO_4); buffer A was 5 m*M* while buffer B was 600 m*M*; alternatively, a molarity gradient was used of 5–600 m*M* KCl in buffer A. The elution was monitored by measuring the UV absorption at 230 nm.

The binding capacities of PbHA and CaHA for bovine serum albumin (BSA) were measured by frontal analysis, as follows: various amounts of BSA, dissolved in buffer A, were pumped through the column as a mobile phase, at a flow-rate of 1 ml/min and at 25°C. Since the 5 m*M* phosphate concentration does not suffice to elute adsorbed BSA, the appearance of protein in the eluate permits the determination of the capacity of the column at saturation.

3. Results and discussion

Fig. 3 is a typical chromatogram of a standard mixture of BSA, lysozyme and cytochrome *c* obtained by applying a phosphate buffer molarity gradient to the PbHA packed column. The first eluted peak, BSA, is followed by a peak of

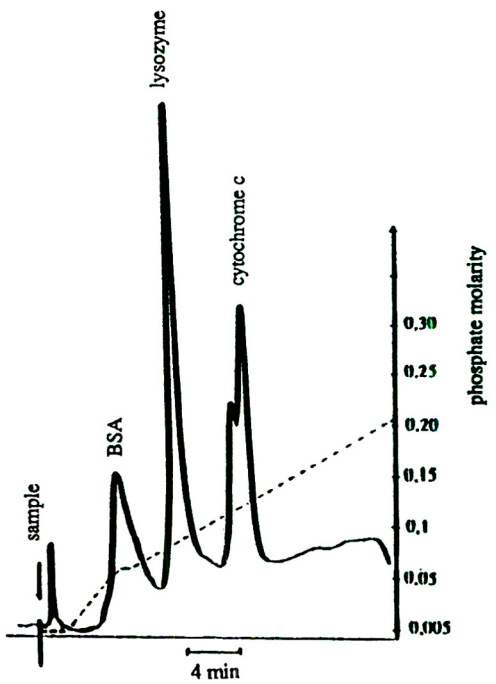

Fig. 3. Chromatogram of a standard mixture of BSA, lysozyme and cytochrome *c* as obtained on the PbHA packed column (75 × 4.6 mm). Conditions: sample load 13.2 μg for albumin, 6.6 μg for lysozyme and 6.6 μg for cytochrome *c*; flow-rate 1 ml/min; inlet pressure 30–32 bar; detection UV at 230 nm. Sample was eluted using a gradient of buffer A to buffer B (0–35% B in 21 min).

lysozyme and a double peak of cytochrome *c* which probably correspond to the oxidized and the reduced forms of cytochrome *c*.

By using the double-gradient method (Fig. 4), it can be seen that BSA, with an acidic p*I*, is eluted with the second potassium phosphate gradient whereas both cytochrome *c* and lysozyme, with basic p*I*, are eluted with the first KCl gradient. Two types of effective surfaces appear on the crystal. From the work of Kawasaki et al. [15] on CaHA, acidic protein molecules are adsorbed mainly onto the a (or b) surface, whereas basic protein molecules are adsorbed mainly onto the c surface. Knowledge of this mechanism permitted selective elution of acidic components in the protein mixture to be developed on the PbHA column. The basic proteins that had been adsorbed on c crystal surfaces were first desorbed through competition with potassium ions from the KCl gradient while the acidic molecules adsorbed on a (or b) crystal surfaces remained adsorbed. When elution of the basic molecules was completed, the phosphate buffer gradient was applied; the acidic molecules were desorbed from a (or b) crystal surfaces through competition with phosphate ions.

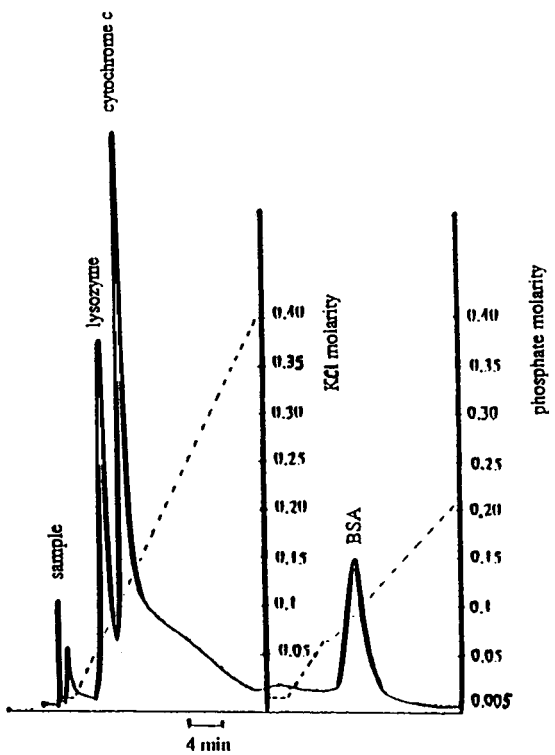

Fig. 4. Double gradient chromatogram for a mixture of BSA (20 μg), lysozyme (10 μg) and cytochrome *c* (10 μg) obtained on the 75 × 4.6 mm PbHA column. First gradient: 5–600 m*M* KCl in buffer A (5–356 m*M* KCl in 20 min). Second gradient: buffer A to buffer B (0–35% in 21 min). Flow-rate = 1 ml/min.

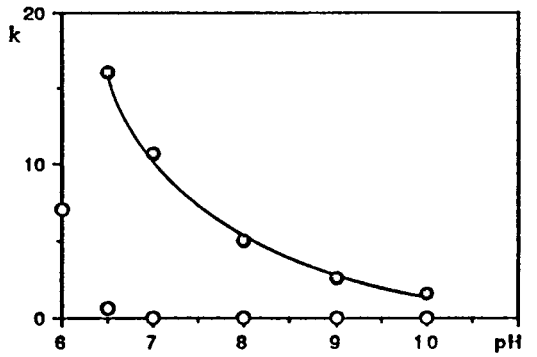

Fig. 5. Effect of pH of eluent on the retention factor (k) of proteins. Proteins were eluted isocratically (0.1 *M* potassium phosphate solution) at various pH values. $k = (t_R - t_0)/t_0$, where t_R is the elution time and t_0 is the elution time for a non-retained solute. ○ = BSA; ● = lysozyme.

Fig. 5 illustrates the effect of the pH of the eluent on the retention factor (k) for BSA and lysozyme. The proteins were injected onto the

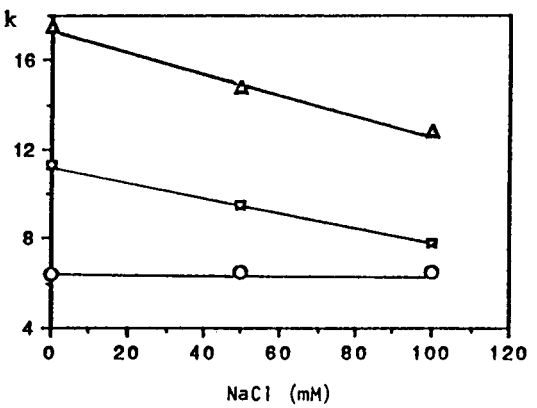

Fig. 6. Effect on NaCl on the retention of proteins on PbHA. A mixture of BSA (○), lysozyme (□) and cytochrome *c* (▲) was eluted from the column under the same conditions as in Fig. 3.

Table 1
Parameters A and Q_m determined from the linearized form of a Langmuir equation

Protein	Adsorbent	Q_m		A
		mg BSA/g adsorbent	mg BSA/mol adsorbent	
BSA	PbHA	4.97	$13.32 \cdot 10^3$	0.308
	CaHA	12.45	$12.54 \cdot 10^3$	0.226

column, and were eluted isocratically at various pH values of the 0.1 M phosphate buffer solution. Both proteins were adsorbed at pH 6. BSA, an acidic protein, was eluted at pH 6.5. Lysozyme, a basic protein, was eluted at pH 10. Generally proteins are adsorbed strongly in low-pH eluent and weakly in high-pH eluent, because adsorption depends on the charges existing on the local molecular surface.

We analysed the effect of sodium chloride on the PbHA chromatography of proteins at pH 6.8. As demonstrated in Fig. 6, addition of sodium chloride to the phosphate buffers had a significant effect on retention; elution of basic proteins (lysozyme and cytochrome c) was facilitated by the addition of sodium chloride whereas no effect was observed on the elution of an acidic protein (BSA). The adsorption of sodium ions to the c crystal surface is analogous to that of potassium ions, and the effects of NaCl on the chromatography are similar to those of KCl.

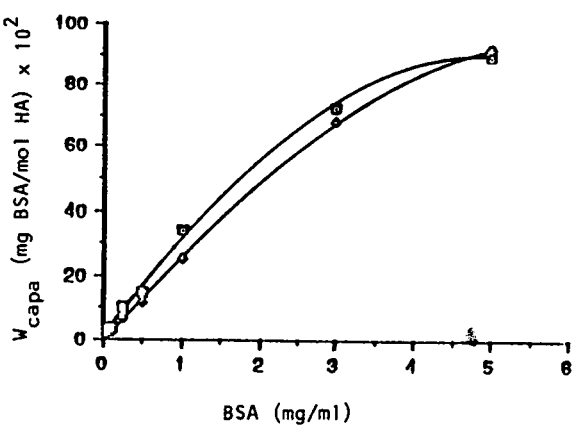

Fig. 7. Adsorption isotherm of bovine serum albumin (BSA) to PbHA (□) and CaHA (◆). The ordinate indicates the binding ratio of BSA to PbHA and CaHA; the abscissa indicates the concentration of BSA (mg/ml) at pH 6.8.

The adsorption isotherms of PbHA and CaHA packings were measured and the amounts of BSA adsorbed per unit mass of the adsorbent (W_{capa}, mg/g) was determined together with C_M, the concentration of BSA in the supernatant.

The adsorption isotherm can be represented by a Langmuir equation:

$$W_{capa} = AQ_mC_M/(1 + AC_M)$$

where A is related to the affinity of the adsorbent and Q_m indicates the maximum capacity of the adsorbent.

To determine the relevant parameters, a linearized form of the above equation can be employed:

$$1/W_{capa} = (1/A)(1/Q_m)(1/C_M) + 1/Q_m$$

Fig. 7 displays the adsorption isotherms of BSA on both CaHA and PbHA. The A and Q_m parameters were determined (Table 1). Little difference is evident when comparing CaHA and PbHA. The affinity A and Q_m are slightly higher for PbHA than CaHA.

The Pb released from PbHA during the adsorption of BSA and lysozyme was determined by inductively coupled plasma mass spectrometry (ICP-MS). The amount of Pb is, in the range 0.2–0.4 ppm, quite low and we can consider that the contamination is minimum. It shall be kept in mind however that this work was more aimed at analytical than preparative separations.

This study shows that it is possible to prepare lead apatites for use as adsorbents in HPLC. Initial experiments with proteins show that the chromatographic behavior of this adsorbent is

similar to CaHA. This may be due to the similar apatitic structure between PbHA and CaHA; the large variation between the a (or b) and c parameters of these two apatites does not lead to a significant difference in protein adsorption. Nevertheless the differences in these parameters, and the difference in electronegative potential between Pb^{2+} and Ca^{2+}, could result in differences in selectivity for closely related proteins. Further study is required to determine the utility of PbHA in chromatography of proteins as well as other small molecules, such as sugars.

References

[1] J.C. Trombe, *Ann. Chim*, 8 (1973) 252.
[2] A. Tiselius, S. Hjertén and O. Levin, *Arch. Biochem. Biophys.*, 65 (1956) 132.
[3] G. Bernardi, *Biochim. Biophys. Acta*, 174 (1969) 423.
[4] G. Bernardi, *Methods Enzymol.*, 22 (1971) 325.
[5] G. Bernardi and M.G. Giro, *Biochim. Biophys. Acta*, 278 (1972) 409.
[6] M. Spencer, *J. Chromatogr.*, 166 (1978) 435.
[7] A. Atkinson and P.A. Bradford, *J. Appl. Chem. Biotechnol.*, 23 (1973) 517.
[8] M. Spencer and M. Grympas, *J. Chromatogr.*, 166 (1978) 423.
[9] M. John and J. Schmidt, *Anal. Biochem.*, 141 (1984) 466.
[10] T. Kawasaki and W. Kobayashi, *Eur. J. Biochem.*, 157 (1986). 291.
[11] T. Kawasaki and M. Niikura, *Biochem. Int.*, 13 (1986) 969.
[12] T. Kawasaki and M. Niikura, *Biochem. Int.*, 15 (1987) 1137.
[13] D.M. Roy and L.E. Drafall, in A.M. Alper (Editor), *Refractory Materials*, Vol. 6-v, Academic Press, New York, 1978, pp. 187–206.
[14] R.D. Shannon, *Acta Crystal.*, 32 (1976) 751.
[15] T. Kawasaki, S. Takahashi and K. Ikeda, *Eur. J. Biochem.*, 152 (1985) 361.

ELSEVIER

Journal of Chromatography A, 694 (1995) 492–497

JOURNAL OF CHROMATOGRAPHY A

Short communication

Resolution of isotoxins in the β-bungarotoxin family

Chen-Chung Chu[a], Sheng-Hsiang Li[b], Yee-Hsiung Chen[a,b,*]

[a]*Institute of Biochemical Sciences, College of Science, National Taiwan University, Taipei 106, Taiwan*

[b]*Institute of Biological Chemistry, Academia Sinica, Taipei 106, Taiwan*

First received 27 September 1994; revised manuscript received 24 November 1994; accepted 25 November 1994

Abstract

Although only five isotoxins of the β-bungarotoxin family had been claimed, this work indicated the existence of more than sixteen isotoxins. Crude snake (*Bungarus multicinctus*) venom was divided into four main fractions by gel filtration on a Sephadex G-50 column. β-Bungarotoxin appeared in a major fraction that contained mainly the M_r 20 000 protein components. The fraction could be further resolved into eighteen peaks designated P1–P18 by HPLC on a Protein Pak SP 5PW column that was eluted with a linear gradient of 0.1–0.6 *M* CH_3COONa in 20 m*M* NaH_2PO_4–Na_2HPO_4 at pH 7.4. P3–P18 were demonstrated to be isotoxins of the β-bungarotoxin family. Results of protein sequencing for P8, P9 and P11, the three main isotoxins, confirmed that they shared a common phospholipase A_2 subunit, which was very similar to although not completely identical with the A1 chain reported previously.

1. Introduction

The β-bungarotoxin (β-BuTX) family consists of a group of isotoxins that constitute the main portion of snake (*Bungarus multicinctus*) venom. As the toxin is very specific and unique in the blockade of neuromuscular transmission [1–3], it has been exploited as an important tool in physiological, biochemical and pharamacological studies. The isotoxins of the β-BuTX family have a similar primary structure [4–6]. Each is composed of two subunits linked by a disulfide bond. One is an M_r 13 000 phospholipase A_2 (PLA_2) subunit and the other is an M_r 7000 non-PLA_2 subunit. As the isotoxins show a wide range of lethal potency, their separation to avoid contamination with one another is critical in order to correlate their structures with neurotoxicity. In this regard, the resolution of the protein components in crude venom has been attempted many times by chromatography on a CM-Sephadex column, but the reported chromatograms varied with the batch of venom [7–11]. It was often confusing to define clearly an isotoxin on the chromatogram and to compare the neurotoxicity of an isotoxin reported by

* Corresponding author. Address for correspondence: Institute of Biochemical Sciences, College of Science, National Taiwan University, P.O. Box 23-106, Taipei, Taiwan.

0021-9673/95/$09.50
SSDI 0021-9673(94)01173-7

different groups. This complicates the elucidation of the structure–function relationship of β-BuTX. Here, we report the effective resolution of the isotoxins.

2. Experimental

2.1. Materials

Crude snake venom was supplied by Chen Hsin Tong Chemical (Taipei, Taiwan). CM-Sephadex C-25 and Sephadex G-50 were obtained from Pharmacia (Uppsala, Sweden). A Protein Pak SP 5PW column was purchased from Waters (Milford, MA, USA) and Chemcosorb-ODS-H from Chemco Scientific (Osaka, Japan). All chemicals were of analytical-reagent grade.

2.2. Purification of isotoxins in the β-BuTX family

Crude venom was fractionated by gel filtration on a Sephadex G-50 column in 0.05 *M* CH_3COONa at pH 5.0, and the fraction containing M_r 20 000 protein was further resolved by HPLC on an SP column which was washed with a linear gradient of 0.1–0.6 *M* CH_3COONa in 20 m*M* NaH_2PO_4–Na_2HPO_4 at pH 7.4. The elution was modified from our previous procedure [12].

2.3. Analysis

Protein at a concentration of 5 mg/ml in 0.1 *M* NH_4HCO_3 at pH 8.5 was digested with trypsin (protein:trypsin = 50:1, w/w) at 37°C for 24 h. The trypsin digests were reduced in 6 *M* guanidine hydrochloride–50 m*M* Tris buffer at pH 8.6 in the presence of 20 m*M* 2-mercaptoethanol at 60°C for 1 h. The reduced samples were alkylated in 20 m*M* 4-vinylpyridine in the dark at 25°C for 3 h [13]. The alkylated derivatives were resolved by HPLC on a C_{18} column (Chemcosorb-ODS-H, 7 μm, 250 × 4.6 mm I.D.).

The amino acid sequences of proteins were determined by automated Edman degradation with a gas-phase microsequencer (Model 477A protein sequencer with on-line Model 120A analyser; Applied Biosystems).

Antisera were collected from rabbits immunized with β_1-BuTX fraction which was purified by CM-Sephadex C-25 chromatography of crude venom [11,14]. Protein size was determined by sodium dodecyl sulfate polyacrylamide gel electrophoresis (SDS-PAGE) on a 15% (w/v) gel slab (7 cm × 5 cm) in Tris–glycine buffer [15]. Electrophoresis was conducted at 60 V for 30 min and then at 120 V for 1 h. The protein bands were revealed when the gel was stained with Serva blue. Alternatively, proteins were transferred overnight from slab gels into nitrocellulose membranes by a diffusion method in phosphate-buffered saline (PBS) at pH 7.4. Blots were immunodetected by treatment with the antisera, followed by treatment with ^{125}I-labelled donkey anti-rabbit IgG antibody and fluorography.

3. Results

3.1. Resolution of isotoxins in the β-BuTX family

Crude venom was divided into four main fractions, denoted Fr. I–IV in Fig. 1, by gel filtration on a Sephadex G-50 column. Only Fr. II, which contained mainly the M_r 20 000 protein as tested by SDS-PAGE, gave a strong immunoaffinity to anti-β_1-BuTX. Taking into account the basicity of β-BuTX, we further resolved it by HPLC on an SP column into eighteen well defined peaks designated P1–P18, as shown in Fig. 2A. P1 and P2 were non-retarding fractions. P3–P18 were washed out from the column by a linear gradient of 0.1–0.6 *M* CH_3COONa at pH 7.4. Apparently, they were basic proteins: the longer the retention time of a protein, the higher may be its basicity. Under the same experimental conditions, the β_1-BuTX fraction obtained from CM-Sephadex C-25 chromatography of crude venom was resolved into three peaks (Fig. 2B), SP I–III, as defined previously [12]. Appar-

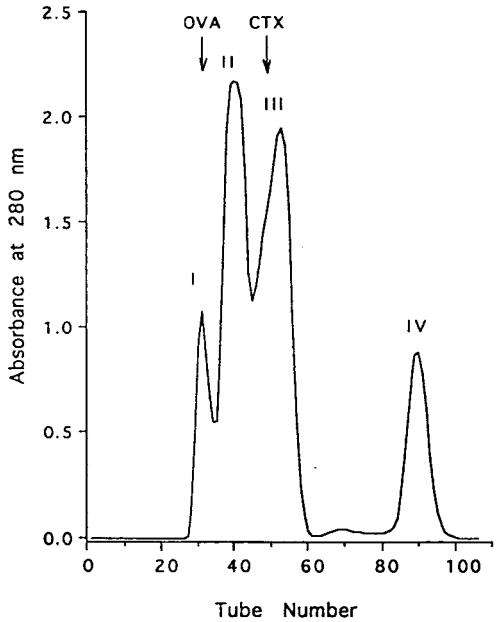

Fig. 1. Fractionation of crude venom by gel filtration. Crude venom (100 mg) in 2 ml of 0.05 *M* CH_3COONa at pH 5.0 was subjected to chromatography on a Sephadex G-50 column (110 × 1.6 cm I.D.). Fractions of 2 ml were collected and their absorbances at 280 nm recorded. The column was calibrated with ovoalbumin (OVA, M_r 45 000) and cobra cardiotoxin (CTX, M_r 7000).

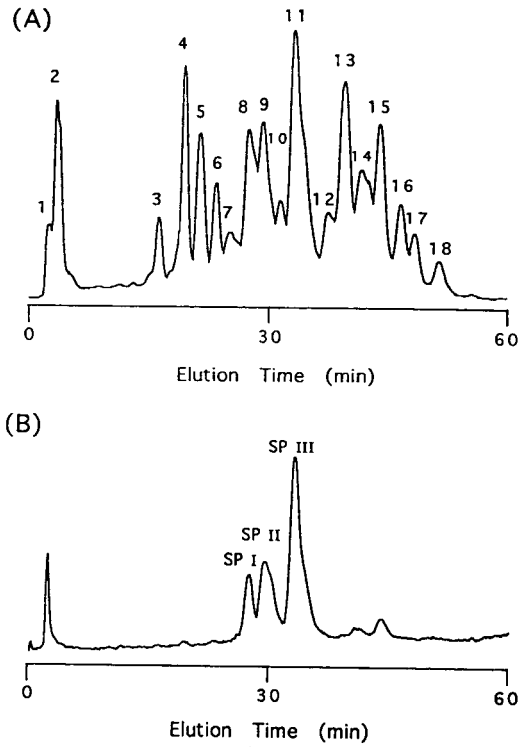

Fig. 2. Separation of isotoxins in the β-BuTX family. (A) Fr. II of Fig. 1 was resolved by HPLC on an SP column, which was washed with a linear gradient of 0.1–0.6 *M* CH_3COONa in 20 m*M* NaH_2PO_4–Na_2HPO_4 (pH 7.4) at a flow-rate of 1 ml/min. The effluent was monitored at 280 nm. Eighteen peaks are marked on the chromatogram. (B) β_1-BuTX fraction obtained from CM-Sephadex C-25 chromatography of crude venom was resolved by HPLC under the same experimental conditions as in (A).

ently, P8, P9 and P11 corresponded to SP I, SP II and SP III, respectively.

The protein samples were analysed by SDS-PAGE. Without reduction of their disulfide bonds (Fig. 3A), only one M_r 20 000 band was found in each of P7–P11 and P16–P18. There appeared one band slightly larger than M_r 20 000 in P4 and two bands around M_r 20 000 in P5, P6 and P12–P15. Traces of these two bands were detected in P1 and P2. P3 contained one M_r 20 000 band and one band smaller than M_r 20 000. Each of P3–P18 was divided into two bands, an M_r 13 000 band corresponding to a PLA_2 subunit and an M_r 7000 band corresponding to a non-PLA_2 subunit, when the protein disulfide bonds were reduced (Fig. 3B). As shown in Fig. 3C, both the M_r 20 000 band and the band slightly larger than M_r 20 000 in P3–P18 showed a strong immunoaffinity towards anti-β_1-BuTX (see Experimental), revealing that P3–P18 may share a similar antigenic determinant(s). This, together with the characteristics of SDS-PAGE shown above, supported the conclusion that P3–P18 are isotoxins of the β-BuTX family. The antisera showed a very weak affinity to the PLA_2 subunit and nearly no affinity to the non-PLA_2 subunit once they were separated by SDS-PAGE after the reduction of each isotoxin (data not shown).

3.2. *Identification of P8, P9 and P11*

Previous results from partial sequence of the N-terminal region analysis revealed that P8, P9

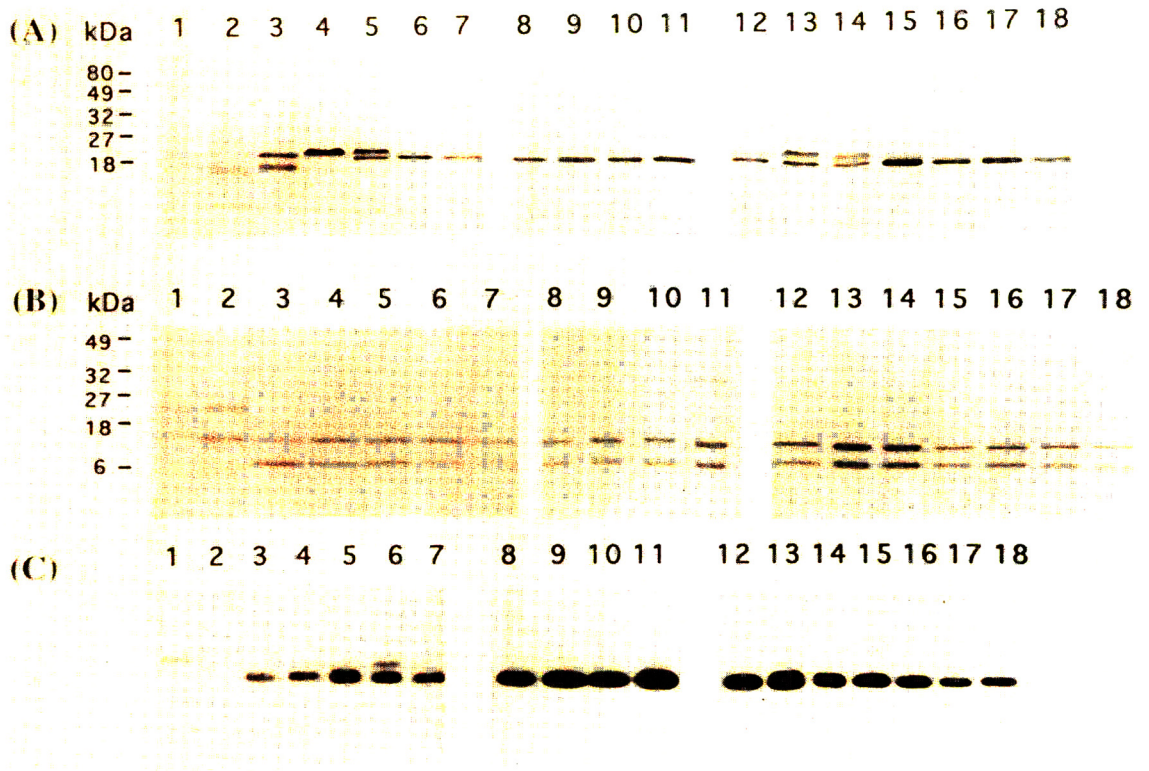

Fig. 3. The protein samples in Fig. 2A were resolved by SDS-PAGE (A) in the absence and (B) in the presence of 2-mercaptoethanol and the gels were stained with Serva blue. (C) The proteins in Fig. 2A were immunodetected by the Western blotting procedure with antisera against the β_1-BuTX fraction. The lane numbers correspond to the protein components denoted in Fig. 2A. kDa = kilodalton.

and P11 differed in their non-PLA_2 subunits and suggested that they might share a common PLA_2 subunit [12]. To corroborate the latter aspect, we determined the primary structures of their PLA_2 subunits. P8, P9 and P11 were rechromatographed on an SP column and were reductively alkylated. The two alkylated subunits of each protein could be separated by HPLC on a reversed-phase C_{18} column [12]. We found that trypsin digestion of the alkylated PLA_2 subunit of each protein remained problematic. Instead, we digested each intact protein with trypsin, followed by reductive alkylation of the trypsin digests with 4-vinylpyridine. The reaction mixture was resolved by HPLC on a reversed-phase C_{18} column (Fig. 4). The peptides of trypsin digests were randomly selected for amino acid sequence determination by automated Edman degradation. Only the peptides having partial sequences that could be aligned with the primary structure of PLA_2 subunit are summarized in Fig. 5. Peptides a–h appeared on the chromatograms of the three trypsin-digested samples. The primary structures of A1, A2, A3 and A2-like chain are also included in Fig. 5 for comparison. The partial sequences of these peptides in P11 confirmed residues 1–10, 11–17, 18–32, 65–71, 76–88, 89–95, 96–111 and 118–120 in the A1 chain reportd by Kondo and co-workers [4–6], except that $S^{66}Q$ and $Q^{103}SDY$ in the A1 chain were replaced by QS in peptide b and NSEY in peptide g, which are present in the A2-like chain deduced from a cDNA sequence [16] (Fig. 5). Nevertheless, the discrepancy between our de-

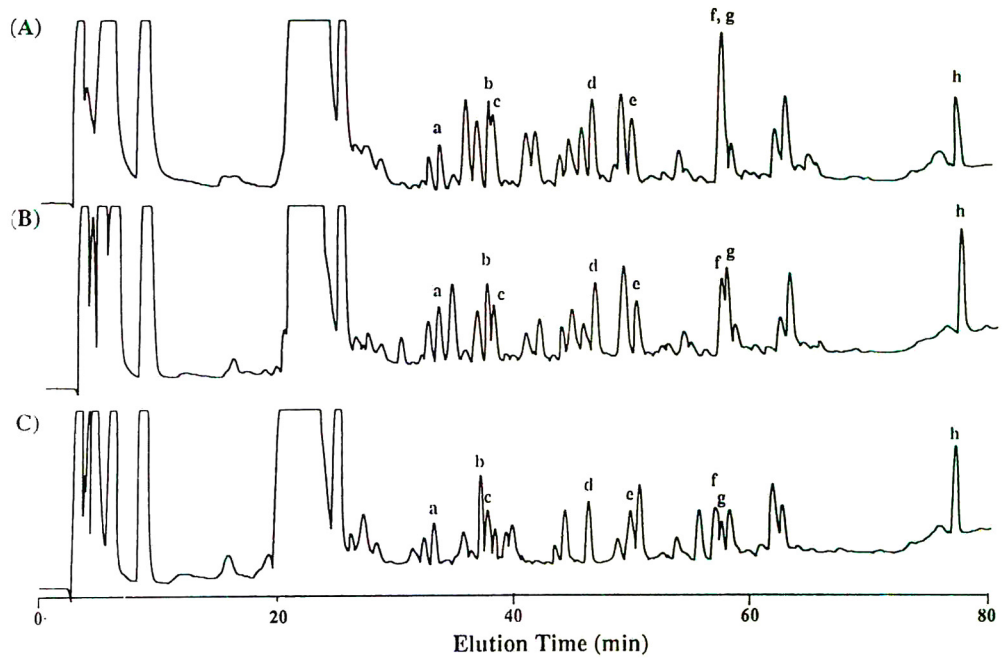

Fig. 4. Resolution of the alkylated trypsin digests of isotoxins. The alkylated derivatives of (A) P8, (B) P9 and (C) P11 were resolved by HPLC on a reversed-phase C_{18} column, which was washed consecutively with 0.1% trifluoroacetic acid (TFA) for 5 min, a linear gradient of 0–30% acetonitrile in 0.1% TFA for 60 min, a linear gradient of 30–60% acetonitrile in 0.1% TFA for 10 min and 60% acetonitrile in 0.1% TFA for 5 min. The flow-rate was 1 ml/min and the effluent was monitored at 214 nm. Peptides a–h of each protein sample were pooled for automated Edman degradation.

```
          1         11        21        31        41        51
          :         :         :         :         :         :
A1        NLINFMEMIRYTIPCEKTWGEYADYGCYCGAGGSGRPIDALDRCCYVHDNCYGDAEKKHK
A2        ------------------------------------------------------------
A3        ----------------------T-------------------------------DAAIRD
A2-like   ------------------------------------------------------------

P8,P9,P11 NLINFMEMIRYTIPCEKTWGEYADYGCYCGAG
          ←— h —→← d →←——— f ———→
```

```
          61        71        81        91        101       111
          :         :         :         :         :         :
A1        CNPKTSQYSYKLTKRTIICYGAAGTCGRIVCDCDRTAALCFGQSDYIEGHKNIDTARFCQ
A2        -------------------------A---------------------R------K-H-R
A3        -------------------------A-V-----------------------------
A2-like   -----QS-------------------A---------------N-E---R------K-H-R

             **                                        * *
P8,P9,P11    TQSYSYK    TIICYGAAGTCGRIVCDCDRTAALCFGNSEYIEGHK       FCQ
             ←b→    ←——— e ———→← c →←——— g ———→          <a>
```

Fig. 5. Partial sequences of peptides a–h in P8, P9 and P11. The corresponding peptides in the three protein samples showed no difference in their amino acid sequences. The partial sequences were aligned with the primary structure of the A1 chain. The primary structures of the A2, A3 and A2-like chains were also aligned with the A1 chain and the homologous residues are indicated by broken lines. The asterisks denote the sequences in peptides b and g, which disagree with the A1 chain but agree with the A2-like chain.

terminations and those of the A1 chain is minor. Peptides a–h of both P8 and P9 were proved to be the same as the corresponding peptides in P11, revealing that P8, P9 and P11 share a common PLA_2 subunit, which is most likely to be the A1 chain.

4. Discussion

This work is the first to give an effective resolution of isotoxins in the β-BuTX family. The results show two important structural features. First, there are more than sixteen isotoxins in the β-BuTX family. Previously, five types of PLA_2 subunit, A1, A2 and A3 chains reported earlier [4–6] and A2-like and A4 chains deduced recently from cDNAs [16,17], and two types of non-PLA_2 subunit, B1 and B2 chain [4–6], have been reported in the β-BuTX family. However, combination of these known subunits is insufficient to account for the formation of more than sixteen isotoxins. It turns out that more types of subunits should exist in the β-BuTX family. The gene regulation for the expression of these isotoxins and the reconstruction of subunits in the formation of isotoxins are of interest for future studies. Second, the two subunits of each isotoxin should interact to stabilize the antigenic determinant(s) of intact toxin. Apparently, the association of two subunits is essential to form an active three-dimensional structure. Therefore, separation of either subunit from the parent toxin in "native format" becomes a formidable task. Under these circumstances, correlation of the isotoxins with a common PLA_2 subunit but with different non-PLA_2 subunits, such as the situation with P8, P9 and P11 or vice versa, with their neurotoxicity may shed some light on the role of each subunit in the PLA_2 activity-dependent and the PLA_2 activity-independent neurotoxic effects, both of which are important in the blockade of neuromuscular transmission by β-BuTX [1,2].

Acknowledgement

This work was partially supported by the National Science Council, Taipei, Taiwan (Grant NSC 84-2311-B-001-069).

References

[1] R.B. Kelly, R.J. Wedel and P.N. Strong, in B. Ceccarelli and F. Vlementi (Editors), *Advances in Cytopharmacology*, Raven Press, New York, 1979, pp. 77–85.
[2] C.G. Caratsch, B. Maranda, R. Miledi and R.N. Strong, *J. Physiol.*, 319 (1981) 179–191.
[3] C.C. Chang, *Proc. Natl. Sci. Conc. B R.O.C.*, 9 (1985) 126–142.
[4] K. Kondo, K. Narita and C.Y. Lee, *J. Biochem. (Tokyo)*, 83 (1978) 101–115.
[5] K. Kondo, H. Toda, K. Narita and C.Y. Lee, *J. Biochem. (Tokyo)*, 91 (1982) 1519–1530.
[6] K. Kondo, H. Toda, K. Narita and C.Y. Lee, *J. Biochem. (Tokyo)*, 91 (1982) 1531–1548.
[7] D.G. Clark, D.D. Macmurchie, E. Elliot, R.G. Wolcott, A.M. Landel and M.A. Raftery, *Biochemistry*, 11 (1972) 1663–1668.
[8] C.Y. Lee, S.L. Chang, S.T. Kau and S.H. Luh, *J. Chromatogr.*, 72 (1972) 71–82.
[9] V.A. Eterovic, M.S. Herbert, M.R. Hanley and E.L. Bennett, *Toxicon*, 13 (1975) 37–48.
[10] T. Abe, S. Alema and R. Miledi, *Eur. J. Biochem.*, 80 (1977) 1–12.
[11] Y.H. Chen, J.C. Tai, W.J. Huang, M.Z. Lai, M.C. Hung, M.D. Lai and J.T. Yang, *Biochemistry*, 21 (1982) 773–779.
[12] C.C. Chu, S.T. Chu, S.W. Chen and Y.H. Chen, *Biochem. J.*, 303 (1994) 171–176.
[13] A.V. Flannery, R.J. Beynon and J.S. Bond, in R.J. Beynon and J.S. Bond (Editors), *Proteolytic Enzymes*, IRL Press, Oxford, 1989, pp. 145–162.
[14] W.Z. Lin, S.T. Chu and Y.H. Chen, *Proc. Natl. Sci. Counc. B R.O.C.*, 8 (1984) 113–118.
[15] U.K. Laemmli, *Nature*, 227 (1970) 680–685.
[16] J.-M. Danse, J.-L. Toussaint and J. Kempf, *Nucleic Acids Res.*, 18 (1990) 4609.
[17] J.-M. Danse, J.-M. Garnier and J. Kempf, *Nucleic Acids Res.*, 18 (1990) 4610.

ELSEVIER

Journal of Chromatography A, 694 (1995) 498–506

JOURNAL OF CHROMATOGRAPHY A

Short communication

Capillary zone electrophoretic separation of proteins using a column coated with epoxy polymer

Yu Liu, Ruonong Fu*, Junling Gu

Department of Chemical Engineering, Beijing Institute of Technology, P.O. Box 327, Beijing 100081, China

First received 2 August 1994; revised manuscript received 1 November 1994; accepted 8 November 1994

Abstract

Fused-silica capillaries used in capillary zone electrophoresis were covalently coated with epoxy polymer and then cross-linked with ethylenediamine to form a stable layer. This coating was of sufficient thickness and hydrophilicity to reduce both protein adsorption and electroosmotic flow. The electroosmotic flow-rate showed about a twofold decrease but was still sufficient to carry both positive and negative species to the detector. As a consequence, high separation efficiencies were obtained in the pH range 2–10. The coatings were stable after more than 350 injections in 2 months. Further, reproducible separations were achieved from run to run and day to day.

1. Introduction

Capillary zone electrophoresis (CZE) is proving to be of great utility in the separation of small molecules such as inorganic ions, amino acids, peptides and nucleotides. Unfortunately, the high resolving power of capillary electrophoresis decreases seriously in the separation of proteins, mainly because of the adsorption of proteins on the inner wall of silica capillaries, which leads to considerable peak broadening and poor reproducibility.

Several approaches have been employed to eliminate the wall adsorption of proteins, e.g., the use of running electrolytes at high [1] or low pH [2]. Although under such circumstances protein adsorption can be greatly decreased, it may limit the selectivity of the system to a narrow pH range and result in protein denaturation. Addition of additives to the running buffer has been applied. Some additives, such as ethylene glycol [3], zwitterions [4] and amines [5], were reported to suppress protein adsorption effectively. However, high concentrations of additives must be used in the running buffer as competitive ions against protein adsorption, and these will also lead to a decrease in the system selectivities. Further, the use of capillary surface coatings has been advocated. The inner surface of silica capillaries was coated with a polymer monolayer which can shield the silanol groups. Several coatings based on the derivatization of capillaries with simple organosilanes have been developed for the CZE of proteins, e.g., glycol [6], polyethylene glycol (PEG) [7,8], poly(methyl gluta-

* Corresponding author.

0021-9673/95/$09.50
SSDI 0021-9673(94)01099-4

mate) [9], carbohydrate [10] and polyacrylamide [11]. Each has attained some success in reducing protein adsorption. However, these silane derivatives are easily hydrolysed under basic conditions and the column performance deteriorates rapidly.

To solve this problem, Cobb et al. [12] treated the capillary surface with a Grignard regent, followed by reaction of acrylamide to form a linear polymer which exhibited enhanced stability at both high and low pH. However, as both the surface adsorption and electroosmotic flow (EOF) were diminished at the same time, cationic and anionic species were swept in opposite directions. Two runs must be made to analyse a mixture of anionic and cationic compounds. Towns and Regnier [13] reported that nonionic surfactant coatings that were adsorbed on the surface of octadecylsilane-derivatized capillaries can reduce protein adsorption. This approach was successful in reducing protein adsorption while still allowing sufficient electroendosmosis to carry both cationic and anionic species to the detector. However, high concentrations of nonionic surfactant must be used in the buffer solution, which may contaminate the sample collected.

Recently, a hydrophilic cross-linked coating based on the polymerization of a bis(epoxide) on the capillary surface was reported [14]. This coating was of sufficient thickness and hydrophilicity to decrease protein adsorption but still allowed sufficient electroosmotic pumping. A high separation efficiency was achieved between pH 5 and 10. However, the results reported were obtained during a 120-h lifetime and the longer use of coatings was not discussed.

This paper is concerned with the preparation of a stable coating that would decrease protein adsorption on capillaries while still maintaining enough electroosmotic flow to carry both positive and negative species to the detector. Towards this aim, an epoxy polymer was covalently bonded on the capillary surface and then cross-linked with ethylenediamine to produce a stable layer that would extend the pH range used and the capillary lifetime.

2. Experimental

2.1. Apparatus

A capillary electrophoresis system was purchased from the Beijing Institute of New Technology Application (Beijing, China). Fused-silica capillaries (Herbei Yongnian Optical Fibre Factory, Herbei, China) of 50 μm I.D. were used to prepare the capillaries. Capillaries were 66 cm long with a separation length of 44 cm. UV detection at 214 nm was applied.

2.2. Reagents

Protein samples were purchased from Shanghai Biochemical (Shanghai, China), except for α-chymotrypsinogen, which was purchased from Sigma (St. Louis, MO, USA). All other reagents were of analytical-reagent grade.

2.3. Electrophoresis

Protein solutions of 1.0 mg/ml were introduced into the capillary by syphoning for a fixed time (3 s) at a fixed height (10 cm). Dimethyl sulphoxide (DMSO) was used as a neutral marker. Between runs, the capillary was flushed with separation buffer for 3 min.

2.4. Preparation of capillary

Pretreatment of capillaries

Capillaries were first treated with 1.0 mol/l NaOH for 30 min followed by 15 min of washing with deionized water. Then the capillaries were flushed with 0.1 mol/l HCl for 10 min. Residual HCl was removed in a gas chromatographic oven at 100°C for 1 h under a nitrogen pressure of 400 kPa.

Preparation of γ-glycidoxypropyltrimethoxysilane (GOX)

The capillary was filled with 5% γ-glycidoxypropyltrimethoxysilane solution in methylene chloride and allowed to react for 3 h. After washing with methylene chloride for 10 min, the

capillary was heated at 100°C for 2 h under a nitrogen pressure of 400 kPa.

Preparation of epoxy polymer coating

A thin film of diglycidyl ether of bisphenol A (DEBA) was deposited on the pretreated capillary by aspirating DEBA in methylene chloride solution and cross-linked with ethylenediamine. Residual reagents were removed in a gas chromatographic oven at room temperature for 2 h under a nitrogen pressure of 100 kPa. Then the temperature was raised to 100°C for 1 h.

3. Results and discussion

Reactions in the epoxy polymer coating process are shown schematically in Fig. 1. It should be noted that the structures do not represent the exact structure of the coating. GOX was firstly

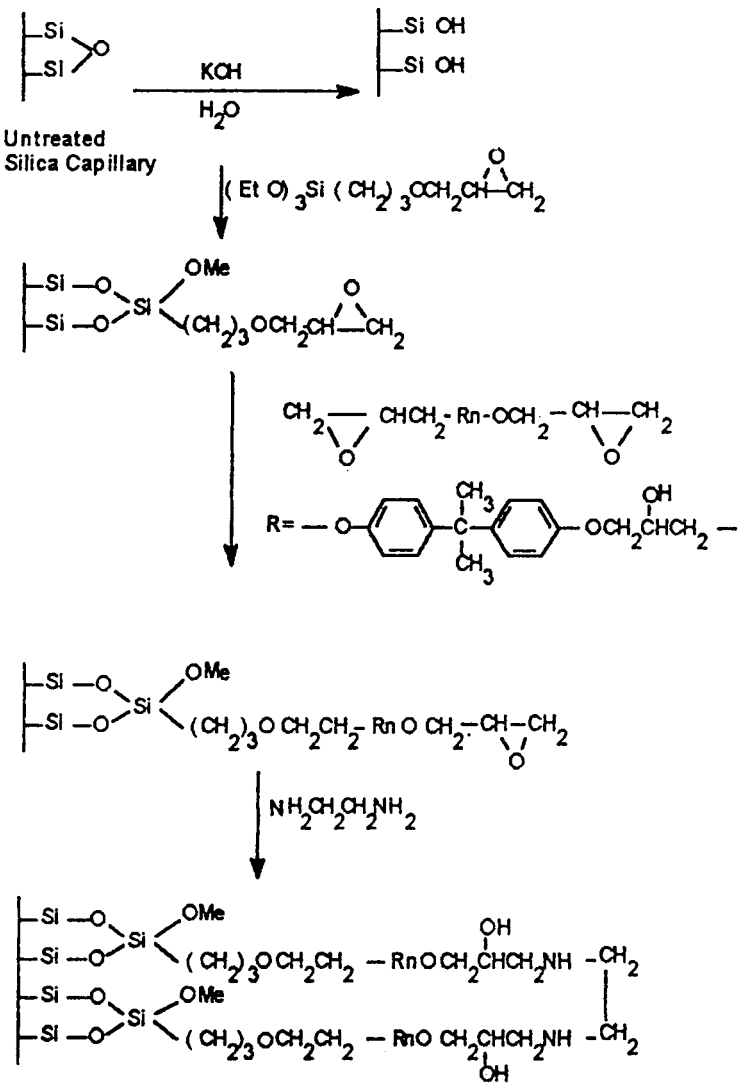

Fig. 1. Typical reaction scheme used in the preparation of epoxy polymer coating.

coupled to the surface silanols and reacted with epoxy polymer (DEBA) to produce a polymer monolayer. Then the surface epoxy groups of DEBA were cross-linked with ethylenediamine to form a stable surface layer. The resulting epoxy polymer contains many ether, hydroxyl and amine groups which may show sufficient hydrophilicity. This cross-linked polymer layer is much more stable than coatings derived from simple organosilanes [6–11]. Towns et al. [14] also used multifunctional oxirane to prepare epoxy polymer coatings, through a five-step process which can effectively reduce protein adsorption at pH 5–10. The present coatings were prepared with only a two-step process and a high-molecular mass epoxy polymer was used to achieve more effective shielding of surface silanols.

3.1. Evaluation of coated capillaries

Masking silanol groups depends on the thickness of the polymer layer deposited on the capillary surface. Therefore, 10%, 50% and 80% epoxy polymer in methylene chloride were used to coat the capillary to determine the optimum conditions. We used four basic proteins to evaluate the coated capillaries. Fig. 2 shows the separation of protein mixtures with coated and uncoated capillaries in 0.05 mol/l phosphate buffer at pH 7.0. Some basic proteins cannot be eluted from the uncoated capillary owing to adsorption on the inner wall (Fig. 2A). However, the four basic proteins can be separated successfully in the coated capillary, which indicates that a substantial decrease in protein adsorption has been achieved.

Table 1 shows the performance of the coated capillaries at the three concentrations examined. With the use of 10% epoxy polymer (coating 1), effective separation can only be achieved at pH 3–5. Above pH 5, the peak shape deteriorated and lysozyme could not be eluted from the capillary. Coating with 50% epoxy polymer (coating 2) showed good efficiency in the pH range 3–7, but the efficiency dropped quickly and both lysozyme and chymotrypsinogen A showed long tailing at pH above 7. This is because the polymer layer deposited on the capillary surface is still not thick enough to mask silanols sufficiently. The use of an 80% epoxy polymer (coating 3) to mask further the surface silanol groups gave good results in terms of efficiency, lifetime and the useful pH range. It should be noted that the efficiency of coating 3 is not as good as that of coating 2 at pH 3–7, probably because epoxy polymer was cross-linked in three directions, and therefore a thicker layer could not be coated as uniformly as a thin layer. However, the EOF of coating 3 is much lower than that of coating 2, which means that more effective shielding of silanols was achieved (Fig. 3). This is very important for a good separation because higher resolution will be achieved at a lower EOF. Further, coating 3 has the longest lifetime and was more stable than others, so it can be used in the pH range 2–11.

3.2. Electroosmotic flow

In CZE, the EOF plays a major role in protein mobility. The protein elution rate is the sum of the EOF and electrophoretic mobility, so decreasing the EOF will improve protein resolution. This is especially true when there is only a small difference among the electrophoretic mobilities of proteins. On the other hand, the EOF is like a pump in liquid chromatography which pumps both positively and negatively charged samples to the detector. Hence it was necessary to maintain a sufficient EOF while decreasing protein adsorption.

The effect of pH on the EOF was examined over the pH range 3–11, using DMSO as a neutral marker. Fig. 3 shows the results obtained for both treated and untreated capillaries. The coated capillaries exhibited a much lower EOF than uncoated capillary because of the effective shielding of surface silanols. However, there was still some increase in EOF over the pH range 3–11, which means that these coatings cannot completely mask all the surface silanols.

The EOF characteristics are different for capillaries coated with different concentrations of epoxy polymer, although they show the same silylation of surface silanols. Coating with 80%

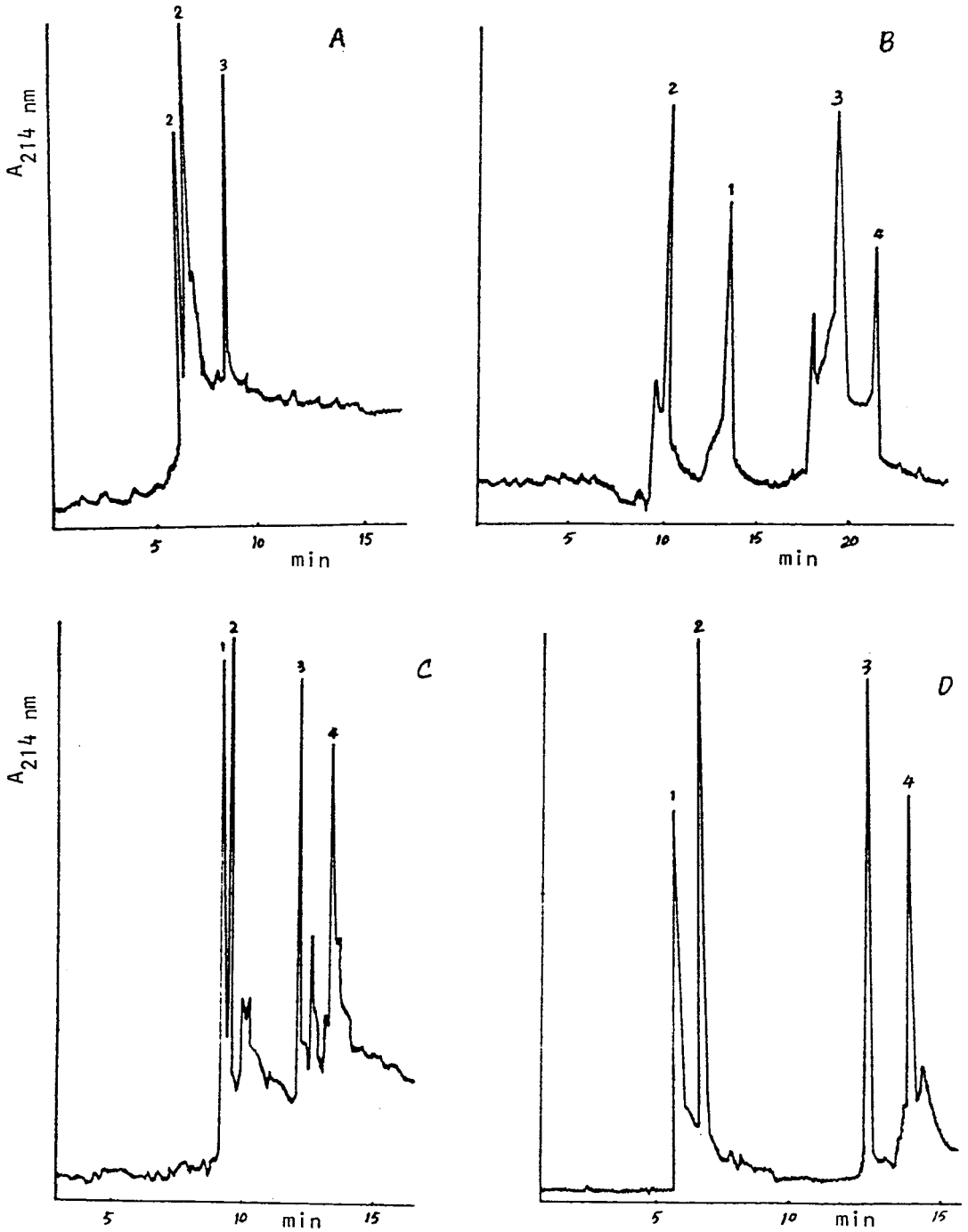

Fig. 2. Capillary electrophoretic separation of a basic protein mixture, using (A) uncoated, (B) epoxy polymer-coated (1), (C) epoxy polymer-coated (2), and (D) epoxy polymer-coated (3) silica capillaries. Electrophoretic conditions: capillaries, 66 cm × 50 μm I.D., 44 cm to detector; 0.05 mol/l phosphate buffer (pH 7 for A, C and D; pH 5 for B); hydrodynamic injection, 5 s at 10-cm height; applied voltage, 19 kV. Peaks: 1 = lysozyme; 2 = cytochrome *c*; 3 = ribonuclease A; 4 = chymotrypsinogen.

Table 1
Separation parameters for epoxy polymer-coated capillaries

Capillary	EOF × 10^{-8} ($m^2/V \cdot s$)	Plate No.	Useful pH range	Lifetime
Untreated	5.0			
Coating 1	3.3		2–5	20 days
Coating 2	2.1	103 114	2–7	>1 month
Coating 3	1.7	51 210	2–10	>2 months

Electrophoretic condition: capillaries, 66 cm × 50 μm I.D., 44 cm to detector; 0.05 mol/l phosphate buffer (pH 7); applied voltage, 19 kV for protein separation, 24 kV for EOF; lysozyme used to evaluate column efficiency (pH 7); DMSO as neutral marker.

epoxy polymer, the highest concentration used, gives the lowest electroosmotic flow-rate. This is because the higher the concentration of epoxy polymer used, the thicker was the cross-linked layer formed. Hence it can further mask the silanol groups towards the atmospheric binding of electrolyte cations, thus further decreasing the EOF. However, compared with an untreated capillary, the EOF showed a ca. twofold decrease in the pH range 4–7 for all the coated capillaries. This moderate EOF was sufficient to carry both positive and negative species to the detector.

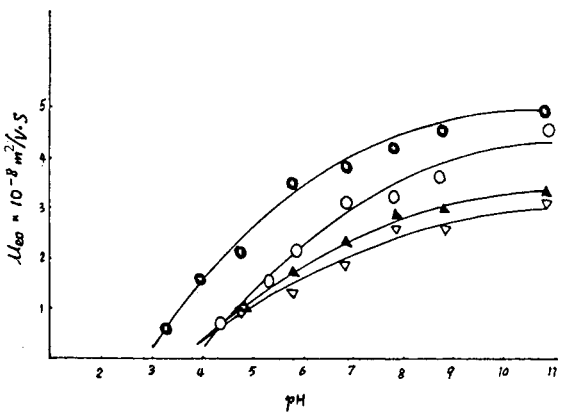

Fig. 3. Dependence of EOF on pH for (●) uncoated, (○) epoxy polymer-coated (1), (▲) epoxy polymer-coated (2) and (△) epoxy polymer-coated (3) silica capillaries.

3.3. Effect of pH on separation

According to the literature [6–11], many coatings based on derivatization with simple organosilanes have been found to be easily hydrolysed above pH 7, because of the unstable Si–O–Si–C bonds. In this work, we also prepared capillaries by silanol derivatization, but the polymer monolayer was further cross-linked with ethylenediamine to form a stable layer. This coating was found to be stable over a wide pH range (2–11). Fig. 4 shows the separation of proteins in coated capillary 3 over the pH range 2–10. Sharp peaks and good efficiencies were obtained at all the pH values used. Therefore, the resolution can be optimized very easily by finding the optimum pH for the specific separation of a protein mixture. Table 2 shows plate numbers for four basic proteins at different pH. It was found that excellent efficiencies and separation were achieved in the pH range 3–8. Below pH 3, although the efficiency is very high, protein denaturation will occur. At pH 10, lysozyme showed slight tailing, which indicated that there were still some unshielding silanols. Chymotrypsinogen A and ribonuclease A, which have a negative charge, should exhibit a slight increase in efficiency; however, the efficiency of ribonuclease A dropped considerably because of its denaturation. Hence both acidic and basic conditions, which may result in protein denaturation, cannot give good separation and efficiencies.

3.4. Reproducibility and stability of the coatings

These studies were carried out on capillaries with coatings 2 and 3. Table 3 summarizes the run-to-run, day-to-day and month-to-month migration reproducibility expressed in terms of relative standard deviation (R.S.D.) with four basic proteins at pH 5.0. It should be noted that the month-to-month reproducibility reflects results obtained when the capillary was further used over the pH range 3–10 for 1 month. Both coatings exhibit good run-to-run and day-to-day reproducibility over their useful pH range. However, after the capillary had been further used

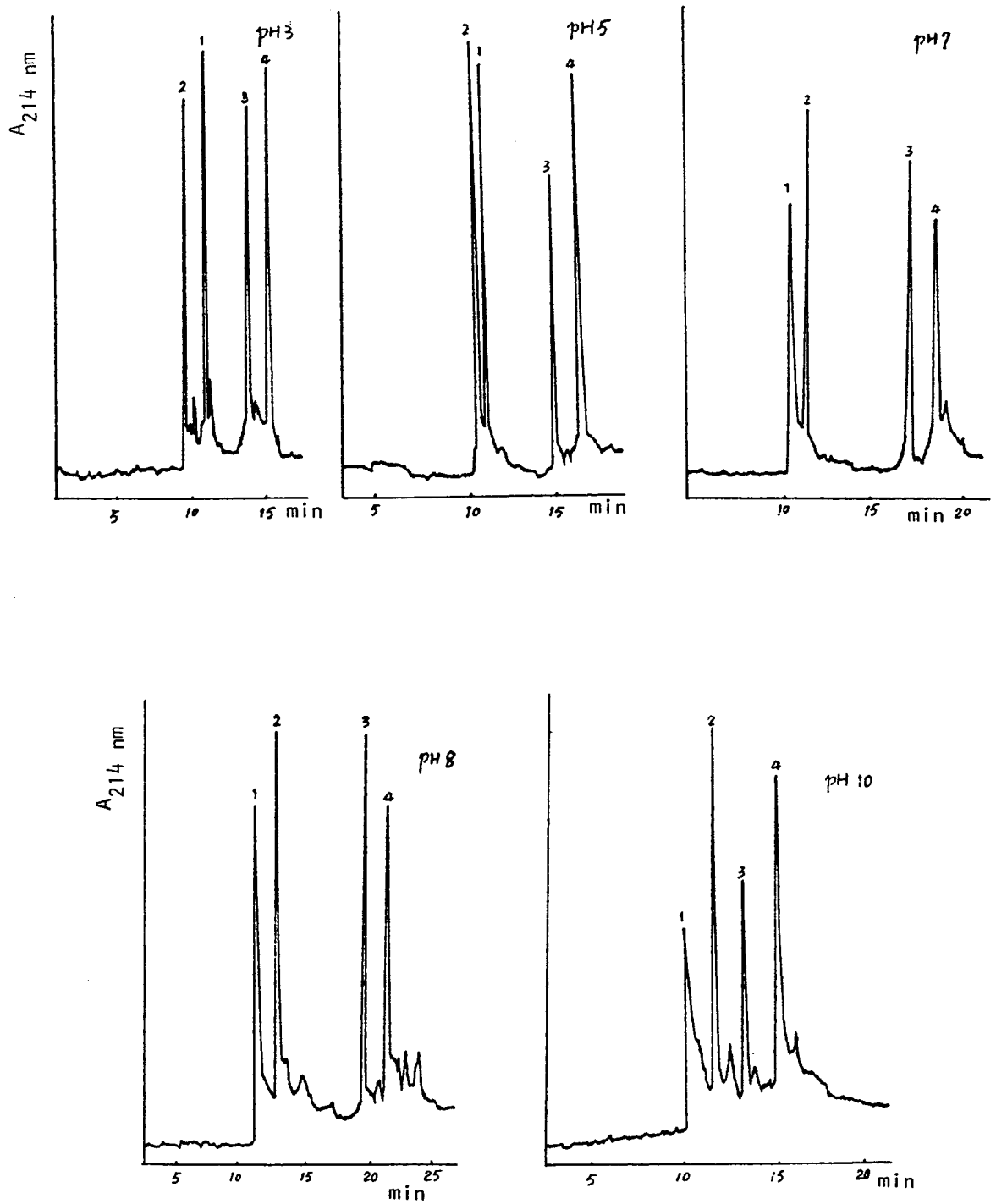

Fig. 4. Separation of basic proteins over the pH range 3–10 on epoxy polymer-coated (3) capillary. Peaks: 1 = lysozyme; 2 = cytochrome *c*; 3 = ribonuclease A; 4 = chymotrypsinogen.

Table 2
Efficiency (plate number) for four basic proteins at various pH values

Protein	pH 2.9	pH 5.0	pH 7.0	pH 8.2	pH 9.5	pH 5 (after 2 months)
Lysozyme	115 070	81 450	51 210	50 850		58 730
Cytochrome *c*	119 170	95 690	104 430	86 560		92 380
Chymotrypsinogen A	87 720	51 060	59 010	58 520	65 410	45 690
Ribonuclease A	167 250	196 990	227 580	100 400	67 030	91 240

Electrophoretic conditions: capillary with coating 3, 66 cm (44 cm to detector); 0.05 mol/l phosphate buffer; applied voltage, 19 kV.

over a wide pH range (2–11), it can be seen that coating 3 is more reproducible than coating 2 simply because the former is thicker and more stable than the latter.

Both coatings 2 and 3 are fairly stable over their usable pH ranges (Table 1). It should be noted that although slight protein adsorption on the coated capillaries was observed under basic conditions, e.g., lysozyme showed slight tailing on coating 3 at pH 10 (Fig. 3), the coatings were still stable and did not hydrolyse under the conditions used. After capillary 3 had been further used for several days over the pH range 9–11, we again used four basic proteins to evaluate its efficiency at pH 5. Table 2 shows the performance parameters of coating 3 that was used after 2 months over a wide pH range (2–11). Sharp peaks were still obtained and there was only a slight decrease in performance in comparison with the plate number obtained earlier. This indicated that coating 3 is fairly stable at basic pH. The slight adsorption problem probably occurred because the coating still does not have enough thickness to mask all the silanols.

4. Conclusions

Capillaries covalently coated with epoxy polymer can produce a hydrophilic cross-linked layer. Compared with other approaches, this coating, which involves only a two-step process, is easy to prepare. It was found that epoxy polymer coatings can greatly reduce protein adsorption and electroosmotic flow. However, it still allows sufficient electroosmotic pumping to carry both positive and negative samples to the detector. High efficiency, symmetrical peaks and reproducible separations can be achieved over a

Table 3
Reproducibility of migration times of proteins on epoxy polymer-coated capillaries

Protein	R.S.D. (%)[a]					
	Coating 2			Coating 3		
	Run-to-run	Day-to-day	Month-to-month	Run-to-run	Day-to-day	Month-to-month
Lysozyme	1.4	2.0	21.2	1.2	2.0	10.6
Cytochrome *c*	0.8	1.1	24.8	1.4	2.3	11.5
Chymotrypsinogen A	2.1	2.9	28.7	1.8	2.4	15.3
Ribonuclease A	2.5	3.2	31.5	2.7	3.6	18.8

Capillaries, 66 cm × 50 μm I.D., 44 cm to detector; 0.05 mol/l phosphate buffer (pH 5); applied voltage, 19 kV.
[a] $n = 6$.

wise pH range of 2–10. Although slight protein adsorption still existed above pH 10, these coatings are fairly stable over the pH range 2–11 and can be used for more than 2 months.

References

[1] M. Zhu, R. Rodriguez, D. Hansen and T. Wehr, *J. Chromatogr.*, 516 (1990) 123.
[2] R.M. McCormick, *Anal. Chem.*, 60 (1988) 2322.
[3] M.J. Gordon, K.J. Lee and A.A. Arias, *Anal. Chem.*, 63 (1991) 69.
[4] M.M. Bushy and J.W. Jorgenson, *J. Chromatogr.*, 480 (1989) 301.
[5] D. Corradini, A. Rhomberg and C. Corradini, *J. Chromatogr. A*, 661 (1994) 305.
[6] J.W. Jorgenson and K.D. Lukacs, *Science*, 222 (1982) 266.
[7] G.J.M. Bruin, J.P. Chang, R.H. Kuhlman, K. Zegers, J.C. Kraak and H. Poppe, *J. Chromatogr.*, 471 (1989) 429.
[8] W. Nashabeh and Z.E. Rassi, *J. Chromatogr.*, 559 (1991) 367.
[9] D. Bentrop, J. Kohr and H. Engelhardt, *Chromatographia*, 32 (1991) 171.
[10] G.J.M. Bruin, R. Huiselen, J.C. Kraak and H. Poppe, *J. Chromatogr.*, 480 (1989) 339.
[11] S. Hjerten, *J. Chromatogr.*, 347 (1985) 191.
[12] K.A. Cobb, V. Dolnik and M. Norotny, *Anal. Chem.*, 62 (1990) 2478.
[13] J.K. Towns and F.E. Regnier, *Anal. Chem.*, 63 (1991) 1126.
[14] J.K. Towns, J. Bao and F.E. Regnier, *J. Chromatogr.*, 599 (1992) 227.

ELSEVIER

Journal of Chromatography A, 694 (1995) 507–514

JOURNAL OF CHROMATOGRAPHY A

Short communication

Micellar electrokinetic capillary chromatographic determination of artificial sweeteners in low-Joule soft drinks and other foods

Catherine O. Thompson, V. Craige Trenerry*, Bridget Kemmery

Australian Government Analytical Laboratories, 338–340 Tapleys Hill Road, Seaton 5023, Australia

First received 13 September 1994; revised manuscript received 9 December 1994; accepted 12 December 1994

Abstract

A rapid method for the determination of artificial sweeteners in low-Joule soft drinks and other foods by micellar electrokinetic capillary chromatography (MEKC) is described. Caffeine, benzoic acid and sorbic acid, which are often added to soft drinks, can also be determined with this procedure. The artificial sweeteners, aspartame, saccharin, acesulfame-K, alitame and dulcin, and the other food additives are well separated in less than 12 min using an uncoated fused-silica capillary column with a buffer consisting of 0.05 *M* sodium deoxycholate, 0.01 *M* potassium dihydrogenorthophosphate, 0.01 *M* sodium borate operating at 20 kV. Dehydroacetic acid was used as the internal standard for the determinations. The levels of artificial sweeteners, preservatives and caffeine were in good agreement with those determined by the high-performance liquid chromatographic (HPLC) procedure currently used in our Laboratory. The MEKC procedure has the same order of repeatability, is faster and less costly to operate than the HPLC method.

1. Introduction

A number of methods for the quantitative determination of artificial sweeteners and preservatives in a variety of foods using high-performance liquid chromatography (HPLC) as the determinative step have been reported in the literature [1–7]. HPLC is currently the method of choice for these determinations because all of the components can be separated in the one run. Micellar electrokinetic capillary chromatography (MEKC) is rapidly gaining acceptance as a rugged analytical tool [8–10]. MEKC procedures exhibit greater resolution than HPLC and have the same order of repeatability. MEKC is faster and less costly to operate than HPLC, and, in some instances, has replaced HPLC as the analytical method of choice [11–13]. We recently reported the quantitative determination of sorbic acid and benzoic acid in a number of foods and beverages using an uncoated fused-silica capillary column with a borate buffer modified with sodium dodecyl sulphate [11]. *l*-Ascorbic acid has been determined in a number of foods with a phosphate–borate buffer containing sodium deoxycholate as the micelle modifier [12,13]. This paper describes the rapid separation and quantitation of aspartame, saccharin, acesulfame-K, benzoic acid, sorbic acid and caffeine in a variety of low-Joule soft drinks and the quantitation of aspartame and saccharin in table-top sweeteners, low-Joule tomato sauce and diet marmalade jam. Two other artificial sweeteners, alitame and dulcin, were also separated from the other com-

* Corresponding author.

0021-9673/95/$09.50
SSDI 0021-9673(94)01224-5

pounds. Dehydroacetic acid was used as the internal standard for these determinations [11].

2. Experimental

2.1. Reagents

Aspartame, sodium saccharin, potassium sorbate, sodium benzoate, sodium deoxycholate, sodium cholate, sodium taurodeoxycholate and sodium dodecyl sulphate were obtained from Sigma, St. Louis, MO, USA. Acesulfame-K and alitame were gifts from Hoechst, Frankfurt, Germany and Pfizer, Groten, CT, USA, respectively. Dulcin was obtained from ICN Biochemicals, Cleveland, OH, USA. Dehydroacetic acid was obtained from BDH, Kilsyth, Australia. Caffeine was obtained from the Curator of Standards, Australian Government Analytical Laboratories, Pymble, Australia. All other chemicals and solvents were analytical-reagent or HPLC grade and used without further purification.

2.2. MEKC buffer

A 2.16-g amount of sodium deoxycholate was dissolved in 100 ml of a 1:1 mixture of 0.02 *M* sodium borate and 0.02 *M* potassium dihydrogenorthophosphate. The pH of the solution was 8.6. The solution was filtered through a 0.8-μm cellulose acetate filter disc before use.

2.3. Apparatus

MEKC

The samples were analysed with an uncoated fused-silica capillary column (75 cm × 75 μm I.D.) with an effective length to the detector of 50 cm purchased from Polymicro Technologies, AZ, USA. An Isco Model 3140 electropherograph (Isco, Lincoln, NE, USA) operating at 20 kV and at 27°C was used for all of the determinations. The capillary was flushed with running buffer for two min between runs. The capillary was cleaned on a weekly basis by washing with 0.1 *M* sodium hydroxide for 10 min followed by deionised water for 10 min before filling with running buffer. The solutions were loaded under vacuum (vacuum level 2, 20 kPa s) and were detected at 220 nm. Aspartame and caffeine were determined quantitatively at 0.005 AUFS, while saccharin, acesulfame-K, sorbic acid and benzoic acid were determined quantitatively at 0.02 AUFS. Electropherograms were recorded with either the ICE data management and control software supplied with the electropherograph or a HP 3350 laboratory data system (Hewlett-Packard, Palo Alto, CA, USA).

HPLC

The analyses were performed with a 501 HPLC pump, 712 WISP, 490 programmable multiwavelength UV detector using a C_{18} μBondapak 10 cm × 8 mm Radial-Pak cartridge equipped with a C_{18} pre-column (Waters Chromatography Division of Millipore, Milford, MA, USA) with a mobile phase consisting of 10% acetonitrile in 0.01 *M* potassium dihydrogenphosphate, adjusted to pH 4.0 with dilute orthophosphoric acid at a flow-rate of 2.0 ml/min. The compounds were detected and quantitated at 220 nm at 0.06 AUFS, except for acesulfame-K, which was determined quantitatively at 254 nm. The chromatograms were displayed on an Omniscribe chart recorder (Houston Instruments, USA). Peak areas obtained from a HP 3350 laboratory data system (Hewlett-Packard) were used in the calculations.

2.4. Samples and standards

MEKC

Samples. The low-Joule soft drinks, cordials, tomato sauce, marmalade jam and table-top sweeteners were purchased from local outlets and analysed within the recommended "use by" dates. Sample solutions were prepared by diluting the products with an appropriate amount of deionised water. Dehydroacetic acid was used as the internal standard at a final concentration of 10 μg/ml. The solutions were filtered through a 0.45-μm cellulose acetate filter disc before analysis.

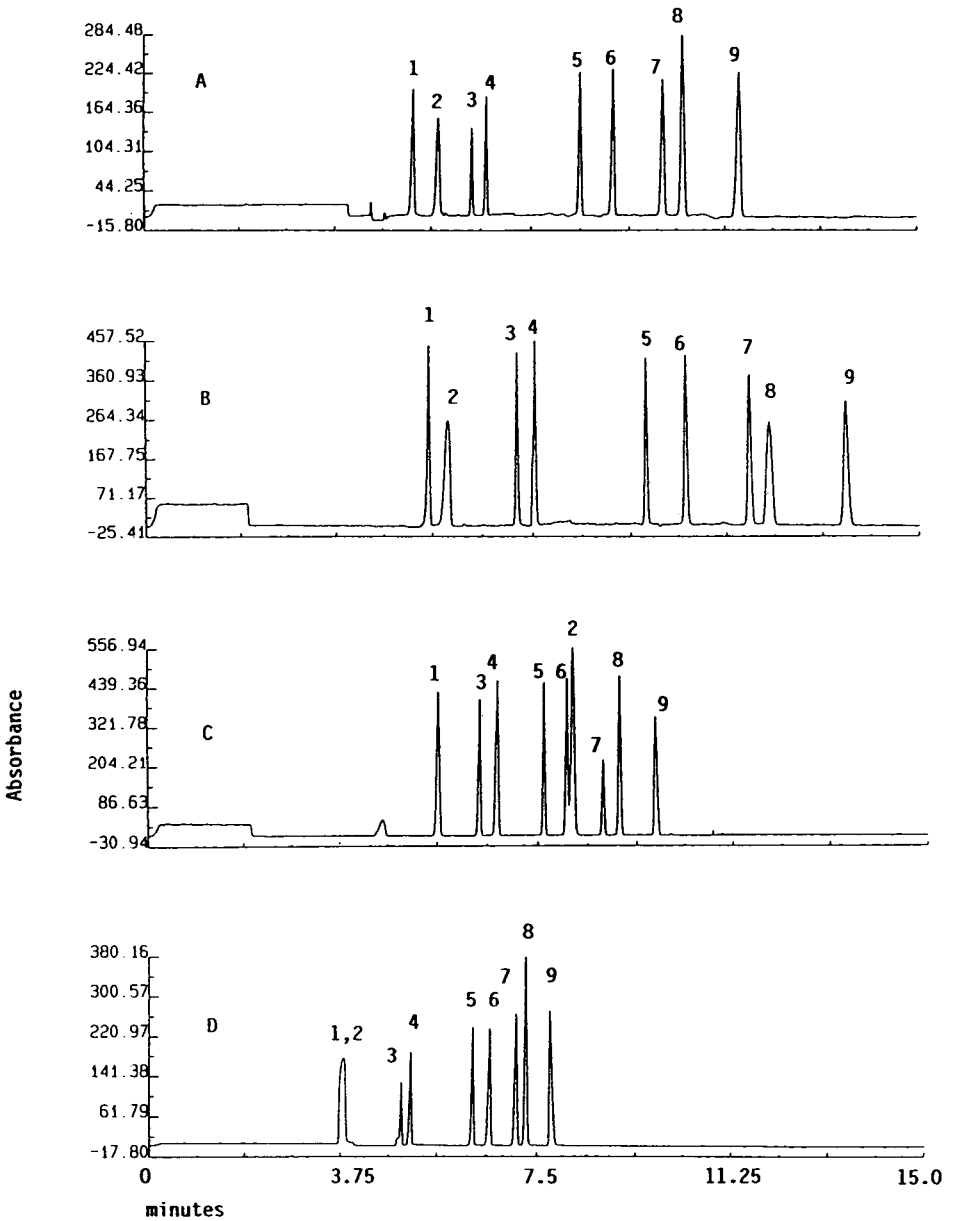

Fig. 1. Electropherograms showing the separation of caffeine (1), dulcin (2), alitame (3), aspartame (4), dehydroacetic acid (5), sorbic acid (6), benzoic acid (7), saccharin (8) and acesulfame-K (9) using (A) a buffer consisting of 0.05 *M* sodium deoxycholate, 0.01 *M* potassium dihydrogenorthophosphate, 0.01 *M* sodium borate pH 8.6, (B) a buffer consisting of 0.05 *M* sodium cholate, 0.01 *M* potassium dihydrogenorthophosphate, 0.01 *M* sodium borate pH 8.6, (C) a buffer consisting of 0.05 *M* sodium dodecyl sulphate, 0.01 *M* potassium dihydrogenorthophosphate, 0.01 *M* sodium borate pH 8.6 and (D) a buffer consisting of 0.01 *M* potassium dihydrogenorthophosphate, 0.01 *M* sodium borate pH 8.6. The *x* axis gives the migration time in minutes.

Standards. Standard solutions were prepared in deionised water with dehydroacetic acid as the internal standard at a concentration of 10 μg/ml. The solutions were filtered through a 0.45-μm cellulose acetate filter disc before analysis.

HPLC

The sample and standard solutions were prepared as described for the MEKC analyses, except that no internal standard solution was used.

3. Results and discussion

Caffeine, dulcin, alitame, aspartame, dehydroacetic acid, sorbic acid, benzoic acid, saccharin and acesulfame-K were well separated using an uncoated fused-silica capillary column with a 0.01 *M* phosphate–0.01 *M* borate buffer containing 0.05 *M* sodium deoxycholate operating at 20 kV (Fig. 1). For the MEKC determinations, the compounds were detected at 220 nm, as this is the most suitable wavelength to determine aspartame, which is the preferred artificial sweetener in the samples analysed. This wavelength was also used for the HPLC determinations, except for acesulfame-K, where 254 nm was the preferred wavelength. The addition of 0.05 *M* sodium deoxycholate to the phosphate–borate buffer was necessary to achieve complete separation of the nine compounds. Caffeine and dulcin co-migrated when the buffer consisted only of the phosphate–borate mixture (Fig. 1). Other micelle modifiers were trialed to see if the separation could be improved or the analysis time shortened. The compounds were well separated when sodium deoxycholate was replaced with either of the related compounds, sodium cholate or sodium taurodeoxycholate [14]. However, in both cases, the run times were longer. Sodium taurodeoxycholate was also unsuitable as a buffer additive as it absorbs at 220 nm, resulting in a very noisy baseline. The noise was eliminated when the detection wavelength was changed to 230 nm. In doing so, the responses for aspartame and alitame were greatly diminished, making this system unsuitable for quantitative work. Replacing sodium deoxycholate with sodium dodecyl sulphate resulted in a slightly shorter run time, but with this system, dulcin and sorbic acid partially coeluted (Fig. 1). Sodium deoxycholate was therefore the modifier of choice. Dehydroacetic acid was used as the internal standard for the quantitation of the food additives, as it is not listed as a food additive in the Australian Food Standards Code and is unlikely to be present in any of the samples to be analysed [15].

Separation of the nine compounds was maintained over 20 repetitive injections. Linearity was established for all of the compounds. Even though all of the compounds were well separated, they could not be all be determined in the one run, as acesulfame-K, saccharin, sorbic acid

Table 1
Comparison of MEKC and HPLC data for standard solutions of varying concentrations showing relative standard deviations (R.S.D.s) between instruments with a sodium deoxycholate-modified buffer

Concentration (μg/ml)	R.S.D. (%)											
	Aspartame		Saccharin		Acesulfame-K		Caffeine		Benzoic acid		Sorbic acid	
	MEKC	HPLC	MEKC	HPLC	MEKC	HPLC	MEKC	HPLC	MEKC	HPLC	MEKC	HPLC
5	2.6	2.0	1.7	0.9	2.5	0.9	1.9	0.9	0.9	2.3	2.0	3.0
50	1.4	1.2	0.5	0.5	1.3	0.8	1.2	1.2	0.7	2.0	1.1	0.7
100	0.6	2.5	–	0.5	1.0	2.2	–	1.6	1.5	2.0	2.9	3.3

and benzoic acid have much greater extinction coefficients than aspartame and caffeine at 220 nm. Therefore aspartame and caffeine were determined at 220 nm and 0.005 AUFS, while the remaining compounds were determined at 0.02 AUFS. Aspartame and caffeine were linear to 200 μg/ml and 50 μg/ml respectively, while acesulfame-K, sorbic acid and benzoic acid were linear to 100 μg/ml and saccharin was linear to 50 μg/ml. The repeatability data (R.S.D.) for seven consecutive injections of a number of standards of different concentrations were comparable to those obtained for the HPLC procedure that is currently used in our laboratory. These data are displayed in Table 1.

A range of soft drinks were then analysed by MEKC and the levels of additives and the instrument repeatability data (R.S.D.) compared with the data obtained from the HPLC procedure. None of the samples analysed had any naturally occurring compounds that comigrated with the internal standard (dehydroacetic acid)

Table 2
Comparison of MEKC and HPLC quantitation of aspartame, benzoic acid and caffeine in low-Joule soft drinks showing R.S.D.s between instruments with a sodium deoxycholate-modified buffer

Sample	Amount (mg/l)					
	Aspartame		Benzoic acid		Caffeine	
	MEKC	HPLC	MEKC	HPLC	MEKC	HPLC
Cola 1	510	530	170	165	140	130
R.S.D. (%)	0.5	3.0	0.9	3.0	0.7	1.0
Recovery (%)	104	87	112	88	112	91
Cola 2	440	405	170	160	100	100
Cola 3	450	430	175	175	90	95
Cola 4	470	450	170	165	85	85
Cola 5[a]	335	335	150	150	60	60
Cola 6[b]	–	–	320	320	80	80
Lemonade 1	405	420	265	260		
R.S.D. (%)	2.1	3.4	0.7	1.1		
Recovery (%)	105	106	103	100		
Lemonade 2	480	470	155	155		
Lemonade 3	395	415	180	175		
Orange 1	450	440	230	235		
R.S.D. (%)	0.5	1.2	1.2	1.3		
Recovery (%)	100	94	104	97		
Orange 2	335	335	170	165		
Lemon 1	395	395	230	230		
R.S.D. (%)	0.5	0.0	1.0	0.5		
Lemon 2[c]	295	295	190	190		

[a] This sample also contained acesulfame-K (MEKC 45 mg/l, HPLC 40 mg/l).
[b] This sample contained saccharin (MEKC 75 mg/l, HPLC 80 mg/l) and cyclamate.
[c] This sample also contained sorbic acid (MEKC 50 mg/l, HPLC 50 mg/l).

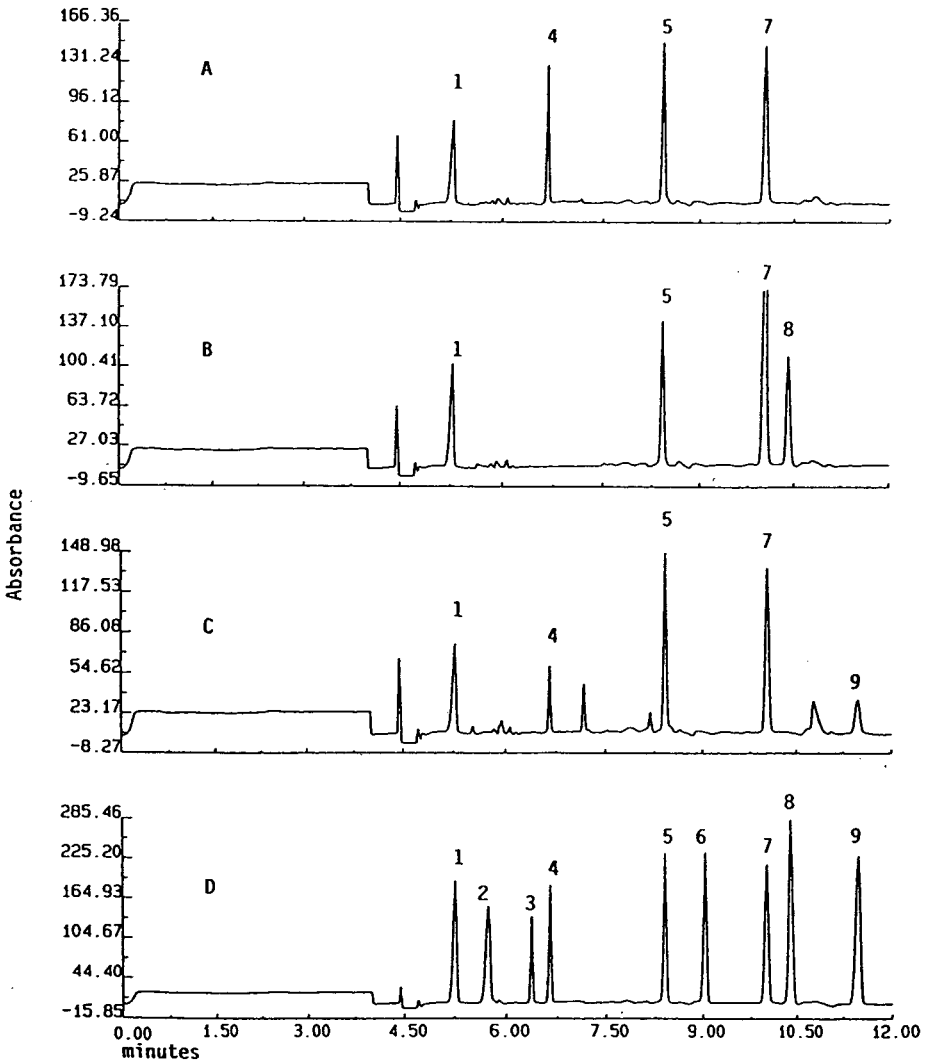

Fig. 2. Electropherograms of (A) low-Joule cola containing caffeine (1), aspartame (4) and benzoic acid (7), (B) low-Joule cola containing caffeine (1), benzoic acid (7) and saccharin (8), (C) low-Joule cola containing caffeine (1), aspartame (4), benzoic acid (7) and acesulfame-K (9) and (D) standard solution with a buffer consisting of 0.05 *M* sodium deoxycholate, 0.01 *M* potassium dihydrogenorthophosphate, 0.01 *M* sodium borate pH 8.6. The *x* axis gives the migration time in minutes. Peak 5 = dehydroacetic acid.

when analysed by MEKC. The levels for aspartame, caffeine and benzoic acid, the R.S.D. data for one sample of each of the soft drinks and recoveries for a number of analytes added to the samples before analysis are listed in Table 2.

One sample of low-Joule cola contained cyclamate as well as saccharin as the artificial sweetener. Cyclamate could not be determined with the MEKC or HPLC procedures as it does not absorb UV light at 220 nm. The determination of cyclamate in various foods by capillary electrophoresis will be reported in a forthcoming article.

Another low-Joule cola contained acesulfame-K as well as aspartame as the artificial sweetener. Acesulfame-K was determined at 254 nm by HPLC, as another compound present in the sample interfered with the quantitation at

220 nm. The levels of additives and the instrument repeatability data (R.S.D.) for all of the samples were in good agreement with the HPLC data. Electropherograms of three colas containing different sweeteners and additives are displayed in Fig. 2, and an electropherogram of a low-Joule lemon drink containing sorbic acid is displayed in Fig. 3.

The levels of saccharin in low-Joule cordials (MEKC 105, HPLC 120 mg/l; MEKC 220, HPLC 225 mg/l; MEKC 350, HPLC 345 mg/l), a low-Joule tomato sauce (MEKC 0.26, HPLC 0.25 g/kg) and a table-top sweetener (MEKC 330, HPLC 315 g/kg) and the levels of aspartame in table-top sweeteners (MEKC 21, HPLC 23 g/kg; MEKC 56, HPLC 56 g/kg) and in a low-Joule marmalade (MEKC 0.32, HPLC 0.31 g/kg) were also in good agreement.

The separation of the standard mixture by HPLC was inferior to the MEKC separation, as dulcin, alitame and sorbic acid coeluted with the HPLC system used for this study. Also, the separation of the nine components by MEKC was much faster than by HPLC. Great care had to be taken when the HPLC mobile phase was prepared, as the elution times for benzoic acid and sorbic acid were very dependent on the pH of the mobile phase. The order of elution of aspartame, saccharin and acesulfame-K was also reversed with HPLC.

4. Conclusions

A rapid method for the separation of aspartame, saccharin, acesulfame-K, alitame, dulcin, caffeine, sorbic acid, benzoic acid and dehydroacetic acid by MEKC is described. The levels of the artificial sweeteners, preservatives and caffeine in a range of soft drinks and the levels of artificial sweeteners in low-Joule tomato sauce, low-Joule cordial, diet marmalade and table-top sweeteners were in good agreement with those determined by the HPLC procedure currently used in our laboratory. The MEKC procedure has the same order of repeatability, is faster and less costly to operate than the HPLC method.

Acknowledgement

The authors wish to thank the Australian Government Analyst, Dr. C.J. Dahl, for his permission to publish this work.

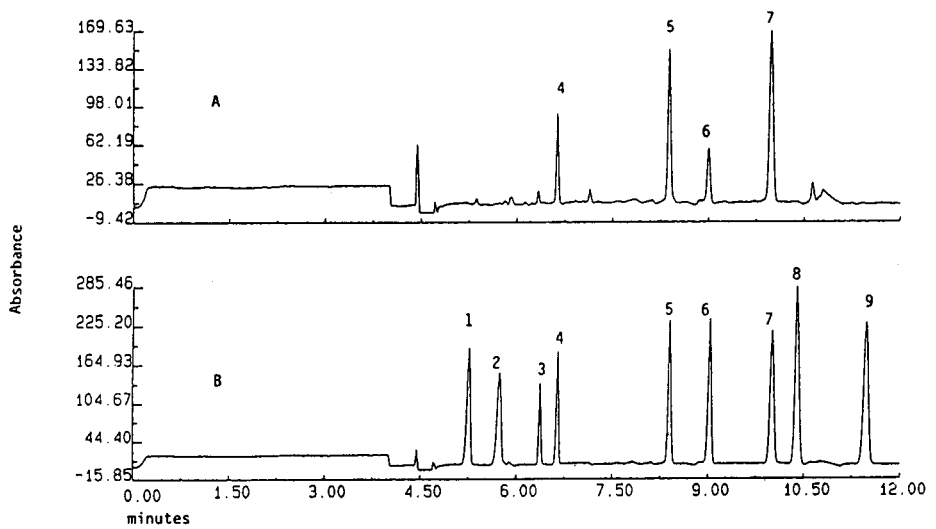

Fig. 3. Electropherograms of (A) low-Joule lemon drink containing aspartame (4), sorbic acid (6) and benzoic acid (7) and (B) standard solution with a buffer consisting of 0.05 *M* sodium deoxycholate, 0.01 *M* potassium dihydrogenorthophosphate, 0.01 *M* sodium borate pH 8.6. The *x* axis gives the migration time in minutes. Peak 5 = dehydroacetic acid.

References

[1] D.S. Smyly, B.B. Woodward and E.C. Conrad, *J. Assoc. Off. Anal. Chem.*, 59 (1976) 14.
[2] B.B. Woodward, G.P. Heffelfinger and D.I. Ruggles, *J. Assoc. Off. Anal. Chem.*, 62 (1979) 1011.
[3] T.A. Tyler, *J. Assoc. Off. Anal. Chem.*, 67 (1984) 745.
[4] M. Veerabhadrarao, M.S. Narayan, O. Kapur and C. Sastry, *J. Assoc. Off. Anal. Chem.*, 70 (1987) 578.
[5] J.F. Lawrence and C.F. Charbonneau, *J. Assoc. Off. Anal. Chem.*, 71 (1988) 934.
[6] J. Prodolliet and M. Bruelhart, *J. Assoc. Off. Anal. Chem. Int.* ,76 (1993) 268.
[7] J. Prodolliet and M. Bruelhart, *J. Assoc. Off. Anal. Chem. Int.* ,76 (1993) 275.
[8] S.F.Y. Li, *Capillary Electrophoresis —Principles, Practice and Applications (Journal of Chromatography Library*, Vol. 52), Elsevier, Amsterdam, 1992.
[9] V.C. Trenerry, R.J. Wells and J. Robertson, *J. Chromatogr. Sci.*, 32 (1994) 1.
[10] V.C. Trenerry, R.J. Wells and J. Robertson, *Electrophoresis*, 15 (1994) 103.
[11] I. Pant and V.C. Trenerry, *Food Chem.*, submitted for publication.
[12] P.A. Marshall, C.O. Thompson and V.C. Trenerry, *J. Chromatogr. Sci.*, submitted for publication.
[13] C.O. Thompson and V.C. Trenerry, *Food Chem.*, in press.
[14] R. Weinberger, *Practical Capillary Electrophoresis*, Academic Press, San Diego, CA, 1993.
[15] *Australian Food Standards Code 1994*, Australian Government Publishing Service, Canberra, 1994.

ELSEVIER

Journal of Chromatography A, 694 (1995) 515–516

JOURNAL OF CHROMATOGRAPHY A

Book Review

Basic Protein and Peptide Protocols, (*Methods in Molecular Biology*, Vol. 32), edited by J.M. Walker, Humana Press, Totawa, NJ, 1994, xii + 490 pp., price US$89.50 (hardbound), US$ 59.50 (comb bound), ISBN 0-89603-268-X (hardbound), 0-89603-269-8 (comb bound).

General comments

The title of the text suggests that the reader can expect that a wide range of protein techniques will be described in the text. This is a challenge clearly in a book of some 480 pages and so not all of the techniques that a reader would desire or all of the details that would be desired for a given technique can be included in this relatively compact volume. The advantage is that this is a book that is readily carried home, so that details of silver straining procedures can be shared over the dinner table.

The book is basic in a less desirable sense in that some of the more recent techniques are not well represented and the absence of electrospray mass spectrometry is a pity in sections on protein, peptide and glycoprotein characterization. Also absent is matrix assisted laser desorption. The production and purification of antibodies were well described but affinity chromatography received only one mention as a specific purification.

The reviewer feels that the text offers a sensible and low cost approach to many aspects of polypeptide studies and thus can be recommended for many laboratories. However the text is rather monodimensional in its approach and most of the techniques are centered around the use of gels. Also the approaches used are not always what is the consensus in other laboratories. This may be due to the rather clustered location of the authors e.g. of the 36 authors I noted that 25 were from the British Isles and 4 of the 5 USA authors were from the same university. Such grouping can be a problem with chapters where the reference list is over-restrictive. For example, in Chapter 31 on reversed-phase HPLC purification of peptides there were only five references despite the popularity of the technique and all references were self-citations by the author. I am not suggesting that there is anything wrong with the work (in fact it is of high standard), but it is thus difficult for the reader to access the literature and receive other approaches to a method.

Specific comments

Chapter 18, p. 145: The discussion on profiling of oligosaccharides by mass spectrometry does not include the recent contribution of flow fast atom bombardment and more recently electrospray mass spectrometry. The latter technique is ideal for M_r 2000–5000 glycopeptides and unfortunately the reader is not directed to the work of Henion, Stults, Carr etc. Also the recent application of capillary electrophoresis to oligosaccharide separations is not noted.

Chapter 23 does not give a good account of modern use of reversed-phase HPLC in that it concentrates on the use of radiolabelled proteins and does not discuss the use of capillary HPLC on on-line UV detectors which can give high

SSDI 0021-9673(94)01186-9

femtomole sensitivity. The advantage of such general detection is that in principle all structural modifications can be detected, whereas radiolabelling limits the information to those residues that have been radiolabelled. The references are similarly constrained and mainly refers to the author and do not refer to the many who have contributed to the HPLC field e.g. Horváth, Hodges, Hearn, Nice etc.

On p. 202 the use of a in-line γ counter is described, in many cases such a system suffers from contamination of the detector, particularly with hydrophobic samples.

On pp. 200 and 275 the authors use the term *reverse* phase HPLC when the correct term is usually agreed on as *reversed*-phase HPLC because of the reversal of the polarity encountered in normal-phase chromatography i.e. the column is less polar than the mobile phase in RPLC.

At times useful cross-references are not present e.g. in Chapter 23, p. 194 it would have been useful to have a cross reference to chapter 32, p. 290 where there is a good description on the use of trypsin so as to minimize the occurrence of nonspecific cleavages.

Technical comments

On p. 277 I would have mentioned the use of different concentrations of trifluoroacetic acid (say 1% vs. 0.8%) in buffers A and B to help smooth out baseline drift. On p. 194 no steps are described to minimize the occurrence of nonspecific cleavages such as the use of inhibitors or high purity enzymes.

On p. 353 the reader is not warned of the possibility of disulfide scrambling if the protein is exposed to higher pH values during steps such as enzyme digestion.

In Chapter 29 the reader is directed immediately to phenylthiohydantoin derivatives for sequencing; I prefer post-column ninhydriny –it is still the gold standard and avoids the pre-separation, derivatisation step.

Concluding comments

The reviewer feels that it is possible to go too far with minor quibbles and much of what is included will be the choice of the author. The text is compact for the breadth of subjects covered and contains few errors and is carefully produced. The reader needs to beware that this text gives one view of the approaches to polypeptide analysis and thus the reviewer recommends that this text is not the only source for recent methodologies.

Palo Alto, CA, USA W.S. Hancock

ELSEVIER

Journal of Chromatography A, 694 (1995) 517–518

JOURNAL OF CHROMATOGRAPHY A

Book Review

Liquid Chromatography for the Analyst (*Chromatographic Science Series*, vol. 67), by R.P.W. Scott, Marcel Dekker, New York, 1994, XII + 328 pp., price US$ 75.00, ISBN 0-8247-9184-3.

Rarely are expectations with regard to a book so high and is the disappointment so deep. It seems to be a good idea to write a book, in the author's own words, "to present a clear perception of the chromatographic process together with the function of its associated instrumentation, the rationale behind the choice of appropriate phase systems and the procedures necessary to obtain accurate qualitative and quantitative analyses" for chemists who are not specialists in liquid chromatography but who use the technique in their daily work. The result is a text with few highlights (if any), too many words and too little inspiration.

The main concept is "interaction": dispersive, polar or ionic, plus size-exclusion and chiral separation mechanisms. Although not wrong, the concept is overstrained by endless discussions. I doubt if "the analyst" can gain really useful and practical information about how to solve his or her separation problems by studying adsorption isotherms. A scheme which gives a guideline which liquid chromatographic technique could be useful if a certain class of compounds needs to be separated cannot be found in the book; there is no question that such proposals are highly welcome to beginners although nobody will expect final answers from them. The text is not only limited with regard to practical problems but also the presentation of theory is not convincing. There is no statement that the ideal peak is Gaussian in shape (which could be done by using the written term or by presenting the formula), no straightforward advice is given how the theoretical plate number can be calculated, a thorough discussion of the resolution equation is missing, and the fruitful concept of reduced parameters (after Knox) cannot be found. In the last chapter the author calculates peak capacities in a wrong manner and seems not to know Grushka's formula which is valid for isocratic separations. Even the drawings illustrating chromatography theory show peaks with a very queer shape (see, e.g., p. 21 or p. 46).

Unfortunately even this list of shortcomings is not complete. In the discussion of liquid chromatographic applications, especially in the part about adsorption chromatography (here "polar interaction chromatography"), chemical formulas would be very useful in order to understand why a certain mode has been chosen (nobody knows Verrucarin A or Roridin). Fig. 9-17 with the separation of proteins and a peptide on a glycerylpropyl phase is clearly based on size exclusion and not on "mixed interactions". The chapter on sample preparation is not convincing because it discusses some practical examples without giving useful advice. And why is enantioselective chromatography limited almost exclusively to separations on cyclodextrin phases? One single example, mentioned at the wrong place, is devoted to brush-type phases. Even some clearly wrong statements can be found, e.g. a 4σ separation is "quite adequate"

SSDI 0021-9673(94)01280-6

(p. 109) —but what about extreme peak size ratios?

The book has a total of 111 references with 23 of them from the author himself. Only 13 of the 111 are from 1990 or later. It seems as if Scott wants to present his personal view (and merits) of liquid chromatography to the public. However, "the analyst" who is in charge of performing difficult analyses and who has little time for personal education is looking for a text with a lot of "hands-on" information; and today a book with this title *needs* to discuss apparatus tests, validation, accreditation and the concept of ruggedness. It is a pity that all this cannot be found here.

Berne, Switzerland Veronika R. Meyer

Author Index

PUBLICATION SCHEDULE FOR THE 1995 SUBSCRIPTION

Journal of Chromatography A and *Journal of Chromatography B: Biomedical Applications*

MONTH	1994	J	F	M	A	M	
Journal of Chromatography A	Vols. 683–688	689/1 689/2 690/1 690/2	691/1 + 2 692/1 + 2 693/1 693/2	694/1 694/2 695/1 695/2	696/1 696/2 697/1 + 2 698/1 + 2	699/1 699/2 700/1 + 2 702/1 + 2	The publication schedule for further issues will be published later.
Bibliography Section				713/1			
Journal of Chromatography B: Biomedical Applications		663/1 663/2	664/1 664/2	665/1 665/2	666/1 666/2	667/1 667/2	

INFORMATION FOR AUTHORS

(Detailed *Instructions to Authors* were published in *J. Chromatogr. A*, Vol. 657, pp. 463–469. A free reprint can be obtained by application to the publisher, Elsevier Science B.V., P.O. Box 330, 1000 AH Amsterdam, Netherlands.)

Types of Contributions. The following types of papers are published: Regular research papers (full-length papers), Review articles, Short Communications and Discussions. Short Communications are usually descriptions of short investigations, or they can report minor technical improvements of previously published procedures; they reflect the same quality of research as full-length papers, but should preferably not exceed five printed pages. Discussions (one or two pages) should explain, amplify, correct or otherwise comment substantively upon an article recently published in the journal. For Review articles, see inside front cover under Submission of Papers.

Submission. Every paper must be accompanied by a letter from the senior author, stating that he/she is submitting the paper for publication in the *Journal of Chromatography A* or *B*.

Manuscripts. Manuscripts should be typed in **double spacing** on consecutively numbered pages of uniform size. The manuscript should be preceded by a sheet of manuscript paper carrying the title of the paper and the name and full postal address of the person to whom the proofs are to be sent. As a rule, papers should be divided into sections, headed by a caption (*e.g.*, Abstract, Introduction, Experimental, Results, Discussion, etc.). All illustrations, photographs, tables, etc., should be on separate sheets.

Abstract. All articles should have an abstract of 50–100 words which clearly and briefly indicates what is new, different and significant. No references should be given.

Introduction. Every paper must have a concise introduction mentioning what has been done before on the topic described, and stating clearly what is new in the paper now submitted.

Experimental conditions should preferably be given on a *separate* sheet, headed "Conditions". These conditions will, if appropriate, be printed in a block, directly following the heading "Experimental".

Illustrations. The figures should be submitted in a form suitable for reproduction, drawn in Indian ink on drawing or tracing paper. Each illustration should have a caption, all the *captions* being typed (with double spacing) together on a *separate sheet*. If structures are given in the text, the original drawings should be provided. Coloured illustrations are reproduced at the author's expense, the cost being determined by the number of pages and by the number of colours needed. The written permission of the author and publisher must be obtained for the use of any figure already published. Its source must be indicated in the legend.

References. References should be numbered in the order in which they are cited in the text, and listed in numerical sequence on a separate sheet at the end of the article. Please check a recent issue for the layout of the reference list. Abbreviations for the titles of journals should follow the system used by *Chemical Abstracts*. Articles not yet published should be given as "in press" (journal should be specified), "submitted for publication" (journal should be specified), "in preparation" or "personal communication".

Vols. 1–651 of the *Journal of Chromatography*; *Journal of Chromatography, Biomedical Applications* and *Journal of Chromatography, Symposium Volumes* should be cited as *J. Chromatogr.* From Vol. 652 on, *Journal of Chromatography A* (incl. Symposium Volumes) should be cited as *J. Chromatogr. A* and *Journal of Chromatography B: Biomedical Applications* as *J. Chromatogr. B.*

Dispatch. Before sending the manuscript to the Editor please check that the envelope contains four copies of the paper complete with references, captions and figures. One of the sets of figures must be the originals suitable for direct reproduction. Please also ensure that permission to publish has been obtained from your institute.

Proofs. One set of proofs will be sent to the author to be carefully checked for printer's errors. Corrections must be restricted to instances in which the proof is at variance with the manuscript.

Reprints. Fifty reprints will be supplied free of charge. Additional reprints can be ordered by the authors. An order form containing price quotations will be sent to the authors together with the proofs of their article.

Advertisements. The Editors of the journal accept no responsibility for the contents of the advertisements. Advertisement rates are available on request. Advertising orders and enquiries can be sent to the Advertising Manager, Elsevier Science B.V., Advertising Department, P.O. Box 211, 1000 AE Amsterdam, Netherlands; Tel: 31 (20) 485 3796; Fax: 31 (20) 485 3810. Courier shipments to street address: Molenwerf 1, 1014 AG Amsterdam, Netherlands. *UK*: T.G. Scott & Son Ltd., Tim Blake, Portland House, 21 Narborough Road, Cosby, Leics. LE9 5TA, UK; Tel: (0116) 2750 521/2753 333; Fax: (0116) 2750 522. *USA and Canada*: Weston Media Associates, Daniel S. Lipner, P.O. Box 1110, Greens Farms, CT 06436-1110, USA; Tel: (203) 261 2500; Fax: (203) 261 0101.

HPLC'95: Innsbruck, Austria

19th International Symposium on Column Liquid Chromatography

May 28–June 2, 1995

Chairman: **W. Lindner**
University of Graz
Austria

Honorary Chairman: **J.F.K. Huber**
University of Vienna
Austria

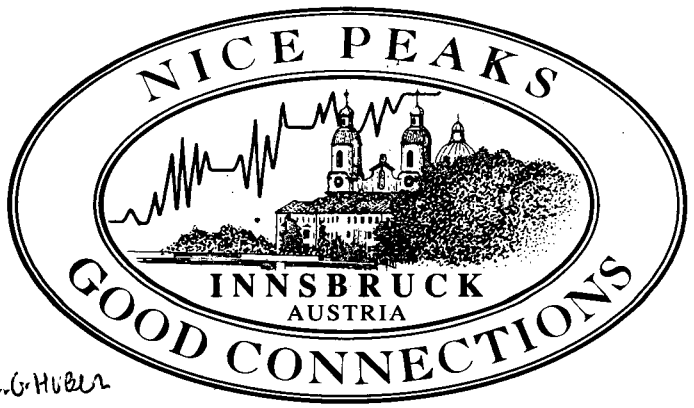

C.G. Huber

FORMAT: The HPLC'95 Symposium in Innsbruck follows the eighteen successful meetings held earlier in this series in Europe and the U.S.A. The format will be similar, covering a broad range of topical issues in Separation Science by oral and poster presentations, together with a series of Poster Discussion Sessions. An International Technical Exhibition on instrumentation, accessories and services will form an integral part of the scientific program.

TOPICS: The broad spectrum of Lecture and Poster Sessions will highlight recent advances in:
o Separation Methods, HPLC, SFC, HP-Affinity Chromatography, etc. o Capillary Electrophoresis o Hyphenated Techniques, Mass Spectrometry o Separation of Stereoisomers and Chiral Recognition o Separation Techniques in Biotechnology o New Developments of Sorption Materials o Preparative Techniques in Chromatography o Sample Preparation and Derivatization o Selective and Sensitive Detection Principles o Clinical, Pharmaceutical, Environmental Applications and Implications o Applications in Food Analysis o Chemometrics in Separation Science, Validation and Regulatory Issues.

The central core of the Symposium will focus on the **Poster Sessions**, which will provide a unique forum for lively discussions on recent research and new developments and for the exchange of ideas together with an informal opportunity to meet colleagues from all over the world. To facilitate a wider discussion of current research and its implications Poster Presenters will be invited to make short oral presentations in discussion group format.

HPLC'95 POSTER AWARD: To acknowledge the major input of Poster Presentations to the continuing success of these Symposia, a number of "HPLC'95 Poster Awards" have been established in order to recognize outstanding contributions to Separation Sciences. The First Prize will be US$ 3000.- to enable the winner to attend the next meeting in the series, HPLC'96 in San Francisco. Scientific calculators will be presented as second and third prizes. This endowment has been make possible by courtesy of Hewlett-Packard and will continue for subsequent Symposia in the series.

LAST MINUTE CONTRIBUTIONS: In view of the rapid development taking place in separation science, the Organisers will be happy to receive *last minute contributions* as **POSTER PRESENTATIONS**, if an Abstract is submitted by **May 10, 1995**

KEY DATES:	January/February 1995	Preliminary Program
	April 20, 1994	Deadline for early registration

ENQUIRIES: If you are interested in attending HPLC'95, please contact:
HPLC'95 Secretariat, Tyrol Congress, Marktgraben 2, A-6020 Innsbruck, Austria
Tel.: +43-512-575600, Fax.: +43-512-575607
or: Professor W. Lindner, Institute of Pharmaceutical Chemistry, Karl-Franzens-University of Graz, A-8010 Graz, Austria, Tel.: +43-316-380-5373, Fax: +43-316-384-6324.

0021-9673(19950310)694:2;1-0